UCRL 5484

Tory IIA

A NUCLEAR RAMJET TEST REACTOR

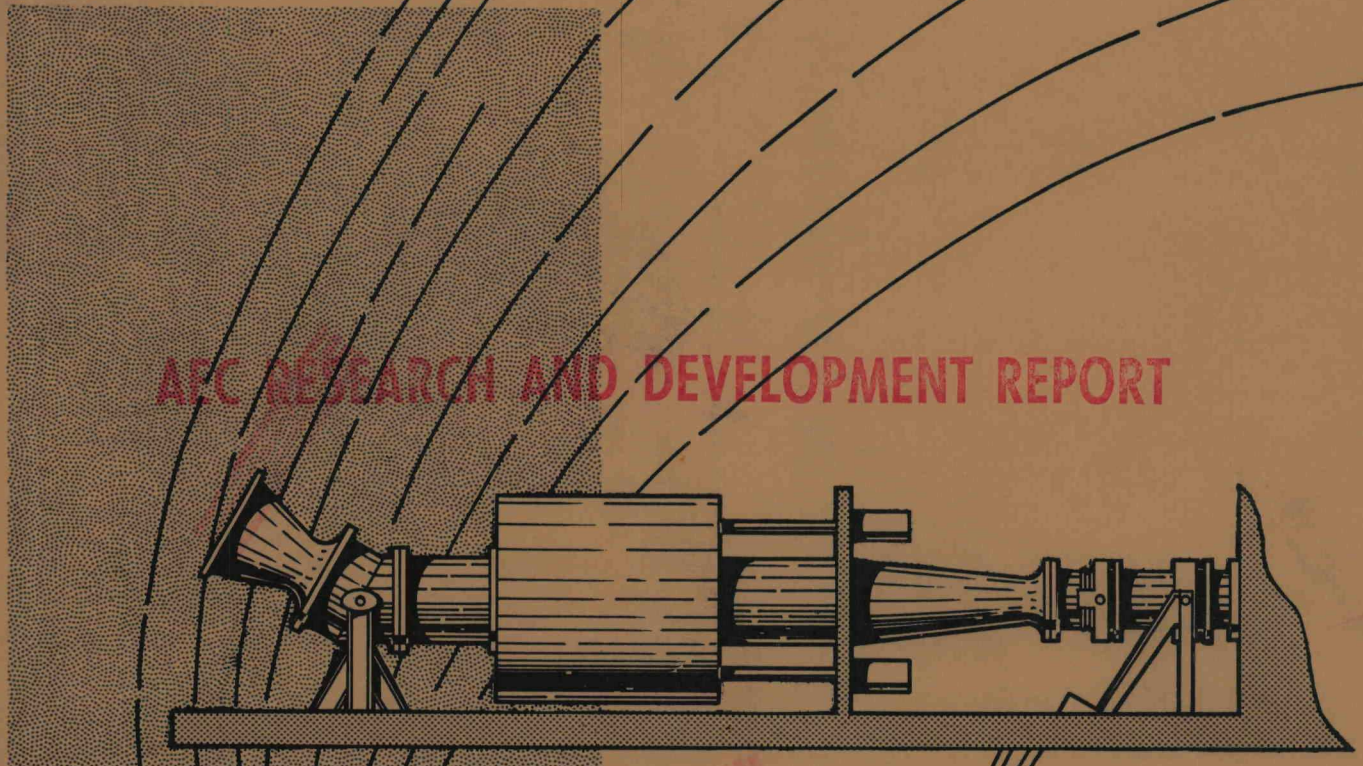

LAWRENCE
RADIATION LABORATORY
Livermore

DISCLAIMER

SECRET

UCRL-5484
Nuclear Rocket &
Ramjet Engines C-86
M-3679 (23rd. Ed.)
This document contains 295 pages.
This is copy 131 of 175 Series A .

UNIVERSITY OF CALIFORNIA
Lawrence Radiation Laboratory
Livermore, California

Contract No. W-7405-eng-48

TORY II-A

A Nuclear Ramjet Test Reactor

(Classification of Title: Unclassified)

Edited by
James W. Hadley

November 4, 1959

Printed for the U. S. Atomic Energy Commission

SECRET

DISTRIBUTION

Series A

	Copy No.
UCRL Livermore,	
Information Division	1 - 6
Edward Teller	7
Theodore C. Merkle	8
James W. Hadley	9
Charles S. Barnett	10
R. F. Finnigan	11
Eugene Goldberg	12
Albert J. Hodges	13
James S. Kane	14
Henry C. McDonald	15
William H. Moran	16
Jerauld H. Moyer	17
W. Blake Myers	18
Ethan A. Platt	19
Harry L. Reynolds	20
Albert J. Rothman	21
Paul M. Uthe	22
Robert J. Vetterlein	23
Albert J. Kirschbaum	24
Harold Brown	25
John S. Foster	26
Sidney Fernbach	27
Gerald W. Johnson	28
Duane C. Sewell	29
William M. Pierson	30
Roger E. Batzel	31
Barney Rubin	32
Arthur J. Hudgins	33
C. M. Van Atta	34
Charles L. Blue	35
Edward H. Hulse	36

DISTRIBUTION (Contd.)

Series A

	Copy No.
UCRL Livermore (Contd.),	
Jack M. Peterson	37
Arthur B. Williams	38
UCRL Berkeley,	
W. B. Reynolds	39
H. S. Gordon	40
UCRL Nevada, Dale Nielsen	41
DASA Liaison Office, Livermore,	
Lt. Richard Leonard	42
ANPO, Div. of Reactor Dev., USAEC, Wash., D. C.,	
Brig. Gen. Irving Branch	43 - 46
Capt. G. F. Helfrich	47
USAEC, Wash., D. C., Comm., John A. McCone	48
Div. of Reactor Dev., USAEC, Wash., D. C.,	
Frank Pittman	49
DMA, USAEC, Wash., D. C.,	
Brig. Gen. A. D. Starbird	50
Div. of Biology & Medicine, USAEC, Wash., D. C.,	
Charles L. Dunham	51
SAN, USAEC, Ellison C. Shute	52 - 54
ALOO, USAEC, K. F. Hertford	55 - 57
DOD, Director of Research & Engineering, Wash., D. C.,	
H. F. York	58
A. T. Biehl	59
ARPA, DOD, Wash., D. C., C. L. Critchfield	60
LASL, Los Alamos, N. Mex.,	
Norris E. Bradbury	61 - 63
Raemer Schriber	64
Sandia Corp., Livermore, R. E. Poole	65
Sandia Corp., Albuquerque, J. P. Molnar	66
AFSWC, Research Directorate, Kirtland AFB, N. Mex.,	
Col. Leonard Eddy	67
Atomics International, Stephen Carniglia	68 - 69

DISTRIBUTION (Contd.)

Series A

	Copy No.
Marquardt Aircraft Co.,	
Don Walter	70
Alan Gruber	71
Air Command and Staff College	72
AFPR, North American, Downey	73
Air Force Special Weapons Center	74
Air Research & Development Command (RDRAP)	75
Air Research & Development Command (RDZN)	76
Air Technical Intelligence Center	77
Albuquerque Operations Office	78
Argonne National Laboratory	79
Armed Forces Special Weapons Project, Sandia	80
Armed Forces Special Weapons Project, Wash.	81
Army Ballistic Missile Agency	82 - 83
Assistant Secretary of Defense, R&D (WSEG)	84
Atomic Energy Commission, Washington	85 - 88
Atomics International	89
Battelle Memorial Institute	90
Brookhaven National Laboratory	91
Bureau of Aeronautics	92
BAR, Chance Vought, Dallas	93
Bureau of Ordnance	94
Bureau of Ordnance (AD-1B)	95 - 96
Bureau of Ships	97
Chicago Operations Office	98
duPont Company, Aiken	99
General Electric Company (ANPD)	100
General Electric Company, Richland	101 - 102
Lockland Aircraft Reactors Operations Office	103
Los Alamos Scientific Laboratory	104 - 105
Marquardt Aircraft Company	106
National Aeronautics & Space Administration, Cleveland	107 - 108
National Aeronautics & Space Administration, Wash.	109 - 110

DISTRIBUTION (Contd.)

Series A

	Copy No.
New York Operations Office	111
Oak Ridge Operations Office	112
Office of Naval Research	113
Office of the Assistant for Operations Analysis DCS/O	114
Office of the Chief of Naval Operations	115
Patent Branch, Washington	116
Phillips Petroleum Company (NRTS)	117
Pratt & Whitney Aircraft Division	118
San Francisco Operations Office	119
School of Aviation Medicine	120
Union Carbide Nuclear Company (ORNL)	121
USAF Project RAND	122 - 123
U.S. Naval Postgraduate School	124
Wright Air Development Center	125 - 130
Technical Information Service Extension	131 - 175

PREFACE AND ACKNOWLEDGMENTS

Because of the length of time necessary for the preparation of such a report as this one, while the design of the reactor which it describes undergoes steady evolution, it will be understood that the finished report cannot be taken as an accurate source of information on the detailed characteristics of the reactor. For the same reason, some minor inconsistencies may be noticed among different chapters, which were written at different times by different persons. Additional and corrected information will be made available in future UCRL reports.

Tory II-A is a complex device; the development of its design, and of materials for use in it, have come from many sources, both inside and outside the Lawrence Radiation Laboratory. To give full attention to the subject matter of the report, individual credit has been omitted in all cases.

This report was written by a number of workers at LRL. The sections to which they contributed are listed below:

Section 3	J. H. Moyer
4	R. J. Vetterlein
5.2	R. E. Lingenfelter G. W. Leppelmeier
5.3	R. G. Finke T. J. Tyson
5.4	E. Goldberg A. Lorenz
6	R. F. Finnigan
7	P. M. Uthe C. S. Barnett
8	W. C. Miller
9	R. B. Meuser
10	P. M. Uthe
11	E. Goldberg

TABLE OF CONTENTS

TABLE OF CONTENTS (Contd.)

TABLE OF CONTENTS (Contd.)

TABLE OF CONTENTS (Contd.)

TABLE OF CONTENTS (Contd.)

TABLE OF CONTENTS (Contd.)

TABLE OF CONTENTS (Contd.)

TABLE OF CONTENTS (Contd.)

TABLE OF CONTENTS (Contd.)

TORY II-A

A Nuclear Ramjet Test Reactor

Edited by

James W. Hadley

Lawrence Radiation Laboratory, University of California

Livermore, California

ABSTRACT

The first test reactor in the Pluto program, leading to development of a nuclear ramjet engine, is called Tory II-A. While it is not an actual prototype engine, this reactor embodies a core design which is considered feasible for an engine, and operation of the reactor will provide a test of that core type as well as more generalized values in reactor design and testing.

The design of Tory II-A is essentially complete at the time of writing, and construction of the reactor and of its test facility is in progress. Test operation of the reactor is scheduled to start late in 1960 at the Atomic Energy Commission's Nevada Test Site.

Operation of the Tory II-A core at a total power of 160 megawatts, with 800 pounds of air per second passing through the core and emerging at a temperature of 2000°F, is the central objective of the test program. All other reactor and facility components exist to support operation of the core, and preliminary steps in the test program itself will be directed primarily toward ensuring attainment of full-power operation and collection of meaningful data on core behavior during that operation.

The core, 3 feet in diameter and 4-1/2 feet long, will be composed of bundled ceramic tubes whose central holes will provide continuous air passages from end to end of the reactor. These tubes are to be composed of a homogeneous mixture of UO_2 fuel and BeO moderator, compacted and sintered to achieve high strength and density.

Surrounding the core will be a thick graphite reflector containing moveable boron-loaded nuclear control elements. The entire reactor, together with control actuators, a duct to bring coolant air up to and away from the core, and other auxiliaries, will be mounted on a railroad flatcar for convenient transportation between assembly-disassembly shops and the test point.

A group of steel tanks will store 100,000 pounds of air, enough to cool the reactor at full power for at least a minute, with sufficient reserve for startup and shutdown phases. In addition, blowers will furnish a continuous supply of air at a much lower rate for low-power operation and for protracted cooling after a full-power run.

Operation of the reactor will be controlled from a building about two miles distant from the test point. In addition to information on inlet air conditions and on neutron flux level which will be necessary for reactor control, very extensive data on air and structure temperatures throughout the reactor, on air pressure distribution, and on strain and vibration in the reactor will be transmitted to the control building for display and recording.

A heavily shielded disassembly building, fitted with remote-handling equipment, will provide for inspection and repair during the course of test operations, as well as dismantling of the reactor after completion of tests, to permit thorough examination of components.

TORY II-A

A Nuclear Ramjet Test Reactor

Edited by

James W. Hadley

Lawrence Radiation Laboratory, University of California

Livermore, California

1. PURPOSE OF THE TORY II-A EXPERIMENT

The Tory II-A reactor described in this report is to be the first of a series of experimental reactors leading to the development of a nuclear ramjet engine. It will be a small, air-cooled, high power-density reactor operating at very high temperature.

Design of the reactor is now nearing completion. First high-temperature operation is scheduled for late 1960 at the Nevada Test Site of the Atomic Energy Commission.

The Pluto program, devoted to development of a nuclear-powered ramjet engine, requires development of a reactor having decidedly unconventional qualities. This reactor, to be used as a heat source in the ramjet engine, must be run at exceptionally high power while its size and mass are kept to a minimum. Half of the volume of the reactor must be devoted to open coolant flow area. Temperature of the reactor core material must approach 2500°F, well above the temperatures at which most conventional structural materials lose their strength. Furthermore, this reactor must withstand the thrust of a large air pressure drop across its length, and the additional loads due to the acceleration of maneuvering. It must stand up under severe thermal stress caused by large changes in core temperature. Extremely high radiation flux levels present severe problems in heat removal as well as in avoidance of radiation damage to many components of the reactor and its control system.

Although it is intended to be the forerunner of such a nuclear ramjet reactor, Tory II-A does not attempt to meet all these requirements, but instead attempts to sidestep as many as possible without avoiding the main problem of producing a core structural design at least approaching satisfaction of the ramjet needs. The Tory II-A program is regarded as a mechanical and chemical engineering test of a likely core design. The core is designed to resemble the core of a feasible ramjet reactor in materials, structure, power

density, temperature, and air-flow properties. Other features of the reactor have been chosen to support this basic aim. Development of more rugged support structures, of reflectors having minimum size and weight, and of compatible small control elements will come later in the series of Pluto reactors.

The three principal ways, then, in which Tory II-A differs from a flyable ramjet reactor are these:

a. To avoid excess drag and weight, a flying ramjet engine will have a reflector of minimal thickness. Tory II-A, on the other hand, will be provided with a very thick graphite reflector. Movement of absorber vanes within this reflector will provide more than ample control for all reactor operations.

b. The engine reflector may not provide sufficient incremental reactivity to cover all operating conditions of the engine. Consequently, at least some of the engine control elements may have to be located within the high temperature reactor core. Tory II-A will not contain any control elements in its core.

c. Tory II-A will not be designed for the stresses to be expected in ramjet maneuvering, but only for those resulting in pressure drop in the cooling air and from the reactor's own weight. An effort will be made to ensure that vibration loads do not damage the reactor, although information on this problem is still meager and is looked for as one of the benefits of actual Tory II-A operating experience.

For a more extensive discussion of the aims of the Pluto program and of the general requirements for the engine, the reader is referred to UCRL reports dealing more specifically with those topics.[1, 2]

It should be noted that the experience and information gained with the operation of Tory II-A will be of benefit not only to the Pluto program but also in its application to the more general field of high-temperature power reactors.

2. GENERAL DESCRIPTION

Before going into a detailed description of the Tory II-A reactor, with a discussion of the analysis upon which its design is based, we will undertake a brief but general descriptive chapter. Each topic is taken up in much greater detail in the chapters that follow.

2.1 Reactor

The Tory II-A program is strongly centered upon operation of the core. Everything else is designed to assist or make possible this operation.

The core is cylindrical in form, about 45 inches long, and 32 inches in diameter. It consists of a very large number of small thin-walled beryllia tubes, supported in the openings of a honeycomb-like grid of beryllia links. The links are joined by metal tie rods which pass completely through the core from end to end and support the axial thrust of air pressure on the core. All of the small beryllia tubes which contain U^{235} fuel, are lined up end-to-end to provide continuous flow passages down the length of the reactor. Air flowing through these passages receives heat directly from the fueled tube walls. Each opening of the honeycomb link structure is capped at the rear of the reactor by a base plate supported on the six surrounding tension rods. These base plates in turn support the matrix of fuel tubes within each honeycomb section. At the front, or inlet, end of the reactor, about six inches of core will be left unfueled to provide a neutron reflector; an appreciable saving in fuel at the cost of only a slight increase in core power density can be effected by this reflector.

About half of the total volume of the core is void space.

A 1-1/2-in.-thick metal gamma-ray shield, perforated by holes for the air stream, is placed directly in front of the inlet end of the core.

The core is supported throughout its length by the tension rods. The upstream ends of the rods are supported by a grid mounted on the air duct. The load at the downstream end is carried to a metal sleeve or shroud which entirely surrounds the core. This shroud, in turn, is entirely supported, cantilever-wise, from the air duct at the upstream end of the core. The shroud, which is provided with internal air-cooling passages, serves also as a heat shield to isolate the high temperature core from the air duct.

The section of air duct passing through the reactor is composed of 1/2-in.-thick aluminum alloy and is water jacketed.

The main reflector for Tory II-A is annular in form and is composed of a layer of graphite about 2 ft thick supported outside the air duct. It extends the full length of the core.

Eight graphite cylinders within the reflector, each 20 inches in diameter, are free to rotate on axes parallel to the axis of the reactor. A 90° sector of each rotating cylinder is provided, near its outside surface, with a layer of boron. The eight cylinders rotate in unison and regulate the effective neutronic thickness of the reflector, providing reactivity regulation for gross control of the reactor.

Four absorbing rods spaced symmetrically around the reflector near its inner surface slide in and out length-wise through the whole reflector. These four rods are identical in construction and interchangeable, although normally one will be used for fine control of reactivity and the other three held withdrawn, with two to be inserted in case of sudden need for rapid decrease in reactivity.

The eight rotating vanes are driven by individual hydraulic actuators which will respond alike to a single electrical signal. The four sliding rods will be driven by individual hydraulic cylinders.

2.2 Air Duct

Upstream from the reactor, air passes through a diffuser section, consisting first of a constriction, then an expanding section containing a grid. This section is designed only to satisfy the requirements of Tory II-A as a test reactor, and is not intended to represent a likely ramjet inlet configuration.

Air leaving the reactor passes through another nozzle which is directed upward, at a 30° angle to the horizontal. The throat of this nozzle, at which the air reaches Mach 1, holds desired air pressure against the exit face of the reactor. In producing a supersonic exhaust jet, the exhaust nozzle also serves the purpose of helping effluent air to reach a considerable height, so that noxious exhaust materials will not be deposited on the ground behind the reactor.

2.3 Test Facilities

The reactor together with the inlet air duct and exhaust nozzle is to be mounted on a railroad flat car, with such auxiliary equipment as cooling water ducts and the hydraulic control actuator system. Figure 2-1 shows the arrangement of the test vehicle.

The complete test car and reactor will roll on tracks up to the face of a test bunker containing air controls and racks of amplifiers, relays, and recording

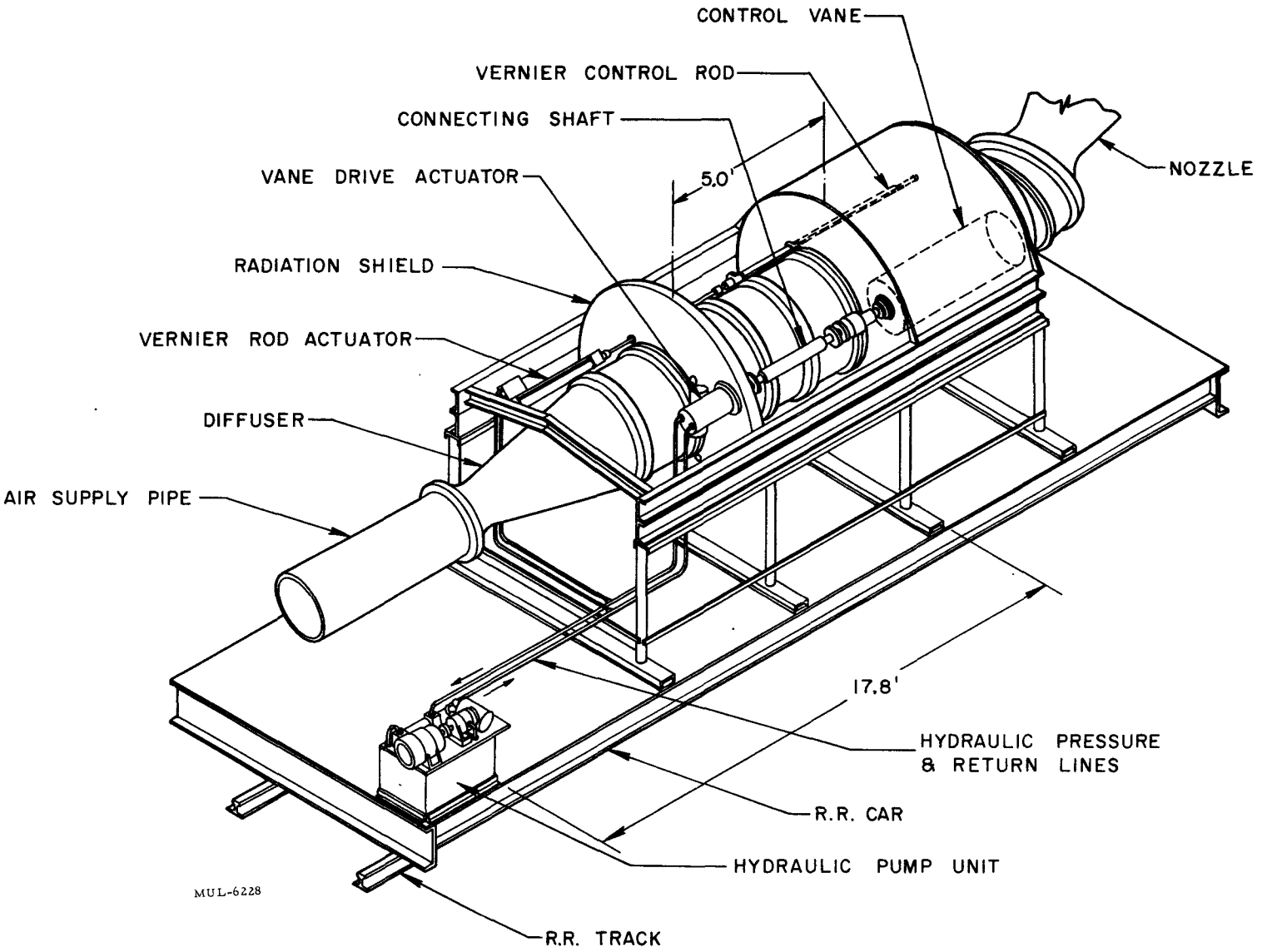

Fig. 2-1. Reactor and test vehicle.

instruments. Positioning of the car at the bunker face will be done by remote control.

The bunker, entered through a 500-ft-long earth-covered tunnel, will provide access to the air supply system and to electronic racks between reactor runs. No one will remain in the bunker during actual operation of the reactor or of the air supply.

Control of the reactor system during a run will be accomplished from a building located about two miles from the test bunker. Recording and display of all quantities of primary importance will also be at the control building.

Air for full power reactor runs will be supplied from a blowdown system consisting of a set of large steel tubes, storing sufficient air at 4000 psi for a run of about two minutes duration at full rated reactor power. When the reactor is operated below about 10% of full power, cooling air may be supplied for an indefinite period by a set of large blowers.

Before it enters the reactor, air will be passed through a stored-energy heater consisting of a bank of heavy steel tubes suspended in a cell, preheated by an oil-fired furnace. This steel will supply heat to the incoming air to raise it to a temperature of 1063°F at the reactor inlet, corresponding to the ram air temperature at the inlet of a ramjet engine flying at Mach 3.0 at 1000 ft altitude.

For inspection or disassembly after a series of runs the reactor car will be moved to a building about two miles from the test point. Facilities will be provided in this heavily shielded building for complete disassembly and packaging of reactor components as well as inspection of the reactor. A bay at the side of the disassembly building will provide space for initial assembly of the reactor and car.

The reactor car will be moved between the disassembly building and test point by an electric mine locomotive controlled remotely from the reactor control building.

2.4 Operation

Tory II-A is scheduled for first critical operation in Nevada in late-1960. A test program lasting about five months will then be carried out, hopefully passing through achievement of a number of limited experimental objectives to final tests of operation at full rated power and temperature. At the end of this period the first core will be removed for thorough examination and a second

core substituted for continuation of the test program. Since fabrication of the second core will have to start before initiation of the first tests, it will not be possible to use first-core test results to any great degree to improve the design of the second core. However, some improvements in concept gained during design and construction of the first core should be available for inclusion in the second.

There are many questions about reactor behavior that can be answered at very low power and temperature and which must be answered before operation at higher power and temperature points is risked. The reactor test program will be laid out so that by any time during the program a maximum of information with a minimum of risk of reactor loss will have been achieved. Power, temperature, and air flow will thus be held below fixed limits at any time. As the experimental program progresses, these limits will be raised until finally the design-point values are reached.

The principal objectives of the Tory II-A experimental program fall under a few main headings: first will be a study of the structural behavior of a core design showing promise for ramjet engine application; the second will be a study of the aero-thermodynamic behavior of the core-air heat exchange system; a third class of information to be obtained falls under the heading of reactor neutronic behavior; and finally, valuable experience will be gained in the operation of a test reactor. Aside from information classifiable under any one of these subjects, it is of course of the greatest interest, and only possible with an actual reactor, to study the reactor system as a whole with interactions among all of the separate systems of interest.

Actual operation of Tory II-A will take place during a long series of runs of varying individual duration. The reactor power, temperature and air flow program for each run will be fixed for the run, with a set of specific objectives and limitations kept in mind. Enough instrumentation and recording equipment will be provided that information will be available, after each run, on the behavior of all important parts of the reactor. Information of primary importance will be displayed in the control room for observation during the run and more will be recorded there. In addition, a considerable amount of additional information will be recorded on charts in the test bunker for later reference. Thus, an immediate evaluation of reactor behavior during a run will be available to the operators, while more extensive data will be available for detailed analysis later if it is deemed of interest.

3. STRUCTURE OF CORE

3.1 General Features of Core Design

The core is the element of central importance in the Tory II-A reactor, containing those material and structural features whose testing is the main purpose of the Tory II-A experiment. The design features embodied in this core are those which, at the time of its inception, seemed most promising for early use in a nuclear ramjet engine. This core, however, is not specifically a model of an engine core; its size is small, it is not designed for acceleration loads, and no attention has been paid to the likely need for nuclear control elements within the core. In addition, the thick Tory II-A reflector produces a steeper neutron flux gradient in the outer core regions than would probably be present in an actual engine.

The core is characterized by some basic features which distinguish it from other possibly feasible designs. These are summarized in the following paragraphs.

First, the core must function as a power generator and heat exchanger. Various means of coupling the power-generating regions to the air stream are possible; the one chosen here consists in making the core of a ceramic material, solid homogeneously mixed oxides of uranium and beryllium, perforated by smooth straight holes extending through the entire length of the core. The uranium fuel material is distributed in such a way that every hole receives an equal amount of power and imparts an equal air temperature increase to its share of the air stream.

Many large temperature differences will exist in the core during operation; to minimize the danger of breakage through thermal stresses, the core is divided into a very large number of small pieces in the form of tube sections which fit closely together.

To provide uniform load distribution, and to prevent dislocations and displacements from spreading through this large bundle of little tubes, it is provided with an internal skeleton of unfueled beryllium oxide links, (usually called "dogbones," in reference to their shape) pinned together at their intersections by metal tie rods extending from end to end of the core.

The gravitational weight of the core rests upon the internal links, which are supported by the tie rods. The thrust of air pressure drop in the core is carried through its body to the downstream end and caught by the tie rods.

This entire core and tie rod assembly is supported at its ends within a cylindrical metal can (shroud), attached at the relatively cool upstream end to the main air duct.

This mechanical system is described in more detail in the following sections, and is illustrated by several figures showing different aspects of the core. Figure 3-1 is a schematic diagram indicating the mode of support of the principal loads. Figure 3-2 shows some fuel tubes and model structural links (not beryllia). Figure 3-3 shows a detailed cross-sectional view through the reactor, and Fig. 3-4 is an artist's view of the core, showing more clearly how the fuel tubes and structural links are assembled.

3.2 Description of Mechanical System

The Tory II-A core has roughly the form of a right circular cylinder whose axis is horizontal. The primary mechanical load imposed on it arises from the loss in pressure experienced by cooling air in passing through the reactor. This pressure drop load is about 130,000 lb at design conditions of temperature, pressure, and power level. The overall mechanical requirements of the core are thus characterized by a need to resist a substantial nonsymmetrical load in the horizontal plane.

This axial load is carried to ground by the core support structure, a hexagonal grid attached to the forward vessel adapter. The core support structure is placed at the inlet end of the reactor so that its temperature may be kept within the useful range of available high-temperature alloys.

Attaching the core to the support structure, and extending through the core, are 72 tension tubes (also referred to as tie rods). These members serve to transfer the axial load from the core to the core support structure. They are made of a high-nickel alloy and are internally cooled by the same air flow that supplies the reactor.

The downstream end of each tension rod is fitted with a flange. Together these flanges engage 37 base plates which restrain the fuel elements axially and are perforated to pass the reactor cooling air. The base plates are made of a coated molybdenum alloy.

Within the active portion of the core all parts except the tension rods are made of beryllium oxide. The basic increment of construction is a hexagonal module approximately 5 inches across flats, extending the length of the core, with the tension rods located at its corners. The module is formed by structural links (dogbones) of beryllium oxide which connect the tension rods. The

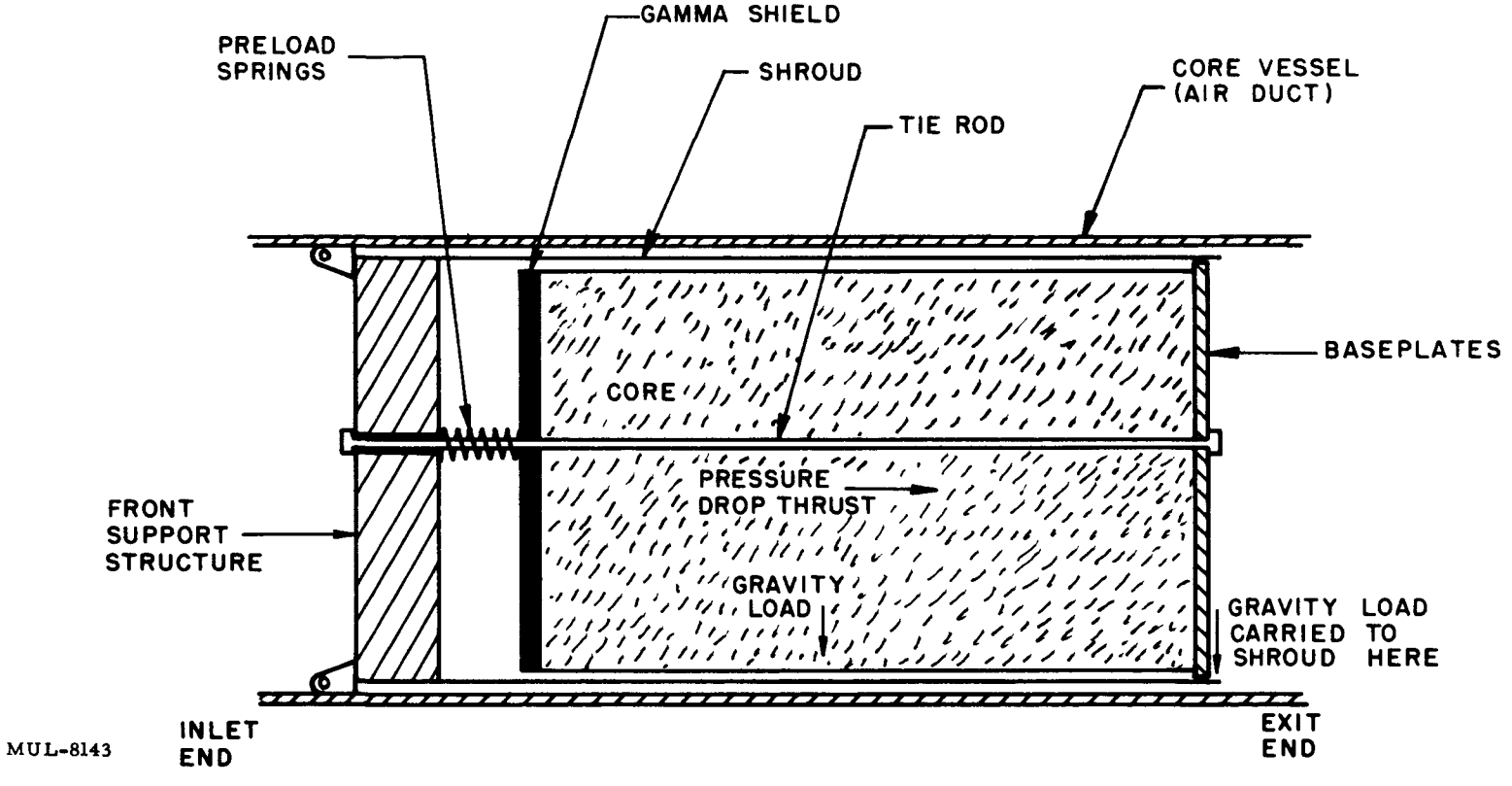

Fig. 3-1. Schematic representation of load support in core.

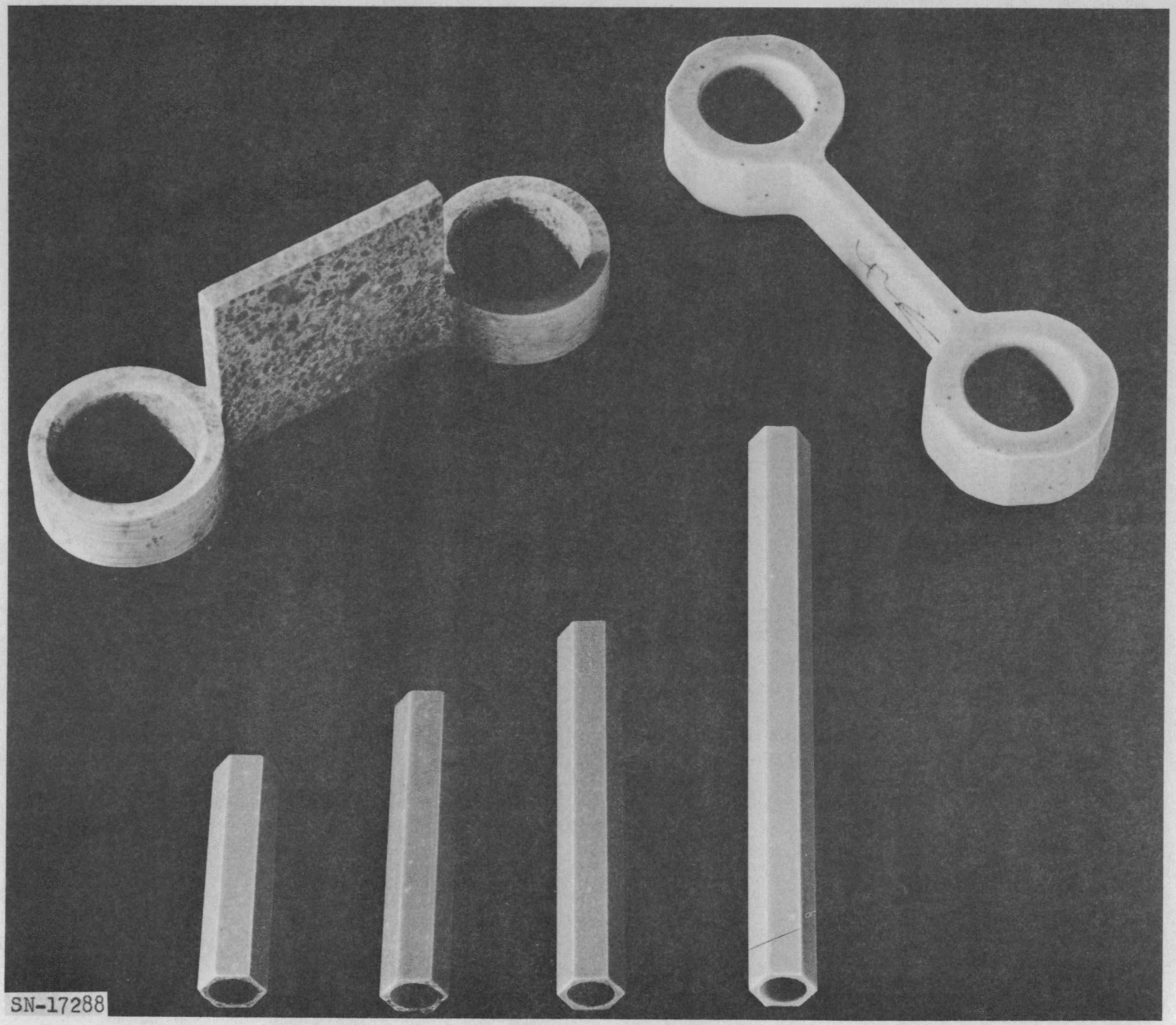

Fig. 3-2. Typical fuel elements and structural links.

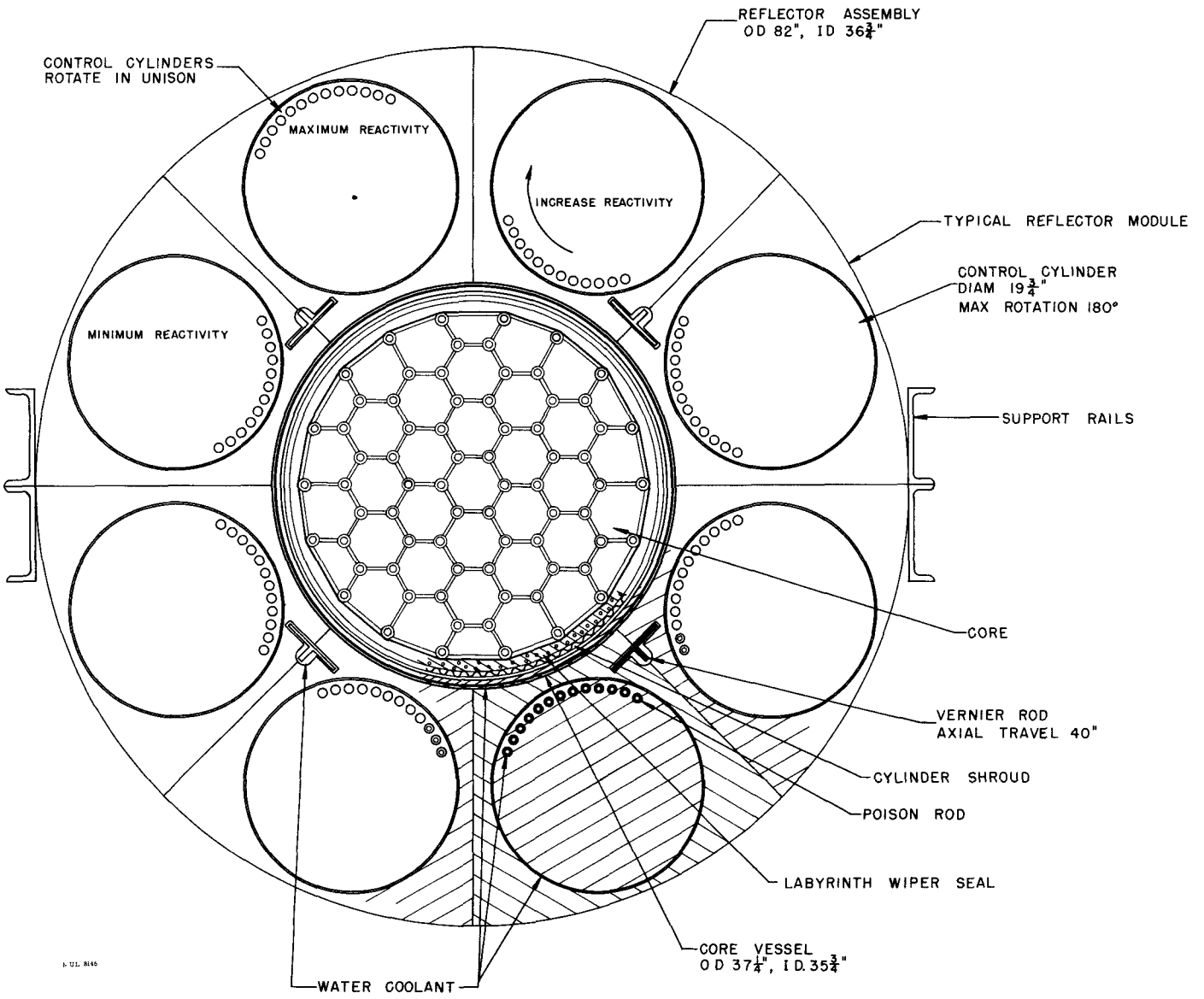

Fig. 3-3. Cross section of reactor.

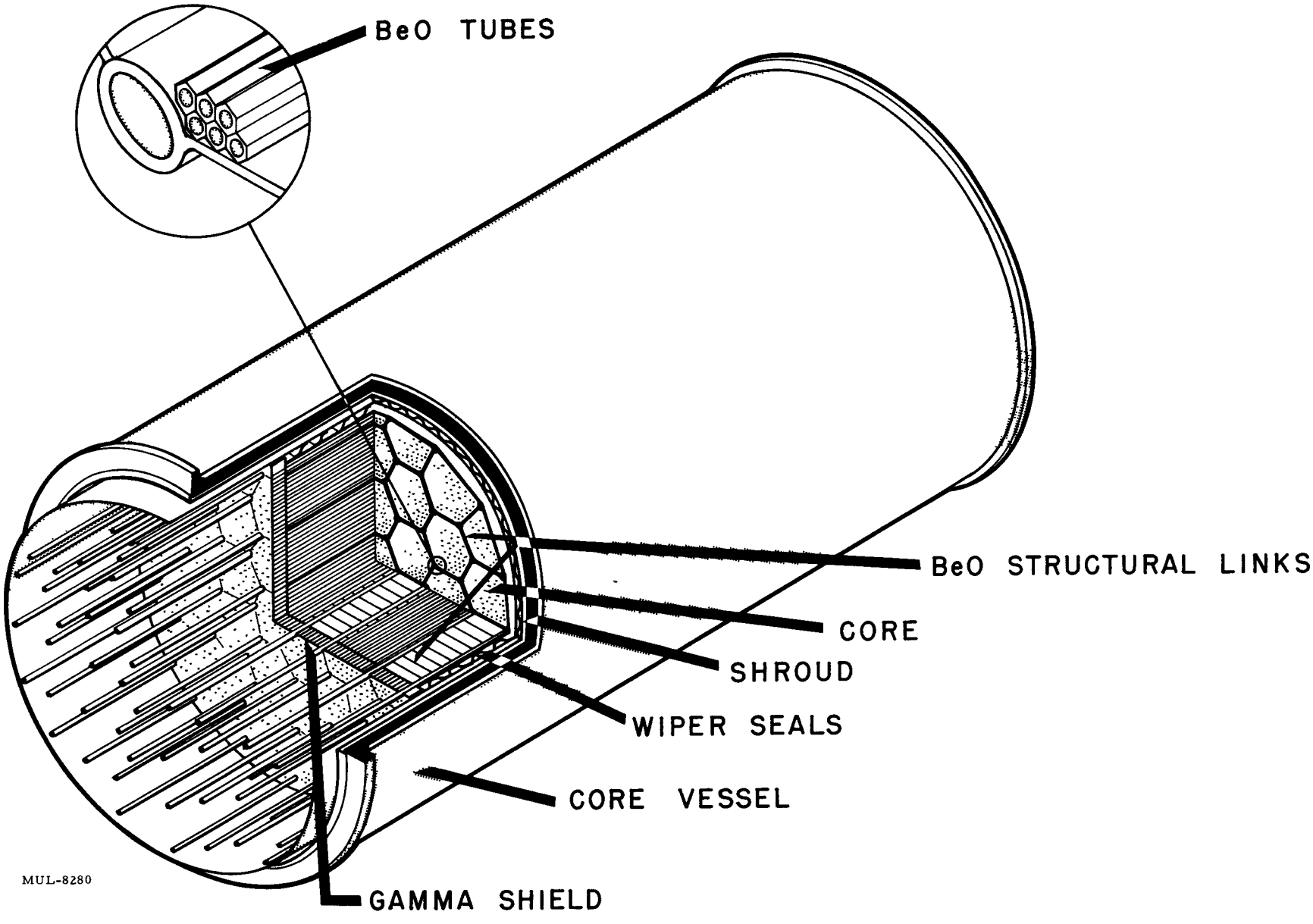

Fig. 3-4. Detailed view of core structure.

volume within the module is filled with fuel elements of a sintered $BeO-UO_2$ compact. These are hexagonal tubes about 4 inches in length, 0.30 inch across flats, with a central hole of 0.22 inch diameter. Their exterior form allows stacking to fill the module, with the holes forming continuous air flow passages through the reactor. The fuel elements are staggered in their axial location, forming an interlaced arrangement to minimize misalignment of holes. A more detailed discussion of the fuel elements and other ceramic parts may be found in Section 9.

The horizontal position of the core makes it necessary to provide support against dead loads transverse to the air flow axis. This is accomplished through the combined action of the tension rods and a sheet metal shroud which fits inside the core pressure vessel and encloses the core except at the ends.

The shroud is composed of two concentric cylinders connected by a corrugated cylinder between them. The three parts are assembled by spot welding at the crests of the corrugation, in order that shearing stresses may be transmitted from one cylinder to the other. The corrugations are aligned axially to provide cooling air passages for the shroud. The upstream end of the shroud is attached by means of machine screws to the circular outer rim of the core support structure. Its downstream end is unsupported, so that the shroud becomes a cantilever beam. Attached in this way the shroud has sufficient rigidity to support a large proportion of the core weight. The base plates, which fit inside the exit end of the shroud, are therefore supported by the shroud, through an arrangement of high-temperature springs which accommodate differential expansion and hold the base plates in contact with each other. The base plates serve to support the ends of the tension rods, which become simply-supported beams carrying the core weight.

The inlet face of the core is closed with perforated plates of a high-tungsten alloy, nearly identical in shape to the base plates. These plates perform the dual function of restraining fuel-element movement (beyond an allowance for differential thermal expansion) and protecting the core support structure from excessive heating by absorption of gamma energy from the core. This gamma shield is also effective in protecting some components external to the core, such as control components, from excessive heating and radiation damage.

At the inlet end of the core, between the gamma shield and the support structure, are 72 light preload springs (belleville type); one assembly on each

tension rod. These springs serve to hold the core components in the proper position axially while permitting differential expansion between tension rods and beryllium oxide parts. They bear on the structural links rather than the fuel elements. Space is permitted both axially and radially for differences in expansion between fuel elements and structural links. Although these parts are made of the same material, their temperatures will in general be different.

In the initial design a 4-in. length of removable spacers is left between the preload springs and the gamma shield. The purpose of the spacers is to allow some adjustment of the active core length after assembly, if the initial critical experiment shows that more or less length is required to achieve the proper neutronic configuration.

The foregoing description has said little about air flow through the reactor. Flow through the fuel elements, of course, constitutes the major portion of the throughput, but flow is also permitted through the tension tubes and the shroud, to cool these components. The shroud cooling air emerges at a temperature low enough to provide cooling for the base-plate retaining springs as well.

Two annuli are left through which no flow is desired: between the core proper and the inner surface of the shroud, and between the shroud and the core pressure vessel. The latter space is sealed at the inlet end by a lip of the shroud which engages a metallic ring at the flanged joint between the core vessel and the forward vessel adapter. This is not a positive seal but merely provides a high-impedance flow path. The purpose of this seal is to conserve air and to prevent scrubbing of the aluminum core vessel with high-temperature air. It has the incidental effect of creating a substantial pressure differential across the outer cylinder of the shroud, because the pressure outside the shroud is essentially core exit static pressure.

The annulus between the core and the shroud requires a different treatment. Obviously a seal at either the entrance or the exit would induce a bursting or crushing force on the core comparable in magnitude to that created in the shroud by the seal on the outer annulus. Such a force is not tolerable in the beryllia. Ideally the pressure in this annulus should match that in the interstices between outer fuel elements at the same axial station. To approach this condition the annulus is divided into short sections by circumferential metallic seals, or wipers. These are thin metal strips which are attached to the shroud and contact the core, thus to a large degree isolating

the spaces between them. The pressure in these spaces is then controlled by the leakage from the core itself. If the leakage path across the seals is small compared with the leakage paths between the many small pieces comprising the core, the pressures would be expected to equalize rather closely.

3.3 Structural Analysis

A tenet of the Tory II-A design is that forces arising from the weight of beryllia in a module are isolated within that module and are not transmitted laterally throughout the core. This is accomplished by allowing the proper clearance between the structural links and the tension rods. The weight of beryllia in one module is low enough that the stress it produces in the surrounding links is very low compared with the thermal stress they are likely to sustain (see Section 9).

The beryllia structural links are sized to permit unrestrained expansion and to avoid transferring loads between modules. The exact fuel-element dimensions are determined, with due regard to fabrication tolerances, to assure that the fit within the module is as snug as possible without loading the surrounding links through differential thermal expansion.

The tension tubes in Tory II-A are subjected both to tension (from pressure drop loads) and to bending (from the weight of beryllia). The material selected is Hastelloy R-235, having the advantages of high strength and high elastic modulus at elevated temperature. The controlling factor in their design is deflection in bending, which must be no more than 3/16 inch. A simple tubular shape is used, with 7/8 inch outside diameter and 0.090 inch wall thickness.

The tubes are expected to reach a maximum temperature about 1250°F, if air flow through them is unrestricted. However, it may be necessary to limit the cooling air and force the tension tube temperature up in order to protect the beryllia structural links from excessive thermal stress. This interaction is being investigated experimentally.

The core support structure is a hexagonal grid 6-3/4 inches deep, welded within a circular outer ring. The outer ring carries six support fittings which mate with clevis attachments on the forward vessel adapter to form the only mechanical connection between the reactor core and its air duct. The 72 tension tubes extend through sleeves in the support structure and transmit both axial and radial force components to it. The shroud is attached to the outer ring of the support structure and transmits a bending moment.

The core support structure is fabricated of N-155, a weldable alloy with adequate mechanical properties at the operating temperature. Radiation heating will raise its temperature above the inlet air temperature of 1063°F but it is not expected to exceed 1250°F at any point, for the design operating conditions.

Design of the core support structure has been checked by tests at room temperature on a geometrically similar structure made of low-carbon steel. The controlling feature in design is deflection rather than stress, because this structure and its attachment fittings establish the alignment of the core within the duct.

3.4 Fuel Loading

The beryllia tubes in the first six inches of core length behind the inlet-end gamma shield, and those in the final two inches at the exit end, will not contain any uranium fuel. These regions thus constitute neutronic reflectors.

The fuel loading in the remainder of the core tubes will be distributed in such a way that the power density will be approximately uniform at any axial station, and the total power supplied to the full length of each air passage will be constant over the core to ±2-1/2%. The core neutron-flux distribution has perturbations due to the control elements in the reflector, and to the lumped moderator and poison material at link-tie rod intersections, superimposed upon a strong radial variation; the fuel distribution varies inversely as the flux, giving flat power. Figure 3-5 maps one quadrant of the core, showing the loading class into which each fuel element falls. In the regions of rapidly varying loading, individual tubes are marked with their class number; elsewhere, general areas are designated by class number. The four core quadrants are mirror images in loading pattern; hence only one quadrant is mapped in this figure. Table 3-1 lists the fuel concentration for each of the loading classes and gives the total number of tube positions falling into each class. The fuel concentration is listed as weight percent of oralloy oxide in the tube material.

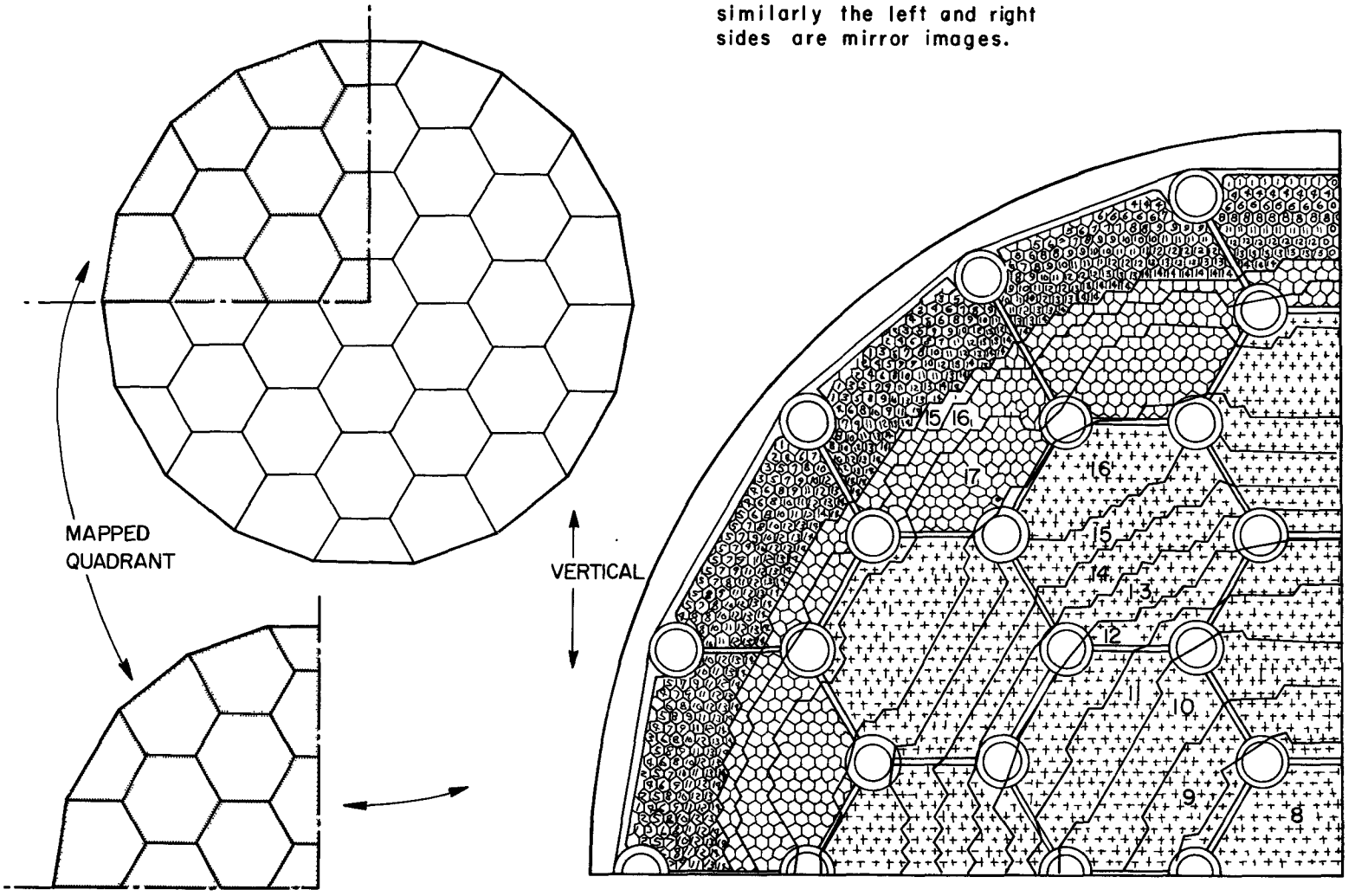

Fig. 3-5. Fuel loading distribution.

Table 3-1. Fuel tube loading distribution.

Loading class	% UO_2	Number of tube positions in class
1	4.70	60
2	4.93	40
3	5.28	40
4	5.41	102
5	5.68	120
6	5.95	128
7	6.25	124
8	6.52	423
9	6.87	480
10	7.16	624
11	7.49	604
12	7.88	702
13	8.27	548
14	8.70	714
15	9.12	1074
16	9.53	1492
17	10.00	1348
18*	0	72

* The elements of class 18 are unfueled and have no central hole.

Total fuel loading: 65.0 kg UO_2, containing 57.2 kg oralloy.

4. REFLECTOR, VEHICLE, AND AUXILIARIES

4.1 Reactor Components

4.1.1 Reflector and Control Elements

The position of the reflector on the reactor is indicated in Fig. 2-1 which shows the general arrangement of the test car. The structure of the reflector is shown in greater detail in Fig. 4-1.

Eight identical sections fit together to form an annular reflector, coaxial with the core and covering its full length. The reflector is assembled in two halves, splitting vertically along the reactor centerline. Each half is mounted on a carriage, movable on the car by a screw-jack mechanism, permitting separate removal of either reflector half or of the core-air duct section alone.

The reflector is composed of graphite having the following average properties:

Density	1.82 g/cm^3
Water absorption	2.2 wt %
Water tranmission at 40 psi, 3/4-in. -thick sample	0.01 $gal/min\ ft^2$
Thermal neutron macroscopic absorption cross section	$2.0 \times 10^{-3}\ cm^{-1}$

The cylindrical center sections of the eight reflector segments rotate on axes parallel to the core axis. These rotating cylinders ("vanes") are provided with 90° edge sectors containing boron-loaded stainless steel tubes. Rotation of the vanes moves the boron toward or away from the reactor core, giving large changes in reactivity for reactor control.

Additional control is provided by four sliding boron-steel rods placed symmetrically around the inner portion of the reflector. These rods move through a 40-inch stroke parallel to the reactor axis.

Each of the twelve control elements is moved by a separate hydraulic actuator, although normally the eight vanes are electrically ganged and move in unison.

Cooling water will be in direct contact with the reflector graphite, so that the graphite is expected to remain water-saturated at all times after initial filling of the cooling system. Loss of water by percolation through the graphite will be negligible, however.

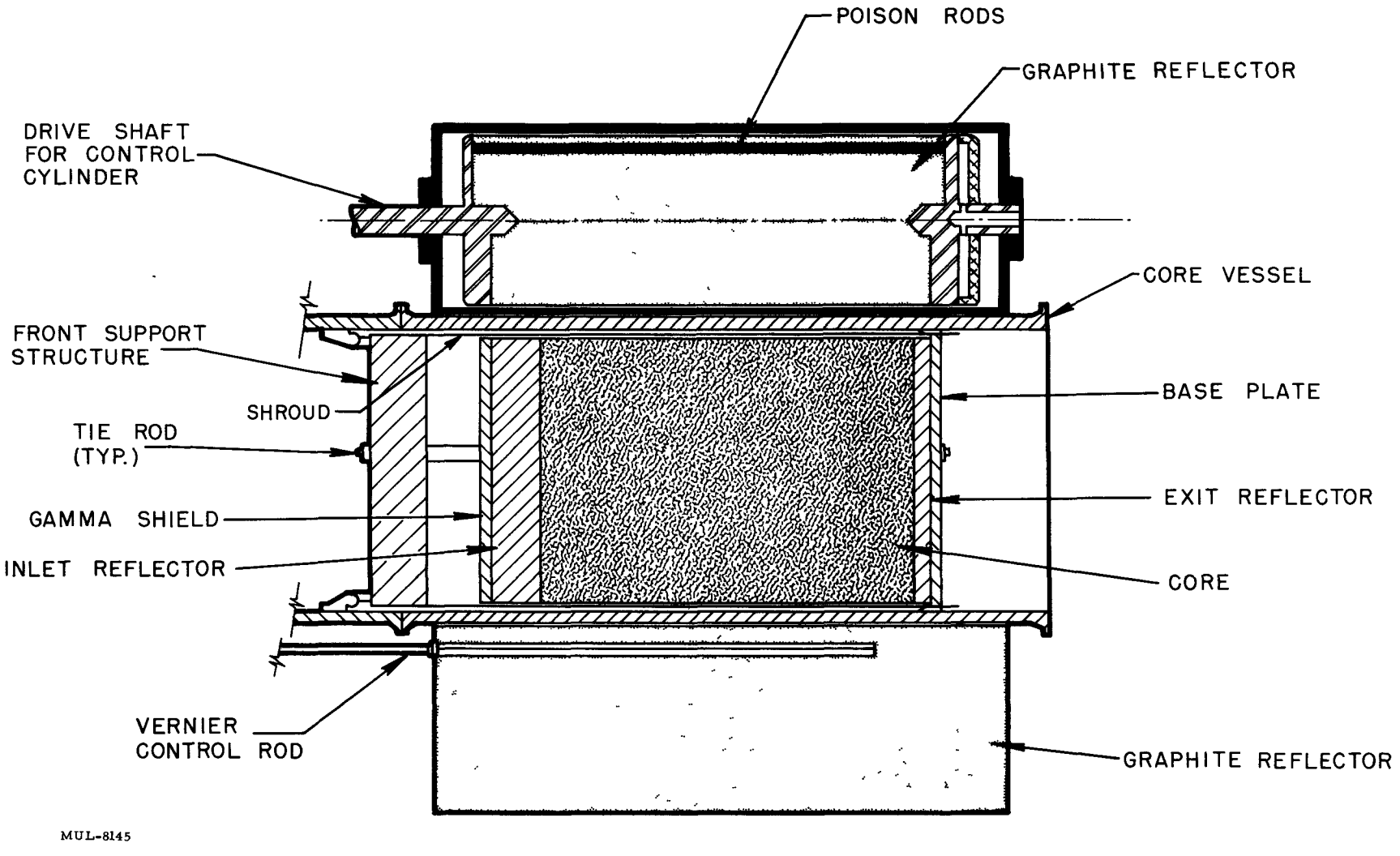

SECTION A–A

Fig. 4-1. Reactor cross section.

Total heat deposition in the reflector will be 3.8 Mw, of which 3.2 Mw will be deposited in the graphite, about 0.5 Mw in the vane poison tubes, and 0.1 Mw in the sliding control rods.

Heat transfer rates will be low, generally in the region of 100 to 400 watts per square inch. The peak heat load in the reflector will be about 100 watts per cubic inch. Peak temperature in the graphite will be held below 200°F.

The main cooling circuit for the reflector and control vanes will provide a flow of 800 gal/min with a temperature rise of 34°F. A separate circuit will provide 15 gal/min to each of the sliding rods, with a 19°F temperature rise.

Continuous circulation of this water will also provide protection against reflector damage through freezing of the wet graphite during reactor shutdown in cold weather.

4.1.2 Core Vessel

The core vessel (pressure shell), shown in Fig. 4-2, is that part of the air duct which contains the core. This vessel is mounted inside the reflector, but has no direct mechanical connection to the reflector. A gap of design thickness 1/4 inch at ambient temperature is maintained between these components, to allow thermal expansion of the core vessel and to isolate the reflector and control assembly from possible vibrations generated in the air duct system.

The pressure vessel will be fabricated of 6061-T6 aluminum, with a total weight of 600 pounds. It is designed for an operating pressure of 225 psi with a metal temperature of 250°F. It is expected that a stress safety factor of 2.5 will be realized in the design.

A cooling water flow of 300 gal/min removes the total heat load of 2.0 Mw, largely produced by neutron and gamma radiation. Thermal radiation and heat conduction from the air within the shell contribute only about 0.02 Mw.

4.2 Air Duct Sections

Structure of the inlet and exit duct sections may be seen in Fig. 4-2.

The inlet (diffuser) section is basically a convergent-divergent nozzle designed to deliver Mach 0.1 air to the core with a reasonably flat velocity profile. An aerodynamic grid (with 25% open area) is incorporated into the diffuser cone to ensure that no separation of air flow from the diffuser wall will occur (see Section 5.3).

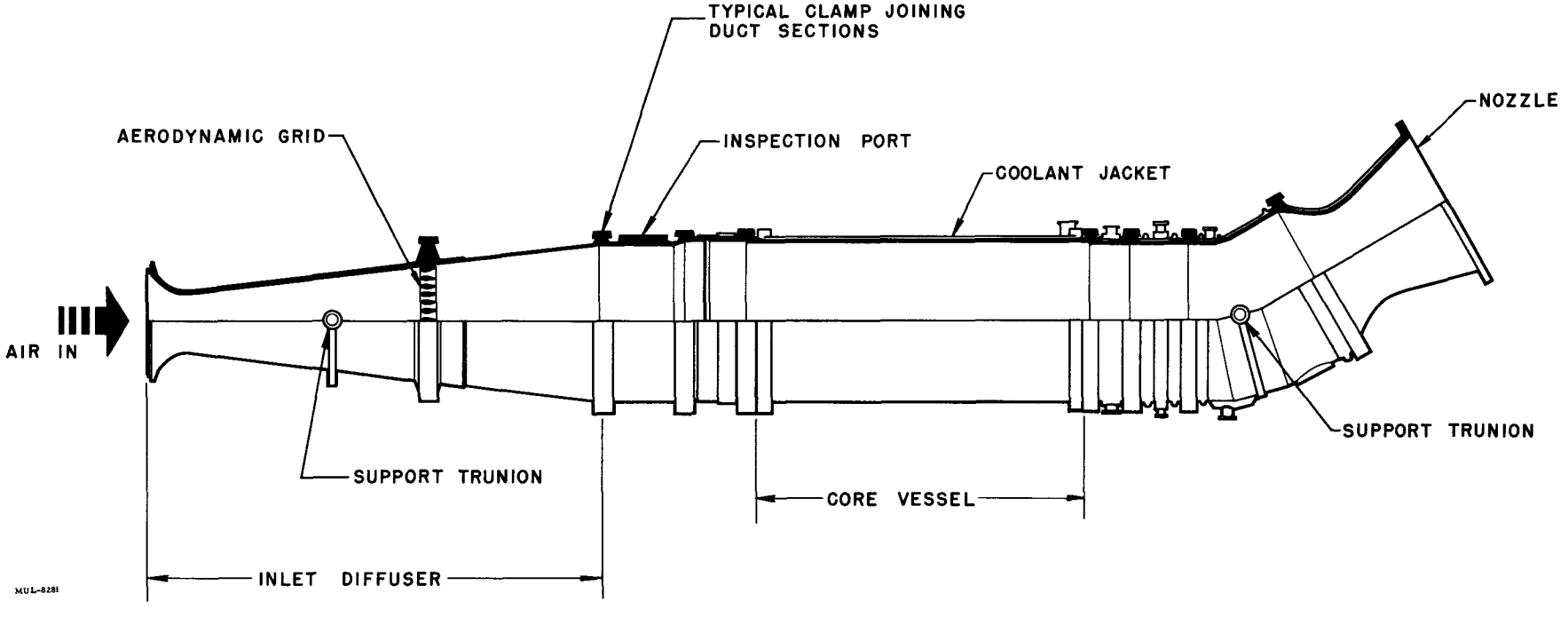

Fig. 4-2. Air duct.

The exit nozzle function of converting internal energy to directed velocity in the emergent air stream will not be needed for thrust development on Tory II-A; however, a high velocity exhaust stream is of value in carrying radioactive material entrapped in the exhaust away from the immediate area of the reactor. For this reason, a divergent exit section is used, together with a turning section in the exit duct which raises the exhaust stream to an angle of 30° above the horizontal. Aside from fulfilling this function, a choked exit nozzle is needed to produce ramjet engine-like conditions of air flow in the reactor. Specifically, by raising the reactor exit stagnation pressure to a uniform value over the rear face of the reactor, the nozzle assists greatly in providing uniform air flow throughout the reactor core.

It should be noted that the exhaust turning section is provided with a port for a television camera, to provide a view of the exit end of the core during runs.

A removable plate on the inlet section provides inspection access to the core support structure.

The entire air duct is supported on mounts forward and aft of the reactor, as shown in the overall car view, Fig. 2-1. The rear mount is fixed to the car, while the forward mount is free to slide with thermal expansion.

4.3 Cooling Water System

The cooling system is designed to accomplish two jobs. It will handle a high heat rate for short periods and low heat rates for long periods. These have been estimated, respectively, at 15 Mw for 90 seconds and 1.5 Mw continuously. The higher heat rates are handled by utilizing a pumping capability of 2000 gpm at 90 psig and the thermal capacity of a 50,000-gal storage tank. For the lower power runs, water coolers are used to keep temperatures down. Tanks, valves, and pumps are arranged so that the water system can accommodate any sequence of operation within the air supply capability.

The cooling water is brought to and from the test vehicle by 8-in. pipes which are coupled to the bunker. The flow is divided among several circuits on the car.

Valves and flowmeters are provided on the car so that the flow balance can be adjusted between runs.

Emergency cooling water is provided by a 20-psig, 500-gpm pump which is run from a separate power source and cuts in when pressure is lost on the normal system.

The water system also contains a deionizer to maintain a resistivity of 10^6 ohm cm.

In addition, a flow of 3 lb/sec of air will be taken from the bunker and directed over the test car. This serves to remove heat from components which do not require water cooling and also serves to reduce migration of dirt into the equipment.

4.4 Air Supply System

The air supply system is designed to deliver about 1000 pounds of air per second, with 350 psia pressure and 1100°F temperature at the reactor inlet face.

The possibility of providing a continuous high-capability air supply was investigated and found to be impractical under the existing budget and time schedule. It was decided instead to use a stored-air system which would permit runs of minimum useful duration. The system selected will store 120,000 lb of air at 3600 psia, permitting runs of about 100 seconds at full flow rate, with enough residual air for after-cooling. In addition, blowers will be provided for continuous air supply at low reactor power levels. The system also contains a heater, and valving and instrumentation sufficient to permit considerable versatility. Figure 4-3 is a schematic diagram of the air supply system.

The following rules were used as a basis for the air supply design.

1. Full-power runs shall be spaced at least 48 hours apart.
2. All equipment requiring frequent service and inspection shall be located either in a shielded position, or at least 500 feet away from the test point.
3. The system shall be operated, during runs, from a remote point (the control building is about 2 miles away).
4. Operation of the system during charging of the air tanks and stored energy heater shall be from the compressor house, about 2500 feet from the test point.
5. The temperature of air delivered to the reactor face shall be essentially stable for at least 20 seconds during a full power run.
6. Flow shall be calculable to 1% accuracy at any of six specified flow rates and shall be displayed in the control room within 5% accuracy over the entire range from 0 to full flow rate.

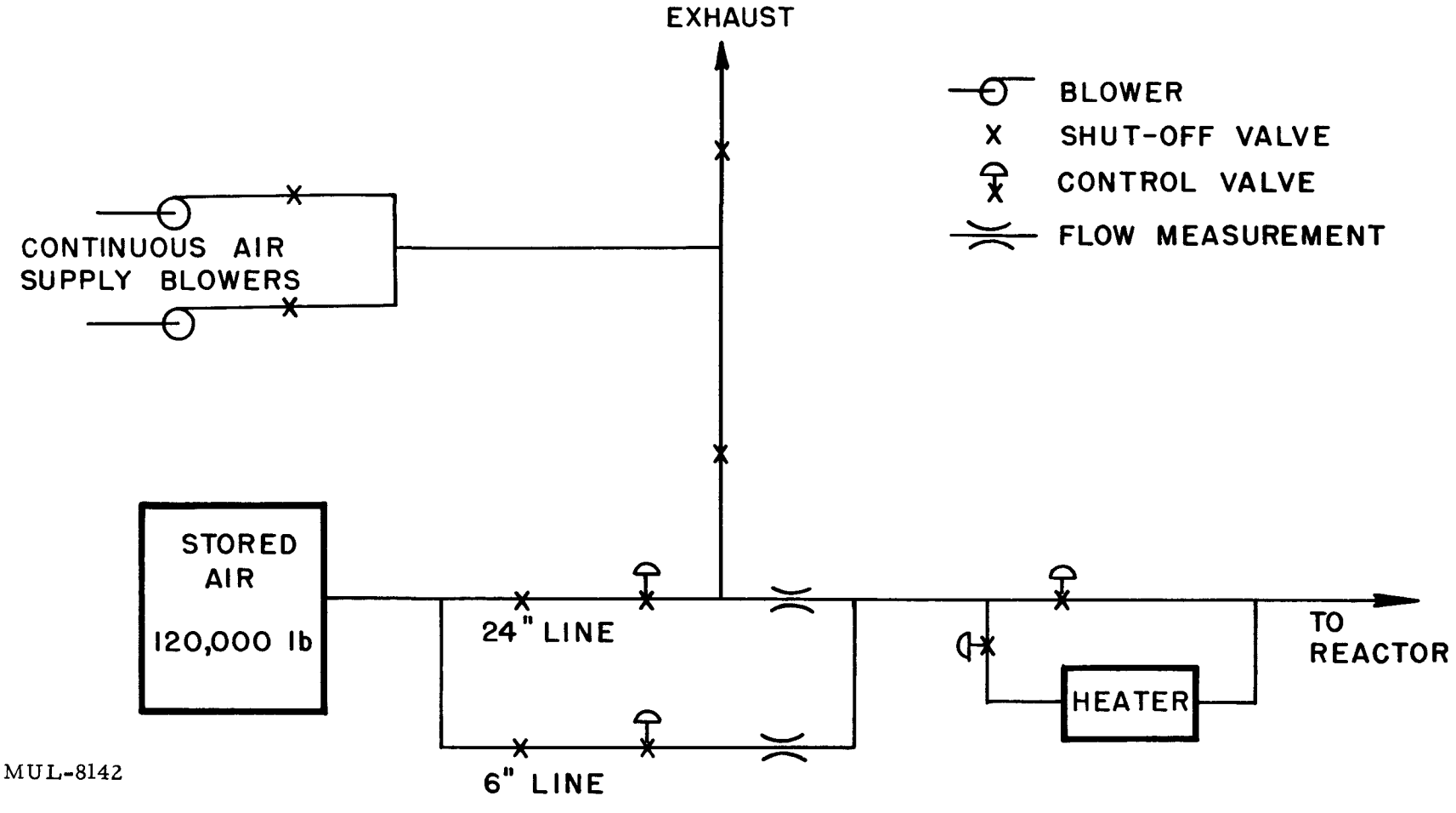

Fig. 4-3. Air supply system schematic.

7. 25 pounds per second of air at 5 psig pressure shall be available continuously for indefinite periods.

8. Automatic control shall be provided for the air supply.

Several parts of the air supply system warrant separate consideration:

Compressor

Two 450-hp compressors, each capable of delivering 1 lb of air per second at 4000 psi maximum pressure, are installed in the compressor house. Either compressor can charge the air tanks in 33 hours, and this time can be cut in half using both units together. The air is dried before storage, in order to prevent rust in the storage tanks, to a water content of 10^{-5} lb of water per lb of air. The air is filtered before it enters the compressors. The use of two compressors is intended to eliminate test cancellation because of failure of a single unit. The compressors will be shut down during a test run.

Heater

For bringing reactor inlet air to the required temperature, a stored-energy heater will be used. Before each run, air heated by an oil furnace will be circulated through an assembly of heavy steel plates by an auxiliary duct system. This steel heat storage unit, which has no direct contact with combustion products, will be brought to a temperature of 1200°F in a time of 80 hours starting at ambient temperature or 40 hours starting immediately after a run. During either a stored-air run or a run using air from the blowers, the test air supply can be directed partly through the steel heater plates and partly through a by-pass duct so that delivery air temperature can be controlled. The furnace and secondary heating loop are shut off during a test run.

Continuous Blowers

For continuous runs, two 400-hp blower units, delivering together 25 pounds of air per second at a pressure of 5 psig, are provided. These blowers pick up air from inside the test bunker, which in turn is supplied by filtered air from blowers in the tunnel head house. These latter blowers send their discharge down the tunnel toward the test bunker, maintaining a pressure slightly above atmospheric in the bunker.

Power limitations at the site make it necessary to phase the operation of some of the large electrical units. For example, it is possible to run either two blowers, or two compressors, or one blower and one compressor at the same time, but not two blowers and a compressor.

Piping and Valving

The entire system downstream from the main air control valves is designed for a pressure of 600 psi, except for those areas which are isolated for lower pressure operation, such as the blowers and the furnace area. Blow-off ports are provided to protect the system from over-pressure.

Basically the piping and valving system can be described as follows:

There are two lines which leave the inlet header. One has a 24-inch diameter and the other varies from 6 to 12 inches in diameter. The operator has the option of routing the air through either line. The first valve in each line is the shutoff valve. These valves operate through a complete cycle in 60 seconds and are located in a chamber outside the bunker area to reduce personnel hazards. The next valves are the main control valves (6 in. and 24 in.), used for actual flow control. These valves operate through a full cycle in 2 seconds and have essentially a linear response. Bleed valves are located between the shutoff and control valves to prevent pressure buildup due to leakage of the main valves.

Next in line are the venturi tubes used to measure air flow. The desire to measure flow to high accuracy over a wide range led to selection of the two-pipe system. Downstream, the main air pipes join and the air can then be valved through or around the heater to control temperature. Finally, the flow is again combined and directed to the reactor.

The continuous blower system supplies filtered but undried air at about 170°F and feeds into the 24-in. high-pressure line upstream from the flow-measuring venturi. The blower air flow will be measured at this venturi.

Piping is insulated where required to reduce heating in the bunker.

Flow Measurement

Flow will be determined by transducers selected to give maximum accuracy at six operating points with flow rates between 3 and 870 lb/sec. These are listed in Table 7-3. In addition, the data will be displayed as mass flow to 5% accuracy in the control room.

Automatic Control

The operator will have the option of automatic air control, providing pre-programmed air flow and utilizing feedback from the mass flow meter. The system is designed so that the operator can trim the air flow as required during the automatic program. This also permits operator control under emergency conditions.

Emergency Control

Two conditions must be avoided: first, loss of air flow, which would permit the reactor to overheat; and second, too much air, resulting in a destructive fast quench to the core.

The combination of shutoff and control valves will provide maximum safety under emergency conditions. It is planned that separate electrical power will be provided to the shutoff and control valves. In case of main power failure, regulation will be retained on the control valves. In the case of control valve failure, the inoperative valve will lock in place and the shutoff valves can be used to bring the reactor off the line in a period of minutes.

5. ANALYSIS

5.1 Reactor Dimensions

Dimensions and composition of the reactor are listed below, in a form useful for neutronic and aero-thermodynamic analysis. No attempt is made here to describe detailed mechanical design.

A. CORE

Moderator material			BeO
Equivalent circular radius			16.35 in.
Length			44.50 in.
Volume			21.62 ft^3
Total core frontal area			839.5 $in.^2$
Fractional Frontal Area Displacements:			
Fuel tube BeO		0.397	
Structural BeO		0.111	
Total BeO		0.508	
Tension tubes with cooling passages		0.051	
Propellant flow		0.379	
Incidental void		0.062	
		1.000	
Fuel tubes (with holes)		0.802	
Number of fuel tubes			8635
Fuel element average (dimensional) porosity			0.488
BeO density			2.9 g/cm^3
Mass of BeO in core			1990 lb
Heat transfer passage diameter			0.214-0.219 in.
Fuel element outside flat to flat dimension			0.294-0.296 in.
Fuel element wall thickness			0.039 in.
U^{235} mass			71 kg
Fuel elements: Atom ratio, moderator/fuel			103.7-187.0;
Average			113.7
Fuel mass/fuel element mass			0.0605-0.1040;
Average			0.0916

B. SHROUD AND AIR SEAL REGION

Material	Hastelloy
Equivalent thickness of material at full density (ρ = 8.22)	0.085 in.

Equivalent inside radius of seal region	16.350 in.
Equivalent outside radius of seal region	17.050 in.
Equivalent outside radius of shroud region	17.375 in.
Outside radius of gap between shroud and core vessel	17.875 in.
Maximum material temperature	1200°F
Length	66 in.
Mass	220 lb

The above table assumes the following:

1) 0.010 in. of wiper seal included in seal region;

2) 0.250 in. cooling air passage in shroud.

C. CORE VESSEL

Material	Aluminum, type 6061-T6
Thickness of structural shell	0.515 in.
Equivalent thickness of cooling jacket	0.140 in.
Cooling jacket water gap	0.125 in.
Inside radius	17.875 in.
Maximum temperature	200-250°F
Thickness of air gap between pressure vessel and reflector	0.235 in.

D. SIDE REFLECTOR (including control cylinders, less support sturcture)

Material	Graphite
Thickness	22.6 in.
Outside radius	41.5 in.
Inside radius	18.875 in.
Length (overall)	65.5 in.
Cross-sectional non-graphite fraction	0.0608 total
Water	0.0294
Air gaps	0.0025
Aluminum	0.0077
Absorber (boron steel)	0.0143
Vernier rod region	0.0069
Material density:	
Graphite	1.85 g/cm^3
Absorber	7.90 g/cm^3

Weight (approximate total)	18,800 lb
Maximum temperature	200°F
Cooling	Water

E. END REFLECTORS

Material and structure identical with core, but without fuel.

Inlet reflector thickness	6 in.
Exit reflector thickness	2 in.

F. METALLIC END PLATES

1. Inlet gamma shield:

Material	0.95 W, 0.033 Ni, 0.017 Cu
Thickness	1.5 in.
Density	18.0 g/cm^3

2. Exit base plate:

Material	0.995 Mo, 0.005 Ti
Thickness	1.0 in.

Porosity and hole sizes identical with core.

5.2 Neutronics

5.2.1 Calculational Methods

Analysis of the neutronic characteristics of the reactor depends largely on the use of high-speed digital computers. Input parameters, such as cross sections and transfer coefficients, are taken from the best available experimental and theoretical data on characteristics of the nuclei involved. As a check on the validity of the results, a large number of simple experimental critical assemblies have been run, together with corresponding calculations. Correspondence between actual and calculated results has been quite good, and efforts are continuing to improve it further.

Two computing machine codes are in use for neutron diffusion calculations. The most frequently used of these, called Zoom,[3] is a one-space-dimension code, handling spherical, cylindrical, or slab geometry with up to thirty space zones. As many as eighteen energy groups may be used, with transfer from any group to any other group.

The second code, Angie,[4] describes two space dimensions and up to eighteen energy groups. The version in use here permits a choice of any three kinds of transfer from a group to the three groups immediately above and the three immediately below it (e.g., up one, down one, down two; or down one, down two, down three; etc.).

Angie can describe either slab or cylindrical geometry, with space zones arranged in a 40 × 50 rectangular array. The cylinder normally described is strictly two-dimensional, with no azimuthal variations; thus it cannot take account of the control absorber elements in the Tory II-A reflector in a realistic way. However, it is possible to describe an end-on view of the reactor with Angie's slab mode, and introduce an artificial absorption cross section throughout the reactor to represent endwise leakage (axial buckling). Control element effects have been studied in this way.

Reactor configurations actually treated by the codes are limited to those that can be outlined on the rectangular array of space zones described by each code. Thus, any curved boundaries must be represented approximately by a series of straight-line segments. Region boundaries are chosen to preserve actual material quantities and approximate locations.

Since the number of available space zones is limited, no attempt is made in coded problems to represent fine goemetrical details of the reactor. Instead, a number of different materials, existing side by side in layers in the real reactor, are generally lumped together into single zones specified as containing a mixture of materials. Here again, care is taken to ensure that the total amount of each component material is conserved, and that it is placed in approximately its correct position.

Void spaces cannot be handled as such by the codes, so they are represented by wider bands of material of lowered density, giving an equivalent local void fraction. An additional hand-calculated correction is applied to the reactivity to provide for neutron loss by direct streaming from large voids.

To take advantage of the symmetry properties of the two-dimensional codes, the four reflector quadrants are represented as mirror images, which is realistic when the eight main control elements are turned full in or full out, and leads only to a slight error when the controls are in an intermediate position.

Figure 5-1 shows a typical reactor end view as seen by a code.

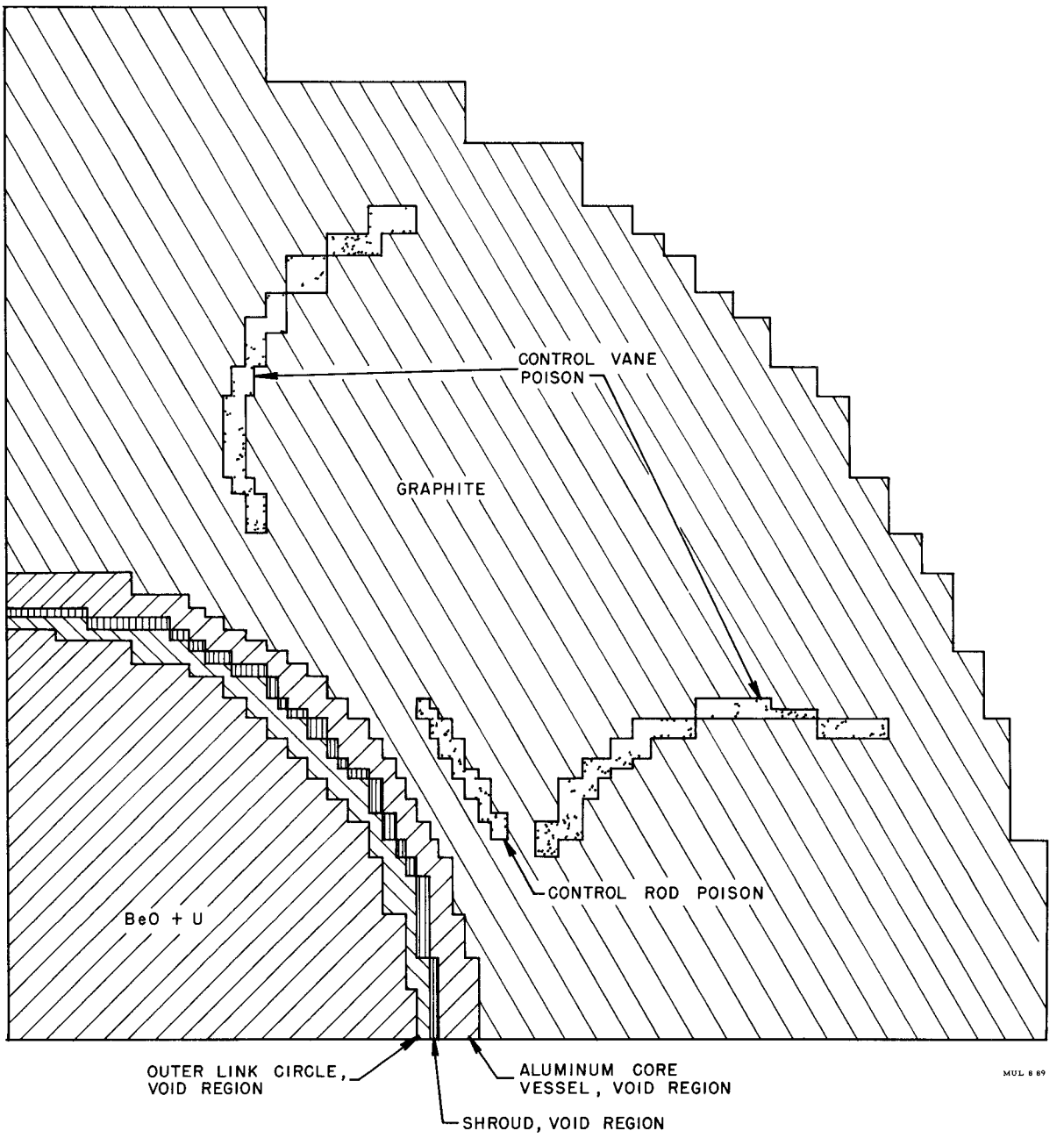

Fig. 5-1. Reactor cross section as described by neutronics code.

Configuration and material concentrations are specified as inputs to the codes; k_{eff} and neutron flux distributions are received as output.

To obtain the most reliable results, eighteen energy groups are used. But since the running time for a problem, and hence the number of problems that can be run, depends very strongly on the number of energy groups used, it is desirable to cut down this number whenever possible. Sets of four-group constants and ten-group constants have been compiled and used for many problems. The general principle followed is to calculate reactivity and flux distributions for a particular configuration with eighteen-group constants, and then to determine the effects of slight perturbations in geometry or material concentrations using fewer groups.

Cross Sections

The average cross section σ_i for the ith energy group is defined as

$$\sigma_i = \frac{\int_{E_{i-1}}^{E_i} \sigma(E)\, \phi(E)\, dE}{\int_{E_{i-1}}^{E_i} \phi(E)\, dE} ,$$

where $\sigma(E)$ and $\phi(E)$ are the cross section and the neutron flux as functions of energy, and E_{i-1} and E_i are the lower and upper energy bounds of the ith group. This necessarily assumes that the neutron flux distribution $\phi(E)$ is known, whereas generally it is not known. Initial sets of average cross sections have been computed on the basis of reasonable assumptions for flux distribution, and then used to calculate flux distributions which in turn can be used to improve the cross-section values.

The handling of two particular types of cross section may be noted:

1. Transport Cross Section

To take into consideration the effects of absorption and anisotropic scattering, the transport cross section has been calculated from the relationship*

* Derived similarly to an expression given in Glasstone and Edlund, The Elements of Nuclear Reactor Theory, 1954 edition, p. 396. We believe their equation 14.35.3 to be in error.

$$\sigma_{tr} = \frac{K^2}{3_a\sigma} ,$$

where K is determined by the expression

$$\frac{{}_s\sigma}{2K} \ln \frac{\sigma+K}{\sigma-K} = \frac{1 + (3_a\sigma_s\sigma\ \bar{\mu}_0)/K^2}{1 + (3_a\sigma\ \sigma\ \bar{\mu}_0)/K^2} ,$$

and σ, ${}_s\sigma$, and ${}_a\sigma$ are, respectively, the total, scattering, and absorption cross sections and $\bar{\mu}_0$ is the average of the cosine of the scattering angle in the laboratory system.

2. (n, 2n) Cross Sections

To describe properly the (n, 2n) reaction process, the absorption cross section entering the calculations (not that used to calculate σ_{tr} above) has been taken as equal to the (n, γ) reaction cross section minus the (n, 2n) reaction cross section. This allows it to be a cross section for the production of a new neutron, while still conserving the original neutron. In addition, a positive cross section twice as large as the (n, 2n) cross section has been added to the scattering cross section to allow both neutrons resulting from the (n, 2n) reaction to be downgraded in energy. The transfer coefficients have also been adjusted to describe the interaction, as will be seen below.

Fission Spectrum

Only one fission spectrum can be used in the eighteen group codes for which these numbers were devised. Therefore, the U^{235} fission spectrum has been integrated for each group and any U^{238} fissions are of necessity assumed to yield a U^{235} fission spectrum properly normalized to the higher incident neutron energy. For U^{238} concentrations equal to that in oralloy, this assumption introduces an error in the multiplication factor of less than 10^{-5} for thermal reactors. The fission spectrum was normalized to give a value of the average number of neutrons per thermal fission, $\bar{\nu}_{th}$, equal to 2.486. This corresponds to 2.47 ± 0.03 prompt neutrons and 0.0158 ± 0.0005 delayed neutrons per thermal fission, given in Reactor Physics Constants, ANL-5800, as the "best" values.

Transfer Coefficients

The energy transfer coefficients have been calculated with the same assumptions for neutron flux energy distribution as were used in the cross

section calculations. In addition, they have been corrected for anisotropic scattering and (in the case of beryllium) for energy losses due to the (n, 2n) reaction:

1. Anisotropic Scattering

The anisotropic scattering correction is a reduction of the transfer coefficient by the ratio of the actual average logarithmic energy decrement to that calculated for isotropic scattering. The actual average decrement was computed from data on angular scattering distributions.[5]

2. (n, 2n) Reaction

In beryllium a further correction has been made to account for the energy losses in the (n, 2n) reaction. Rosen and Stewart[6] have measured the combined energy spectrum of the two neutrons resulting from (n, 2n) reactions in beryllium produced by incident 14-Mev neutrons. Assuming the same general shape of the spectrum to hold for lower incident neutron energies, (n, 2n) reaction transfer coefficients were calculated. These were combined with the anisotropic scattering transfer coefficients to give a group transfer coefficient defined by

$$\mu_i^j = \frac{{}_s\mu_{i\,s}^j\sigma^j + 2\,{}_{n,\,2n}\mu_{i\;n,\,2n}^j\sigma^j}{{}_s\sigma^j + 2\,{}_{n,\,2n}\sigma^j} \quad ,$$

where μ_i^j is the transfer coefficient for transition from the jth to the ith energy group.

Values in Current Use

These numbers are not yet wholly satisfactory, and improvements are continuously being made. Among corrections now under study are the effect of crystal and molecular binding on scattering in the thermal groups, and improved treatment of uranium absorption in the resonance region.

As an example of neutronic parameters currently in use and giving good agreement with experimental critical assemblies, values applying to the most important reactor materials are given in Tables 5-1 through 5-5. The quantities f_i, not previously defined, describe the fission spectrum, determining the distribution of fission neutrons among the groups i. All values refer to materials at normal room temperature. Table 5-1 also lists the values of E_i.

Table 5-1. Group energies and neutronic parameters for U^{235}

i	$F\sigma$	$a\sigma$	$tr\sigma$	$s\sigma$	f_i	μ^i_{i-1}	μ^i_{i+1}	E_i
18	1.255	0.060	2.299	6.222	0.4665	0.00160	0	10.0 Mev
17	1.275	0.096	3.304	5.734	1.2510	0.00316		3.3
16	1.206	0.179	4.567	6.001	0.5919	0.00473		1.00
15	1.480	0.315	7.956	8.814	0.1437	0.00604		333 kev
14	2.34	0.584	10.7	10.08	0.0265	0.00729		100
13	3.26	1.06	11.0	10.16	0.0052			33
12	3.99	1.68	12.0	10.83	0.0010			10.0
11	5.9	2.83	14.3	12.27	0.0002			3.3
10	10.5	5.25	17.2	13.4	0			1.00
9	18.8	9.24	21.0	14.0				333 ev
8	39.4	17.8	29.2	14.0				100
7	48.9	19.9	33.1	14.0				33
6	44.7	13.3	29.4	13.8				10.0
5	28.5	6.7	22.3	13.2				3.3
4	82.9	17.0	42.7	12.5				1.00
3	191	42.4	85.1	11.0				0.33
2	337	62.3	139.8	9.5		0.03637		0.10
1	660	119	264.5	8.2		———	0.05462	0.033

Table 5-2. Neutronic parameters for U^{238}

i	F^{σ}	a^{σ}	tr^{σ}	s^{σ}	f_i	μ^i_{i-1}	μ^i_{i+1}
18	0.65	0.02	1.99	7.0		0.00160	0
17	0.35	0.06	3.15	6.6		0.00316	
16	0	0.15	5.62	8.5		0.00473	
15		0.22	9.20	11		0.00604	
14		0.4	13	13		0.00729	
13		0.6	14	14			
12		0.8	14	14	Use		
11		0.8	14	14	same		
10		1.7	14.3	14	fission		
9		15.44	15.6	12	spectrum		
8		49.626	23.9	10	as		
7		54.72	25.2		U^{235}		
6		117.18	45.8				
5		1.7	10.3				
4		2.3	10.5				
3		2.2	10.4				
2		2.5	10.5			0.03637	
1		2.75	10.6			———	0.05462

Table 5-3. Neutronic parameters for beryllium

i	σ_a	σ_{tr}	σ_s	μ^i_{i-1}	μ^i_{i-2}	μ^i_{i+1}
18	-0.474	1.165	2.593	0.2994	0.2429	0
17	-0.002	1.928	2.427	0.1384	0	
16	0	3.646	3.938	0.1643		
15		4.510	4.871	0.1643		
14		5.46	5.90	0.1682		
13		5.56	6.00			
12						
11						
10						
9						
8						
7						
6	0.001					
5	0.001					
4	0.002					
3	0.004	5.56				
2	0.007	5.57	6.00	0.1778		
1	0.013	5.567	6.011	——		0.2700

Table 5-4. Neutronic parameters for oxygen

i	σ_a	σ_{tr}	σ_s	μ^i_{i-1}	μ^i_{i+1}
18	0.01	0.67	1.45	0.0417	0
17	0	1.68	2.30	0.0750	
16		4.51	5.01	0.0938	
15		3.46	3.64	0.0990	
14		3.35	3.50	0.0999	
13		3.35	3.50		
12		3.35	3.50		
11		3.40	3.55		
10		3.55	3.70		
9		3.62	3.78		
8					
7					
6					
5					
4					
3					
2		3.77	3.93	0.1356	
1		4.03	4.20	——	0.2060

Table 5-5. Neutronic parameters for carbon

i	σ_a	σ_{tr}	σ_s	μ^i_{i-1}	μ^i_{i+1}	σ_a*
18	0	1.29	1.49	0.2645	0	0
17		1.97	2.09	0.1548		
16		3.07	3.25	0.1272		
15		3.95	4.18	0.1284		
14		4.25	4.50	0.1317		
13		4.34	4.60			
12		4.39	4.65			
11						
10						0.0001
9						0.0002
8						0.0003
7						0.0005
6						0.0009
5	0.001	4.39	4.65			0.0016
4	0.001	4.44	4.70			0.0028
3	0.002	4.49	4.75			0.0049
2	0.003	4.53	4.80	0.1556		0.0088
1	0.005	4.34	4.60	——	0.2363	0.0169

* Absorption cross section for carbon contains 13 parts per million boron impurity.

5.2.2 Critical Assemblies

Many critical assembly experiments have been made at Livermore to test the validity of results from the multigroup calculations. These assemblies have been kept as simple as possible in order to permit direct comparison with calculated results — that is, no geometries have been used which cannot exactly be described by the neutronic codes. Small corrections were made for the presence of control-vane slots, supporting structure, and inhomogeneity of fuel loading.

A number of assemblies were designed to provide experimental data over a fairly wide range of fuel loading densities and degrees of reflection, as tests of the general validity of the calculations. Others were designed to have a close neutronic resemblance to Tory II-A, either in part or as a whole.

Table 5-6 lists some graphite-moderated assemblies, unreflected and reflected by graphite or beryllium. The reflected assemblies had geometries shown in the following sketches, with critical height H_c measured as shown:

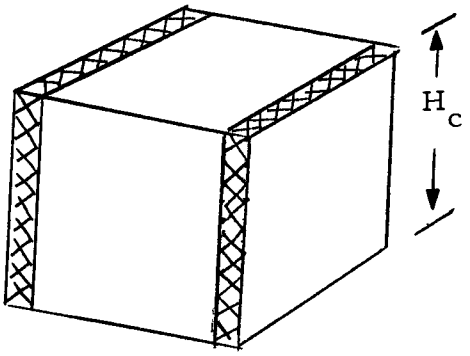

Two sides reflected

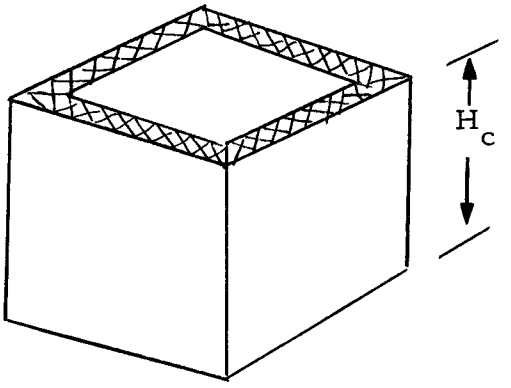

Four sides reflected

The calculated value of k_{eff} is given in the table for each assembly, showing the degree of success of the calculation. The true value of k_{eff} for each assembly is of course exactly 1.0.

Table 5-7 presents a list of unreflected and reflected BeO — moderated critical assemblies which have been run, again with a calculated value of

Table 5-6. Graphite critical assemblies.

Expt. No.	Mole ratio, C/U^{235}	Core base size, inches	Critical height, inches	Reflector thickness	Calculated k_{eff}
1	301	42.50 × 42.50	44.4	None	1.034
2	603	48.50 × 48.50	37.6	None	1.027
3	1,206	48.50 × 48.50	40.3	None	1.023
4	2,355	48.50 × 48.50	44.7	None	1.009
5	10,500	60.50 × 60.50	51.2	None	0.993
6	1,210	48.50 × 36.50	40.7	6.0 in. C on two sides	1.006
7	1,210	36.50 × 36.50	41.3	6.0 in. C on four sides	0.995
8	2,360	48.50 × 36.50	45.1	3.0 in. Be on two sides	0.993
9	2,360	48.50 × 36.50	38.4	6.0 in. Be on two sides	0.994
10	2,360	36.50 × 36.50	34.5	6.0 in. Be on four sides	0.989

Notes:

1. Assembly base is square in all cases except No. 8, where base is 48.5 × 42.5 in.
2. Graphite density is 1.64 g/cm^3, beryllium density is 1.84 g/cm^3.
3. The fuel used is 93% U^{235} and 7% U^{238}.

Table 5-7. BeO critical assemblies

Expt. No.	Mole ratio[a] BeO/U^{235}	Core base[b] size, inches	Critical height, inches	Graphite[b] reflector thickness	Extra material			Calculated k_{eff}
					Composition	Density, g/cm^3	Thickness, inch	
1	245	24×24	20.4	None	None			1.003
2	490	24×24	21.8	None	None			1.002
3	982	24×24	24.2	None	None			0.999
4	1860	24×24	31.0	None	None			1.013
5	3800	36×36	21.3	None	None			0.996
6	243	24×18.1	24.0	8.5	None			0.991
7	246	24×24	14.2	18	None			1.002
8	246	24×24	14.3	12	None			0.999
9	246	24×24	15.8	6	None			1.002
10	490	24×19.4	24.0	6	None			1.002
11	246	24×24	14.2	6	C_nH_{2n}	0.94	0.25	0.991
12	246	24×24	14.7	12	Aluminum	2.70	0.25	0.996
13	246	24×24	15.5	12	Aluminum	2.70	0.75	0.995
14	246	24×24	17.2	12	Cadmium	8.64	0.032	1.012
15	246	24×24	18.8	12	Boral: 82.5% Al, 17.5% B	2.53	0.25	1.003
16	246	24×24	15.2	12	Boral: 82.5% Al, 17.5% B	2.53	0.25[c]	1.007

Notes:

[a] The fuel is oralloy, 93% U^{235} and 7% U^{238}.

[b] BeO density is 2.84 g/cm^3, graphite 1.70 g/cm^3.

[c] In assembly No. 16, the boral sheets were placed inside the reflectors, removed by 6 inches from the fueled core.

k_{eff} for each. Here the reflectors were always graphite, and in some cases thin layers of other materials were placed between the core and reflectors. The reflected assemblies were arranged thus:

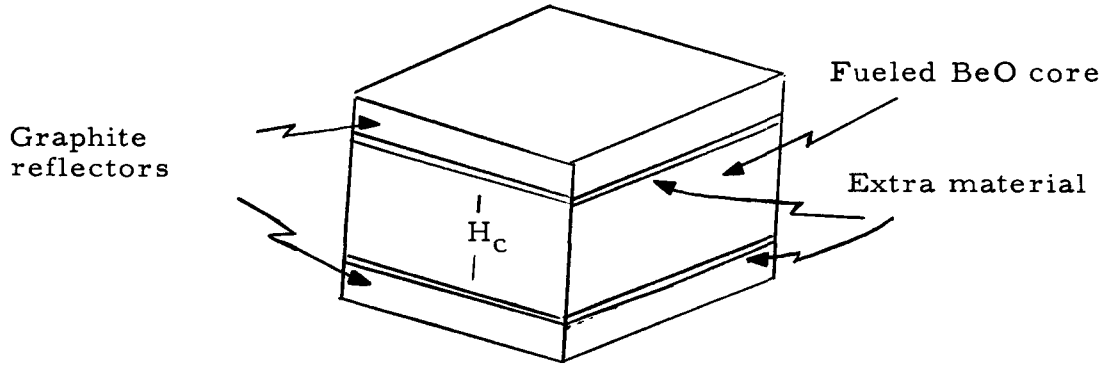

Reflected BeO assemblies of Table 5-7

Some further BeO critical assemblies were run with reflectors on four sides, and with various materials placed between the core and reflectors, or inside the reflectors. The structure of these assemblies is shown in Fig. 5-2, with calculated values of k_{eff} indicated for each.

The assemblies of this latter group are intended more specifically than the others to test the ability of the calculations to handle neutronic systems similar to Tory II-A. In addition to the calculation of overall reactivity, the treatment of differential effects due to addition of structural materials is tested.

This series of room temperature critical experiments is being continued. In addition, the effect of elevated temperature on reactivity is being investigated with a series of experiments conducted in a large oven. This experimental critical facility, called Hot Box,* is located at the Nevada Test Site (see Section 8).

Inspection of the listed values of calculated k_{eff} shows general agreement, within 1%, with the true value in all cases except for the heavily fueled bare graphite assemblies. The changes made from one assembly to another within the series correspond to changes in k_{eff} considerably greater than 1%, as may be demonstrated by noting the variations in critical height and bearing

---

* Hot Box, an elevated-temperature critical facility, is described by H. L. Reynolds and C. E. Walter in report UCRL-5483 (see ref. 22).

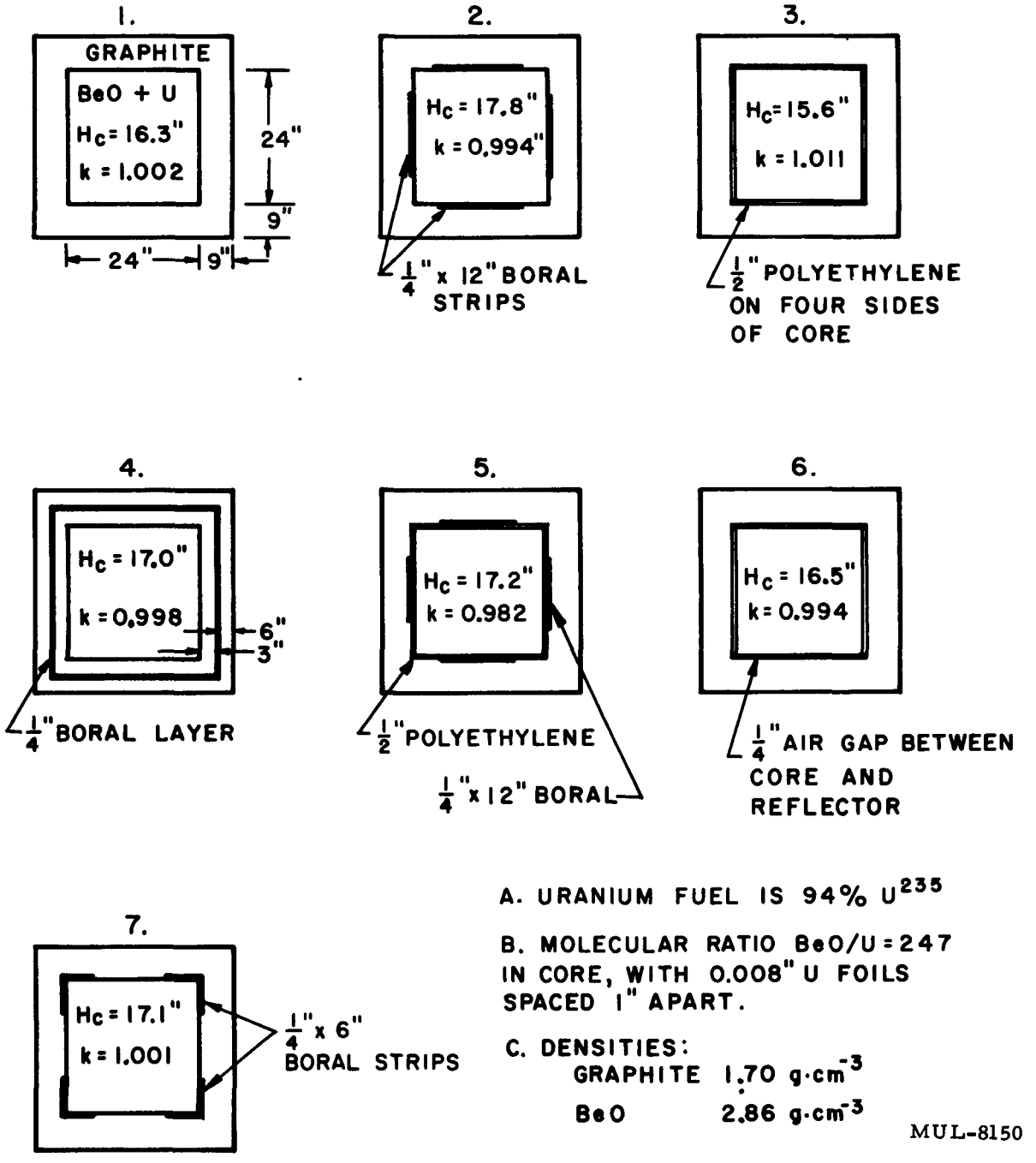

Fig. 5-2. Reflected BeO critical assemblies (plan views).

in mind that 1 inch in critical height is worth about 1% Δk_{eff} for the graphite assemblies, about 2% for the BeO assemblies of Table 5-7, and about 4-1/2% for the BeO assemblies of Fig. 5-2.

It is felt that these results indicate a capability of calculating the reactivity of structures similar to the Tory II-A reactor with an accuracy of about 0.01 absolute. Since (see Section 3) the reactor core length will be adjustable to a degree sufficient to provide a reactivity adjustment of ± 0.025 after the core has been assembled and tested for criticality, and since a large surplus reactivity swing is available in the control vanes, this state of the calculational art should prove satisfactory. The possibility that this good agreement is fortuitous is not overlooked, however, particularly in view of the anomalous bare graphite results. Consequently an intensive critical measurements program is being continued, concurrently with the study of improved calculational methods.

The description of the critical experiments given above has necessarily sacrificed completeness for the sake of brevity. Detailed descriptions of the graphite experiments have been published elsewhere.[7]

5.2.3 Reactor Characteristics

The neutronic characteristics of Tory II-A are presented in the following sections. A description of properties pertaining to the standard reactor design is given first; this is followed by a list of the effects of various changes in dimension or composition which might come about through design changes or through alterations caused by operation of the reactor.

Prompt Lifetime

The prompt lifetime is a quantity equal to the average lifetime, since birth, of those neutrons just undergoing capture in fuel nuclei. If all neutrons in the reactor came from prompt emission in the fission process, the prompt lifetime would be identical with the average generation time of neutrons, and would determine the rate of growth or decay of neutron population, for a given multiplication factor, according to the formulas

$$T = \frac{\ell}{k_{ex}} \quad \text{and} \quad n = n_0 e^{t/T} ,$$

where n = the neutron flux density,

n_0 = a constant,

$k_{ex} = k_{eff} - 1$ the excess multiplication factor,

ℓ = the prompt lifetime.

Since ℓ is to be used in the analysis of reactor kinetics, it was thought best to determine it through the relations given above rather than through direct averaging of neutron lifetimes. Accordingly, an eighteen-group calculation was set up on Zoom to represent the reactor (with no delayed neutrons) in a state of exponentially increasing neutron flux. This was done by introduction of an artificial absorption cross section (macroscopic)

$$a\Sigma_i = \frac{1}{v_i T}$$

into each of the groups i = 1, . . . 18, where v_i is the neutron velocity in group i, and T is an arbitrary time selected more or less at random: say 1 second. The reactor configuration was adjusted to give $k_{eff} \cong 1$. Next, the absorption cross section was removed, and the resulting increase in multiplication factor, Δk_{eff}, was noted. The prompt lifetime was then obtained from the relation

$$\ell = T\, \Delta k_{eff} .$$

Values obtained at ambient temperature and at maximum average core temperature were

$$\ell = 4.8 \times 10^{-5} \text{ at } 300\,^{\circ}\text{K}, \text{ and } 4.5 \times 10^{-5} \text{ at } 1350\,^{\circ}\text{K}.$$

Temperature Coefficient of Reactivity

The reactivity ρ (equal to $k_{eff} - 1/k_{eff}$) changes with core temperature because of thermal expansion of the core, change of effective cross sections with neutron temperature, and change of cooling air density in the core. The latter effect depends on power level and air flow rate as well as core temperature, and so cannot be stated as a simple number. Information on the reactivity contribution of air in the core is given separately later in this section.

Reactivity has been computed for a number of different core temperatures (assuming constant temperature throughout the core) and control-element positions, completely neglecting the effect of air in the core. Detailed results are given later, in Fig. 5-19; they show that the rate of change of reactivity with temperature varies only slightly for different reactor conditions and has an average value of

$$\frac{\partial \rho}{\partial T} = 1.9 \times 10^{-5}\ ^{\circ}\text{K}^{-1} .$$

Neutron Economy

A knowledge of the ultimate fate of the neutrons produced in the reactor is important in understanding its operation and the effect of various changes in geometry or composition. An audit is given in Table 5-8, showing the number of neutrons, per fission event, going into each of the main classes of neutron use or loss. End leakage neutron energies have been separated into fast and slow groups with a boundary at 10 kev, corresponding to the neutron energy below which 95% of fission reactions take place. This table refers to the hot, critical reactor.

Table 5-8. Reactor neutron economy

Neutrons per fission		
To new fissions		1.00
Radiative capture in core	0.32	
in shroud	0.08	
in core vessel	0.05	
in reflector	0.17	
in single, half-inserted vernier control rod	0.02	
in eight control vanes	0.49	
Total radiative capture		1.13
Reflector side leakage	0.04	
Fast neutron leakage from		
front of core	0.01	
rear of core	0.05	
front of reflector	0.02	
rear of reflector	0.06	
Slow neutron leakage from		
front of core	0.01	
rear of core	0.05	
front of reflector	0.03	
rear of reflector	0.08	
Total leakage		0.35
Total neutrons per fission:		2.48

Delayed Neutron Value

The relation between reactivity and reactor period is usually given in terms of the well-known inhour formula,

$$\rho = \frac{\ell}{Tk_{eff}} + \sum_i \frac{\gamma_i \beta_i}{1 + \lambda_i T} ,$$

where λ_i and β_i are the decay constant and fractional yield of neutrons in the ith group, respectively. The fractional yields used in this formula are multiplied by correction factors γ_i to account for the fact that delayed neutrons are more effective than prompt neutrons, being born at lower energies and thus subject to smaller leakage probability. The correction factor γ_i for a particular delayed neutron group, in the Tory II-A reactor, is readily computed as the ratio in k_{eff} brought about in a multigroup calculation by causing all the neutrons to be born at the delayed group mean energy E_i rather than in the usual fission spectrum. The following table gives values of γ_i calculated in this way for U^{235}, together with other parameters taken from a recent compilation of the Reactor Physics Constants Center at the Argonne National Laboratory.[8]

i	λ_i	β_i	E_i	γ_i
1	0.0124	0.00021	250 kev	1.14
2	0.0305	0.00140	460	1.11*
3	0.111	0.00126	405	
4	0.301	0.00252	450	
5	1.13	0.00073	420	
6	3.00	0.00027	---	

* A common group energy of 440 kev was assumed for groups 2-6 in calculating γ_i.

Photoneutrons

Since Tory II-A contains a very large amount of beryllium, the effect on the neutron economy of the $Be^9(\gamma, n)Be^8$ reaction must be considered. Rough calculations, outlined in the following paragraphs, indicate that the total contribution of the photoneutrons amounts to about 0.14% in k_{eff}.

The accuracy of this value is too low to justify making an effectiveness correction, as was done above for the delayed neutrons from fission. No explicit correction has yet been made in our multigroup calculation input parameters to account for photoneutrons; their reactivity contribution is small, and moreover their effect is taken care of by ensuring that results of the calculations fit real critical assembly measurements.

Most of these neutrons are born very soon after the fission event that led to their parent gamma; it is believed that the effect on reactor kinetics will be negligible. Further calculations will be made to check this point.

The contribution of photoneutrons to the multiplication factor was estimated in this way: The threshold for the $Be^9(\gamma, n)Be^8$ reaction is 1.67 Mev; the cross section value for this reaction reaches 1.0 mb at E_γ about 1.7 Mev, drops at higher energies, and then rises to 1.6 mb at about 10 Mev.

During operation, the more energetic gammas, such as prompt gammas, capture gammas, and some of the fission-product gammas can make photoneutrons. Since, on collision, a gamma above 1.7 Mev loses at least half of its energy, it has only one chance to make a photoneutron. Since around 5 Mev of energy per fission resides in gammas above 2 Mev, there are at most three gammas per fission energetically capable of making photoneutrons. Now in the Tory II-A core, in BeO of molecular weight 25 and average density about 1.5 g/cm^2,

$$\Sigma(\gamma, n) = \left(\frac{1.5}{25} \times 0.6\right) \times (1.0 \times 10^{-3} \text{ barns}) \cong 3.6 \times 10^{-5} \text{ cm}^{-1}$$

and the total γ removal cross section is

$$\Sigma \cong 1.5 \times \left(0.022 \frac{\text{cm}^2}{\text{gm}}\right) \cong 0.033 \text{ cm}^{-1} .$$

Therefore, the probability of $Be^9(\gamma, n)$ is $\sim 1.2 \times 10^{-3}$ for a particular gamma, and since we have about 3 gammas per fission capable of making photoneutrons, and we make 2.5 neutrons per fission, we have increased the neutron yield by

$$\frac{3 \times 1.2 \times 10^{-3}}{2.5} = 0.0014 .$$

If $\beta = 0.0064$, this is \$0.22.

Neutrons from the (n, 2n) Reaction

The (n, 2n) reaction is handled in a straightforward way in the multigroup calculations through introduction of appropriate input parameters, as

discussed in Section 5.2.1. A contribution of 0.12 in k_{eff} is made by (n, 2n) neutrons.

Flux and Power Distribution

Various aspects of the Tory II-A spatial flux distribution are shown in a series of figures on the next pages. The quantity plotted here is actually a weighted average flux value, determined by taking the ratio of power density to fuel concentration at a given point. For consistency and convenience, this quantity is used for those regions which will contain no fuel in the actual reactor, as well as for the fueled regions; in unfueled regions, it refers to the power density which would be generated in a very small sample of fuel material placed there.

For simplicity in calculations, the reactor is often treated by replacing the real reflector, with its system of neutron-absorbing control elements, by a homogeneous cylindrical reflector of equivalent thickness (with respect to criticality). It is believed that many valid results can be obtained in spite of this simplification, as, for instance, general flux configuration in the core.

Figure 5-3 shows axial plots of neutron flux calculated under this model, taken at various radii. The variation of axial shape with radial position should be noted; it is evident that radial variation in fuel loading will not alone be able to produce an identical power profile along all air flow passages. Achievement of a near-ideal power profile in all flow passages of a Tory II-A-like core would require fuel-loading variation throughout the core, in all three dimensions. The Tory II-A loading, however, is specified by a single r-θ map, invariant along the length of the core.

Figure 5-4 shows the flux distribution in a cross section perpendicular to the reactor axis, with the real reflector, and the rotary control cylinders in critical position for the core at 1350°K. The sliding control rod for the quadrant shown is not inserted.

Figure 5-5 shows a similar flux contour map with a control rod fully inserted. In the operating condition, three rods will be fully withdrawn and one rod inserted to half the core length, so that the flux distribution in three quadrants will be as shown in Fig. 5-4, and in the fourth quadrant as in Fig. 5-4 near the exit end and as in Fig. 5-5 near the inlet end. Both of these figures neglect the effect of detailed core structure on the flux distribution.

Figure 5-6 shows a typical radial flux profile, at the standard conditions of full operating temperature (1350°K), air at atmospheric pressure in

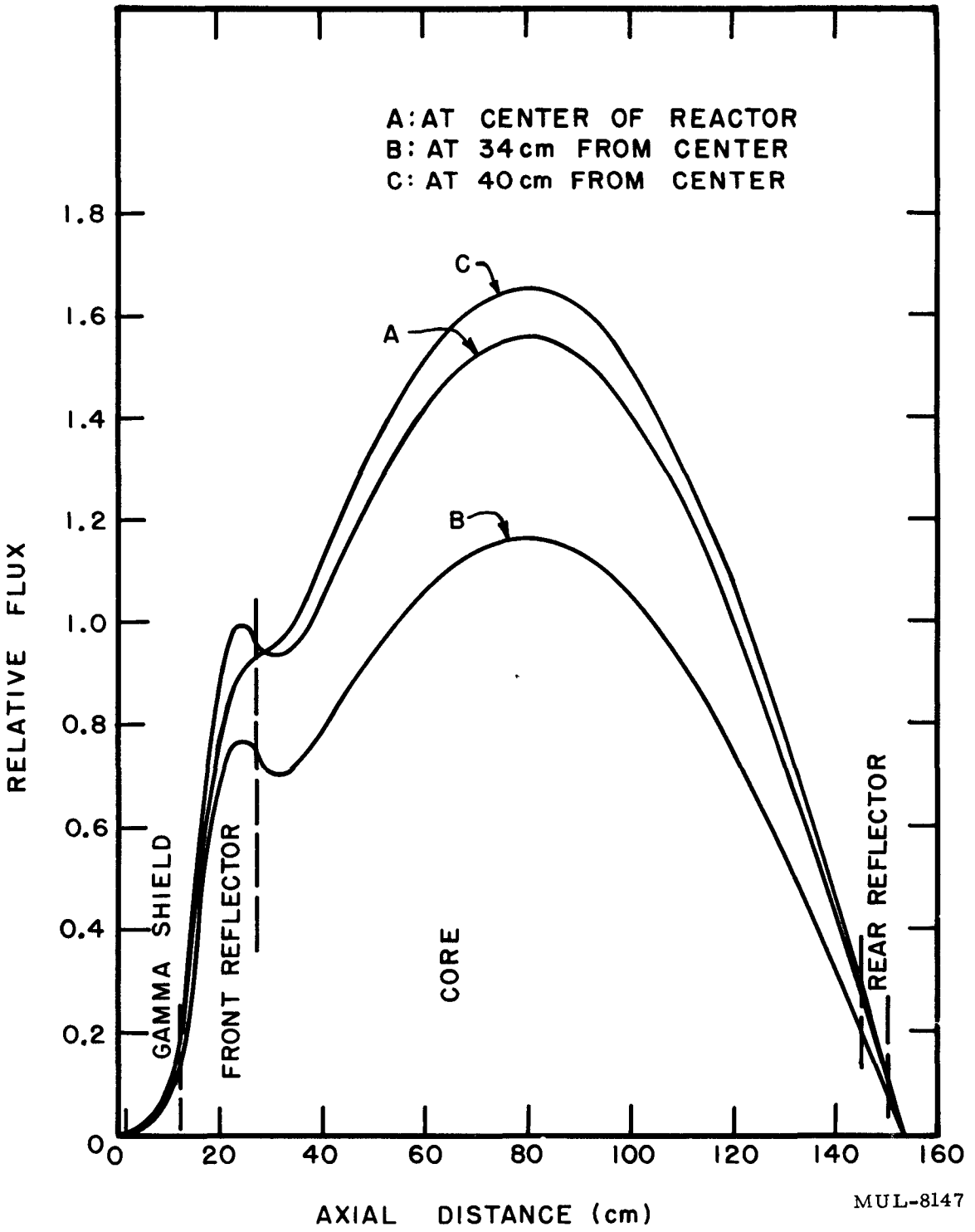

Fig. 5-3. Axial flux distribution.

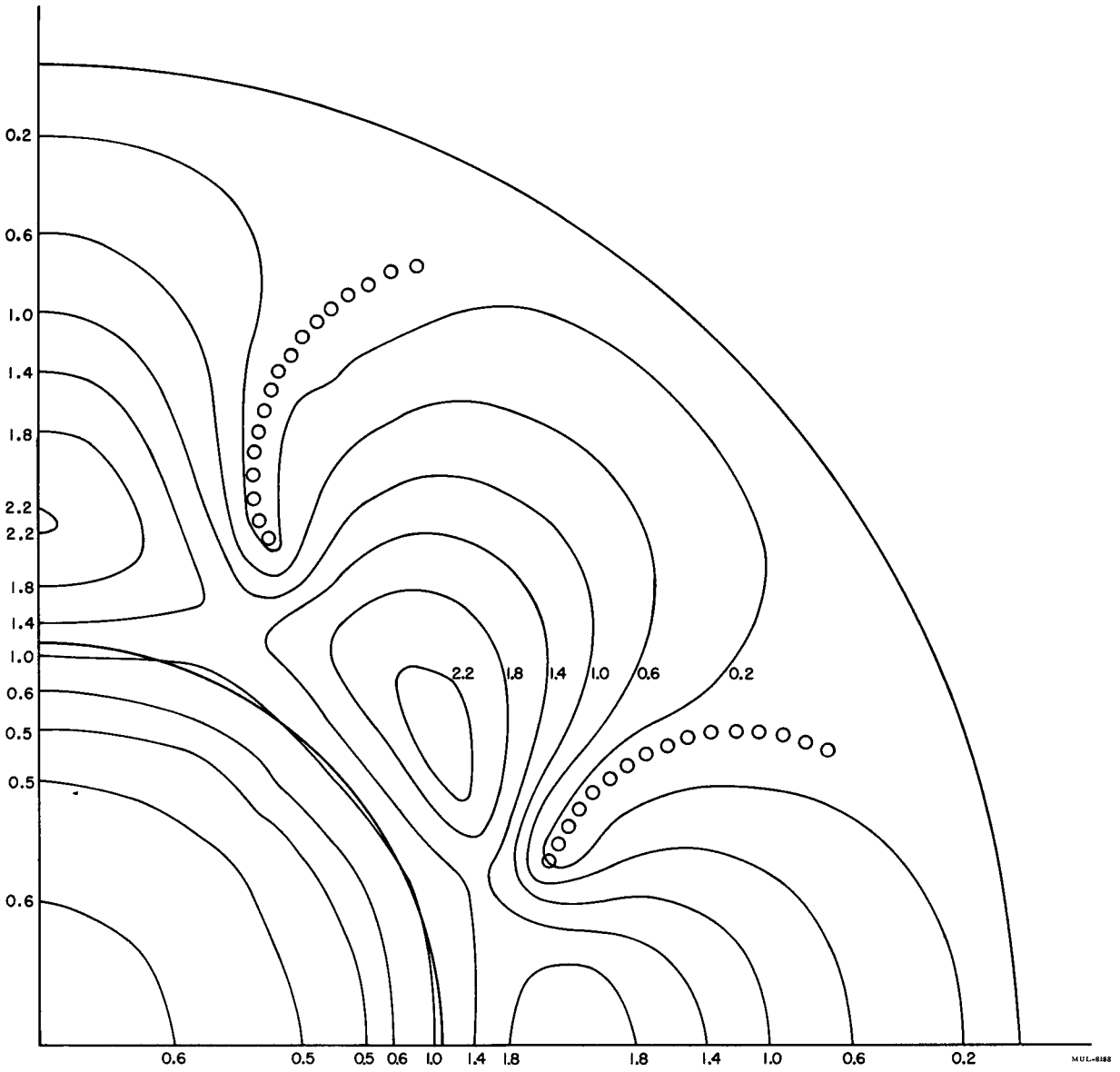

Fig. 5-4. Radial-azimuthal flux distribution without vernier rod.

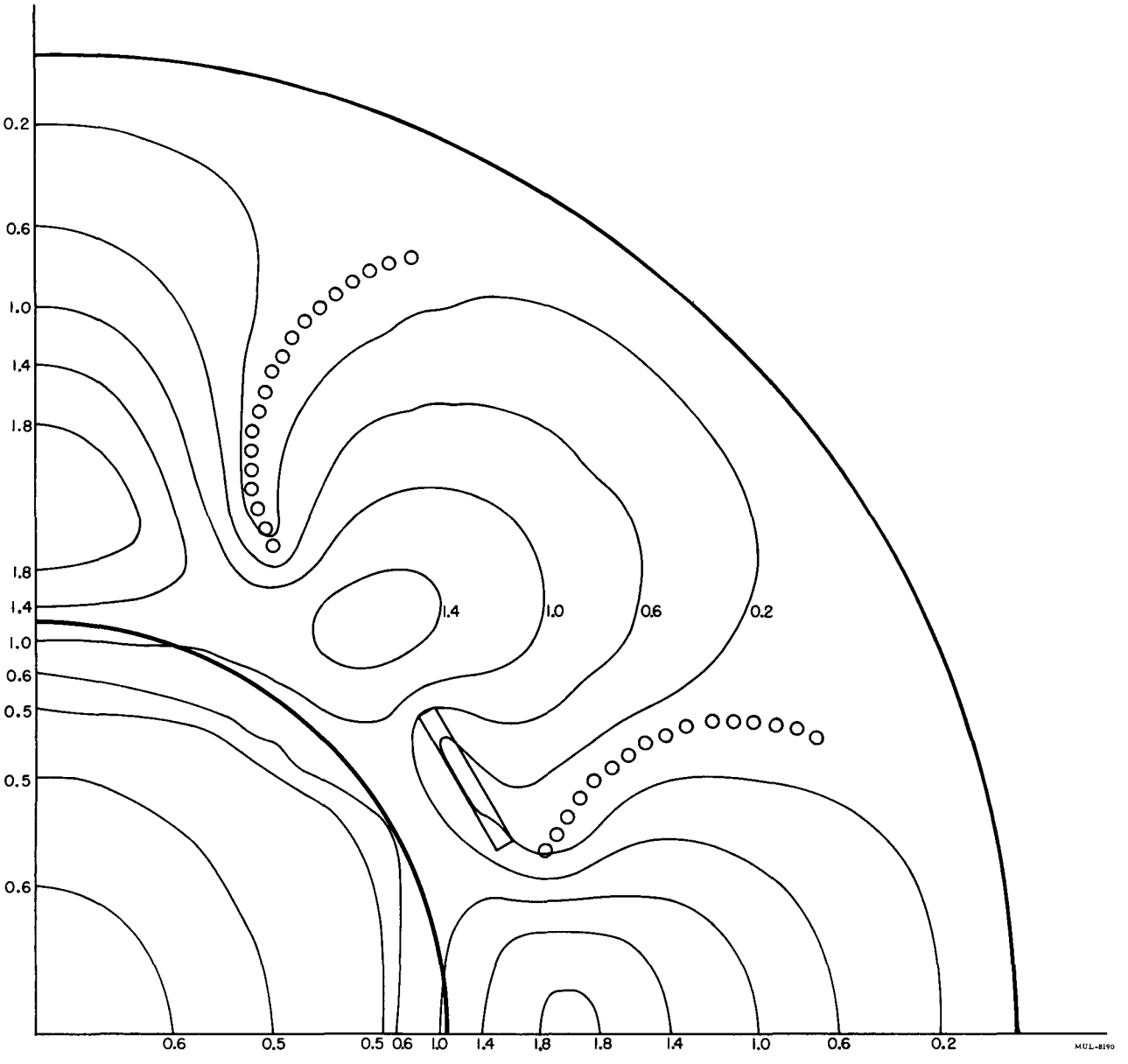

Fig. 5-5. Radial-azimuthal flux distribution with vernier rod.

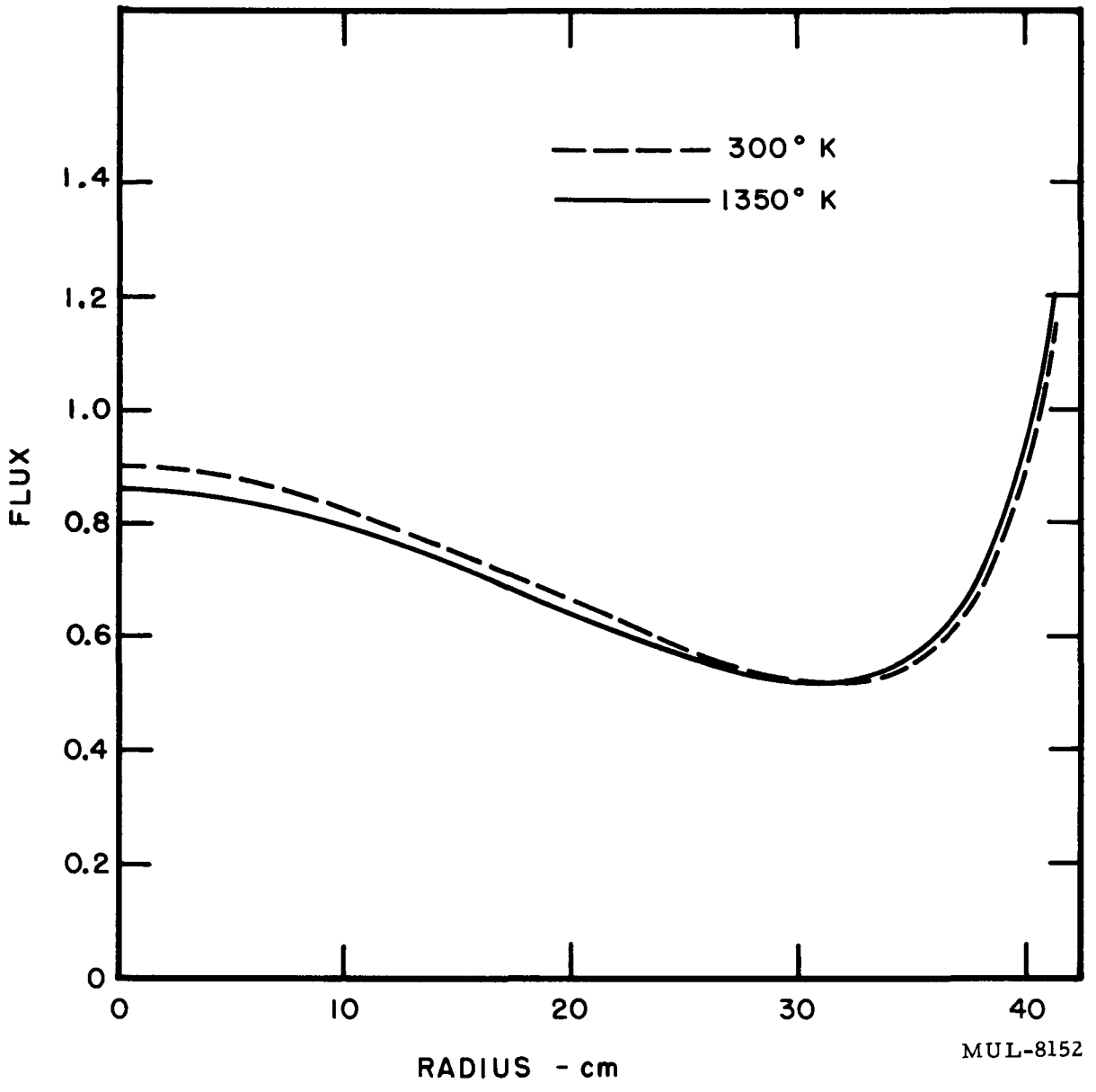

Fig. 5-6. Radial flux profiles at average core temperatures of 300°K and 1350°K.

the core, and the reflector graphite saturated with water (2 weight percent). The effect of a change in temperature is shown in a second curve, representing a cold (300°K), critical reactor.

The local effect on flux distribution of structural elements in the core is shown in Figs. 5-7 and 5-8 a, b. Figure 5-8 shows flux profiles along the paths indicated by dotted lines in Fig. 5-7. The single module shown in Fig. 5-7 is part of an infinite repeating array of similar modules, so that no overall curvature in flux resulting from boundaries, as in the real core, is present. The local flux distortion shown in these figures should be applied as a correction to the overall flux distribution in the core, shown in previous figures.

The core fuel loading varies only with radius and azimuth, in a pattern which is constant along the core length. This pattern, shown in Fig. 5-9, was chosen so that the total power delivered to any flow passage differs by no more than about 5% from that delivered to any other. The actual distribution of discrete fuel-element loadings, approximating this ideal pattern, is shown in Fig. 3-5. Seventeen different fuel concentrations are necessary to achieve this result; Table 3-5 shows the concentrations used, and the numbers of tubes in each grade.

In determining a fuel distribution to produce a flat power distribution, it is of course necessary to take into account the change in flux distribution produced by variations in loading distribution. Fortunately, this interaction is not strong; Fig. 5-10 compares typical radial flux profiles for the actual fuel loading and for a core with uniform loading.

Figure 5-11 shows logarithmic energy spectra $\left(\frac{d\phi}{d \log_{10}(E)} \text{ vs } E\right)$ of the neutron flux at various points in the reactor core and reflector. The numerical values are normalized to a reactor power level of 100 Mw.

Figure 5-12 shows the energy distribution of neutrons causing fission events in the reactor. It may be seen that a very small portion of the fissions are brought about by thermal neutrons; the temperature coefficient of reactivity could be much larger if a greater proportion of fissions took place at thermal energy.

Neutron energy spectra at the external surfaces of the reactor are discussed in Section 5.4.4 and presented graphically in Figs. 5-49 through 5-51.

Reactivity

The effect of various control positions and reactor temperatures on the reactivity, ρ, is shown through various families of curves. Critical

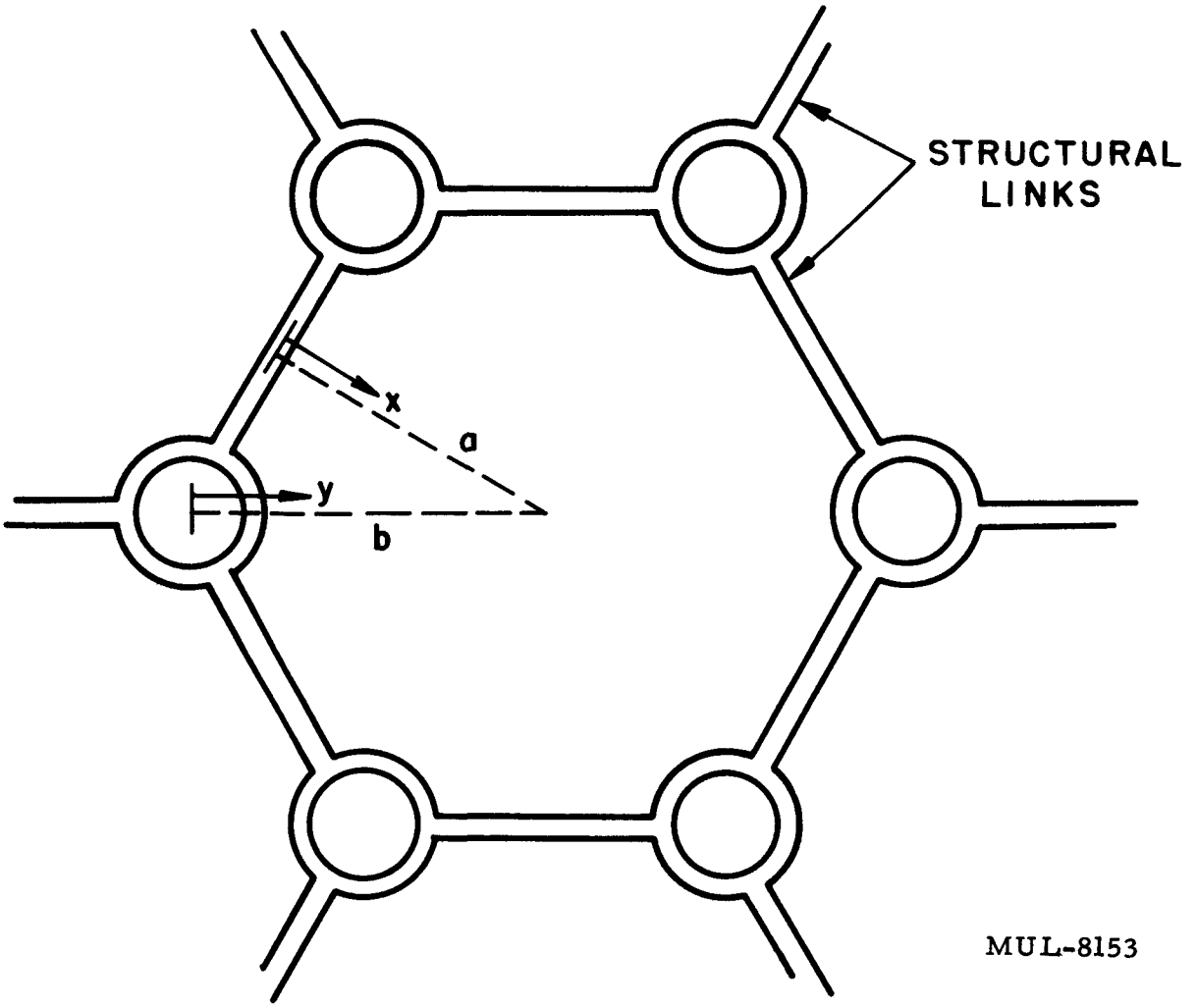

Fig. 5-7. Core module showing location of flux plots given in Fig. 5-8, a, b.

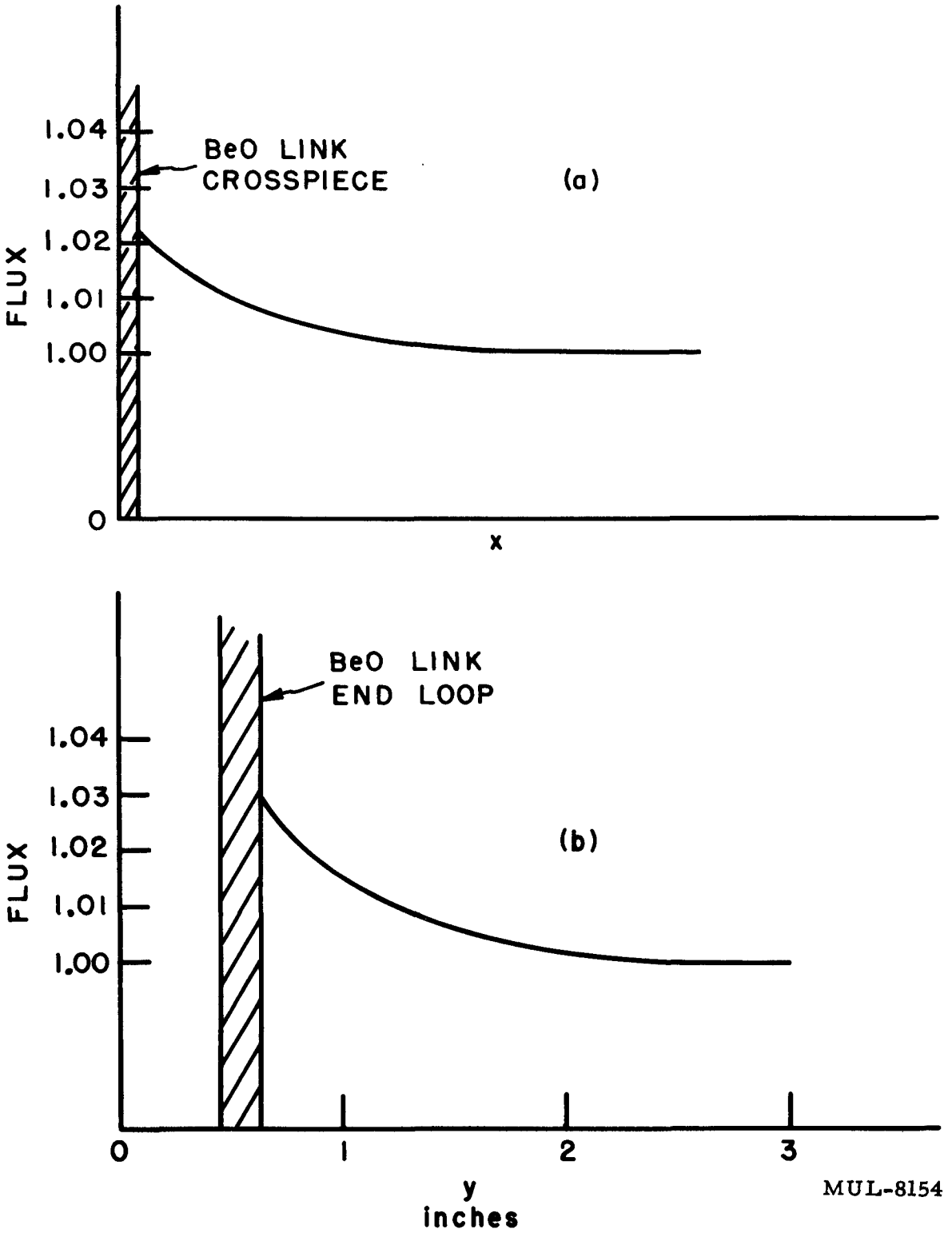

Fig. 5-8. Flux distribution, showing rise near unfueled BeO structural links.

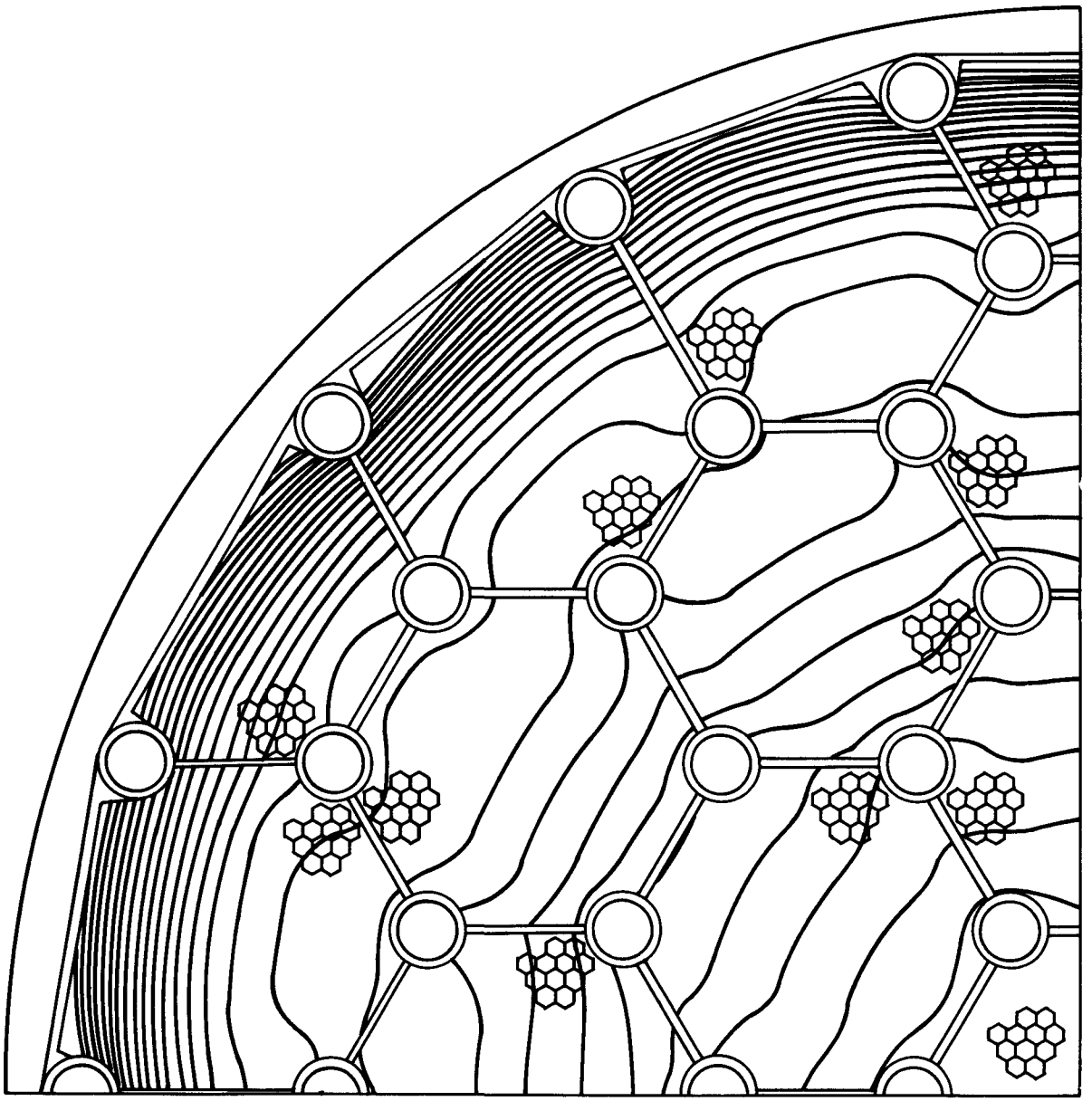

Fig. 5-9. Ideal fuel loading zone boundaries. MUL-8177

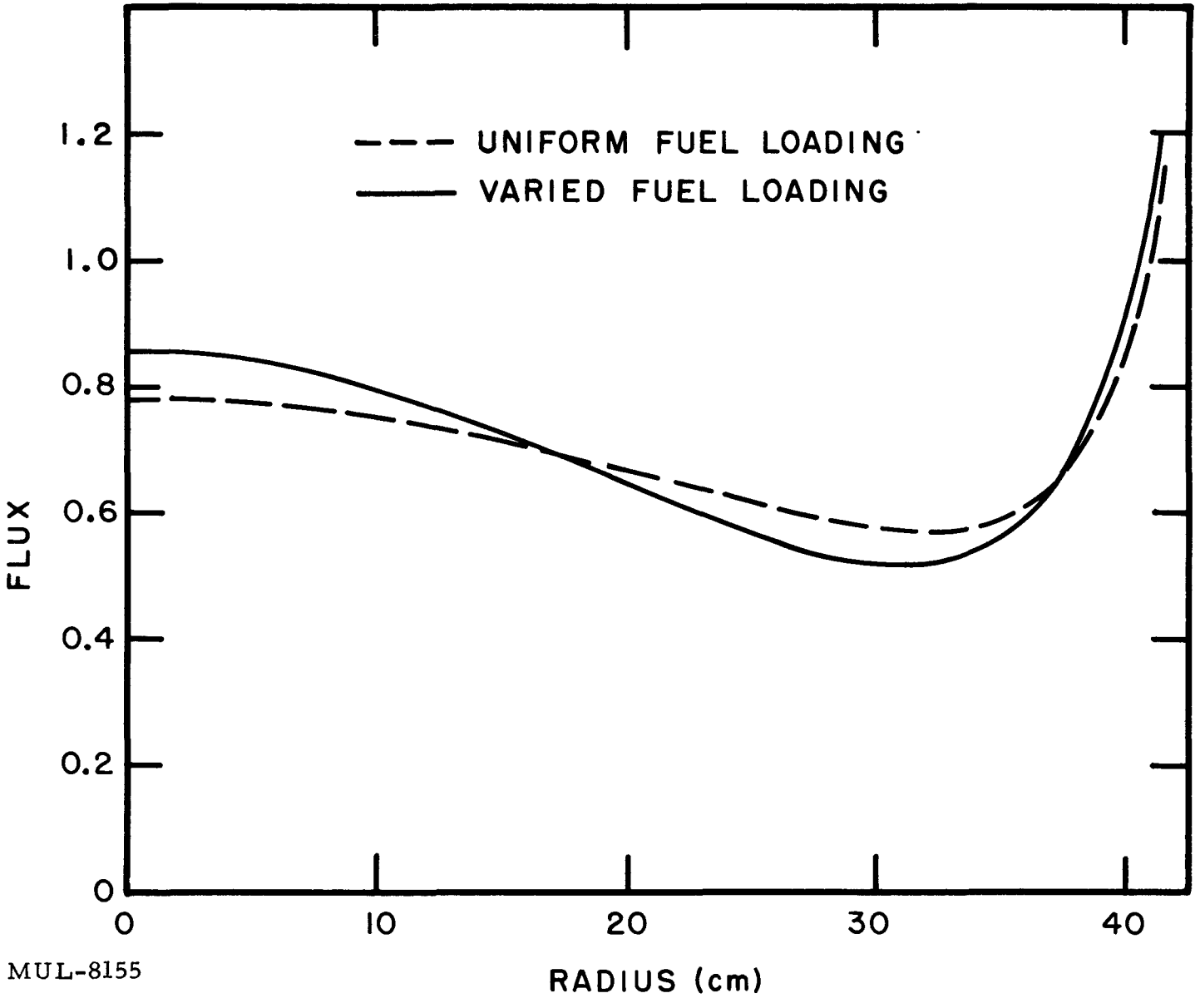

Fig. 5-10. Effect of varied fuel loading on neutron flux distribution.

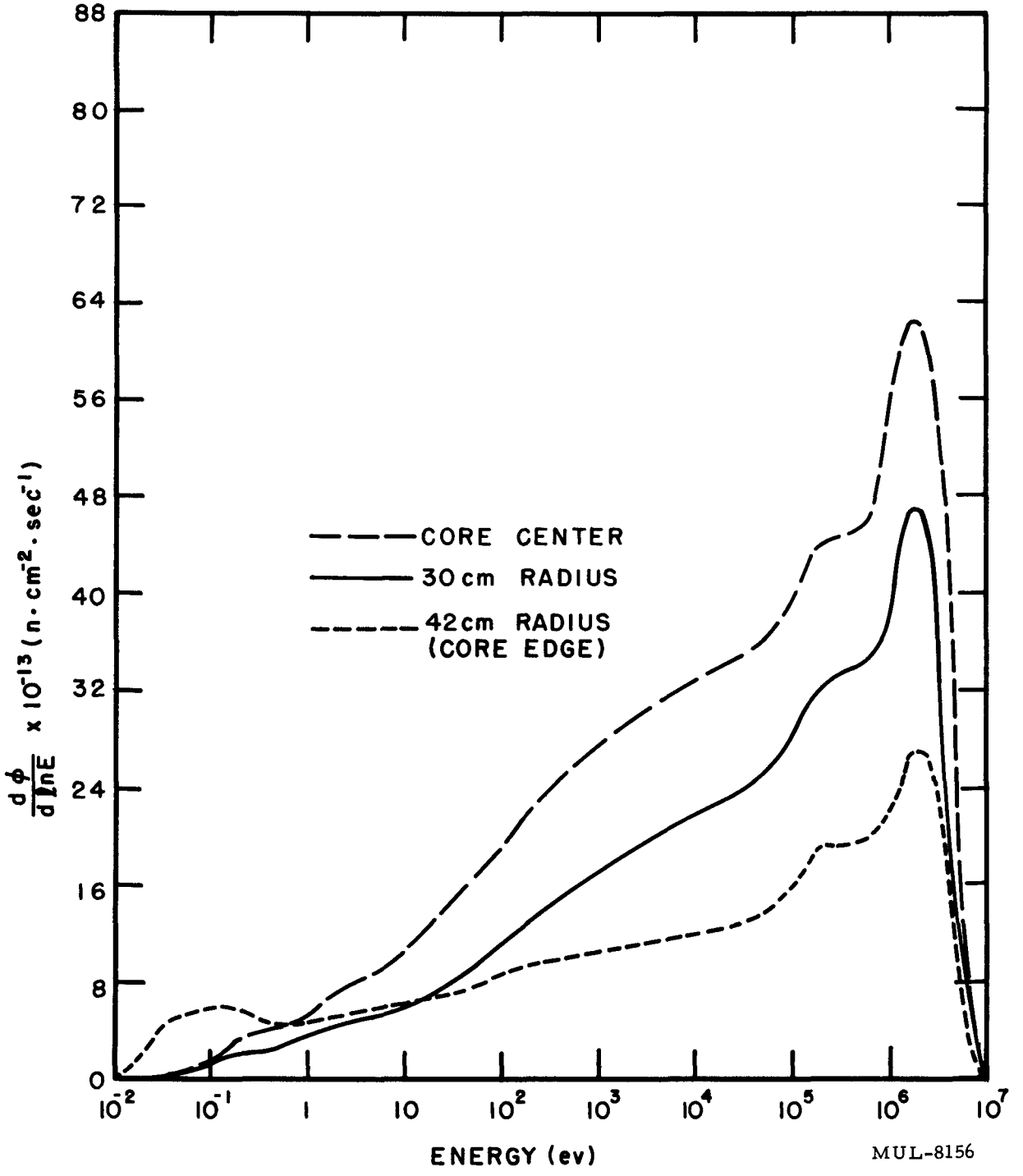

Fig. 5-11. Logarithmic neutron energy spectra in core.

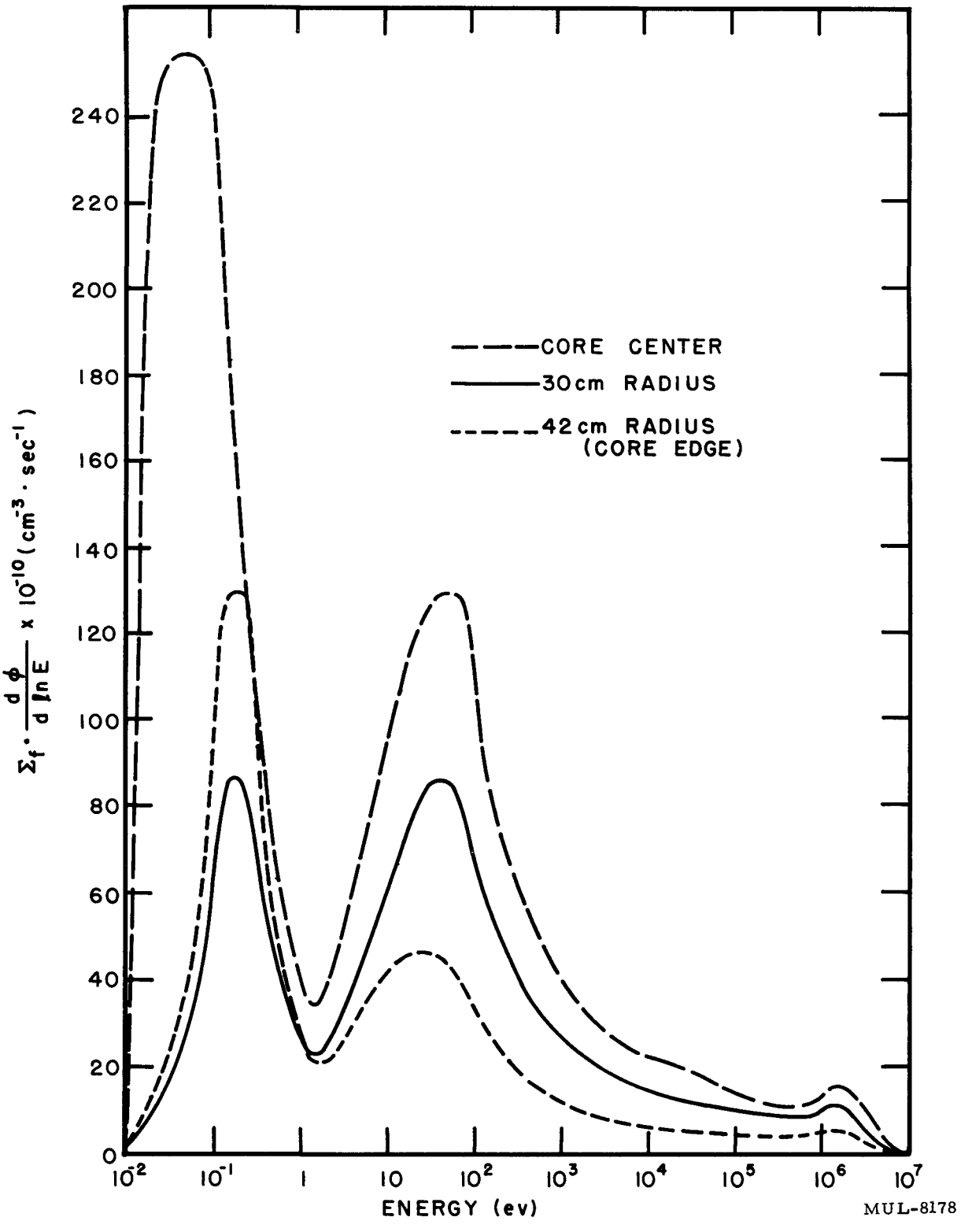

Fig. 5-12. Energy distribution of neutrons initiating fission reactions.

configurations may be identified as lines of zero reactivity. Indicated temperatures are average core temperatures, obtained using the square of the flux density as a weighting function. The assumptions are made that all eight control cylinders always move in unison, and that only one vernier rod enters the reflector at a given time. Unless otherwise stated, air in the core is at atmospheric pressure.

Reactivity as a function of control cylinder angle and core temperature is shown in Fig. 5-13, for the vernier rod in its centered position.

Figure 5-14 shows, for several fixed critical cylinder angles, the variation of ρ with vernier rod position.

The effect on reactivity of varying air density in the core flow passages is shown by comparing the reactivity contribution of this air under three standard conditions: At normal temperature and pressure, $\Delta\rho$ is -0.0002; at peak temperature and flow rate (see design operating conditions in Section 5.1), $\Delta\rho$ is -0.0009; and for the reactor and air at ambient temperature, with the same full air flow rate, $\Delta\rho$ is -0.0036.

Off-Design Situations

Both for design use and for anticipating the effect of changes which may occur during operation of the reactor, it is necessary to know the effect on reactivity and flux distribution of various changes in reactor dimensions or composition.

To achieve general usefulness, such a study has been made in terms of small changes in single parameters. As long as the changes remain small, it is a reasonable approximation to say that the effects brought about are additive, and linearly proportional to the parameter changes causing them.

When looking for the effect of some design change on radial flux distribution in the core, two things must be considered. One is the direct effect of the change; the second is the effect of the change in critical mass necessary to accommodate the design change. It has been found in all cases studied that the second effect is larger than the first by at least a factor of 2 and in most cases masks the effect of the original design change completely. Figure 5-15 is an example of the effect of a change of fuel loading, due to design change, on the flux distribution. The changes from Core 1 to Core 2 were an increase in total void fraction of the core by ~ 1.4% (of the core volume) and a decrease in core length of ~6%. It was necessary to increase fuel density by 50% to

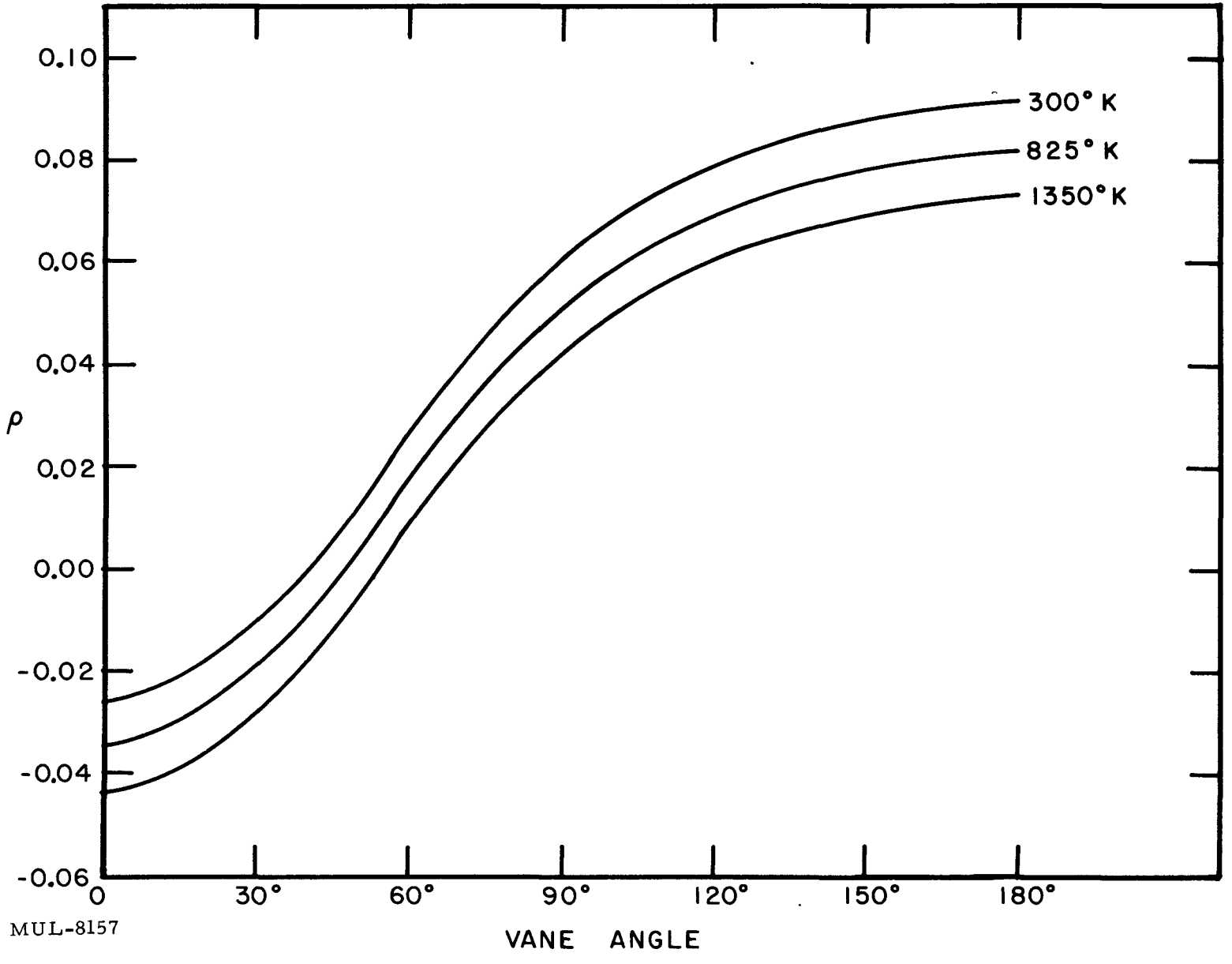

Fig. 5-13. Reactivity ρ as a function of control vane angle and average core temperature.

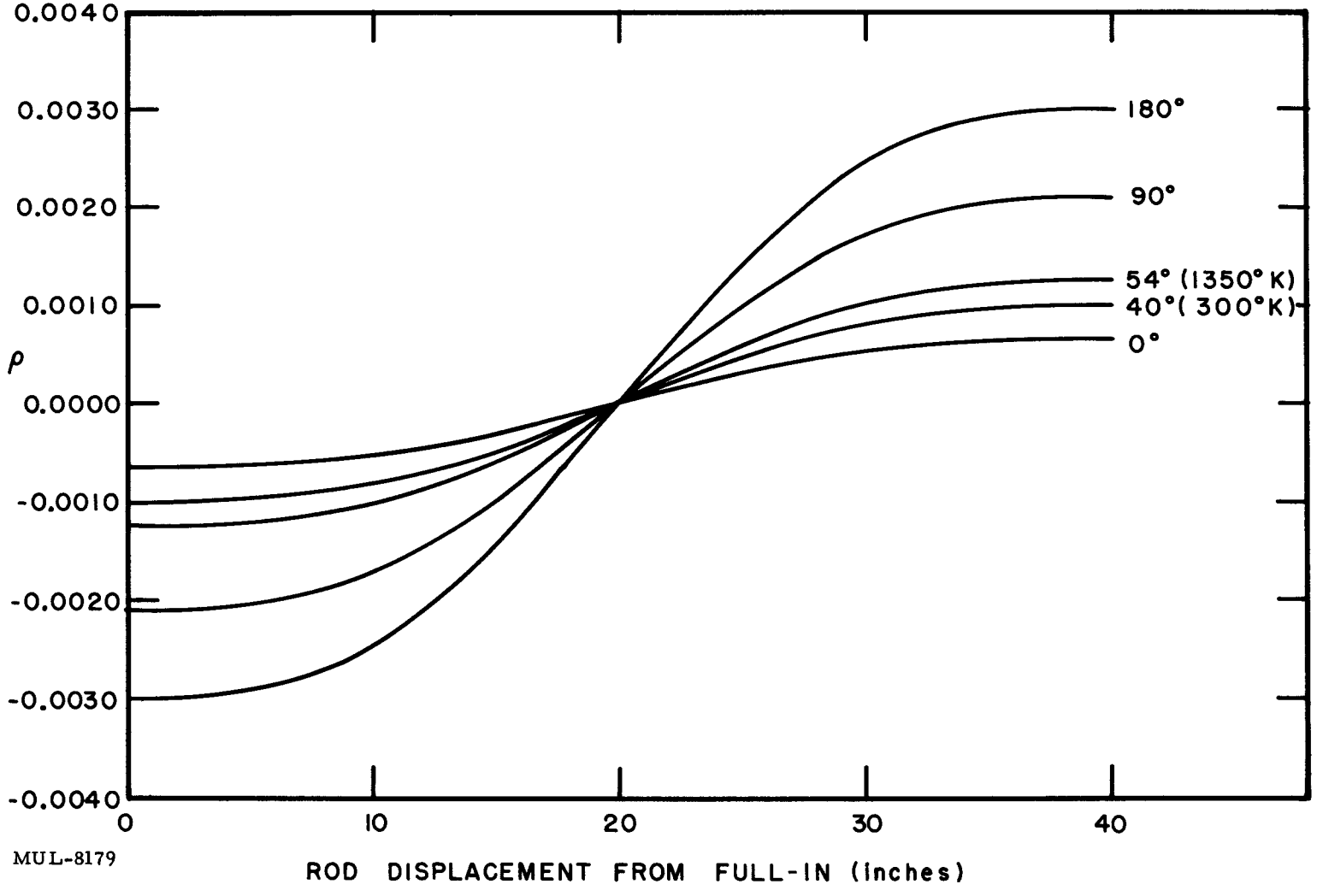

Fig. 5-14. Variation of reactivity ρ with single vernier rod position, for various control vane angles.

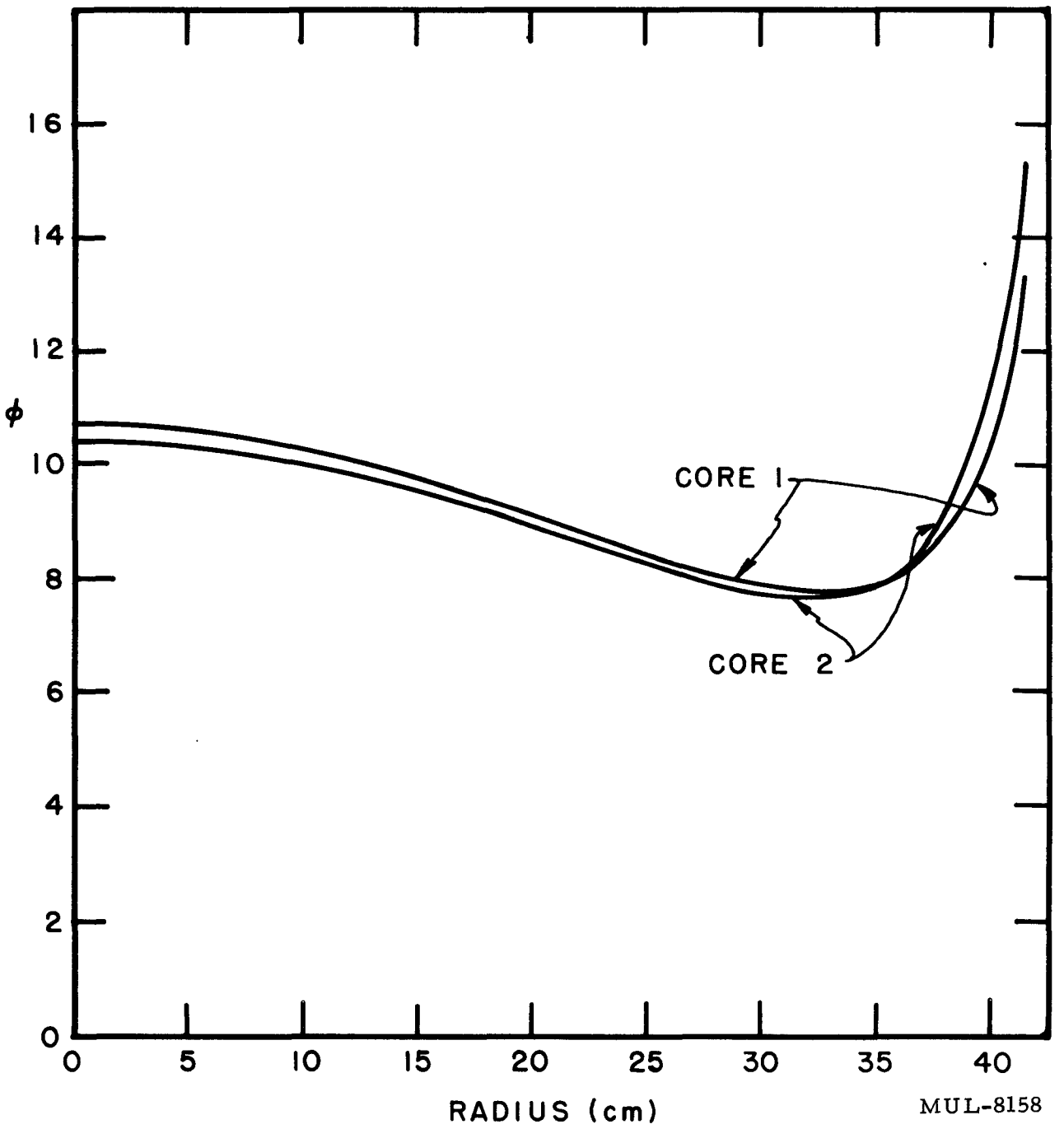

Fig. 5-15. Change in radial flux distribution resulting from 50% change in fuel loading.

maintain criticality. The two curves are normalized to constant total power on an arbitrary scale. The change shown in this figure should be taken as representative of that due to a 50% fuel loading change to accommodate any other design variations. Flux changes due to different loading changes will maintain a similar radial variation, with amplitude in proportion to the fuel change.

In each case to follow, a specified variation has been applied to a critical reactor. The effects are shown in terms of reactivity vs control vane angle. Dotted curves in each figure show the corresponding quantities for the unperturbed reactor. For each change considered, the fuel concentration has been adjusted by an amount sufficient to keep the hot, clean reactor critical at a vane angle of 54°.

For the standard Tory II-A reactor in a clean, hot critical condition an increase of 0.010 in reactivity is produced by a 9.4% increase in total fuel loading. Here and in the following list, % fuel change means 100 times the fractional change in total fuel content of the reactor.

Changes in absorption cross sections are defined in terms of the thermal value, but were actually made in the same ratio in all energy groups, of course.

Figures presented are listed below, with the changes to which they refer:

5-16 Core Void Fraction. Average void space increased uniformly throughout core by 1% of core volume, at expense of fuel element material; fuel increased 14%.

5-17 Reflector Water. Water concentration increased uniformly throughout reflector graphite by 0.04 g/cm^3; fuel loading decreased 5.6%.

5-18 Reflector Poison. Macroscopic thermal absorption cross section increased uniformly throughout reflector graphite by 5×10^{-4} cm^{-1}; fuel loading increased 4.2%.

5-19 Reflector Density. Density of reflector graphite increased uniformly by 0.10 g/cm^3, with no change in absorption cross section; fuel loading decreased 5.7%.

5-20 Pressure Vessel Water Jacket. Thickness of cooling water layer at pressure vessel increased by 0.25 inch; fuel decreased 12.2%.

5-21 Shroud and Pressure Vessel. Absorption cross section raised by amount sufficient to add 0.01 thermal absorption mean free path to effective thickness of metal at core-reflector boundary; fuel increased 3.0%.

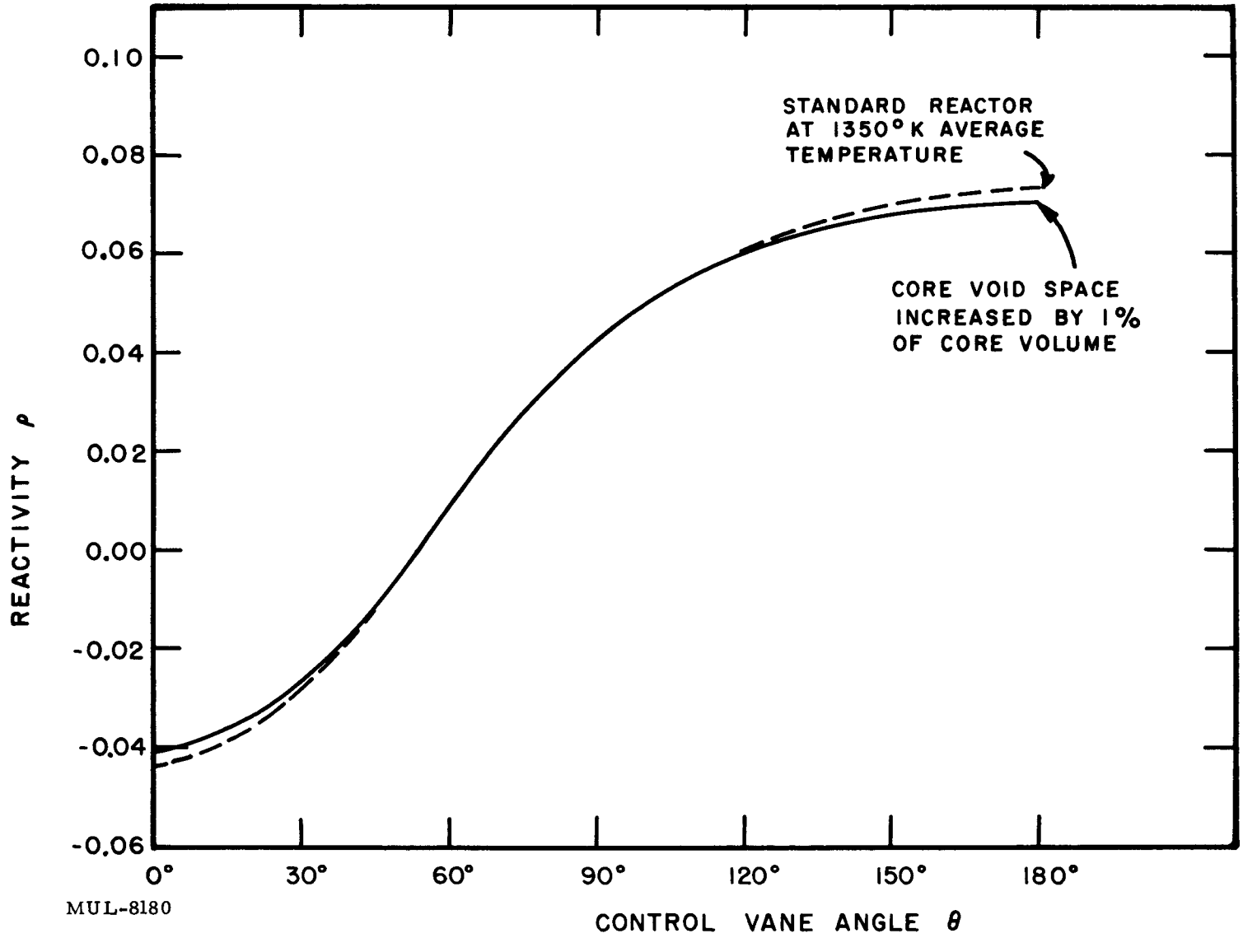

Fig. 5-16. Effect on reactivity vs vane angle of a change in core void fraction.

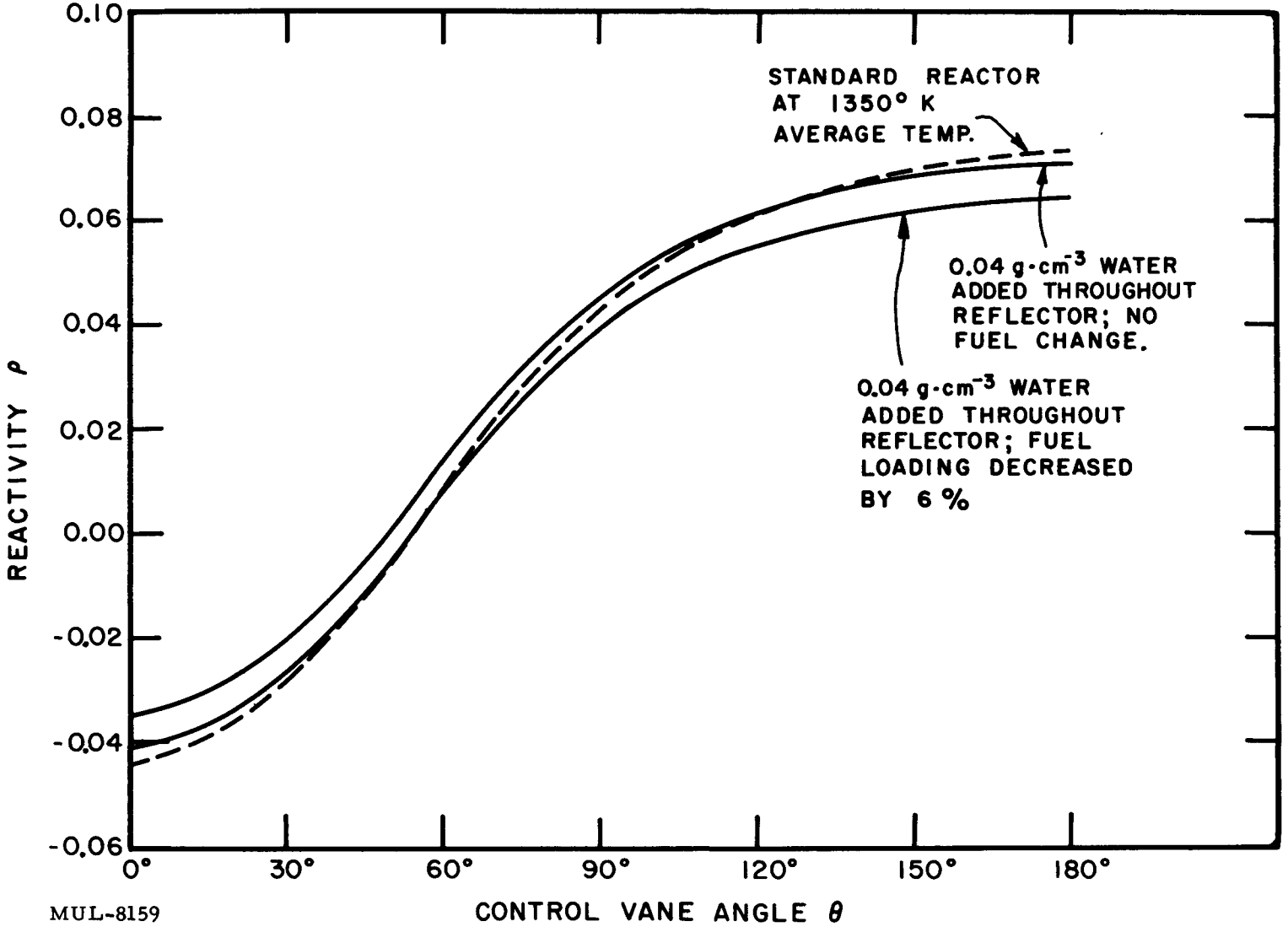

Fig. 5-17. Effect on reactivity vs vane angle of a change in water content of reflector graphite.

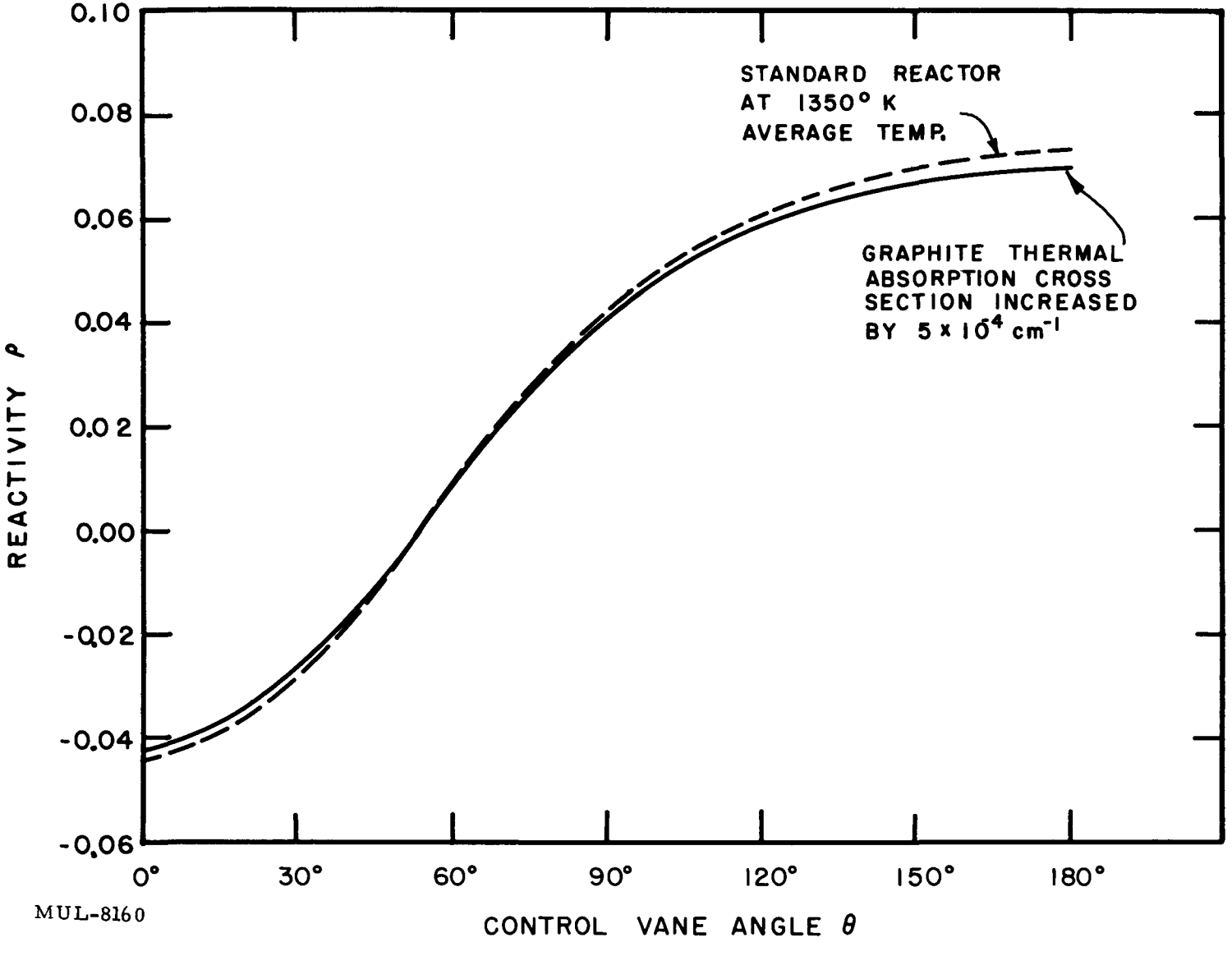

Fig. 5-18. Effect on reactivity vs vane angle of a change in reflector poison content.

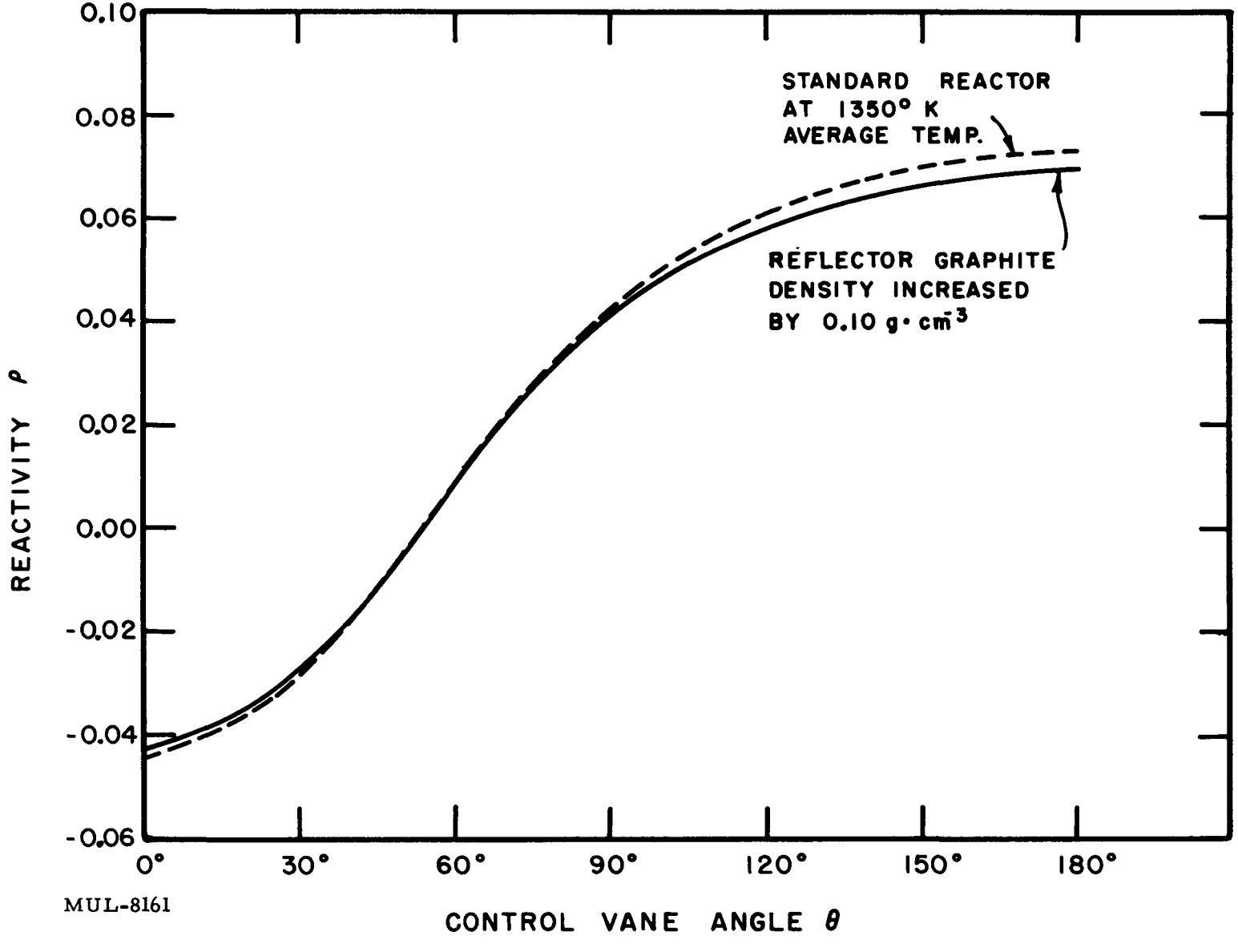

Fig. 5-19. Effect on reactivity vs vane angle of a change in reflector density.

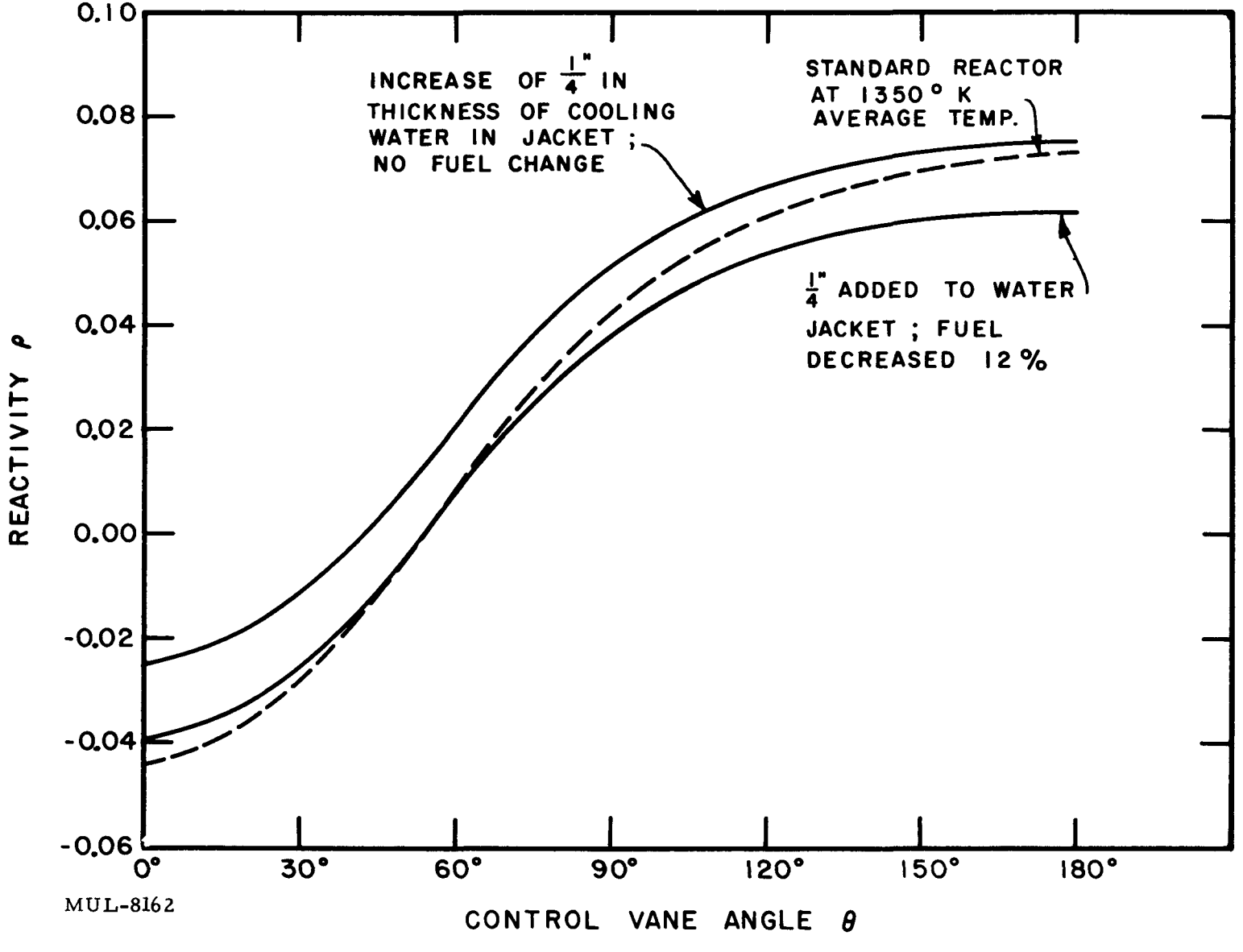

Fig. 5-20. Effect on reactivity vs vane angle of a change in thickness of pressure vessel water jacket.

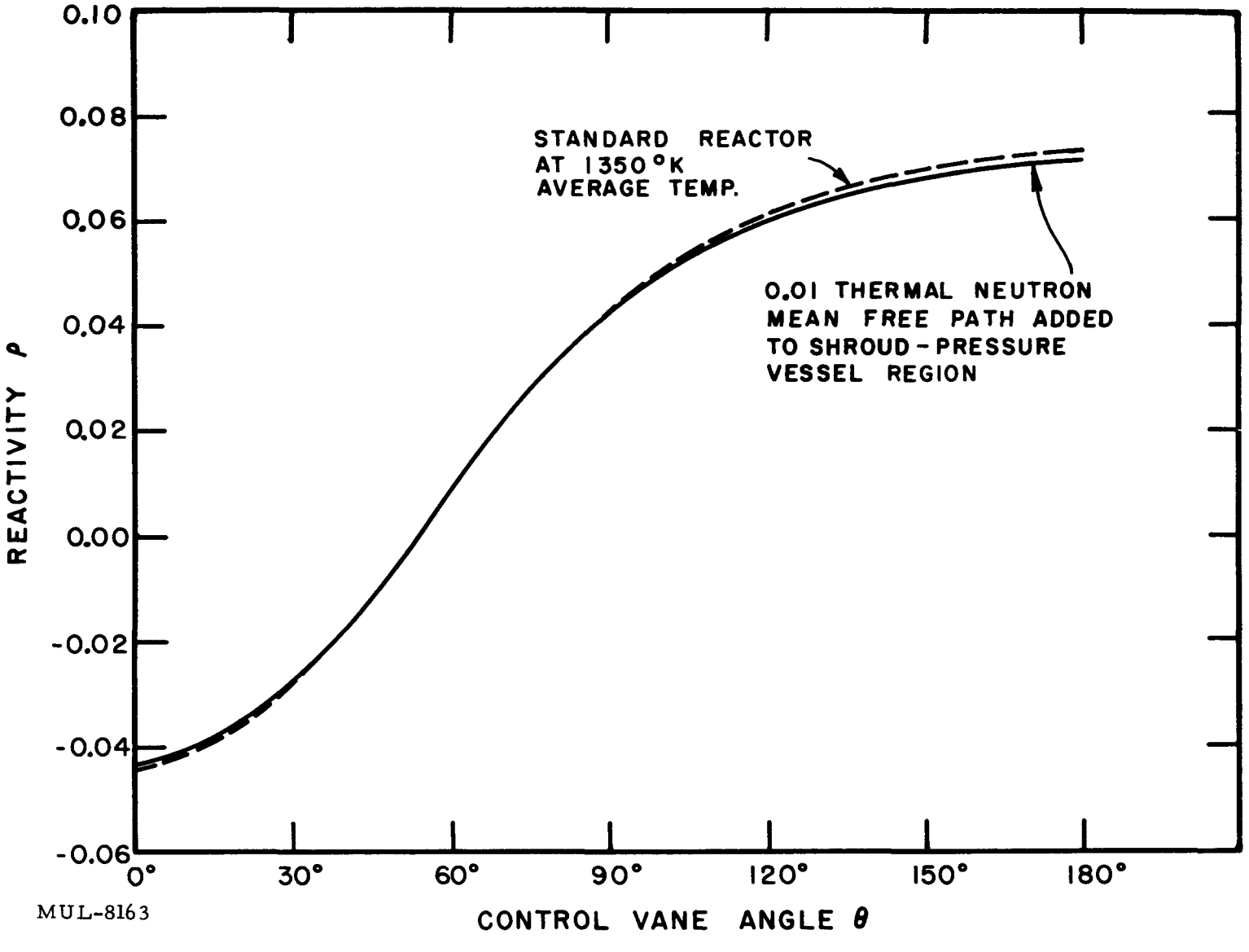

Fig. 5-21. Effect on reactivity vs vane angle of a change in neutron absorption at core-reflector boundary.

5-22 Control Vane Poison. Concentration of poison in rotating control vanes halved; fuel decreased 11.7%.

For each of the reactivity curves given above, the vernier control rod was taken to be in its centered position.

Two other similar changes have been studied, but result in too small a variation in the reactivity curve to be visible in a figure. These are:

a) Core Poison. The macroscopic thermal absorption cross section in the core was uniformly increased by 1×10^{-3} cm^{-1}, necessitating a 5.2% increase in fuel loading.

b) Fuel Loading Distribution. The fuel loading distribution was made uniform throughout the core instead of being shaped for flat radial power; the total fuel loading was correspondingly decreased by 6.6%.

5.3 Air Flow and Thermodynamics

5.3.1 Background of Choice of Tory II-A Design

It has been stated that the purpose of Tory II-A is to investigate the engineering problems associated with achieving the high power density, high temperature, and large air flow at high pressure required to propel a nuclear ramjet at supersonic speeds at low altitudes. In order to establish the realm of these variables of Tory II-A design interest, a digital-computer program was set up to calculate nuclear ramjet performance over the whole region of possible feasibility, from Mach 1 to 10, altitudes from sea level to 150,000 feet, for all encountered ambient temperatures, and for the spectrum of each of the reactor independent variables pertinent to thermodynamic performance: void fraction, maximum material temperature, and axial power distribution shape.*

A simple configuration was chosen for the nuclear ramjet nacelle: the diffuser section was taken to be an isentropic-spike-centerbody nose inlet with payload and controls in the centerbody; the center section containing the reactor and support structure is a right circular cylinder; and the boat-tail section containing the subsonic-supersonic nozzle is a cone frustrum flaring out or converging from the body size to the exhaust area.

---

* A detailed discussion of the methods and results of this program may be found in ref. 1.

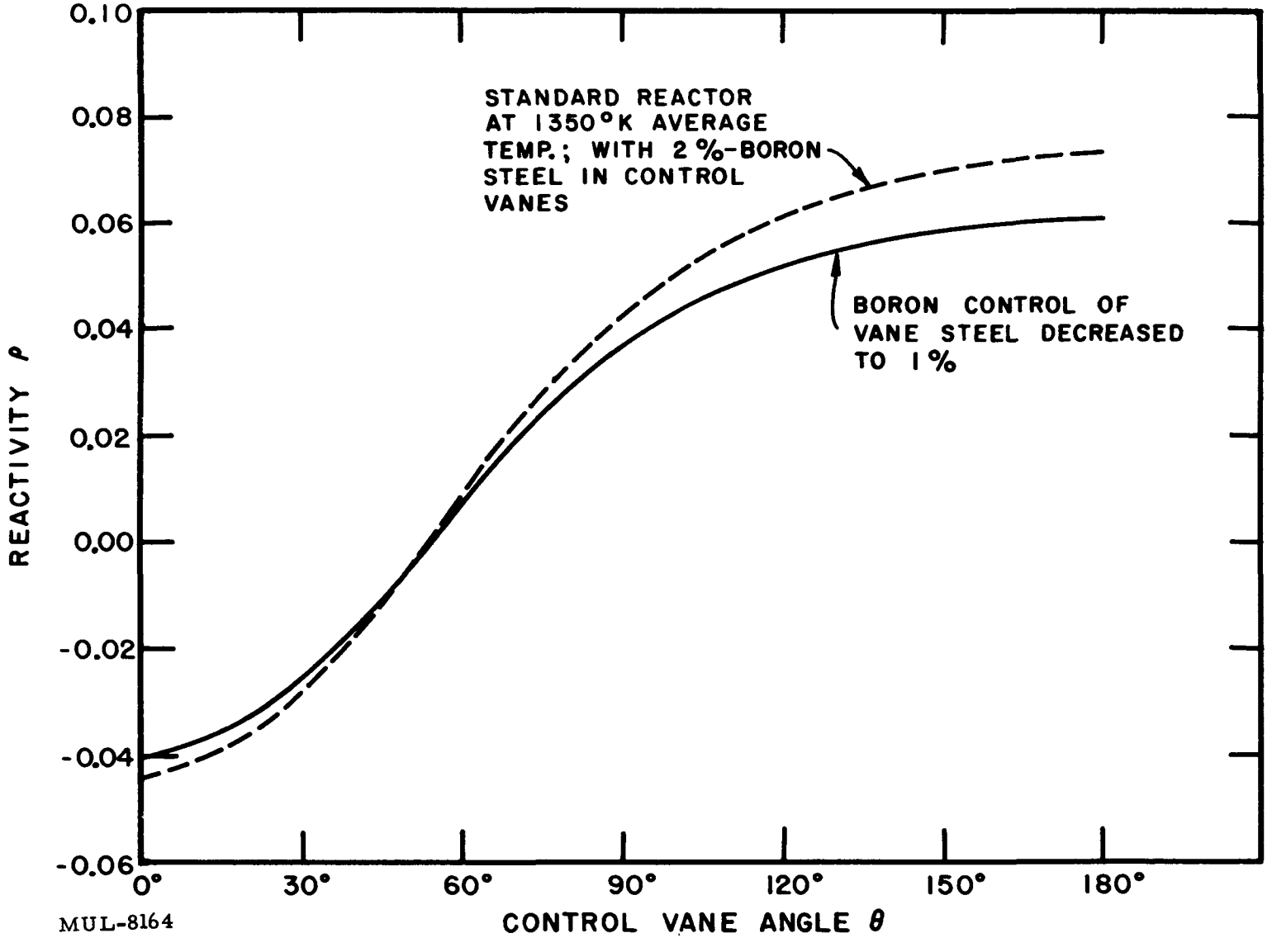

Fig. 5-22. Effect on reactivity vs vane angle of a change in control vane poison content.

The nose length was chosen to be essentially consistent with a subsonic diffuser expansion rate from the throat area to the reactor area equivalent to a 6° half-angle cone; the boat-tail length is consistent with a 30° half-angle converging subsonic nozzle and a 15° half-angle diverging supersonic nozzle with a radius of curvature at the throat equal to the throat diameter. The skin-friction drag of the whole nacelle, and the wave drag for the nose section and boat-tail section were calculated; the latter was balanced by an optimization process against the effect on thrust of varying the nozzle-area expansion ratio.

The diffuser performance was described simply by a pressure recovery factor (a decreasing function of Mach number) based on conservative contemporary values.

The performance of a real nozzle was described in terms of a velocity coefficient, the ratio of the actual velocity attained by the air to the ideal velocity, and a divergence factor, representing the effective component parallel with the nozzle axis of the slightly diverging exhaust velocity vectors.

The problem of calculating the thermodynamic performance of the reactor is considerably more extensive than for the diffuser and nozzle. The temperature increase in the reactor is accomplished at the expense of decreasing the pressure available to accelerate the air through the nozzle. Because of the pressure loss in the duct the air cannot be expanded through the nozzle to an exhaust Mach number as high as the incoming, or flight, Mach number, so the increase in temperature must raise the velocity of sound high enough that it can more than offset the decrease in Mach number and hence lead to a net increase in air velocity and a positive thrust.

The local surface heat transfer coefficient for turbulent flow, given in an NACA[9] report and modified according to a Los Alamos[10] technical note, has been satisfactorily verified in a Livermore reactor-element heating experiment (Blowpipe) and is expressed by the modified Dittus-Boelter correlation, with the nomenclature of Table 5-9:

$$\frac{hD}{k_f} = 0.036 \left(Re_f\right)^{0.8} \left(Pr_f\right)^{0.4} \left(\frac{x}{D}\right)^{-0.1} . \qquad (1)$$

For a given axial power distribution and various values for power, flow rate, and flow-passage size, the steady-state wall temperature contour may be calculated using the above equation and energy conservation, and a simple

Table 5-9 Nomenclature

a	flow passage radius
c	constant; specific heat
D	flow passage diameter
f	friction factor; subscript: film
g	normalized dimensionless local power density
h	surface heat-transfer coefficient
k	thermal conductivity
L	flow passage length
M	Mach number
p	pressure
P	power
Pr	Prandtl number: $C_p\mu/k$
Re	Reynolds number: $\rho VD/\mu$
T	temperature
V	velocity
x	distance along flow passage from inlet
X	power distribution shape factor
z	flow impedance of passage
γ	ratio of specific heats
ϵ	dimensionless length
μ	viscosity
ρ	density

The subscripts 1 and 2 generally indicate the value of a variable at a flow passage inlet or exit end, respectively.

The superscript ^{0} indicates total, or stagnation, gas properties.

correlation is found between the maximum wall temperature, exit air temperature, tube radius and length, and exit friction factor which reads

$$\frac{1}{f_2 L/a} = \frac{1}{z_2} = c_1 - c_2 \left(\frac{T_2^0 - T_1^0}{T_{w_{mx}} - T_1^0} \right), \qquad (2)$$

where the c_1 and c_2 are constants (approximately equal to 2), different for each axial power distribution. The friction factor is given by the standard formula

$$f = \frac{0.046}{\left(Re_f\right)^{0.2}} \tag{3}$$

The pressure drop is calculated on the basis of the exact differential equation for the gas momentum[11] for flow in a smooth tube with friction and heating and with no entrance or exit losses,

$$\frac{dp}{p} = -\frac{\gamma M^2}{1-M^2}\left\{\left(1+\frac{\gamma-1}{2}M^2\right)\frac{dT^0}{T^0} + \left[1+(\gamma-1)M^2\right]\frac{f\,dx}{a}\right\}, \tag{4}$$

which may be integrated exactly by a digital computer program, the Floss code.[12] This code calculates, in addition, the Mach number, gas temperature, and wall temperature variations along a flow passage. An approximate analytical integration of equation(4) has been performed by R. H. Fox,[13] giving pressure ratios only about 0.1% different from Floss results for Mach numbers up to 1 and for either heating or cooling. The result of this integration is

$$\left(\frac{p_1}{p_2}\right)^2 = 1 + \frac{2\gamma_2 M_2^2}{T_2}\left\{\left(T_2^0 - T_1^0\right) + z_2\left[X\left(T_2^0 - T_1^0\right) + T_1^0\right]\right\} + M_2^2\,\ell n\left(\frac{p_1}{p_2}\right)^2. \tag{5}$$

The power distribution shape factor, X, is given in terms of the dimensionless axial power distribution, $g(\epsilon)$,

$$X = \int_0^1 d\epsilon' \int_0^{\epsilon'} g(\epsilon)\,d\epsilon, \tag{6}$$

and is a number between 0 and 1, being less than 0.5 for power distributions peaked toward the exit and greater than 0.5 for distributions peaked toward the entrance.

The exit air temperature may be brought closer to the maximum wall temperature by decreasing the flow-passage radius (for a given length) which, however, increases the pressure loss in the reactor and, consequently, for constant reactor inlet pressure, decreases the nozzle chamber pressure. Benefits of increasing the exit gas temperature must be weighed against the disadvantage of decreasing exit pressure.

The flow per unit area of the reactor may be increased (at constant void fraction and inlet pressure), leading to a more compact reactor, by increasing the velocity of flow or the flow Mach number (larger exit nozzle), which, however, leads to a higher pressure loss. The resulting decrease in drag, due to making the reactor smaller for the same total flow, must be balanced against the loss in thrust due to lower exit pressure.

The decrease in wave drag due to making the boat-tail taper more gradual must be weighed against the loss in thrust due to nozzle expansion to an exhaust pressure different from that giving the highest thrust.

For each group of reactor and flight independent variables: void fraction, maximum wall temperature, and axial power distribution shape; and flight Mach number, altitude, and ambient temperature; optimum values of the reactor-exit-air stagnation temperature, reactor-exit Mach number, and nozzle-exhaust static pressure can be found.

Calculation has been made of performance of nuclear ramjets flying at 1000 ft altitude, standard hot day, at Mach numbers of 2.5, 3.0, 3.5, and higher where reasonable, with reactor void fractions of 0.3, 0.4, and 0.5, and with reactor maximum wall temperatures of 2250, 2500, 2750, and 3000°F. For simplicity and to obtain an upper limit in performance, the calculations were made with the ideal isothermal wall power distribution, no end reflectors, no mixing with auxiliary cooling air, and no exit or entrance pressure losses.

Performance in terms of net thrust coefficient, that is, nacelle thrust-minus-drag per unit "reactor" area (85% of body cross-sectional area), in general increases monotonically without limit with void fraction and maximum wall temperature, so no optimum is indicated for either on the basis of performance alone; some other criterion must be found, therefore, to specify reasonable values for these variables.

The reactor average void fraction is limited by several considerations: 1) The flow passages may be only so close together before the walls become too thin for manufacture and handling; 2) Not all the reactor area is given over to fuel elements; part is occupied by necessary structure which supports the core and must have cooling passages which are not as effective in raising the air temperature as the fuel elements, and 3) The increased neutron streaming loss and smaller moderator volume fraction at higher void fractions lead to prohibitively large uranium requirements. On the basis of these arguments, an average void fraction of 0.3 can easily be accomplished, 0.4 can be

accomplished with some effort, and 0.5 can be accomplished only with great difficulty, requiring extension of presently known limitations in properties of materials.

The tensile strength of beryllium oxide drops rapidly with increasing temperature in the range 2250-3000°F, with no real certainty in its value at any temperature. The resistance to oxidation of metallic structural materials also tends to decrease rapidly with increasing temperature.

It would be very convenient indeed if no more than 0.3 void fraction and 2250°F maximum wall temperature were required to make a nuclear ramjet feasible; this combination, however, leads to virtually zero thrust even with the idealized reactor configuration. Indeed, both the combinations 0.3 and 2500°F, and 0.4 and 2250°F lead to marginal performance. Therefore, for further calculation of performance involving more realistic reactor configurations, a void fraction of 0.4 and a maximum wall temperature of 2500°F were chosen.

For flight at 1000 ft altitude and 100°F ambient temperature, there is in general a very clear-cut optimum flight Mach number varying from Mach 3.0 to Mach 3.25 as the maximum wall temperature is increased from 2250 to 3000°F. For a void fraction of 0.4, the net thrust coefficient at Mach 2.5 is in general less than one-third that at the Mach 3.0-3.25 maximum, indicating low probability of flight at that speed. Therefore, a flight Mach number of 3.0 was chosen as the most probable "design" speed of a real nuclear ramjet.

A more realistic reactor has end reflectors; the ideal isothermal wall power distribution will probably be achieved, even with uranium loading variation, only with the help of a thick entrance reflector to raise the neutron flux and power toward an exponential shape. The more efficient heat-transfer is attained, however, at the expense of increased pressure drop due to the lengthened flow passage, and increased reactor weight.

A bare cylindrical reactor without variation in uranium loading has a simple sinusoidal axial power distribution. For the same maximum wall temperature and same length as the unreal bare isothermal wall reactor, the exit air temperature is greatly reduced with a consequent loss in performance. If the reactor length is increased to bring the exit air temperature back up, the performance suffers due to the increased pressure drop.

Between these extremes there is a compromise reactor which does not suffer too great a performance penalty due to non-ideal power distribution and

does not suffer too great a weight penalty from the end reflectors. This reactor is described approximately as having an inlet reflector of length equal to 20% of the core length and an exit reflector of 5% length, and a power distribution in the core in the shape of a sine curve cut off at 3/4 amplitude before the maximum and 1/4 amplitude after the maximum. This shape gives conservative results, as it will undoubtedly be feasible to further optimize the axial power distribution through variation of fuel loading. This idealized shape is compared with the real axial power distribution of Tory II-A (no axial variation in fuel loading) in Fig. 5-23.

The core length is chosen as about 40 inches as a compromise between neutronic demands for increased length and a desire to minimize weight. A reasonable ramjet "reactor" diameter (for 85% of the body area) is 4 feet, from both neutronic and performance considerations.

On the basis of the selected reactor and flight parameters, and within the framework of the assumptions made above, a calculation was made of the thermodynamic performance and geometry of a nuclear ramjet nacelle optimized in reactor-exit-air stagnation temperature, reactor-exit Mach number, and nozzle-exhaust static pressure. Characteristic reactor dimensions of the ramjet and Tory II-A are listed in Table 5-10; the operating conditions of the two reactors are listed in Table 5-11; and Table 5-12 describes the flight conditions, dimensions, and performance of the nuclear ramjet nacelle. Figure 5-24 illustrates the general configuration of the nacelle.

The final basic criterion of performance is the wing-and-tail lift in Table 5-12 which, from weight studies,[2] appears to be more than adequate for the Pluto mission.

5.3.2 Detailed Calculations for Tory II-A

After determination of the regions of interest in flow passage size, flow rate, inlet and exit temperatures, pressures and Mach numbers, and core power density, a great deal of analysis becomes necessary to establish detailed operating characteristics of the reactor. A number of problem areas will be discussed below, with mention of the calculational methods used and with a discussion of results obtained.

Steady-State Flow in Simple Passages

The Floss code (mentioned earlier) calculates single-tube, steady-state, forced-convection heat transfer, heat conduction in the wall material, pressure

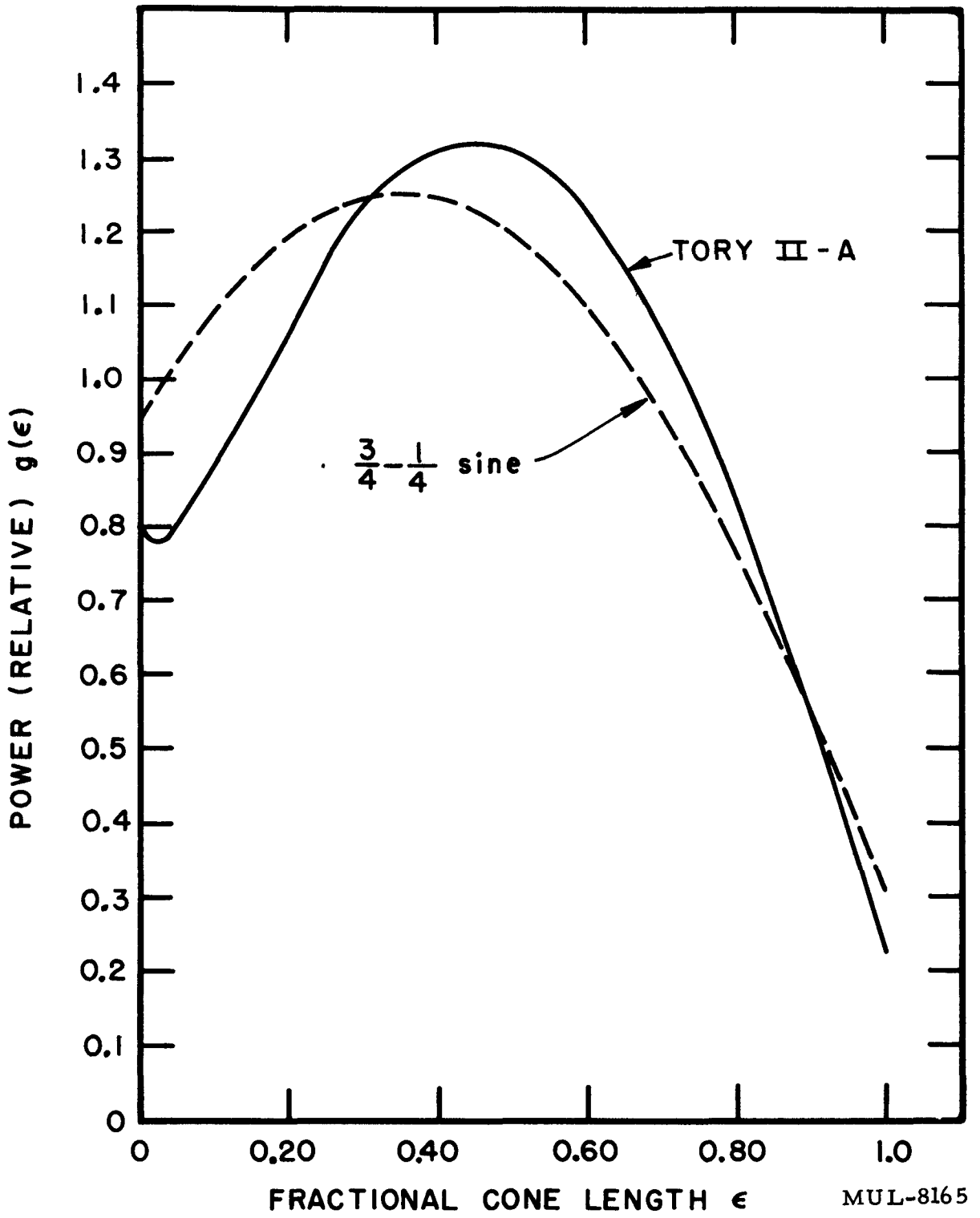

Fig. 5-23. Comparison of axial power distributions.

Table 5-10. Reactor dimensions

	Ramjet	Tory II-A
Core length	44 in.	44.5 in.
Inlet reflector length	8 in.	6 in.
Exit reflector length	2 in.	2 in.
Flow passage diameter	0.230 in.*	0.215 in.
Closest spacing of flow passage centers	0.30 in.	0.30 in.
Fuel element average void fraction	0.53	0.49
Average void fraction (85% of body area)	0.4	†
% core area available for fuel elements	85.4	85.6
Core diameter	45.0 in.	32.7 in.
Core-reflector gap thickness	0.5 in.	†
Reflector thickness (Be)	3.0 in.	†
Body diameter	52.0 in.	†

* Optimized quantity.

† No valid comparison exists between Tory II-A and an engine where components outside the core are concerned.

Table 5-11. Reactor operating conditions

	Ramjet	Tory II-A
Total power (Mw)	474	157
Core average power density (Mw/ft^3)	11.7	7.3
Fuel element average power density (Mw/ft^3)	13.7	9.4
Peak fuel element power density (Mw/ft^3)	17.2	12.5
Axial power distribution	3/4-1/4 sine	(See Fig. 5-23)
Inlet air stagnation temperature (°F)	1063	1063
Maximum wall temperature (°F)	2510	2250
Fuel element exit air stagnation temperature (°F)	2165*	1940
Mixed exit air stagnation temperature (°F)	2165	1770
Flow rate per fuel element (lb/sec)	0.0839	0.0714
Exit Mach number	0.68*	0.50
Inlet stagnation pressure (psia)	357	357
Exit stagnation pressure (psia)	226	235 (after 5% loss)

* Optimized quantity.

Table 5-12. Ramjet description

Flight Mach number	3.0
Altitude (feet)	1000
Ambient temperature (°F)	100
Dynamic head ($lb/in.^2$)	89.7
Isentropic-cone half-angle	10°
Half-angle to lip	20°
Pressure recovery factor includes subsonic diffuser efficiency of	0.66 0.95
Capture-area diameter (in.)	33.5
Nose length — minimum (feet)	12.2
Nozzle divergence factor	0.98
Velocity coefficient	0.97
Nozzle throat diameter (in.)	28.9
Nozzle exhaust diameter (in.)	47.4
Nozzle area expansion ratio	2.70
Boat-tail length (feet)	5.2
Nozzle exhaust pressure (psia)	15.5*
Maneuvering factor (maximum nacelle thrust/wing-and-tail drag)	1.5
Wing-and-tail lift/drag	5.0
Nacelle drag coefficient	0.0739
Reference area	0.85 of body area
Nacelle net thrust coefficient	0.0838
Wing-and-tail lift (lb)	45,000

* Optimized quantity

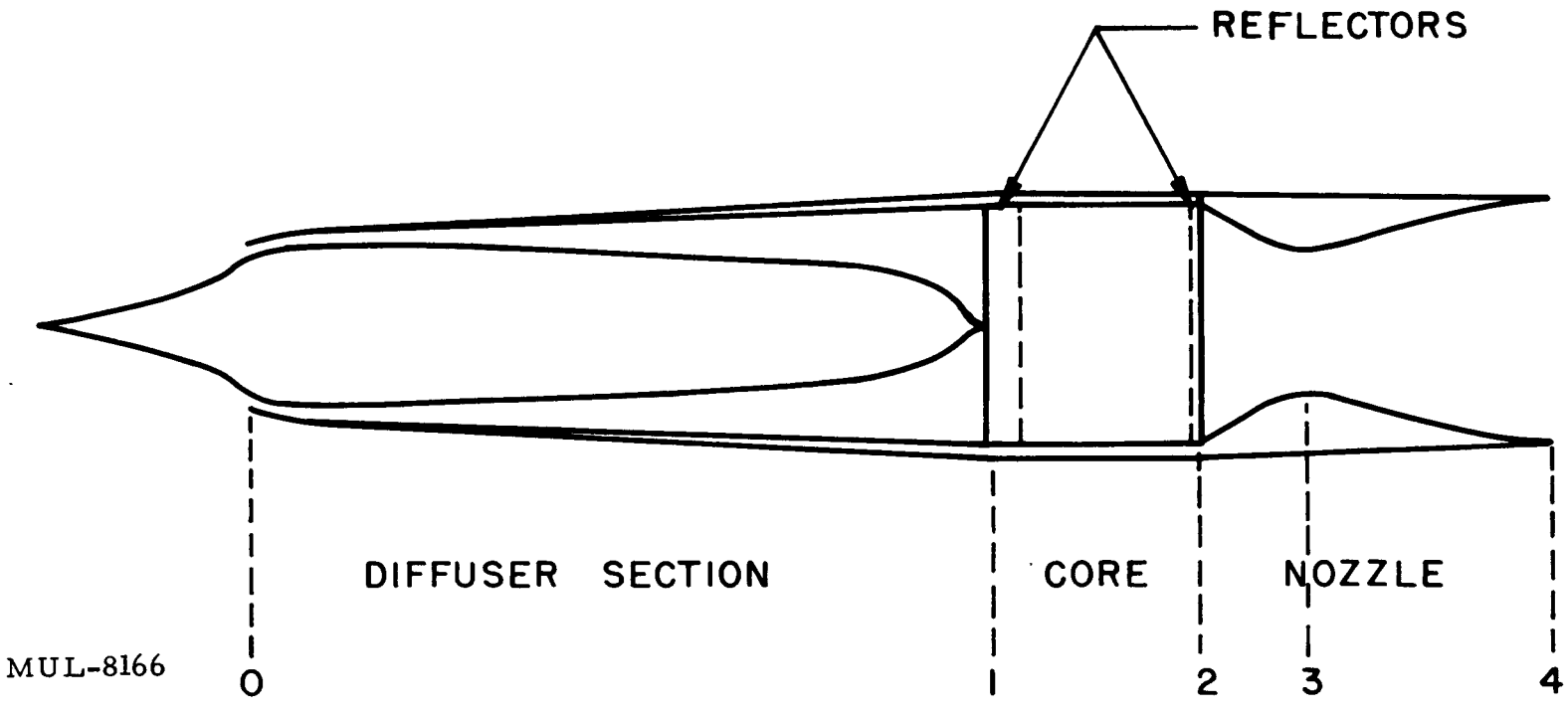

Fig. 5-24. Typical nuclear ramjet nacelle.

drop, and velocity change in gas flow at twenty axial stations from local heat transfer coefficients [Eq.(1)] and friction factors [Eq.(3)], with use of the exact momentum equation for gas flow [Eq.(4)]. The air temperature profile, fuel element wall temperature axial profile, internal temperature profile, and pressure profile including end reflector sections are found with this code (see Figs. 5-25 and 5-26).

Any cooling passage that may be treated as a single circular tube to a first approximation is investigated with this code: the tie-rods, the cooling annulus in the shroud, and the various shaped incidental voids formed by the hexagonal surface of the fuel elements and the adjacent structural members. Flow rates and axial temperature profiles are obtained (see Table 5-13) consistent with the core pressure drop and the local gamma-ray heating.

With the assumption that the overall behavior of the core is characterized by the behavior of an average fuel element, a thermodynamic performance map for Tory II-A was calculated with the Floss code, giving the dependence of flow rate and exit gas temperature on reactor power and inlet stagnation pressure. A range of power from full to 2% of full power, and pressure from 357 psia down to minimum nozzle-choking pressure for inlet gas temperatures of 80°F, 710°F, and 1063°F are considered. The results are shown in Figs. 5-27, 5-28, and 5-29.

Variation of Radial Temperature Profile

Calculation was made with the Flash Univac code of the steady-state axial wall temperature distribution and air flow in each of ten parallel fuel elements, dissimilar only in power and axial power distribution, fed by a common inlet plenum, and emptying into a common exit chamber terminated by a subsonic-supersonic nozzle. The wall temperature at ten axial stations was calculated from local heat transfer coefficients [Eq.(1)] and the pressure drop from inlet to exit was calculated by the approximate integral of the exact momentum equation [Eq.(5)]. Since Tory II-A experiences a change in the shape of the radial neutron flux distribution with temperature, variation of the fuel loading radially can assure a flat radial power distribution at only one average core temperature (Fig. 5-30); this code is necessary to calculate the deviation from a flat radial temperature distribution at core temperatures and operating conditions other than those of the design operating point.

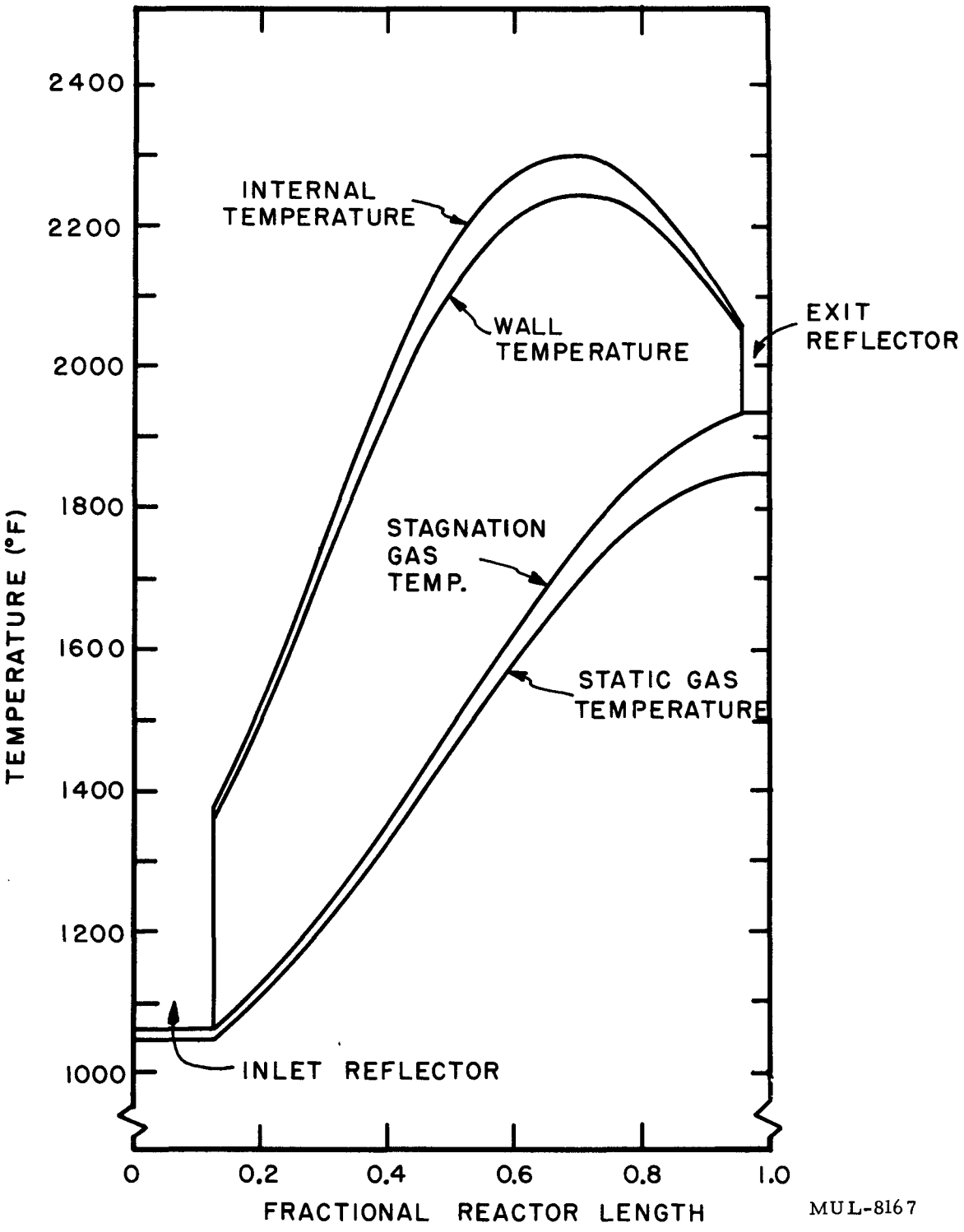

Fig. 5-25. Fuel element temperature contours.

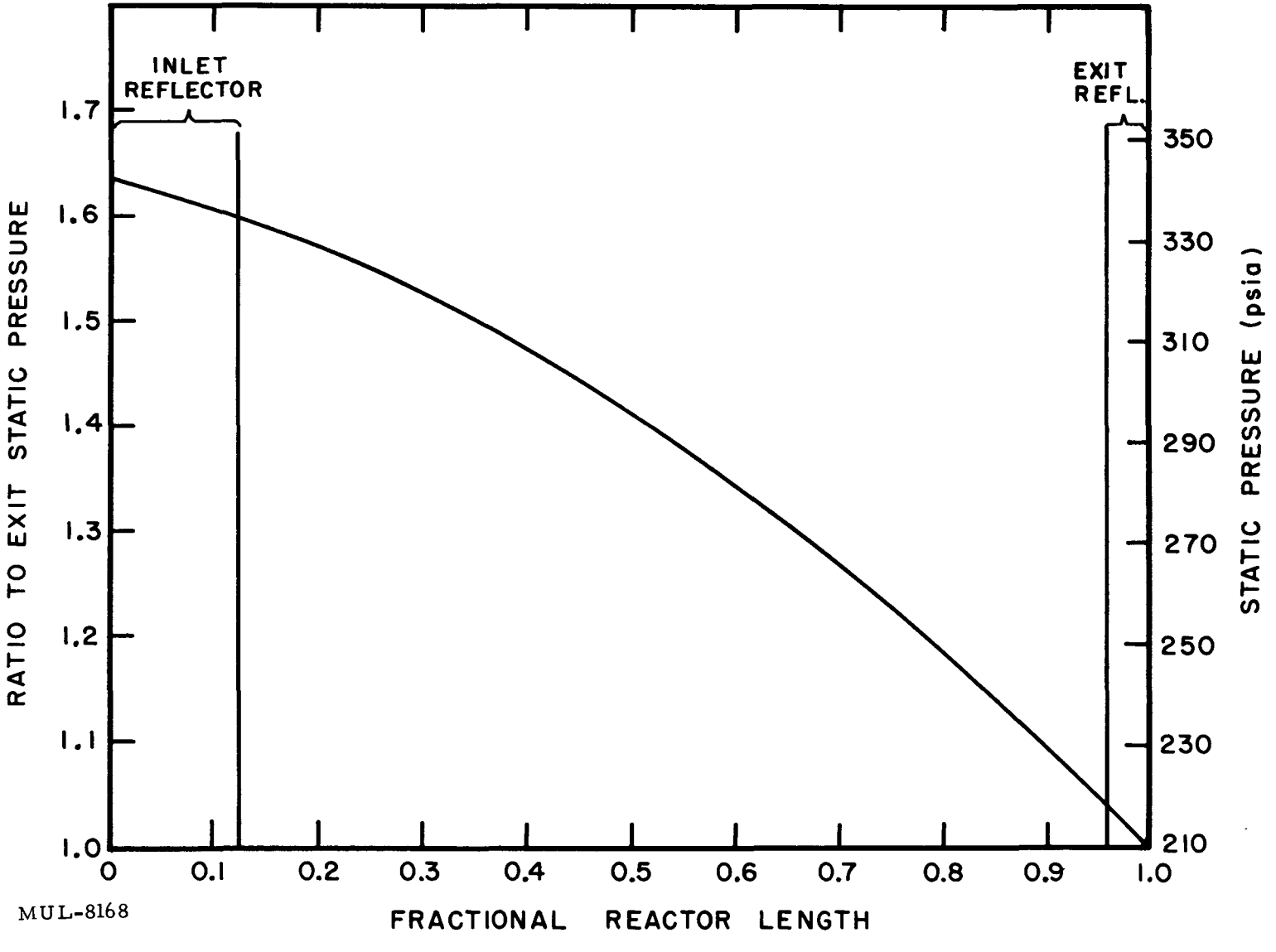

Fig. 5-26. Fuel element static pressure profile.

Table 5-13

Operation of various Tory II-A flow passages under conditions at full temperature ($T_{w_{max}}$ * = 2250°F in fuel tubes), and full inlet pressure (p_1^0 = 357 psia)

Passage	Number	Power/Each (kw)	Flow/Each (lb/sec)	Total flow (lb/sec)	T_2^0 † (°F)	$T_{w_{max}}$ * (°F)	M_2	M_1	$D_{effective}$ (in.)
Fuel element	8623	18.23	0.0715	616	1935	2250	0.50	0.24	0.2165
Tie-rod (and eye)	72	47	1.15	83	1210	1570	0.70	0.40	0.695
Shroud	1	900	70	70	1100	1160	0.60	0.40	0.500
Triangles	1400	1.3	0.015	16	1950	2060	0.30	0.14	0.080
Total other incidental voids				~20	~ 1700				
Total, average		163 Mw		850	1782				

* $T_{w_{max}}$ is wall temperature.

† T_2^0 is exit air temperature.

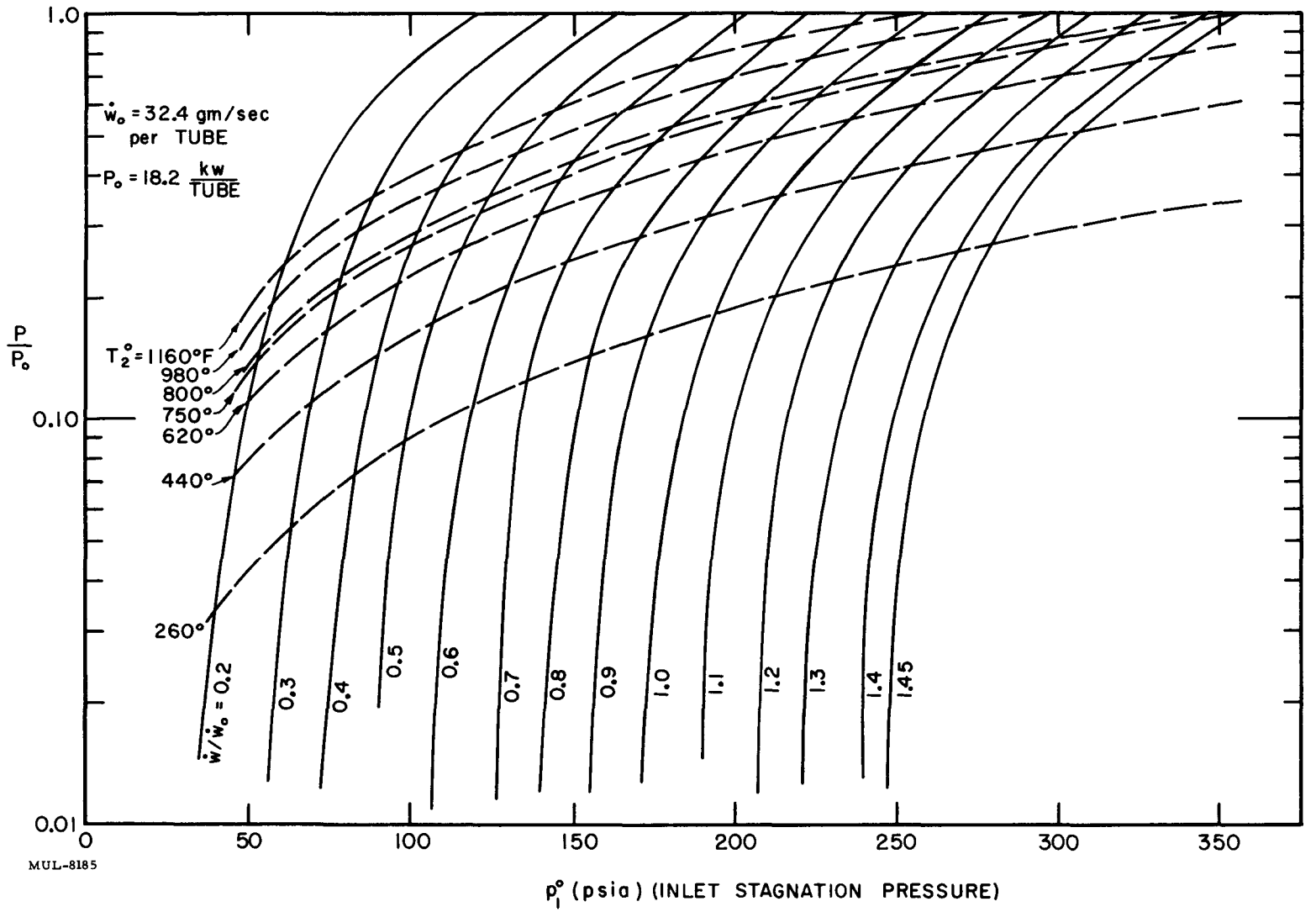

Fig. 5-27. Thermodynamic performance chart for inlet air temperature of 80°F.

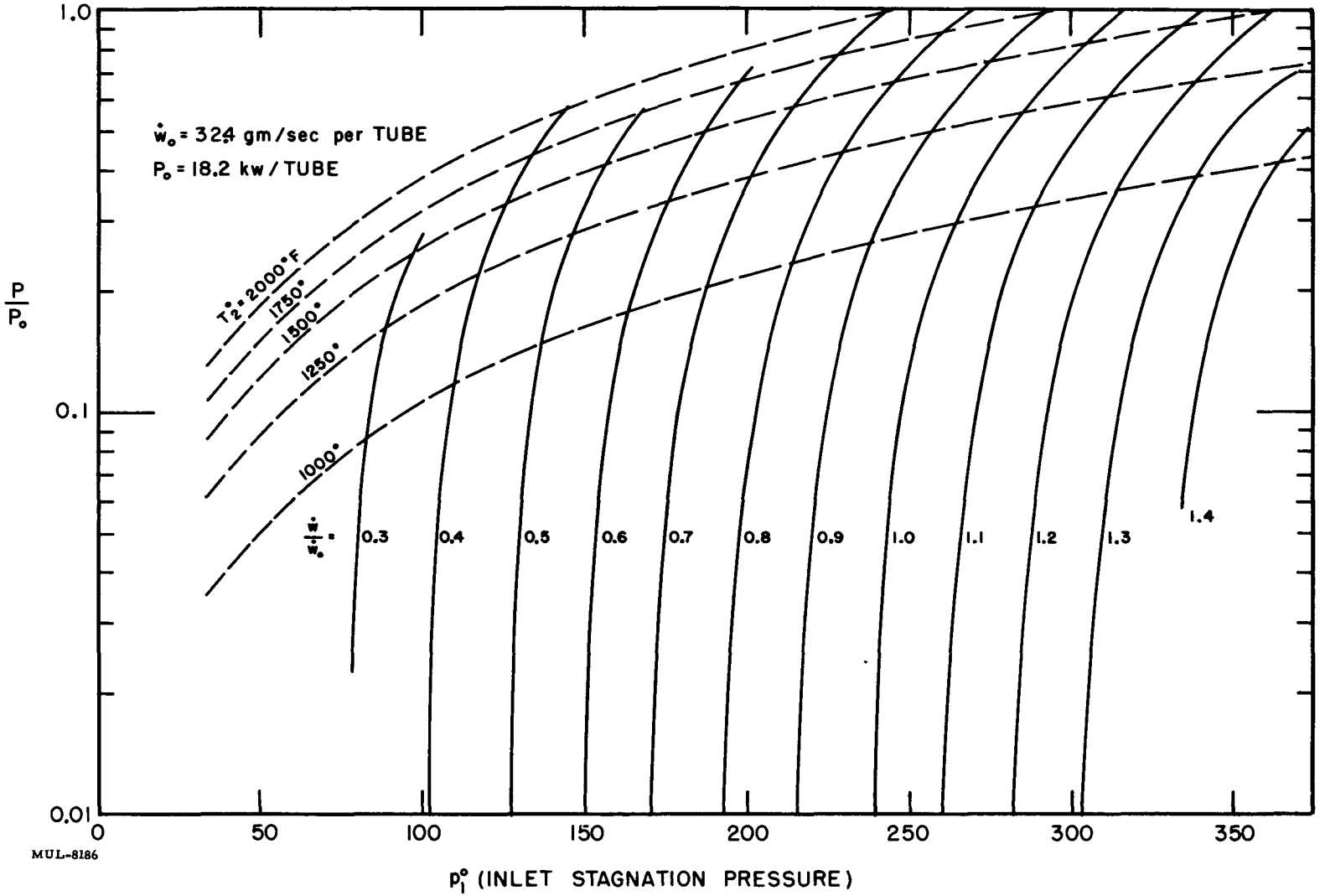

Fig. 5-28. Thermodynamic performance chart for inlet air temperature of 710°F.

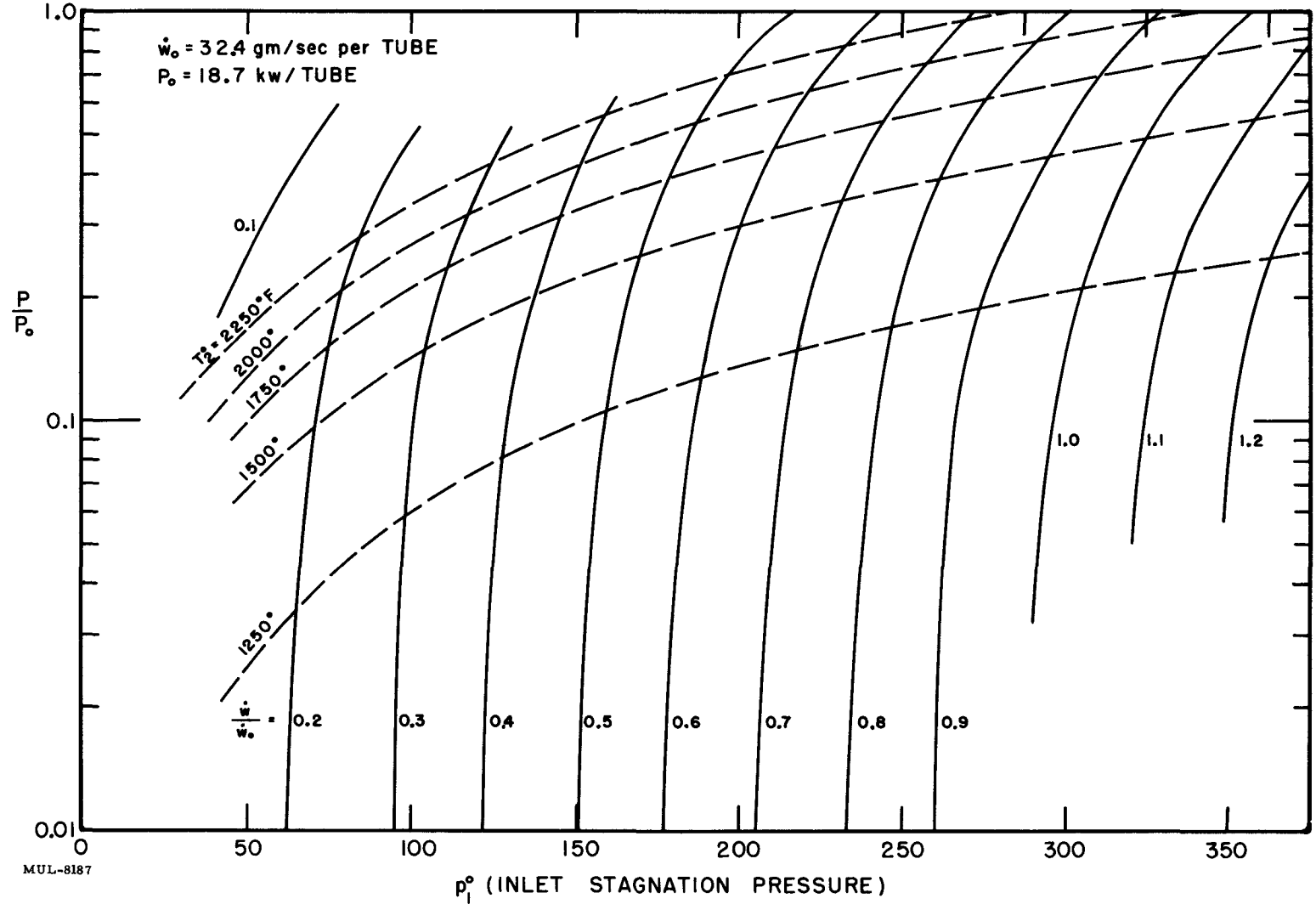

Fig. 5-29. Thermodynamic performance chart for inlet air temperature of 1063°F.

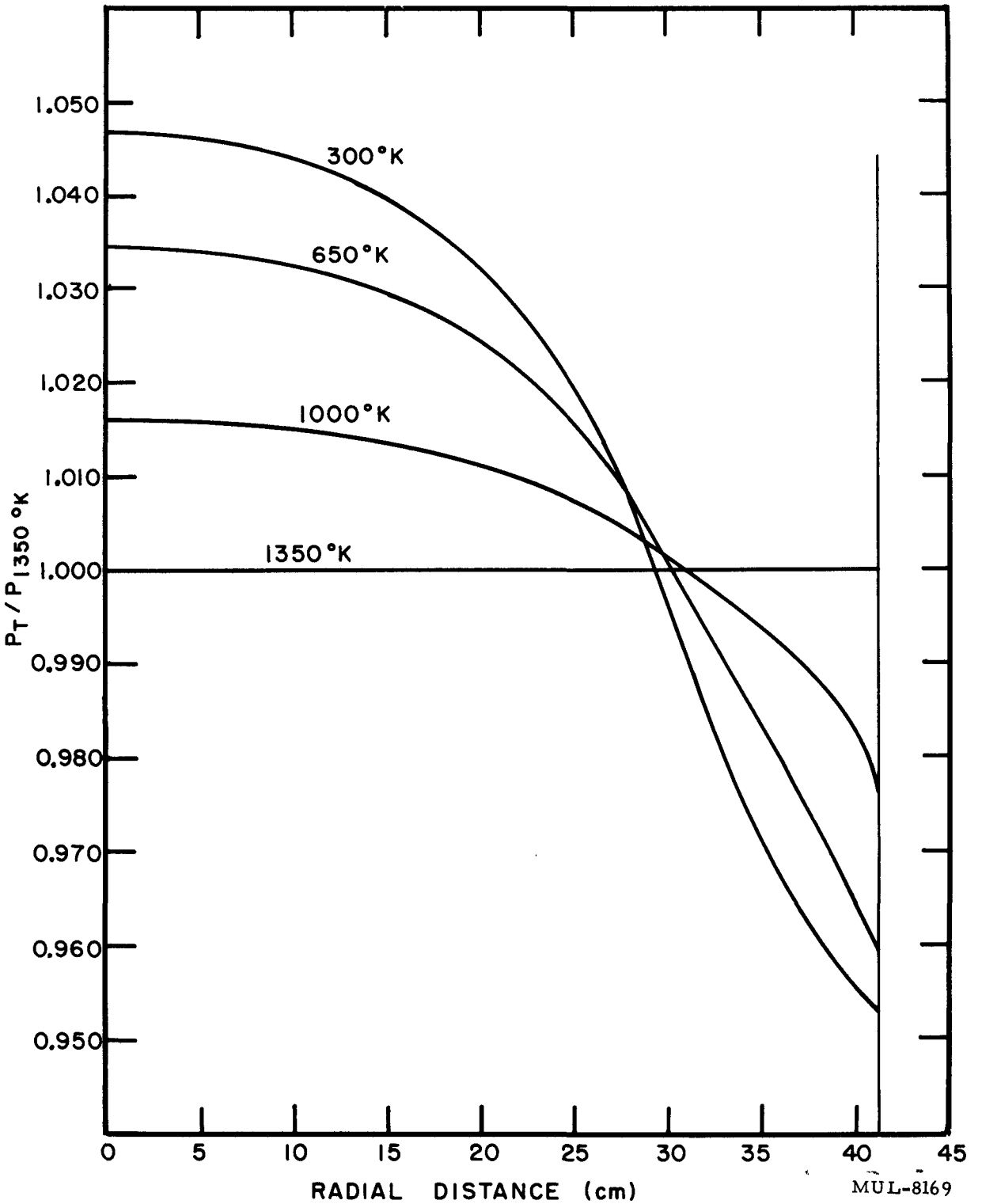

Fig. 5-30. Off-design-temperature radial power distribution.

Detailed calculational results are not yet available for the present reactor design; however, its behavior is well understood from the following data: An early (since superseded) configuration for Tory II-A, when loaded to give a flat radial power distribution at full temperature in neutronic calculations, showed a 30% peak-to-peak deviation from flat power at room temperature. A series of Flash code calculations for this configuration at many different operating conditions for both 80 and 1063°F inlet air temperature, giving complete core temperature maps, indicate that any operating condition which leads to an average core temperature midway between the inlet gas temperature and the design operating temperature gives a worst radial temperature disparity, with little dependence on the values of power and flow rate. The maximum radial temperature difference obtainable at any axial station was about 70°F for 1063°F inlet gas temperature and about 300°F for 80°F inlet gas. The present Tory II-A room temperature radial power distribution has been greatly reduced in its deviation from flatness: The former 30% deviation has been reduced to 9%, and the dissimilarity of the center and edge axial power distribution shapes has decreased. The worst radial temperature disparity is consequently estimated at less than 100°F. No Flash temperature map calculations have been made for the up-to-date design, but the Floss code, with the approximation that the core exit Mach number is equal to 0.5, independent of temperature, was used to calculate the core temperature map for only the two operating temperatures midway between the two inlet gas temperatures and the core design temperature. The radial temperature disparities found in this way are indeed less than 100°F, being 20°F for 1063°F inlet gas and 90°F for 80°F inlet gas.

Temperature Distribution Within Fuel Elements

A steady-state relaxation-method calculation of the detailed temperature distribution within the fuel-element walls was made, with the results shown in Fig. 5-31.

To aid in thermal stress calculations, a comparison was made with the temperature distribution resulting from the simplifying assumption that the outer fuel element boundary is a circular cylinder enclosing the same cross-sectional area as the actual hexagon. As might be expected, the radial temperature difference between the inside surface and the corners of the hexagon is higher than that in the approximating annular cylinder, but it exceeds the

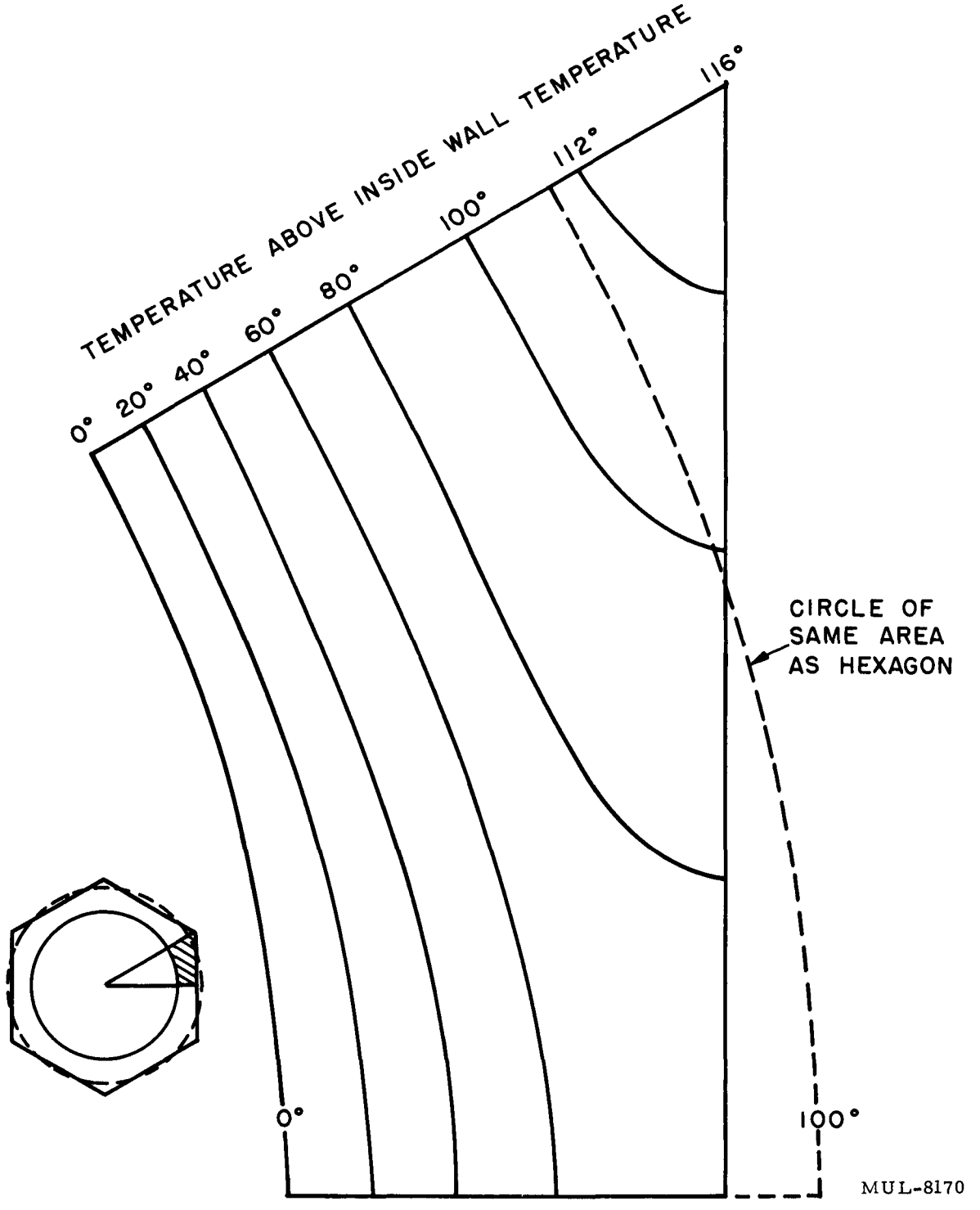

Fig. 5-31. Comparison of temperatures within the wall of a hexagonal fuel element and an approximating annular cylinder.

annular cylinder difference by less than 20%. Estimates of the resulting thermal stresses fail to show any significant difference (5%) between the two configurations. A more detailed discussion has been given in a separate report.[14]

Transient Conditions

A Univac code (Tride) has been set up for the calculation of transient temperature conditions in a single heat-transfer tube extending the length of the reactor. This code calculates gas temperature and internal fuel-element temperature distribution at each of a number of stations along the length of the tube.

The calculation is based on local heat-transfer coefficients and steady-state one-zone hydrodynamics [Eq.(5)], with fixed exit Mach number and programmed inlet stagnation pressure and temperature. Thus for various types of startup and shutdown programs, for power surges, and for sudden changes in the inlet gas temperature, the time-dependent temperature distribution within and along the wall of a characteristic fuel element may be calculated. Thermal stresses resulting from the radial temperature distribution in the wall for drastic temperature changes may then be evaluated.

Some specific problems which have been studied are the following:

Startup—

1. sudden application of full power and air flow,
2. linear ramp increase of flow rate with exponential rise in power,
3. sudden application of ten times full power with negligible flow rate;

Shutdown—

4. instantaneous reduction of power to zero with full continuing flow rate;

General operation—

5. instantaneous, and
6. linear ramp changes in inlet air temperature.

The parameters used for these calculations, somewhat different from current values, were:

$T_1^0 = 1063°F$	$a = 0.115$ in.
$M_2 = 0.75$	$P_0 = 27.9$ kw per tube
$L = 39$ in.	$p_1^0 = 357$ psia

The instantaneous application of full power and flow rate is, of course, more drastic than the ramp startup, but still results in a quite gradual buildup of wall temperature and temperature gradient very nearly reaching steady-state values in about 15 seconds (Fig. 5-32).

Sudden application of ten times full power for essentially zero flow results in a very rapid change in core temperature, reaching full design temperature in a small part of a second (Fig. 5-33), but with a maximum temperature difference within the wall less than one-fifth that for steady-state full power and temperature (Fig. 5-34).

For instantaneous power shutdown with constant inlet gas temperature and pressure, the temperature and wall temperature difference drop exponentially, with the wall temperature difference dropping to one-tenth of that at steady-state full power and temperature in about 5 seconds (Figs. 5-34 and 5-35).

A sudden change in inlet gas temperature from 1060°F to room temperature develops large wall temperature differences (near those for steady-state full power and temperature) and, hence, high thermal stresses at the inlet end of a hot flow passage for a few tenths of a second after the change. Lengthening the time for the change to about 3 seconds is required before the peak transient thermal stress is cut in half. No other hazardous transient situation is found.

Structural Links and Adjacent Fuel Elements

Calculations (Triangle code) were made of the steady-state temperature coupling between the core structural links and adjacent fuel elements. This coupling, principally involving thermal radiation and convective heat transfer through air in the triangular passages between fuel elements and links, as well as gamma heat deposition in the links, was studied for various powers, flow rates, and relative gamma-ray heating rates.

Investigation of the temperature of the structural links is required to determine the effect of differential thermal expansion on the fit of fuel-element bundles within their surrounding links, as well as the load-carrying capacity of the links. Results indicate that convective coupling is so tight due to the high heat-transfer coefficient and low flow in the triangular passage that radiative transfer is relatively negligible, with the greatest steady-state separation in temperature between the links and the adjacent fuel elements being less than 150°F. These fuel elements, however, are reduced in temperature

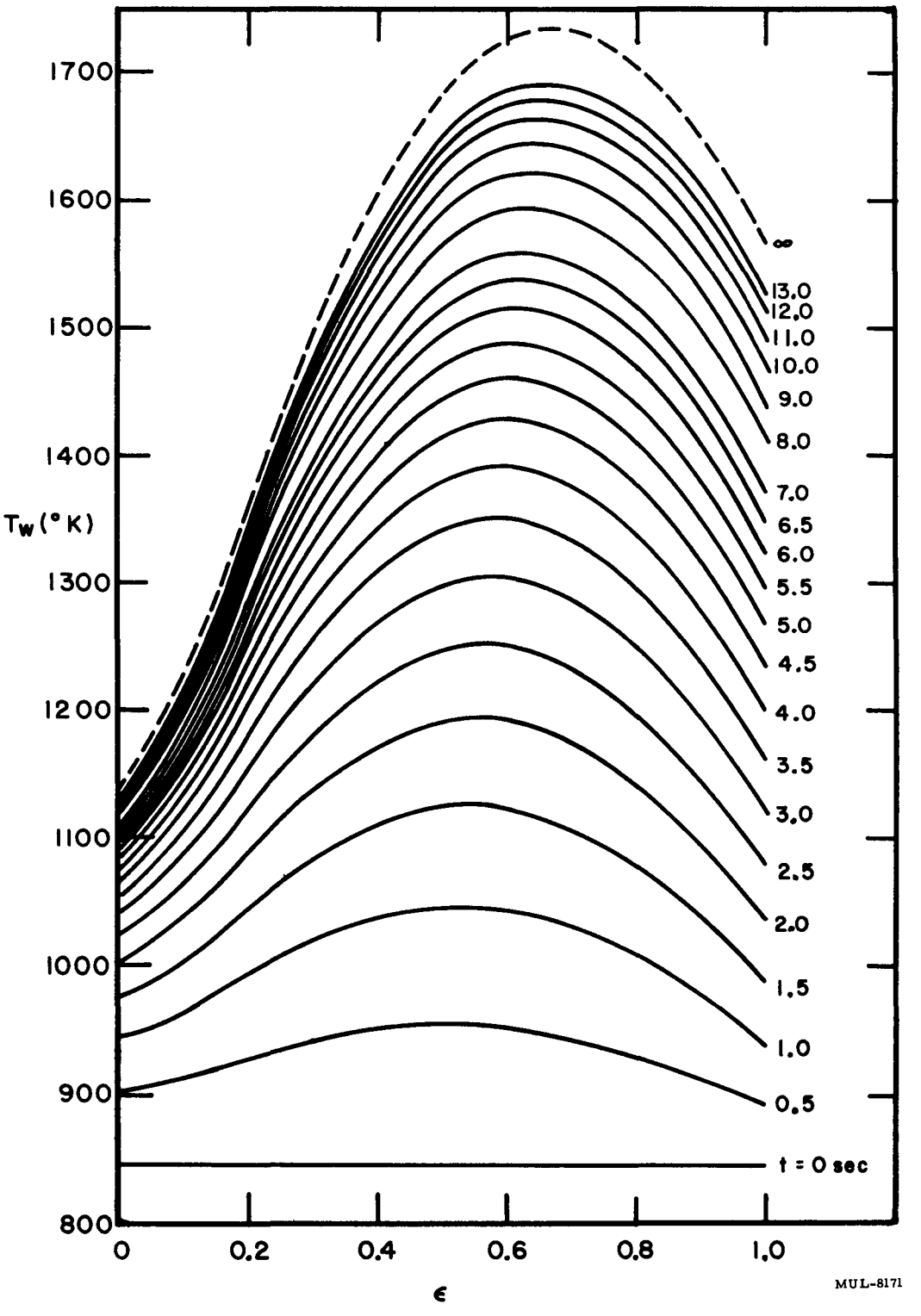

Fig. 5-32. Fuel element wall temperature buildup.

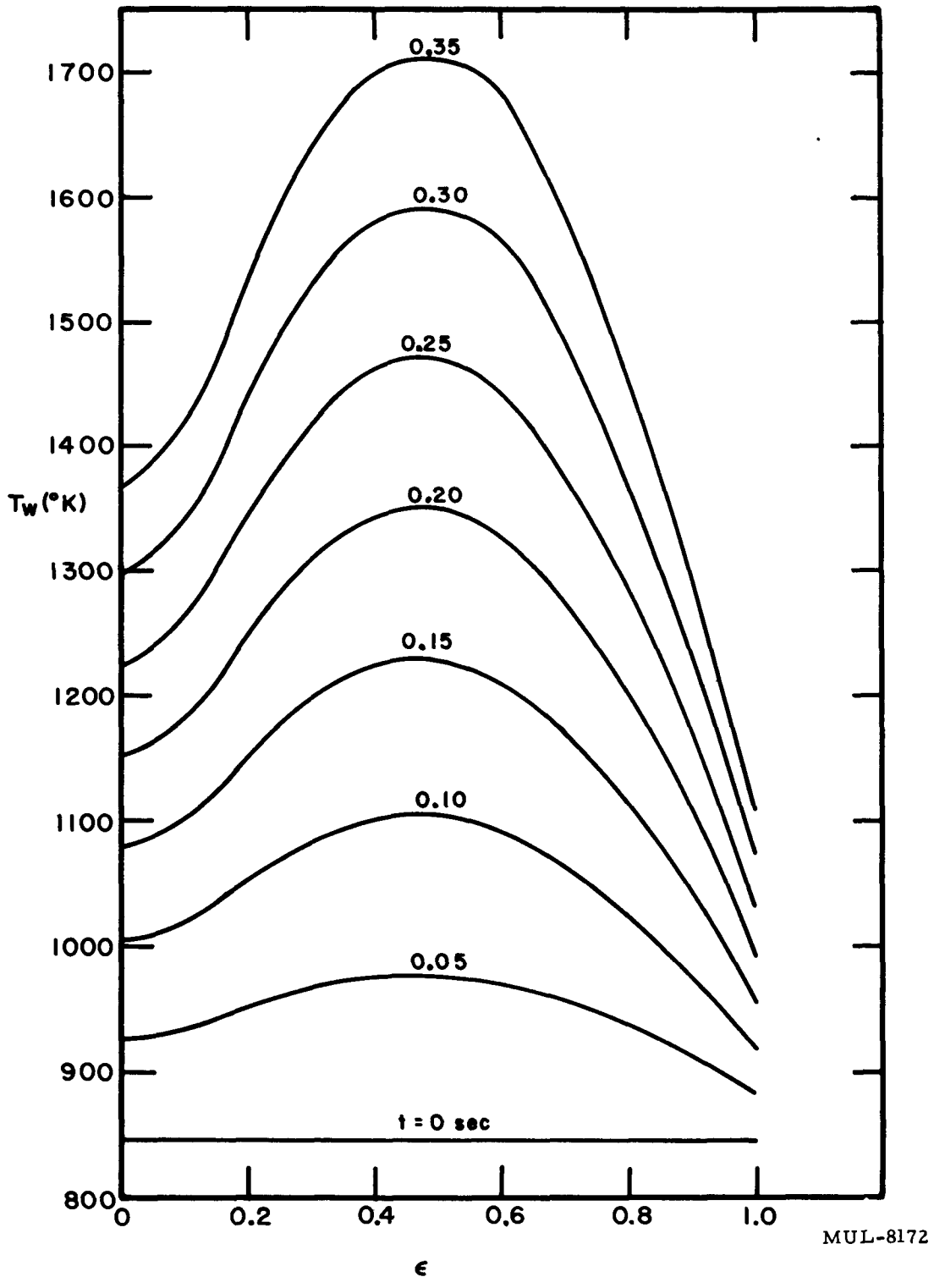

Fig. 5-33. Wall temperature buildup for ten times design power.

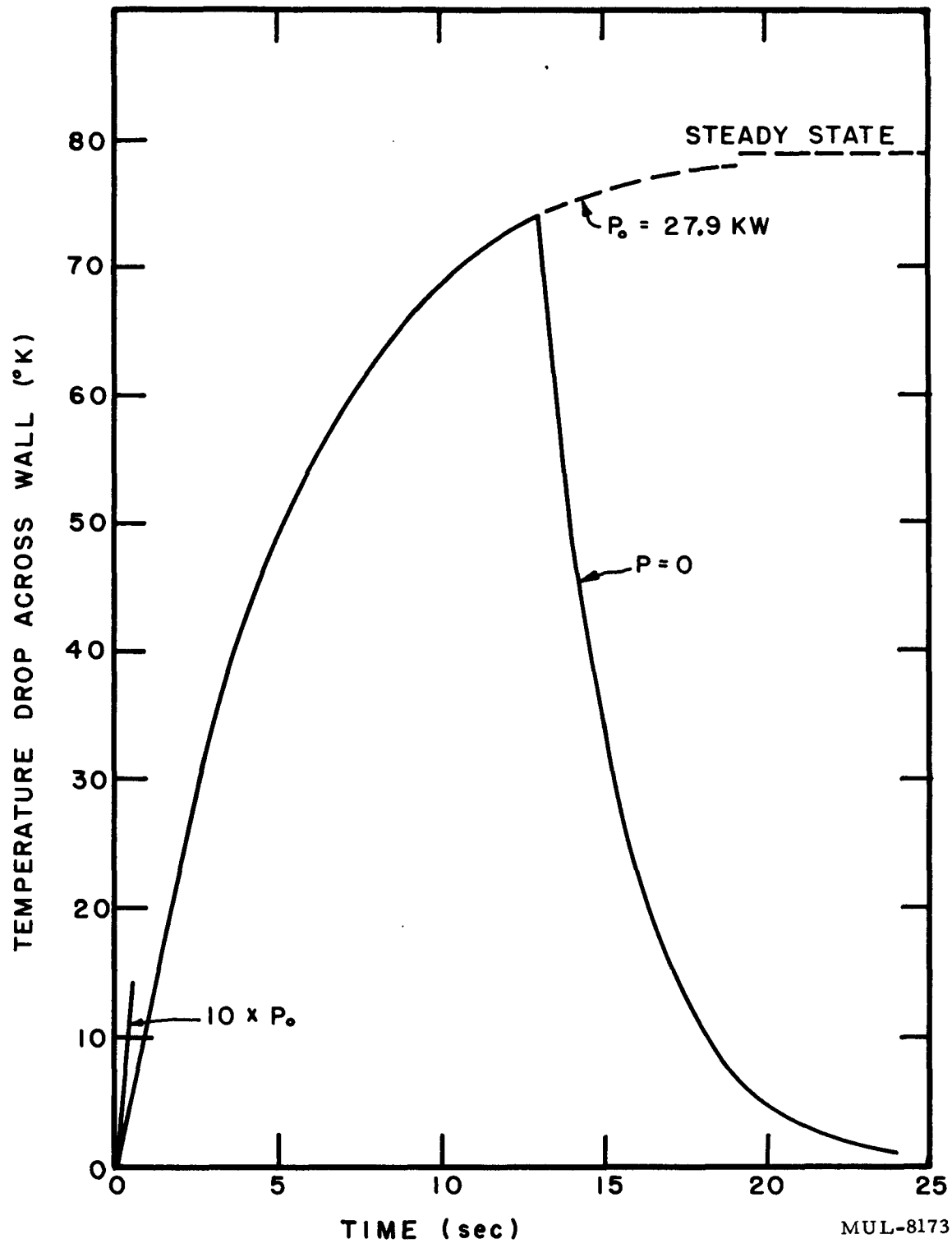

Fig. 5-34. Fuel tube wall temperature difference vs time, at axial station $\epsilon = 0.5$.

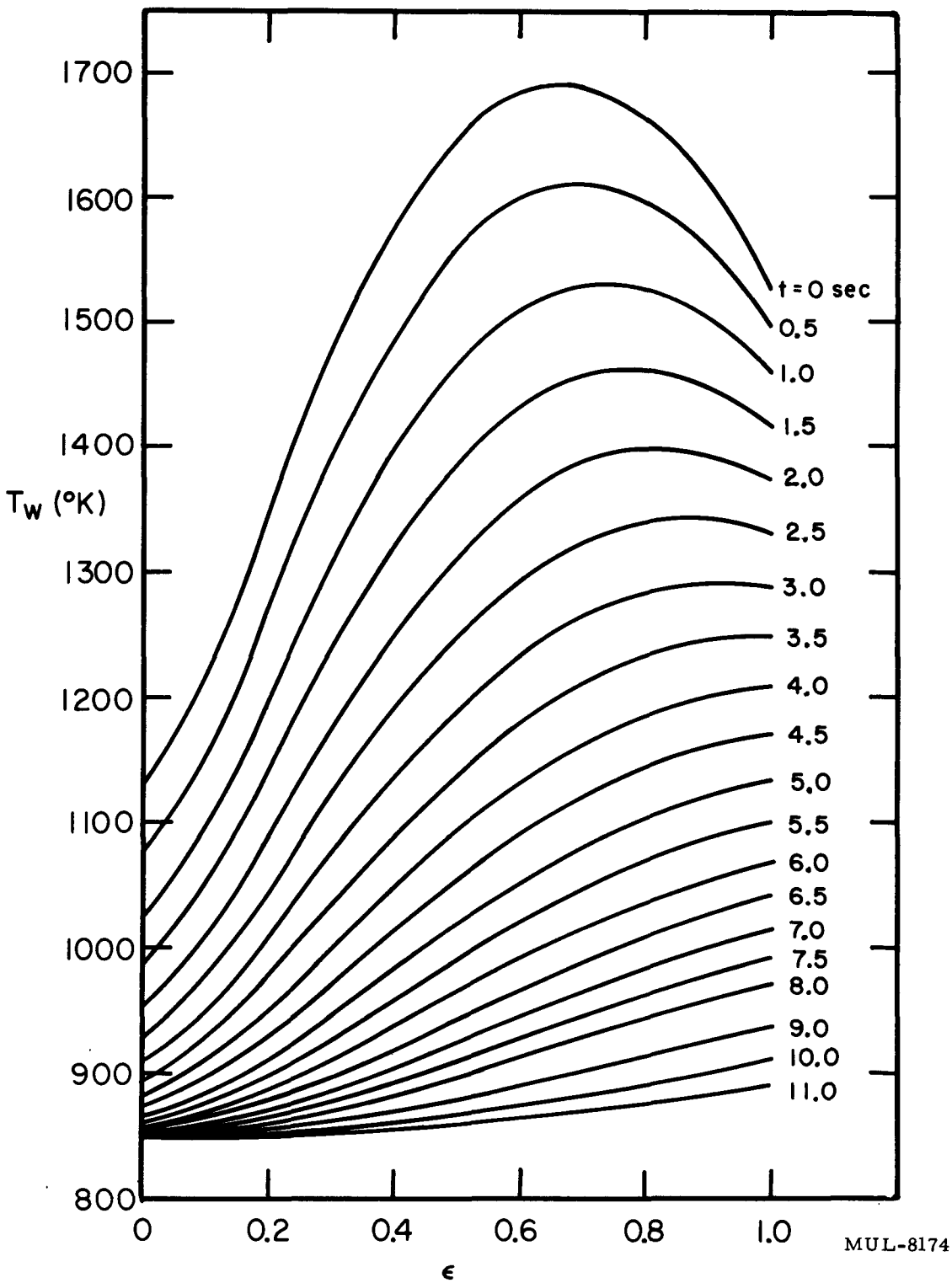

Fig. 5-35. Wall temperature decrease in shutdown.

below unperturbed fuel elements by about 200°F. Figures 5-36 and 5-37 show link, fuel-element and air temperatures for full power blowdown operation (157 Mw, 805 lb/sec) and for operation with air supplied by the blowers (7.1 Mw, 28.4 lb/sec).

A pseudo-time-dependent calculation, accounting for thermal capacity of the links absorbing part of the gamma heat, gave an estimate of the expected temperature lag of the links in startup. For startup steady power levels of about 7 Mw, with blowers supplying 28 lb/sec of air, a maximum structural link temperature lag of 150°F is obtained with a ramp increase to full temperature in 15 minutes.

Design Operating Characteristics

A summary of the design characteristics of Tory II-A, with respect to its performance as a heat-transfer device, is given in Table 5-13.

Table 5-13. Reactor operating characteristics

Power density	
Averaged over total core volume	7.28 Mw/ft^3
Averaged over tube and hole volume	9.39 Mw/ft^3
Total power	157 Mw
Power per flow tube	18.23 kw
Peak core temperature	2305°F
Tube wall temperature (max)	2250°F
Inlet air total temperature	1063°F
Discharge air total temperature (from fuel tubes)	1936°F
Total pressure	
Inlet	357 psia
Discharge (after expansion loss)	235 psia
Air flow rate	
Fueled tubes	618 lb/sec
Tie-rod cooling	97 lb/sec
Shroud annulus	65 lb/sec
Gaps next to links	25 lb/sec
Total	805 lb/sec
Air flow rate per tube	32.4 g/sec
Tube inlet Mach No.	0.244
Tube exit Mach No.	0.500

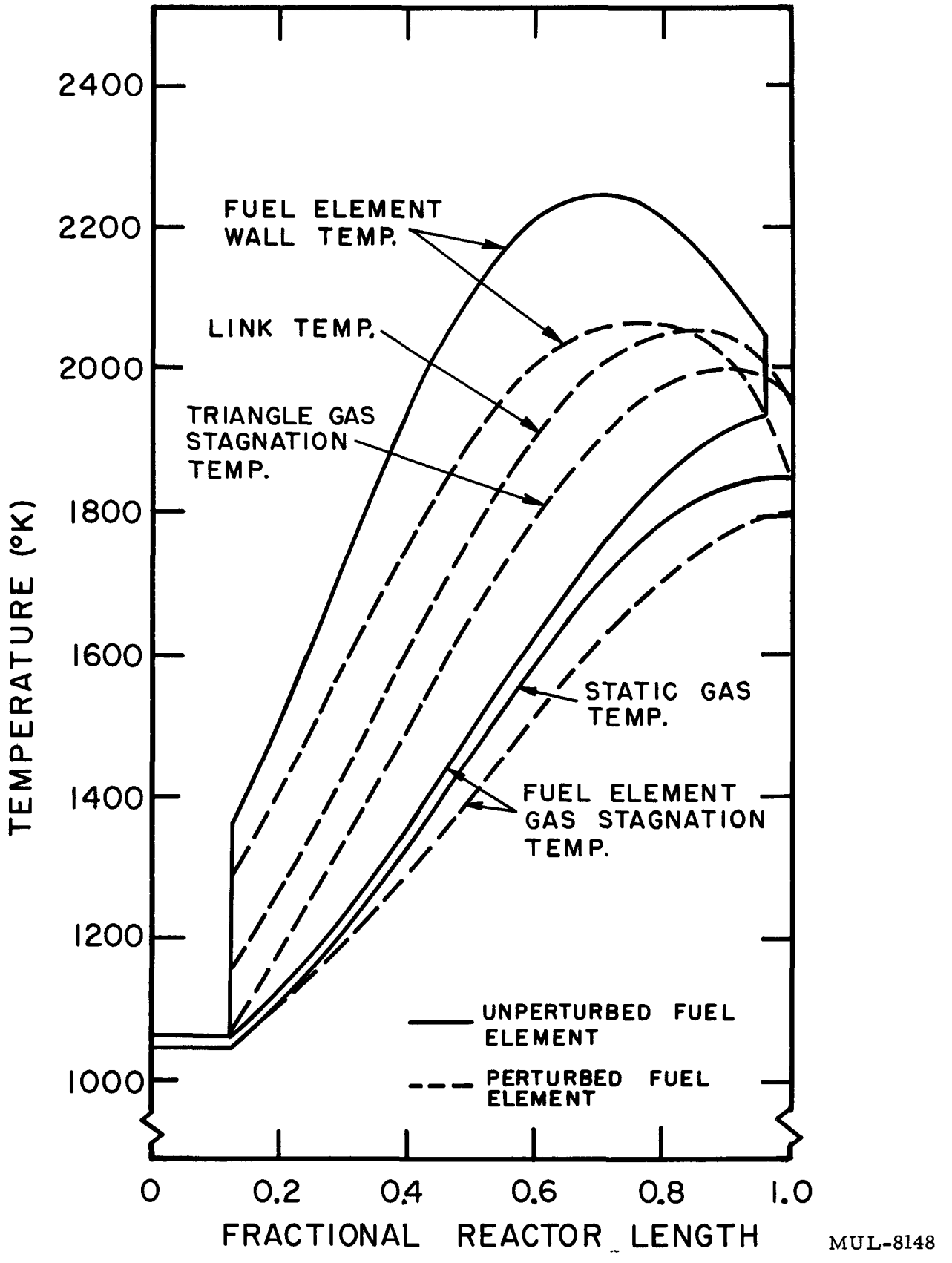

Fig. 5-36. Fuel element-internal link temperature contours (full power).

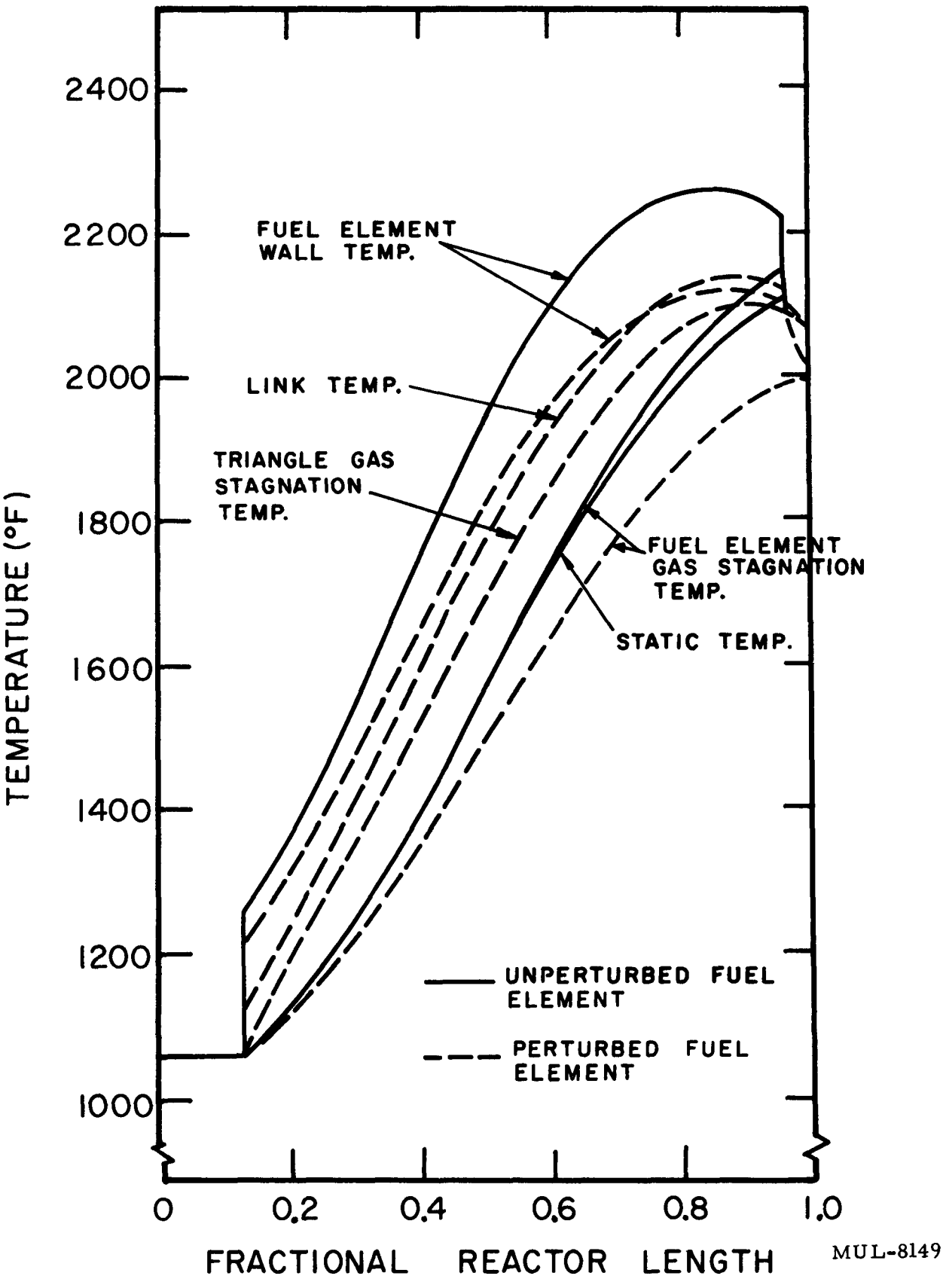

Fig. 5-37. Fuel element-internal link temperature contours (blower operation).

5.3.3 Inlet Diffuser Operation

It is desirable to have a choked nozzle-diffuser system upstream from the Tory II-A test reactor for several reasons. The primary purpose is to separate the reactor from the air supply in such a manner that fluctuations in reactor operating conditions (power level, pressure drop, etc.) cannot be felt by the air supply system. Consequently, a steady flow rate can be maintained which depends only on upstream regulator and heater controls. This separation can be accomplished by maintaining a sonic section (choked nozzle) between the air supply and the reactor. Furthermore, a diffuser system as described herein will give rise to shock-induced turbulence representative of the flow in an actual ramjet application. A choked nozzle also provides an accurate method of measuring the system flow rate.

To give background information for choice of the Tory II-A diffuser design, a discussion is given here of three alternate designs, with reasons for selection of the third as most suitable for our use.

Diffuser Operating Range and Design Criteria

The diffuser must operate satisfactorily over a rather large range of reactor conditions, namely:

Reactor inlet stagnation pressure	0-360 psia
Reactor inlet stagnation temperature	70°F-1070°F
Reactor stagnation temperature ratio (exit/inlet)	1 to 2

Given a set of these three parameters, the reactor thermodynamic characteristics are completely determined, provided the exhaust nozzle is choked. The only reactor parameters, however, that affect the diffuser design (other than scaling effect) are reactor pressure ratio and temperature ratio (these ratios refer to the ratio of stagnation conditions across the reactor). That this is the case can be seen by referring to the calculations presented herewith. As a basis for discussion of the different diffuser systems, the following assumption is made: The reactor pressure ratio is considered to be independent of the flow rate and temperature ratio and is taken to be the design point value of 0.657 (this includes reactor exit losses). Over a large range of flow rates and temperature ratios this ratio is very nearly constant, and hence the assumption is justified for any qualitative discussion. In the quantitive analysis of the last system considered, this assumption is not made. It is the required temperature

ratio range alone, then, that dictates the diffuser design, except for a scaling factor. As for scaling, all diffuser critical dimensions can be scaled directly from the exhaust nozzle size, which is 323.6 $in.^2$. A further requirement is that the diffuser system exit Mach number be approximately 0.10 at the Tory II-A design point conditions (temperature ratio = 1.45).

For systems considered herein, there will of course be some flow rate below which the entire system (diffuser, reactor, exhaust nozzle) will flow subsonically. This condition will occur at very low flow rates and high temperature ratios, hence it should pose no serious problem.

Qualitative Discussion of Systems Considered

1. Single-Throat Diffuser

The first configuration that comes to mind that might satisfy the requirements, is simply a converging-diverging nozzle upstream from the reactor as shown schematically below. Such a system is immediately thrown

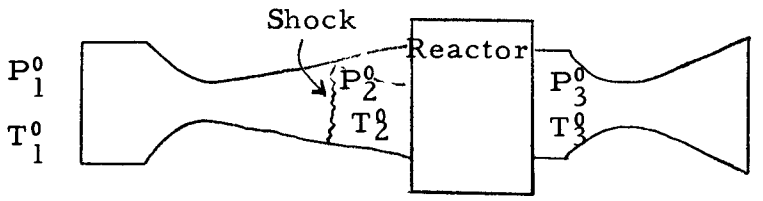

out on the following grounds. If the nozzle is to remain choked under a swing in reactor temperature ratio from 1 to 2, a strong shock must exist in the diffuser at the lower temperature ratio. This can be seen as follows. Consider the throat just choked at the maximum temperature ratio (diverging portion entirely subsonic). The flow rate is fixed by the upstream temperature and pressure. Now let the reactor temperature ratio be reduced; the back pressure (P_2^0) on the diffuser will then drop (since a lower pressure is now required to push the colder air through the exhaust nozzle). In order for the diffuser to compensate for this lower back pressure, a normal shock must form of such a strength that the stagnation pressure drop across it is equal to the difference between the inlet and back pressures ($P_1^0 - P_2^0$). If the temperature ratio is reduced to 1, the stagnation pressure ratio across the shock is approximately $1/\sqrt{2}$. But we cannot permit, in this configuration, any shocks except nearly isentropic ones because of the danger of large scale shock-induced separation. This could starve a portion of the core as indicated

schematically by the dashed line in the figure. The basic criteria governing possible separation is that the static pressure ratio across a normal shock should not exceed 2. This corresponds to a stagnation pressure ratio of 0.97 and a shock Mach number of 1.36. On the basis of this limitation, a diffuser of this type would only operate satisfactorily over a temperature ratio variation such that

$$(\text{Temperature ratio})_{max} = 1.06\ (\text{Temperature ratio})_{min}\ .$$

In selecting a satisfactory system we must meet two basic requirements over a reactor temperature ratio range 1 to 2:

1) upstream throat must remain choked,
2) no possibility can exist of starving a portion of the core due to large scale shock-induced separation.

2. Double-Throat Diffuser

The following double-choked diffuser allows satisfactory operation over a considerably larger temperature ratio range than the single converging-diverging nozzle discussed above. This is accomplished by allowing a con-

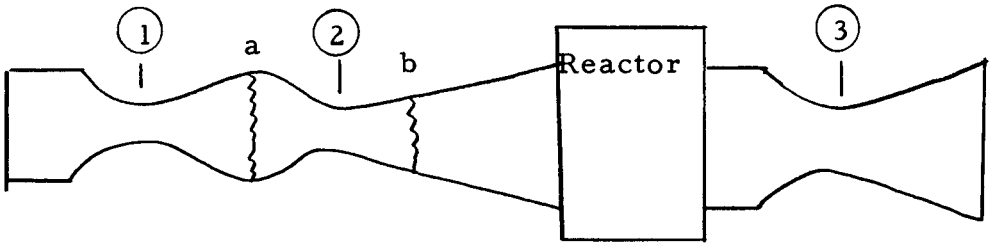

siderably stronger shock to exist between throats No. 1 and No. 2 than in the previous example. If this shock induces separation the flow will be reattached by the converging portion of nozzle No. 2 and by the choking effect of throat No. 2. A shock strength corresponding to a stagnation pressure ratio of 0.90 is considered to be the limiting strength before separation poses a serious problem. The system is designed such that the shock downstream of throat No. 2 is again limited to a stagnation pressure ratio of 0.97 (Mach number of 1.36).

The diffuser works as follows. At maximum temperature ratio (high diffuser back pressure) throat No. 2 is unchoked and throat No. 1 is just barely choked. The flow through the entire diffuser system is subsonic except for the sonic condition at throat No. 1. Now, as the temperature ratio is reduced (back pressure decreases) a shock forms in diffuser No. 1 to accommodate

this lower pressure. The flow remains entirely subsonic downstream from this shock until the temperature ratio has reduced to a point where the shock reaches its maximum strength (maximum area position between the two throats). At this condition, throat No. 2 is sized such that it is just barely choked. As the temperature ratio is reduced further a second shock forms in diffuser No. 2. When the temperature ratio reaches its minimum acceptable value, the second shock is still nearly isentropic (pressure ratio = 0.97) and it will not induce separation. Reiterating, the combination of two throats is for the purpose of containing a strong shock and thereby avoiding any separation problems, while at the same time, always maintaining throat No. 1 choked. A design of this nature will allow a swing in temperature ratio such that

$$(\text{Temperature ratio})_{max} = 1.32 \quad (\text{Temperature ratio})_{min} .$$

Although this is considerably greater range than for the single converging-diverging diffuser, it is still far below the specified requrements.

3. Aerodynamic Grid Diffuser

Another system which has been proposed is similar to the above system, in that it also is a double-throat configuration. This type has been selected for the Tory II-A diffuser. In this case, the second converging-diverging nozzle has been replaced by an "aerodynamic grid" which consists of many small C-D nozzles in parallel as indicated in the sketch below. Strong shocks are allowed to exist in these small nozzles, as no large-scale shock-induced separation can result. The grid will function to break up the shock-induced sep-

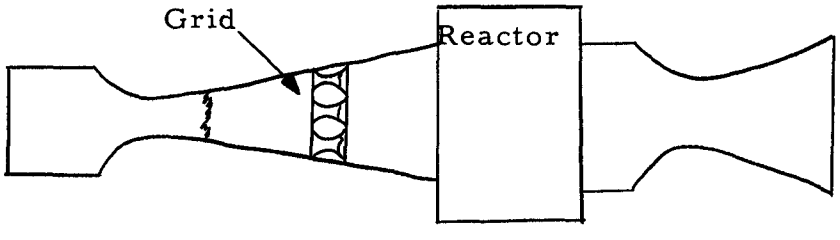

aration into multiple cells. The resulting flow will have a fairly high turbulence level but large scale separation will be avoided. This grid is sized such that it will remain choked over the entire temperature ratio range. The upstream C-D nozzle acts as a convenient method of feeding the grid nozzles. Throat No. 1 is sized such as to give rise to a weak shock between the throat and the grid. This is to insure choking of the throat since flow rate measurements will be made on the basis of this upstream throat area. Again consider this system with the temperature ratio at its maximum value. The nozzle

throat will be choked, a weak shock (pressure ratio = 0.97) will exist between the throat and grid, and the grid will be just choked with all subsonic flow downstream of the grid throats. As the temperature ratio is decreased (back pressure decreases) a normal shock appears in the diverging portion of the grid. This shock reaches a maximum strength (pressure ratio = $1/\sqrt{2}$) when the temperature ratio = 1. It should be noted that in both the double-throat systems discussed, the price paid for satisfactory operation over a large reactor temperature ratio range is substantial pressure loss in the diffuser. However, with a high pressure blowdown system, this will not substantially cut the available air supply.

A brief analysis is given below of the grid system under development to meet the Tory II-A requirements. Figure 5-38 indicates the various modes of operation of the diffuser system. Regions of reactor temperature ratio and flow rate are shown for upstream throat choked and unchoked, grid choked and unchoked, and exhaust nozzle choked and unchoked. These regions are indicated for two inlet temperatures, 530°R and 1530°R.

Aerodynamic Grid Diffuser Analysis

A. Station locations:

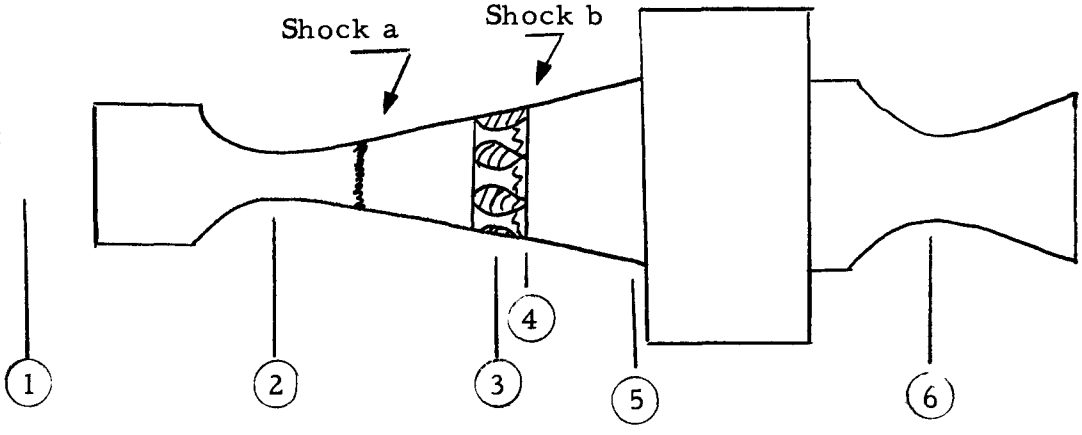

B. The two basic equations:

1) Continuity equation:

$$\frac{\dot{w}}{A} = \frac{P^0}{\sqrt{T^0}} \quad f(M, \gamma) ,$$

where P^0 = stagnation pressure

T^0 = stagnation temperature

$\dot{w}/A$ = flow rate per unit area

f = standard tabulated function of Mach number and specific heat ratio.

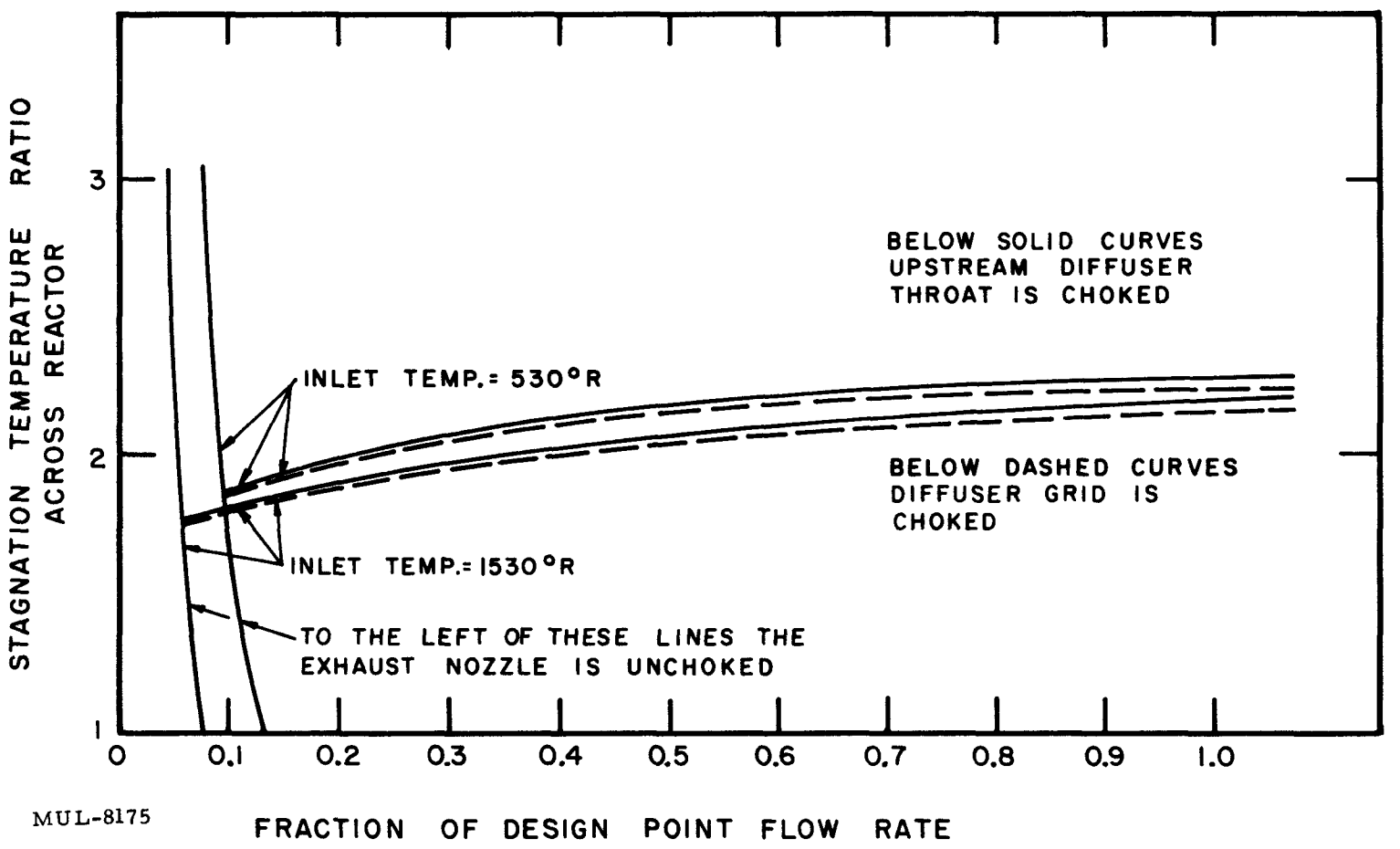

Fig. 5-38. Diffuser operating regions.

2) Total pressure ratio across a normal shock:

$$\frac{P_A^0}{P_B^0} = g(M, \gamma) ,$$

where A = refers to region downstream from shock

B = refers to region upstream from shock

g = is the standard tabulated function of upstream Mach number.

C. Data and assumptions:

Diffuser:

A_2 = upstream throat area = 118.4 in.^{2}

A_3 = grid throat area = 125.5 in.^{2}

A_4 = grid exit area = 457.0 in.^{2}

A_5 = diffuser exit area = 974.0 in.^{2} .

Exhaust nozzle:

A_6 = exhaust nozzle throat area = 323.6 in.^{2} .

Reactor:

The following reactor data was used in this analysis.

1) Individual flow passage pressure ratio, as a function of temperature ratio, exit Mach number, flow rate, and exit temperature.
2) Reactor exit pressure loss, as a function of exit Mach number.
3) Proportion of total flow bypassed for cooling, as a function of fuel-element temperature ratio.
4) Overall reactor temperature ratio, as a function of fuel-element temperature ratio.

Assumptions:

1) Friction losses in ducting.
   a) 3% pressure loss between upstream throat and grid.
   b) 5% pressure loss between grid and reactor.
2) Specific heat ratio.
   a) γ = 1.28 downstream from reactor
   b) γ = 1.40 elsewhere.

D. Operating characteristics:

1) Exit nozzle total pressure to diffuser inlet total pressure ratio, as a function of reactor temperature ratio, for the case where both the exhaust nozzle and upstream diffuser throat are choked:

From continuity,

$$\frac{A_2 P_2^0}{\sqrt{T_2^0}} \; f(M=1,\ \gamma=1.4) = \frac{A_6 P_6^0}{\sqrt{T_6^0}} \; f(M=1,\ \gamma=1.28)$$

$$\frac{P_6^0}{P_2^0} = \frac{A_2}{A_6} \sqrt{\frac{T_6^0}{T_2^0}} \; \frac{f(M=1,\ \gamma=1.4)}{f(M=1,\ \gamma=1.28)} \; .$$

From gas tables,

$$\frac{f(M=1,\ \gamma=1.4)}{f(M=1,\ \gamma=1.28)} = 1.03 \; .$$

From given data,

$$\frac{A_2}{A_6} = \frac{118.4}{232.6} = 0.366 \; .$$

Thus,

$$\frac{P_6^0}{P_2^0} = 0.377 \sqrt{\frac{T_6^0}{T_2^0}} \; .$$

For the case $T_6^0 = T_2^0$, the specific heat ratios will be taken as the same; hence, for $T_6^0/T_2^0 = 1$,

$$\frac{P_6^0}{P_2^0} = 0.366 \; .$$

2) Limiting case for which the upstream throat is choked and no shocks exist (i.e., grid unchoked).

$$\frac{P_6^0}{P_2^0} = \frac{P_6^0}{P_5^0} \cdot \frac{P_5^0}{P_4^0} \cdot \frac{P_4^0}{P_3^0} \cdot \frac{P_3^0}{P_2^0} \; .$$

Then

$$\frac{P_6^0}{P_2^0} = \frac{P_6^0}{P_5^0} \times 0.95 \times 1.00 \times 0.97 = 0.921 \; \frac{P_6^0}{P_5^0} \; .$$

Thus

$$\sqrt{\frac{T_6^0}{T_5^0}} = \frac{0.921}{0.377} \frac{P_6^0}{P_5^0} = 2.44 \frac{P_6^0}{P_5^0} .$$

Let

$$\frac{T_6^0}{T_5^0} = T_r \text{ (reactor temperature ratio),}$$

$$\frac{P_6^0}{P_5^0} = P_r \text{ (reactor pressure ratio) .}$$

Then the condition for the upstream throat to be choked is:

$$\frac{\sqrt{T_r}}{P_r} \leq 2.44 .$$

For values of this parameter > 2.44, the continuity equation requires that $M_2 < 1$.

3) Limiting case for which the grid is just choked (i.e., no shock in grid):

Since the grid is choked, the upstream throat must also be choked, since it has a smaller area than the grid throat.

Then,

$$A_2 P_2^0 = A_3 P_3^0 .$$

Thus

$$\frac{P_3^0}{P_2^0} = \frac{A_2}{A_3} = \frac{118.4}{125.5} = 0.943 .$$

Now since a friction loss of 3% was assumed, a shock with pressure ratio = 0.97 (M = 1.35) must be present. Such a shock is within the design requirements and will not induce separation.

Again,

$$\frac{P_6^0}{P_5^0} \cdot \frac{P_5^0}{P_4^0} \cdot \frac{P_4^0}{P_3^0} \cdot \frac{P_3^0}{P_2^0} = 0.377 \sqrt{T_r} .$$

Thus,

$$\frac{P_6^0}{P_5^0} \times 0.95 \times 1.00 \times 0.943 - 0.377 \sqrt{T_r} .$$

Hence,

$$\frac{\sqrt{T_r}}{P_r} \leq 2.37 \text{ is the limiting condition.}$$

4) Limiting flow rate at which the exhaust nozzle becomes unchoked:

From the data available on subsonic diffusers, it appears that the exhaust nozzle (area ratio = 2.97) will remain choked down to approximately 15 psia for ambient pressure equal to 12.6 psia. Hence the limiting flow rate, for a choked exhaust nozzle, is given by

$$\dot{w} = \frac{P_6^0 A_6}{T_1^0 T_r} f(M=1, \gamma=1.28) ,$$

where $P_6^0 = 15$ psia.

Using reactor flow calculations from the Floss code, these three limiting cases have been investigated for inlet temperatures of 530°R and 1530°R. The results appear in Fig. 5-38.

E. Mach number at the diffuser exit for the design point conditions ($T_r = 1.45$, $P_r = 0.657$):

$$\frac{A_5 P_5^0}{\sqrt{T_5^0}} f(M_5) = \frac{A_2 P_2^0}{\sqrt{T_2^0}} f(M=1) ,$$

$$\frac{f(M_5)}{f(M=1)} = \frac{A_2}{A_5} \frac{P_2^0}{P_6^0} \frac{P_6^0}{P_5^0} = \left(\frac{118.4}{974.0}\right)\left(\frac{1}{0.377\sqrt{1.45}}\right)(0.657) ,$$

$$\frac{f(M_5)}{f(M=1)} = 0.176 .$$

From gas charts

$$M_5 = 0.103 .$$

This value is consistent with the design requirements.

F. Diffuser pressure recovery:

$$\text{Let } P_d = \frac{P_5^0}{P_1^0} = \frac{P_6^0}{P_2^0} \cdot \frac{P_5^0}{P_6^0} = 0.377 \frac{\sqrt{T_r}}{P_r} ,$$

or for $T_r = 1$, making the inlet and exit specific heat ratios identical,

$$P_d = \frac{0.366}{P_r} .$$

The reactor pressure ratio P_r is a function of the reactor temperature ratio, exit Mach number (which is fixed at 0.50 when the exhaust nozzle is choked), flow rate, and exit temperature. P_r varies approximately over a range from 0.55 to 0.66.

At the design point $T_r = 1.45$, $P_r = 0.657$, $P_5^0 = 357$ psia.

Hence

$$P_d = 0.689 \text{ at design point.}$$

Thus

$$P_2^0 = 0.689 \times 357 = 517 \text{ psia.}$$

The minimum P_d occurs at $T_r = 1$ and at high flow rates. At 100% design point flow rate and $T_r = 1$, $P_r \approx 0.65$; thus

$$P_d \geq \frac{0.366}{0.65} = 0.563.$$

G. Required grid exit area:

The pressure ratio across the grid shock is given by

$$\frac{P_4^0}{P_3^0} = \frac{P_6^0/P_2^0}{(P_6^0/P_5^0)\,(P_5^0/P_4^0)\,(P_3^0/P_2^0)}$$

$$\frac{P_4^0}{P_3^0} = \frac{0.377}{0.95 \times 0.943} \frac{\sqrt{T_r}}{P_r} = 0.421 \frac{\sqrt{T_r}}{P_r} ,$$

or for $T_r = 1$

$$\frac{P_4^0}{P_3^0} = \frac{0.408}{P_r} .$$

P_4^0/P_3^0 will be a minimum (maximum shock strength) when $\sqrt{T_r}/P_r$ is a minimum. This occurs at $T_r = 1$ and at high flow rates. Hence the calculation will be made for design point flow and $T_r = 1$. For this case, $P_r \approx 0.65$.

Then,

$$\left(\frac{P_4^0}{P_3^0}\right)_{min} = \frac{0.408}{0.65} = 0.628.$$

From gas tables,

$$M_5 = 2.20 \text{ and } A_5/A_3 = 2.00,$$

where A_5 is the area at which the shock occurs; thus

$$A_5 = 2.00 \times 125.5 = 251.0 \text{ in.}^2 .$$

Hence $A_5 < A_4$ and the design meets the necessary requirements.

H. Diffuser geometry:

The diffuser is designed according to the following accepted rules:

1) Subsonic diffuser half-angle : 7°
2) Supersonic diffuser half-angle : 15°
3) Converging portion half-angle : 45° (max)
4) Throat radius of curvature : 60% throat diam (min)

5.4 Radiation Effects

This section will present estimated levels of gamma and neutron radiation in and around the reactor, with discussion of the effects of this radiation with respect to heating, activation of materials, and structural damage. Most of the estimation of radiation fluxes is on an approximate basis, and the approach used varies according to particular applications. For this reason, and because the material presented here was taken from several different working papers, some repetition or slight differences in calculated levels may be noticed.

Where uncertainty exists as to the exact radiation level existing in a region, or with respect to the effects of that radiation, conservative assumptions have been made to ensure that heating and damage levels will be within safe limits.

5.4.1 Radiation Levels External to the Reactor

Gamma Flux

Leakage of gammas from a medium occurs from that material which is within a few attenuation mean-free-paths of the surface. Gammas originating farther away are heavily attenuated and so contribute very little to the escaping current. If what is of interest is the escaping energy in matters of gamma heating, then the energy attenuation length, λ_e, is the pertinent quantity.

The gamma radiation levels have been estimated by a simplified model in which a constant attenuation length is assumed for the reactor core. This length, λ_e, is found from the energy absorption coefficient averaged over the fission gamma spectrum. Fortunately, λ_e varies only slightly over the fission spectrum so that one can ignore the details of the spectrum when inquiring into the heating of external objects.

Since λ_e $(= 1/\rho\mu_e)$ is found to be 10.9 inches in BeO of average core density, 1.5 g/cc, and this length is small compared to the core dimensions, gamma leakage has been computed on the basis of a model which assumes a semi-infinite medium bounded by a plane; the leakage from this plane per unit area being simply

$$F = \int_V \frac{N(\vec{r})\, e^{-\mu_e \rho r}\, dV \cos\theta}{4\pi r^2}$$

where r is the distance from dV to the unit area through which F leaks, $N(\vec{r})$ is the rate of gamma production per unit volume at $\vec{r}$ in the medium, and $\cos\theta$ accounts for the fact that dV sees only the projection of the unit area on the plane surface. The integral is performed over the semi-infinite medium. In the event that $N(\vec{r})$ is constant, one finds $F = N/4\rho\mu_e$ which is recognized as Lambert's Law.

It can also be shown easily that if $N(\vec{r})$ is not constant, but has the form $N_0 + ax$, where a is the gradient of N and x is measured from the plane surface, then

$$F = \frac{1}{4\rho\mu_e}\left[N_0 + \frac{2a}{3\rho\mu_e}\right].$$

This form has meaning in the case of Tory II-A at both the front and back ends of the active core, as the power level is not axially constant but has an appreciable gradient, with the power level dropping to about $0.7\overline{P}$ at the front end of the active core and $0.4\overline{P}$ at the rear end. As always, one must exercise caution in the use of such approximations, checking their results for plausibility; it is easy to overestimate escaping radiation fluxes.

The radiation from the front face will be considered first. If there were no intervening material between the active core and the external object to be heated, the radiation would leave with a $\cos\theta$ angular distribution, where θ is measured with respect to the core axis. However, a 6-inch BeO

reflector and 4-inch steel* gamma shield, both of half-density, are present directly against the core end. These serve to attenuate gamma rays which pass through normally by 0.5 mean free path and 0.9 mean free path, respectively. However, those gammas that enter at skew angles will be attenuated even more. The modified angular distribution closely resembles a $\cos^2 \theta$ distribution.

If a thin sheet of material of thickness dx is very close to the outer surface of the gamma shield, it is important to recognize that the sheet will be heated by more than $F' dx/\lambda_e$, where F' is the current falling on the sheet. The enhancement is due to the fact that gammas which leave the shield at angles other than $\theta = 0$ travel a distance $dx/\cos \theta$ through the sheet. If the angular distribution varies as $\cos \theta$, the heating is enhanced by a factor of 2. If the distribution varies as $\cos^2 \theta$, the heating is enhanced by a factor of 1.5. In fact, enhancement factor is $(n + 1)/n$ for $\cos^n \theta$. By the same token, one must recognize that the BeO end reflector and steel gamma shield will remove more energy than the 1.4 mean free paths imply.

When proper attention is given to the manner in which the reflector and gamma shield remove energy, it is found that for the current Tory II-A design (total power of 160 Mw), 3.3×10^{17} Mev/sec leaves the front face of the reactor in gamma energy. The maximum current is 6.7×10^{13} Mev/cm^2 sec. For distances greater than a few feet from the face, the current is $1.6 \times 10^{17} \cos^2 \theta/R^2$, where R is in cm units. This latter value does not include the effect of the air pipe, which has steel walls 3/4 in. thick.

The rear face will have a less thick reflector: 2 inches of unfueled BeO plus a 1-inch molybdenum plate, each of half-density. The leakage from the side reflector, on the other hand, will be very strongly attenuated by the graphite as well as the pressure shell.

The results are summarized in Table 5-14. The quantity R refers to the distance from the radiating surface in question, and is in centimeter units. The listed values do not take into account the steel air pipe which is 3/4 in. thick ($\rho\mu_e = 0.24$ cm$^{-1} = 0.61$ in.$^{-1}$).

---

*As indicated in Section 5.1, the gamma shield has been changed to 1-1/2 inches of tungsten. The analysis given here is not materially affected.

Table 5-14. Gamma leakage currents

Source	Total energy (Mev/sec)	Max current (Mev/cm^2 sec)	Current at distance R (Mev/cm^2 sec)
Front	3.3×10^{17}	6.7×10^{13}	$1.6 \times 10^{17} \cos^2 \overline{\theta}/R^2$
Rear	1.0×10^{18}	2.0×10^{14}	$3.2 \times 10^{17} \cos \overline{\theta}/R^2$
Side	0.7×10^{17}	0.3×10^{13}	$5 \times 10^{15}/R^2$

To illustrate the use of these values, let us consider gamma heating of the front support structure. Explicit consideration of the gamma spectrum is unnecessary. Although the spectrum is important in the matter of in-core heating, the spectrum of the gammas emerging from the front end is sufficiently similar to that of a fission spectrum to allow the use of a constant μ_e.

At 1.0 Mev, $\rho\mu_e = 0.207$ cm^{-1}. At 3.0 Mev, the minimum of 0.174 cm^{-1} is found, and at 10.0 Mev, the value is 0.196 cm^{-1}. A conservative value of 0.2 cm^{-1} gives a power density of:

$$6.7 \times 10^{13} \left(\frac{\text{Mev}}{\text{cm}^2 \text{ sec}} \right) \times 1.5 \times 0.2 \text{ (cm}^{-1}) \times 4.54 \times 10^{-15} \frac{\text{Mw/ft}^3}{\text{Mev/cm}^3 \text{ sec}}$$

$$= 0.09 \text{ Mw/ft}^3 .$$

The support structure is sufficiently thick that a careful consideration of self-shielding effects would justify lowering this value slightly.

Neutron Flux

Neutron leakage currents from Tory II-A were computed by multigroup diffusion calculations such as Angie (a two-dimensional code which allows the inclusion of end reflectors). Eighteen neutron groups were employed, as explained in Section 5.2.

Although a diffusion calculation does not include transport effects such as leakage of undegraded fission neutrons from the core, it would be unlikely that the latter effect is important. If it were, the diffusion code would give poor agreement with critical assembly experiments, which is not the case. An estimate of loss of undegraded neutrons can easily be made if one employs

a "removal" cross section which is the total fast neutron cross section. If this is done, it is found that total neutron leakage from the front end is affected by 1 percent and that from the rear by 1.5 percent.

Figures 5-39, 5-40, and 5-41 show the average emergent neutron currents, as functions of energy, from various external surfaces of the reactor. The neutron currents from the ends of the core are listed in Table 5-15, as they fall into the four highest energy intervals considered.

Table 5-15. Fast neutron currents from core at 100-Mw power

Energy group (Mev)	Front face* (neuts/cm^2 sec)	Rear face* (neuts/cm^2 sec)
3.16 - 10.0	4.7×10^{12}	7.2×10^{12}
1.00 - 3.16	6.0×10^{12}	9.3×10^{12}
0.316 - 1.00	2.5×10^{12}	4.7×10^{12}
0.10 - .316	2.6×10^{12}	3.8×10^{12}

* The front and rear faces both have areas equal to 2.21×10^4 cm^2.

A reasonable guess for the angular distribution of the emergent neutrons from the front and rear faces would be cos θ. Accurate determination of the distribution is difficult; a procedure such as the Monte Carlo method would supply such information.

Heating by neutrons can be accomplished in several ways. Fast neutrons can lose energy through elastic collisions. Inelastic scattering leaves the initially stationary nucleus in an excited state, and a gamma ray is produced as the nucleus returns to its ground state. There may also be reactions such as (n, p) and (n, α) reactions where the recoil energies are deposited in the heated material. Thermal neutrons, although possessing very little kinetic energy, can be absorbed in many materials with the result that high energy gammas are emitted. All of these energy sources must be examined closely to permit an accurate determination of heating.

5.4.2 Heating by External Fluxes

To illustrate the determination of external radiation heating, a specific case will be considered, that of the front support structure. To avoid complication, as was done above, the effects of self-shielding in a thick structure

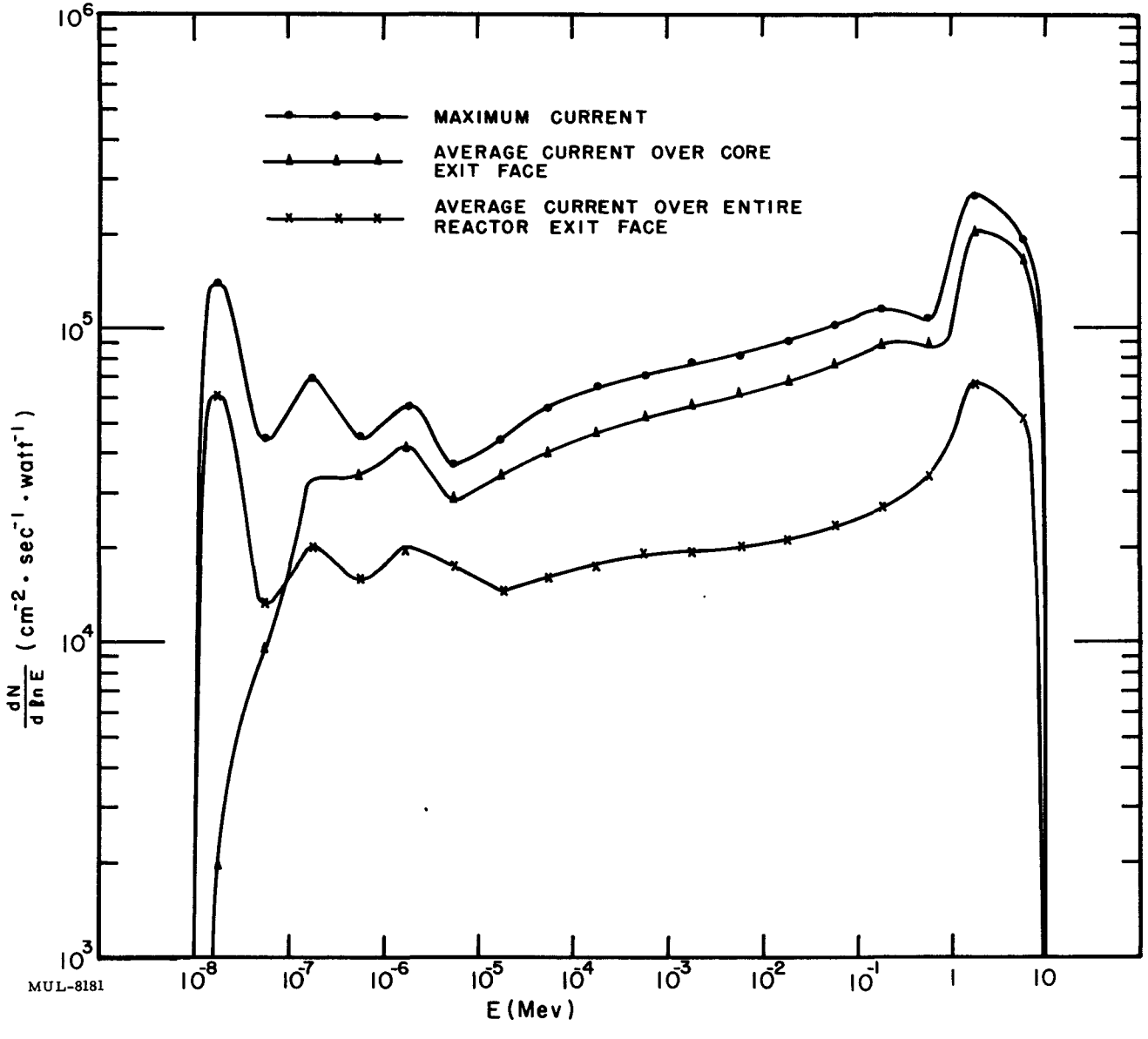

Fig. 5-39. Energy distribution of neutron current leaving exit end of reactor.

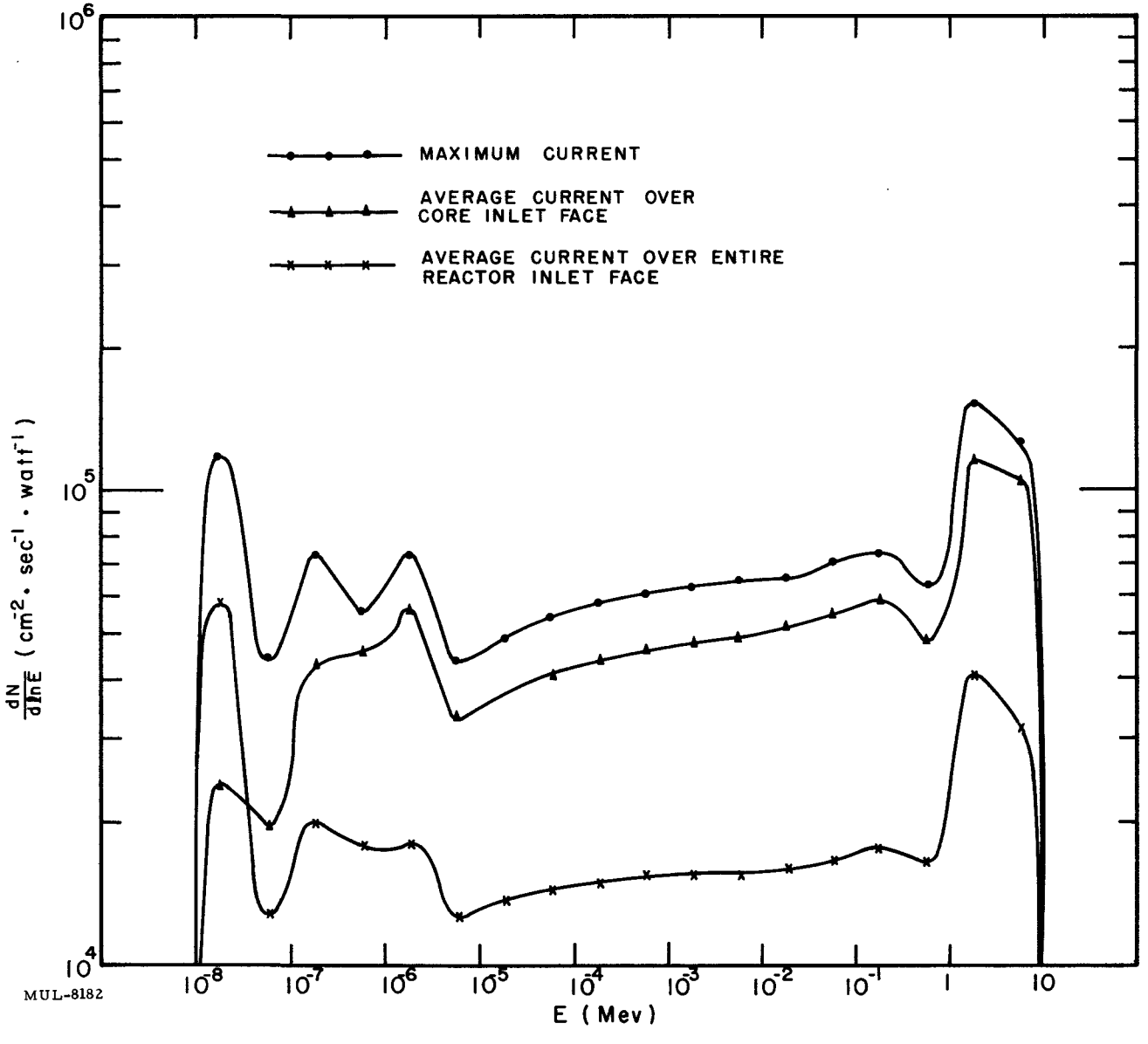

Fig. 5-40. Energy distribution of neutron current leaving inlet end of reactor.

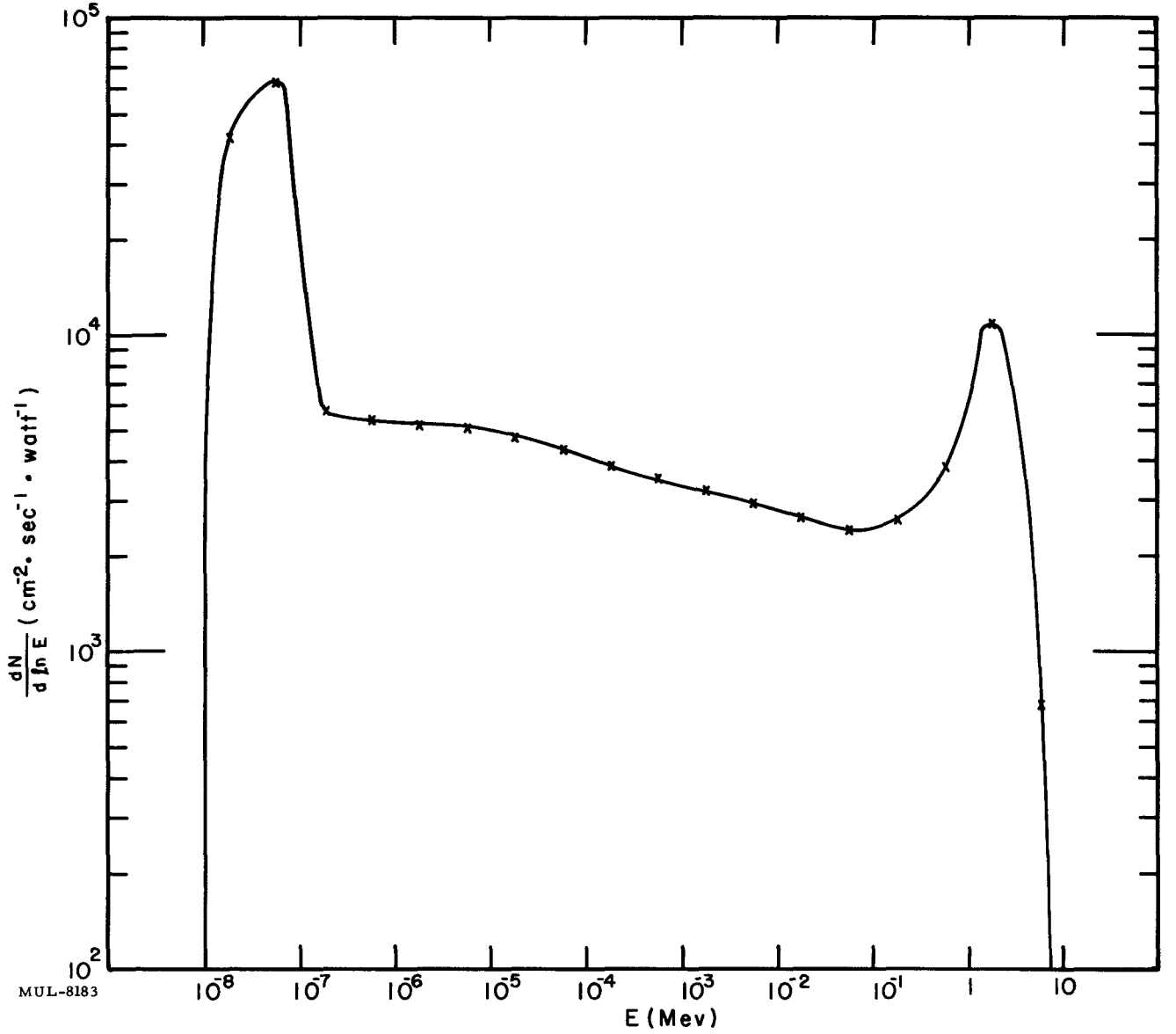

Fig. 5-41. Energy distribution of neutron current leaving cylindrical outer surface of graphite reflector.

will be ignored. The resulting error will be fairly small, giving heating values slightly larger than the true case.

Consider a thin sheet of stainless steel at the front face of the reactor. It was shown before that the power density due to gammas in such a sheet is 0.09 Mw/ft^3; it remains to determine the neutron effects.

For the main constituents of stainless steel (i.e., Fe, Cr, and Ni), $\sigma_{scat.} \sim 2 \times 10^{-24}$ cm^2 and $\sigma_{inel.} \sim 1 \times 10^{-24}$ cm^2. The gammas released have energies of about 1 Mev; E_γ(Fe) = 0.85 Mev while E_γ(Cr) = 1.44 Mev. Since the neutron loses about 0.036 of its energy upon elastic collision, and since the energy of fast neutrons is about 1.0×10^{14} Mev/cm^2 sec, it follows that if the fast neutrons all impinge normal to the thin sheet (which is normal to the core axis), the heating will be 0.0027 Mw/ft^3. Since the emergent neutrons leave with a (more-or-less) cos θ distribution, the value is doubled to give 0.0054 Mw/ft^3.

In the case of inelastic neutron effects, one finds an approximate current of 3.2×10^{13} neutrons/cm^2 sec. Since each inelastic collision releases approximately 1.0 Mev, and since the gamma has an approximate energy attenuation length in full-density steel of about 4.2 cm, the heating from inelastic scattering is 0.0061 Mw/ft^3. This value is based on a cos θ distribution for entering neutrons, and no gamma shield effect.

The thermal neutrons, on the other hand, have the capability of contributing appreciably to the heating through capture gamma production. These gammas, arising from the (n, γ) process, carry about 8 Mev per capture. For type 304 stainless steel, the absorption mean free path for thermal neutrons is 3.9 cm for full-density material; also the gammas released will have a probability dx/λ_e, where λ_e is about 4.2 cm, of being absorbed in a sheet of thickness dx. The average thermal neutron current over the entire front face is 8.6×10^{12} neutrons/cm^2 sec. Although the thermal current will be much lower on the axis if boron steel is used as a gamma shield, the value above will be used since some neutrons from the front face of the side reflector will pass through the heated material (such as the support structure). Therefore, this value of current is a conservative estimate. The resultant heating, assuming a cos θ angular distribution for the thermals, is 0.039 Mw/ft^3.

The previous effect came from direct action of the thermal neutrons. There is also a contribution to heating from the capture gammas made in materials surrounding the support structure. If these materials, such as the air

pipe, are sufficiently thick, they can account for an appreciable secondary gamma flux. If, on the other hand, they are several inches thick, thermal neutron absorption may reduce the direct capture gamma source.

A conservative estimate of the heating due to capture gammas from the steel air pipe and similar structures gave a power deposition rate in the support structure of 0.04 Mw/ft^3, which is about as large as that from the direct action of thermals on the support structure.

Reactions such as $Fe^{56}(n, p)Mn^{56}$ contribute a negligible amount to the heating. Therefore, the total is 0.17 Mw/ft^3 for full-density stainless steel, where 0.09 Mw/ft^3 comes from gamma heating and 0.08 Mw/ft^3 comes from thermal neutron effects.

5.4.3 Nuclear Heating Within the Reactor

During operation of the Tory II-A reactor, many components of the active core as well as reactor components in close proximity to the core will be subjected to nuclear heating which far exceeds thermal heating due to conduction, convection and radiation. Knowledge of the extent of this heating is necessary for design purposes, where questions of differential expansion, coolant flow rates, and other engineering problems arise.

An exact appriasal of nuclear heating is difficult to make because of uncertainties in the gamma energy spectrum, and the complex geometry of the core assembly. Evaluation of nuclear heating has therefore been based on approximations and models which tend to give as realistic an estimate as is possible. This section describes the models adopted and the methods used in the evaluation of nuclear heating of Tory II-A reactor components.

Internal Core Heating

The components of the core most susceptible to nuclear heating are the tie rods. The major source of heating of the tie rods is recognized to be heating by gammas resulting from U^{235} fission. The method employed in this evaluation treated an infinite uniform medium containing a homogeneous mixture of BeO, U and tie rod metal in a ratio equal to that in which these components occur in the Tory II-A core.

The gamma rays are allowed to interact with the materials in accord with branching ratios determined from the abundances and cross sections of the various materials present. Compton and photoelectric interactions were

allowed. An energy transfer matrix describing the Compton scattering process as a function of energy was developed and employed. The gamma heating of a particular material was found by tallying the contributions from photoelectric as well as Compton heating for that particular material. The gamma spectrum employed was that of prompt fission gammas, and it was considered to have 12 Mev/fission.

It was shown that, for the conservative model employed, the tie rods were heated to a power density of 6.3 Mw/ft^3 for a core power density of 10 Mw/ft^3, the uncertainty in the former number being ± 10%. The BeO to uranium ratio considered was 200:1, which represented the lowest expected loading in the core.

A refinement of the above calculation consisted in the consideration of the shielding effect on the tie rods by the uranium in the fueled core. It was found that the low-energy gammas were limited in their ability to diffuse and many were prevented from reaching the rods. Inclusion of this effect reduced the tie rod power density to 5.1 Mw/ft^3. A conventional computation of Compton heating would have given 3.9 Mw/ft^3.

These calculations indicate that increased amounts of uranium in the homogeneous mixture tend to decrease the amount of heat deposited in the rods. Also, in the actual reactor core, self-shielding reduces the tie rod heating. Thus, since the actual moderator to fuel ratio is expected to be smaller than the one considered here, the heating evaluated here can certainly be considered as an upper limit.

Heating External to the Core

While reactor components in the immediate proximity of the active core will undergo nuclear heating to a smaller extent than any internal components, the nuclear heating effect in these components is expected to be more important than thermal heating by at least a factor of 10.

Although heating of high-Z materials is due mainly to gammas, the presence of low-Z materials such as aluminum and water in the region considered has warranted the consideration of heating by neutrons and by other processes; in some cases these heating contributions have been found to be more important than the effect of gammas. Calculations of heating at the periphery of the active core have been done by considering a semi-infinite medium, the heating effect being evaluated at the boundary of the medium.

The gammas are assumed to emerge from the active core radially with an energy distribution similar to the prompt fission gamma spectrum (see Figure 5-42). The gamma energy escaping from the core can be evaluated in a conservative way by means of Lambert's Law, which implies an approximate escape thickness $\lambda_E/4$ for gammas of specific energy E, where λ_E is the energy absorption mean free path in the core material. This model does not take into account gammas that are reflected back into the component in question after having deposited some energy on their way out. However, these back-scattered gammas contribute only slightly to the nuclear heating.

Gamma heating has been calculated by considering a total gamma power of 15 Mev/fission in the reactor core; approximately 7.8 Mev/fission are attributed to prompt gammas, with a spectrum relatively well established (Fig. 5-42), while the remaining 7.2 Mev/fission represents gammas produced in neutron capture, inelastic scattering of fast neutrons, and fission product decay. The delayed fission product gammas approach a saturation value of ~6 Mev/fission exponentially, reaching 80% of this value after one hour of operation. Thus, calculations based on a total of 15 Mev/fission of gamma power released should certainly lead to a conservative estimate. The total 15 Mev/fission were then distributed among gamma energy groups at 0.2 Mev, 1 Mev, and 6 Mev, according to the ratios given by the prompt fission gamma spectrum.

By using this model, the heating by gammas can be computed for any material by:

$$H\left(\frac{Mw}{ft^3}\right) = 2P\left(\frac{Mw}{ft^3}\right) \sum_{E_i} (\Gamma_i \times \Lambda_i)$$

where Γ_i is the ratio of gamma energy in an energy group to the total fission energy, considered here to be 190 Mev; Λ_i the fraction $\frac{\lambda_E}{4}/\lambda_A$ where $\lambda_E/4$ is introduced by virtue of Lambert's Law and λ_A is the energy absorption mean free path in the material under consideration; and P is the reactor power density. The factor of 2 is introduced to account for the fact that the angular distribution of emitted gammas varies as $\cos\theta$.

The following are computed values for the gamma heating of components in the inactive part of the reactor. Note that these results do not take self-shielding or attenuation into consideration; the materials considered appear in thicknesses small enough to omit this effect without gross overestimate. The

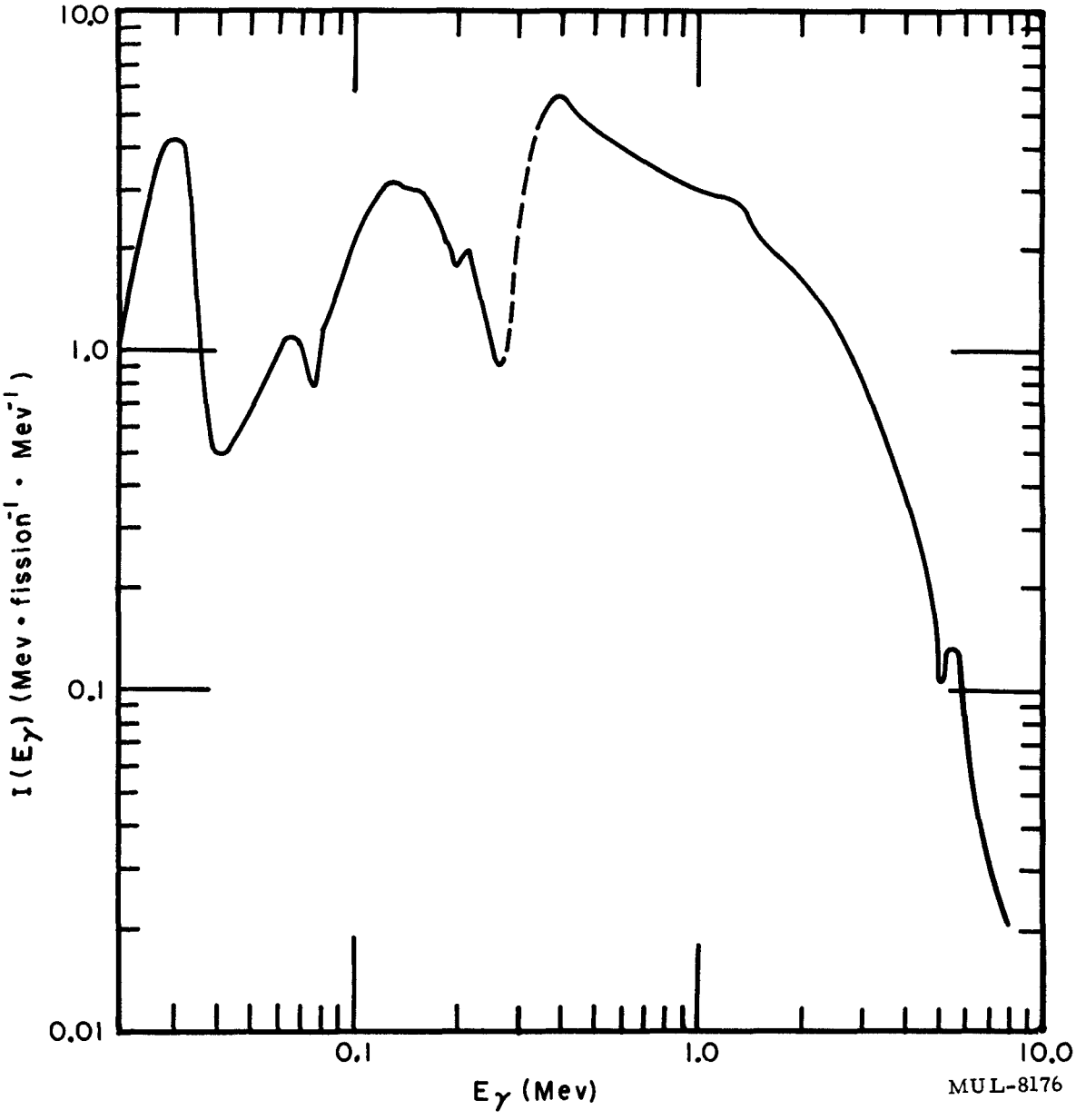

Fig. 5-42. Spectrum of energy carried by fission prompt gamma radiation.

core power density is taken to be 10 Mw/ft^3.

Al (core vessel)	0.66 Mw/ft^3
Hastelloy (shroud)	1.64 Mw/ft^3
Graphite (side reflector)	0.53 Mw/ft^3
H_2O	0.26 Mw/ft^3

In addition to gamma heating, the effect of neutron heating has been evaluated. Also, the gamma heating is enhanced slightly because of other, secondary, processes.

Heating due to moderation of fast neutrons can be calculated by comparing the heating by neutrons of a known material, such as the core elements, with the material of interest. Considering 5 Mev of fast neutrons produced per fission, and a core power density of 10 Mw/ft^3, the following values have been obtained: aluminum 0.028 Mw/ft^3, graphite 0.094 Mw/ft^3, and water 0.46 Mw/ft^3. These were assumed to be at the core's radial surface.

The gamma heating of aluminum is enhanced by products of the $Al^{27}(n, \gamma)$ reaction; Al^{28} has a half life of 2 minutes and releases one 1.8-Mev gamma and an average beta energy of 2.8 Mev. The effect of this process contributes 0.082 Mw/ft^3 to the heating of the core vessel.

The gamma flux in the vicinity of the aluminum pressure vessel is enhanced due to neutron capture so as to increase the heating by gammas of other components in this region. The enhancement factor over the existent gamma flux was found to be 11%. This effect increased the heating of the considered components by the following amounts: aluminum 0.078 Mw/ft^3, graphite 0.063 Mw/ft^3 and water 0.031 Mw/ft^3.

In summary, a table of specific power in the most important reactor components is given below, for a core power density of 10 Mw/ft^3; neither self-shielding nor attenuation has been considered. As a matter of interest, the heat deposition due to gamma heating alone is given in parentheses.

Radiation Power Deposition

Tie rods (partly shielded by U)	(5.10)	5.10 Mw/ft^3
Hastelloy shroud	(1.64)	1.64 Mw/ft^3
Aluminum core vessel	(0.66)	0.85 Mw/ft^3
Graphite side reflector	(0.53)	0.69 Mw/ft^3
Water coolant	(0.26)	0.75 Mw/ft^3

5.4.4 Activation of Materials

In the course of operation of Tory II-A, components of the reactor as well as materials in its vicinity will be irradiated by a relatively high neutron flux. The following discussion summarizes the method of approach and the findings of a more detailed treatment of the problem.

In order to calculate the degree of activation and the possible radiation hazards resulting therefrom, two methods have been used in our evaluation. The first was based on calculations from first principles using the available activation cross section and the estimated chemical compositions of the various materials including trace elements; activation by thermal (n, γ reactions) as well as fast (n, p and n, α) neutrons have been taken into account. The second method was based on experimentally measured decay curves of activated materials; the data used were obtained by C. D. Bopp[15] at the ORNL graphite reactor. Because uncertainties exist in the parameters necessary for the analytical evaluation of activity, the experimental data was used wherever possible.

Calculations

The activity of irradiated materials can be evaluated by means of the following analytical expression

$$A = k(1 - e^{-\lambda t_0})e^{-\lambda T}$$

where A is the activity, k the rate of production of the considered radionuclide during operation, and the exponential terms introduce the familiar buildup and decay mechanisms where t_0 is the time of operation and T is time after shutdown. The activation cross sections for thermal and fast neutrons used in the analytical evaluation of k were obtained from standard compilations.[16, 17] The cross sections for fast neutron reactions were averaged over the pertinent part of the spectrum if average values were not given.

The mathematical basis used in calculating activities from C. D. Bopp's data is essentially the same as the one outlined above, the exception being that the listed macroscopic absorption cross sections were determined experimentally and measured by the extent of induced activity in an irradiated sample. While some of the uncertainties of the analytical method were thereby eliminated, the exact neutron spectrum in the ORNL graphite reactor was not specified, and it was difficult to determine the fraction of activity induced by fast and slow

neutron irradiation respectively. Inasmuch as the neutron spectrum from Tory II-A is weighted more heavily at the fast end than is the spectrum in a thermal graphite reactor, it is estimated that activation by (n, p) and (n, α) reactions is likely to give a somewhat larger contribution than Bopp's data would indicate. Despite these differences, good agreement was found between analytically and experimentally determined activities in most cases. It was felt that any existing discrepancies should not change the final values beyond the limits of the overall estimated error.

Since the expected core lifetime is assumed to be 5 months, it is anticipated that most structural and supporting components of Tory II-A will be subjected to radiation for an equivalent length of time. The total energy output during this five-month operation cycle is assumed to be 9×10^{11} watt-sec. However, it is expected that most of the energy will be released during the last month of the cycle. Therefore, to give a representative estimate of the degree of activation of materials around the reactor core, the following model has been adopted in our calculations. The reactor operates continuously for a period of one month at an average power of 3×10^5 watts, following which the reactor is run full power at 160 Mw for 3 minutes. The total activity is then the sum of two contributions: a long, low-level accumulation plus a short-term accumulation produced during the last high-power run.

Results

Calculations of induced activities have been made for pure metals as well as for engineering materials. Of interest to us are materials used extensively in the reactor vicinity. These are stainless steel AM 355, aluminum 6061 and more generally other iron alloys and concrete. Aluminum and concrete have been found to behave similarly, the activity decreasing approximately by a factor of 10 every 2 days during the first 2 weeks after shutdown, followed by a more gradual decrease thereafter. Stainless steel and other ferrous material activities have been found to drop some three decades within the first day or two after shutdown and to assume a very gradual decay thereafter; flattening out of the decay curve at times of 2 days after irradiation is due mainly to the long half lives of some iron isotopes and other minor components such as Co, Cr, Ni and Mo.

The distribution in energy of neutron currents leaving the physical boundaries of the reactor has been calculated with the aid of the IBM 704 Angie Code and is presented in Figs. 5-39 through 5-41. Hence, the neutron

current levels outside the reactor can be evaluated (see Section 5.4.1). An order of magnitude approximation of the neutron flux levels during operation indicates that:

A. Inside the reactor:

$$\phi_{slow} \cong \phi_{fast} \cong 10^6 \text{ neutrons/cm}^2 \text{ sec per watt.}$$

B. Outside the reactor:

1) Axially, R = 1 meter: $J_{slow} \cong J_{fast} \cong 10^5 \frac{\text{neutrons}}{\text{cm}^2 \text{ sec}}$ per watt

R = 4 meters: $J_{slow} \cong J_{fast} \cong 10^4$ " "

R = 10 meters: $J_{slow} \cong J_{fast} \cong 10^3$ " "

2) Radially, R = 1 meter: $J_{fast} \cong 10^4$ " "

$J_{slow} \cong 10^5$ " "

The potential hazard from activated components has been estimated by considering them as non-self-absorbing isotropic point sources. These upper-limit calculations permit an evaluation of expected dose-rates in an expedient and conservative fashion. Without going through the calculations for all the components, the expected dose-rates from a few typical ones can be evaluated approximately.

The activity of some of the more important components two days after shutdown is presented below:

1) Aluminum core vessel — weight 135 lb.
$\phi_{fast} = \phi_{slow} = 10^6$ neutrons/cm^2 sec per watt
$A = 1.3 \times 10^7$ Mev/sec per gram.
Dose-rate at 1 meter: 25.4 r/hr.

2) Aluminum car cover — weight 500 lb.
$J_{slow} = 10^5$ neutrons/cm^2 sec per watt
$A = 1.3 \times 10^6$ Mev/sec per gram
Dose-rate at 1 meter: 9.4 r/hr.

3) Steel nozzle — weight 1000 lb.
$J_{fast} = J_{slow} = 10^5$ neutrons/cm^2 sec per watt
$A = 9.6 \times 10^5$ Mev/sec per gram
Dose-rate at 1 meter: 14 r/hr.

It must be remembered that these activities are the result of an irradiation period equivalent to a 5-month operation cycle of Tory II-A. Since activity at time T is a function of the integrated power of the reactor up to time T, an estimate of the hazard from activated components at any time during the operation cycle can be made by referring to Section 10.2, which outlines the operating program of Tory II-A. One finds that at the end of four months the hazard from activated components is 10^{-1} of that calculated above, at the end of the third month it is 10^{-2} of the calculated maximum, and it is relatively insignificant during the first two months of operation.

Figure 5-43 gives the specific activity of two alloys as a function of time after shutdown, for specimens located at a point receiving unit neutron flux per watt of reactor power and exposed during the full 5-month operating cycle of the reactor.

A more exact evaluation of induced activities and dose-rates is at this point impractical. The uncertainties existent in the parameters necessary for an exact evaluation have warranted calculations based on upper limit estimates in order to appraise the seriousness of the problem. Generally speaking, the activity of irradiated structural and supporting components is much less significant than the activity of the core itself.

5.4.5 Radiation Damage to Reactor Components

The major effect of radiation on structural materials is contributed by fast neutrons; this effect is attributed to rearrangements of atoms within the structure of the crystal. Radiation damage is thus dependent on the integrated fast neutron flux intercepted by the material under consideration. For Tory II-A, we can obtain an upper limit for integrated fluxes at various points by assuming that during one core lifetime the reactor will be operated with a total output of 250 Mw-hr. The approximate flux levels are tabulated in Table 5-16.

Experimental evidence to date indicates that metal parts are not likely to be damaged by nuclear radiation; integrated doses in excess of about 10^{19} neutrons/cm^2 must be realized before any change in the metal properties can be observed, and current observations indicate that, in general, properties such as yield strength, tensile strength, and hardness increase while creep rate and fatigue strength are not much affected. BeO and graphite also remain unaffected from the radiation levels expected in Tory II-A. Little or no

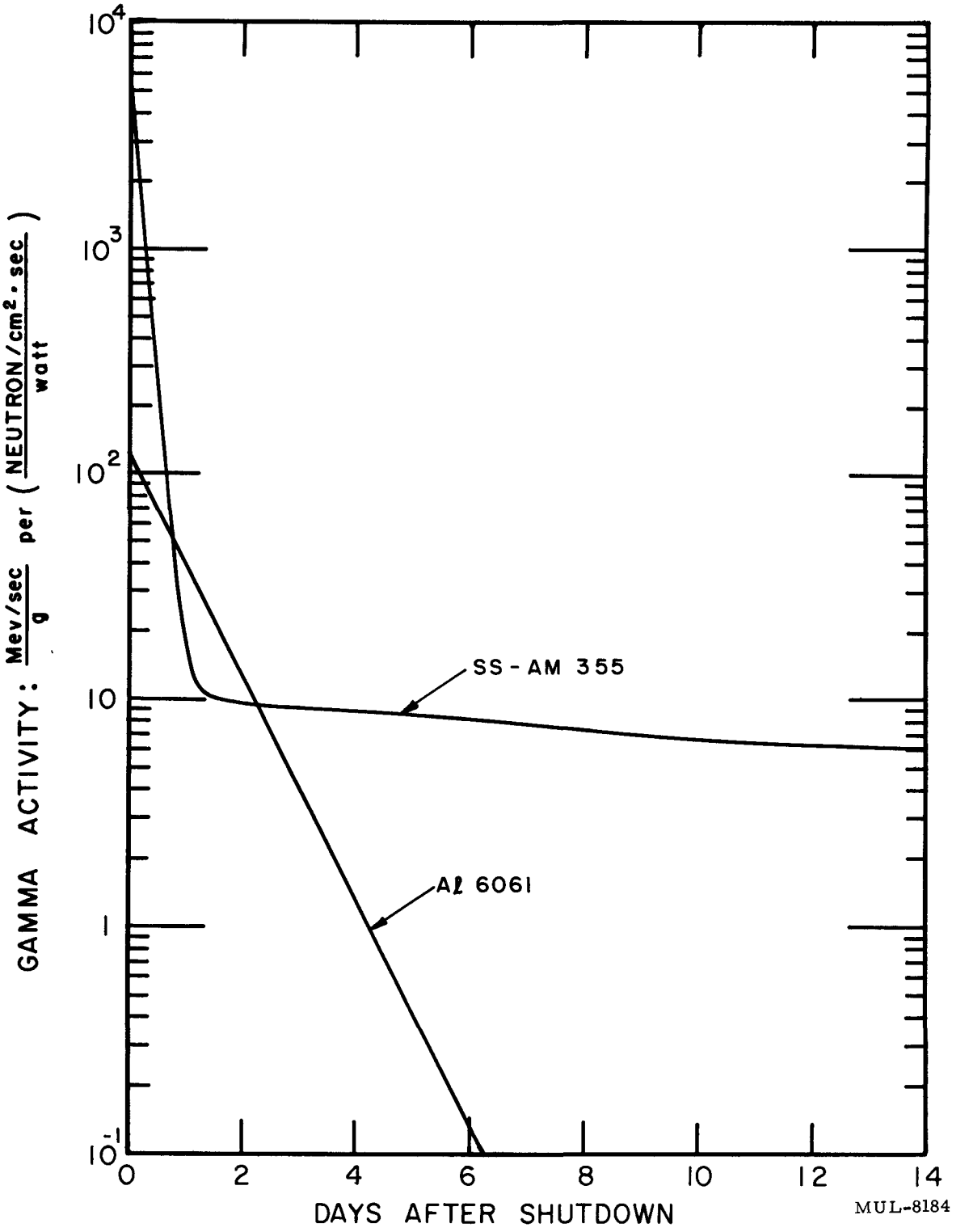

Fig. 5-43. Radioactivity of an aluminum and a stainless steel alloy as a function of time after shutdown.

Table 5-16. Radiation levels and damage thresholds

Material	Region	Integrated flux (neuts/cm^2) Fast	Slow	Threshold dose	Comments	Ref.*
Steel	Various structures near the core	2×10^{17}	2×10^{17}	$> 10^{19}$	No damage problem in Tory II-A	1
Aluminum	Pressure vessel	3×10^{18}	5×10^{17}	$> 10^{19}$	" " " " "	1
Hastelloy	Shroud	5×10^{18}	6×10^{17}	$> 10^{19}$	" " " " "	1
Molybdenum	Tie rods	9×10^{18}	$< 6 \times 10^{17}$	$> 10^{20}$	Improvement of certain physical properties noted	1
Boron steel	Control vanes	2×10^{16}	$< 5 \times 10^{17}$	?	No damage problem in Tory II-A (see text)	2
	Neutron shield	3×10^{16}	2×10^{17}	?		
$BeO-UO_2$	Fueled core material	9×10^{18}	$< 6 \times 10^{17}$	?	No damage problem in Tory II-A (see text)	2
BeO	Core material	9×10^{18}	$< 6 \times 10^{17}$	$> 7 \times 10^{20}$	Slight increase in crushing strength and thermal resistance at 7×10^{20} neuts/cm^2	1
Graphite	Side reflector	2×10^{18}	$< 6 \times 10^{17}$	$\sim 10^{19}$	Crystal structure breaks down from 10^{21} neuts/cm^2	1
H_2O	Reflector coolant	$< 2 \times 10^{18}$	$< 5 \times 10^{17}$	--	~2 moles of hydrogen formed during 100-sec run	3

* The numbers in this column refer to sources given below at the end of this section (Sec. 5.4.5).

experimental data are available on radiation effects on urania-loaded BeO,* or boron alloys. Both acquire imperfections in their crystal lattice owing to uranium fission or breakup of the boron nucleus upon capture of a neutron, and thus may suffer considerable modification of properties as structural materials. Neither is expected to undergo damage to a serious extent in the lifetime of Tory II-A, however.

Under the influence of radiation, water is decomposed chemically to produce approximately one hydrogen molecule per 100 ev of mixed radiation absorbed; in Tory II-A this represents about 50 liters of hydrogen (~2 moles) formed during a 100-second run. While the problem of excess hydrogen production exists where a large quantity of water is used as coolant and where the water is circulated in a closed sealed loop, conditions in the Tory II-A reactor are such as to render this problem negligible.

Organic materials are not allowed in the reactor because of prohibitive radiation levels (see items 3 and 4, two paragraphs below); permissible neutron doses are lower for organics than for structural materials, and, in addition, gamma radiation plays an important part in damage to organic materials.

The estimated radiation damage thresholds for Tory II-A components together with the integrated neutron flux doses at appropriate points are summarized in Table 5-16. It may be seen that expected radiation levels are safely below the threshold values.

Information on radiation damage was derived from the following sources:

1. Battelle Memorial Institute reports — "The Effect of Nuclear Radiation on:

Electronic Components and Systems" — REIC-2;

Ceramic Materials" — REIC-2-C;

Elastomeric and Plastic Materials" — REIC-3;

Lubricants and Hydraulic Fluids" — REIC-4;

Structural Metals" — REIC-5.

2. J. J. Harwood, The Effects of Radiation on Materials (Rheinhold Pub. Corp., 1958).

3. B. T. Price, Radiation Shielding (Pergamon Press, 1957).

---

* Some additional information on radiation damage to BeO is now available — see ref. 2 (UCRL-5515) Chapter VII.

4. General Electric Co. Aircraft Nuclear Propulsion Dept., report No. APEX-357, "Estimated Radiation Stability of Aircraft Components."

5.4.6 Radiation Effects on Control System

The parts of the control actuator system which will be exposed to the highest radiation level are the vane actuators, located about 5 feet from the inlet end of the reactor. These hydraulic actuators, eight in number, encircle the reactor inlet air duct. Not only can the components be heated by gammas and neutrons, but also the hydraulic fluid and the seals can suffer direct radiation damage if the levels are sufficiently high. It is more meaningful, therefore, to solve for the number of rads per gram per second than Mw/ft^3, since the former unit allows an estimate of the temperature rise during a run as well as allowing a direct comparison to be made with known radiation tolerance levels.[18, 19]

The gamma radiation from the core is attenuated by the front support structure, the air duct wall, and a special 4-inch shield immediately in front of the actuators. These attenuate to the extent of four mean free paths. The control system gamma shield receives about 200 rad/sec, or 5×10^{-4} cal/g sec. The temperature rise there from gammas is, therefore, insignificant. Beyond the shield, the primary gamma intensity is 1.2×10^{11} Mev/cm^2 sec. In a material with unit density and a composition like CH_2, the energy attenuation length is about 30 cm; the dose rate is, therefore, 65 rads/sec, or 2.3×10^5 rads/hr. Since a Tory II-A core is expected to have an operating lifetime of about one hour at full power, the latter quantity is an indication of the total gamma dose received.

Conventional seals such as those made of rubber have a gamma damage threshold of 2×10^6 rads, while hydraulic fluids have a limit of more like 10^8 rads;[18, 19] therefore, primary gammas are not likely to cause trouble in the control system. It is now necessary to appraise the effects of fast and thermal neutrons.

Fast neutrons can release considerable energy in hydrogenous materials. A collision of a fast neutron with a proton reduces the neutron energy to one-half of its initial energy on the average. If the support structure and air pipe did not interfere with the fast neutron flux, its intensity at the control system shield would be 1.1×10^{13} Mev/cm^2 sec. Fortunately, since the scattering mean free path in steel is about 6 cm, it is reasonable to expect that any portion of the control system can "see" only one-half of the front face of

the side reflector; furthermore, only one-third of the fast neutron current which leaves the front end departs from the front face of the side reflector. Therefore, the intensity is reduced to 1.8×10^{12} Mev/cm^2 sec. The control system gamma shield is expected to reduce this by another factor of 2 through back scattering; energy degradation in the shield should be insignificant. Therefore, 9×10^{11} Mev/cm^2 sec falls on the seals and hydraulic fluid. The energy degradation length in the latter materials ($\rho \simeq 1.0$) is about 10 cm. This implies a dose rate of 5×10^6 rads/hr, which indicates that conventional seals cannot be tolerated. Hydraulic fluids may be employed, but it will be necessary to check the condition of these fluids occasionally during the operating program to ensure satisfactory operation.

Thermal neutrons contribute to the gamma radiation damage of fluids and seals by direct capture gamma production in the fluid and in the control system shield. The latter effect is actually more important, partly because the gammas from iron are much more energetic than those made from neutron capture by protons. Heating by externally made capture gammas in CH_2 ($\rho = 1$) amounts to 1.2×10^6 rads/hr; direct action of thermals contributes 4×10^5 rads/hr. The sum is the threshold dose for conventional (e.g., rubber) seals. Therefore, one is obliged to avoid the use of rubber seals because of thermals as well as fast neutrons. It is easy to shield for thermals, but the fast neutrons are very difficult to eliminate if space is at a premium.

It is seen that for hydrogenous materials (such as CH_2, $\rho \simeq 1.0$), the primary gamma energy deposition rate in the area of the control system is 2.3×10^5 rads/hr; the fast neutrons contribute 5×10^6 rads/hr. Thermals account for 1.6×10^6 rads/hr through capture in the material itself and capture gammas from the adjoining steel shield. The sum is 6.8×10^6 rads/hr.

6. CONTROL SYSTEM

6.1 Introduction

The Tory II-A control system, described in this chapter, was designed to meet some unusual problems in reactor control.

A desire existed to gain experience with the sort of fast-responding system which will be required for engine control. The combination of very fast actuator motion with the large amounts of reactivity available in the reactor control elements could create great potential hazard to the reactor.

In addition, emergency control or shutdown procedures are complicated by a need to avoid thermal stresses involved in an immediate complete shutdown, so that the usual scram provisions must be avoided except as an ultimate resort under exceptional conditions. Transients at high power levels must occur only in a controlled manner, subject to preselected limitations.

Because of the limited air supply, high power runs can last only for a minute's duration or so; whatever experiments are desired must be carried out in this short period. Thus, there is little opportunity for reflection or choice by the operator during a high power run, and a high penalty for mistakes. For this reason, as well as the need for immediate and accurate response to accident conditions, control of the reactor must be highly automatic. This provision has been extended even to very low power levels, so that the reactor may be brought up many decades in power under completely automatic control.

Finally, a need for exceptionally high reliability of all components is felt, because of the difficulty of making repairs. Direct access to the reactor for parts replacement or repair at the test point will not be possible, because of high radioactivity levels as well as the need for specialized heavy tools. Consequently, each repair will involve disconnection of the reactor and return to the disassembly building, with considerable loss of time.

The Tory II-A control system has been designed to provide safe, stable, reliable control of the Tory II-A reactor at all power levels. It must be capable of performing all steady-state and transient studies which are anticipated, but, in general, has little application to a flight-type control system. Wherever possible, proven methods and state-of-the-art hardware have been used.

6.2 System Characteristics and General Requirements

The variables which must be controlled or held within limits on the Tory II-A reactor are the reactor power level, the period, and the core and air

temperatures. The Tory II-A control system maintains control of the reactor through control of the reactor power level, period (during transients), and air flow rate. The temperatures are thus dependent variables, and can be controlled only indirectly. Direct temperature control is ruled out for the present by the lack of straightforward, reliable methods of temperature measurement, especially in the highest operating ranges of power and temperature.

Requirements which the control system must fulfill are as follows:

1. Temperature Requirements. The control system must:

(a) Take the core temperature from ambient to maximum design temperature in a quasi-linear fashion in approximately 5 minutes.

(b) Produce a 5% change in core temperature in 5 seconds.

(c) Hold the core temperature constant to within 1% of the desired value.

2. Power Requirements. The control system must:

(a) Take reactor from 0.01 watts to 10 kw in 10 minutes (under manual control).

(b) Take reactor from 10 kw to 10 Mw in 1 minute (under manual or automatic control).

(c) Take reactor from 10 Mw to 160 Mw in approximately 15 seconds (under automatic control).

(d) Take the reactor from 160 Mw to 10 Mw in 15 seconds (under automatic control).

3. Period Requirements. It is desirable that the reactor positive period be kept above some minimum value during transients. It is expected that the minimum positive period tolerated during Tory II-A operation will be of the order of 2-5 seconds.

4. Flow Rate Requirements. The air supply automatic control system must be capable of scheduling the air flow rate through the reactor such that the temperature requirements given above can be realized when the power is varied in the manner indicated.

There are four basic modes of power control: Manual, automatic, fast reset, and scram. Control with these four modes, which will be defined later, represents a systems method of maintaining safe, stable, reliable control of the reactor through control of two primary reactor parameters: power level and period. The salient features of the system which employs these four modes are:

1. Control of the reactor power level and period by means of conventional feedback control methods during automatic control. Closed-loop position control of the control elements during manual control.

2. Restriction of the amount of fast positive reactivity available in the system, to provide safe control.

3. Provision of sufficient fast negative reactivity to allow recovery from all foreseeable accident situations. This fast negative reactivity is used in a controlled manner in the fast reset mode so as to avoid thermal shocks at high power levels.

4. Use of a number of control elements, individually actuated, thus providing additional reliability. Reactor operation could be continued in spite of malfunctions in several individual control-element-actuation subsystems.

5. Provision of an independent scram-override actuation system. This system allows fast scram from a stored source of energy as a last resort following loss of all other control. In addition, the system provides a hydraulic override method of actuating any particular control element in the event of a malfunction in the servo system which normally actuates that element. This helps relieve the irrepairability situation.

The control system uses twelve control elements: eight identical control cylinders and four identical control rods. Briefly, the control elements are used as follows:

1. The eight shim cylinders (also referred to as vanes) compensate for reactor temperature changes, and for slow changes in fuel element composition. They also provide negative reactivity for shutdown.

2. One of the control rods is used as a vernier rod, providing primary fast reactivity adjustment to control power level.

3. Two of the control rods are used as safety rods, providing additional negative reactivity in the fast reset mode.

4. One rod can be used as an oscillator rod or as a spare vernier or safety rod. When serving as an oscillator rod, it will be used to:

   (a) Measure the frequency response of the reactor.

   (b) Produce reactivity perturbations to check the control system performance.

   (c) Determine the worth of the shim cylinders.

In addition to the functions outlined above, all twelve control elements are used in the scram mode to shut down the reactor in case of an actual or

potential accident.

Only radiation-resistant materials will be used on components located near the reactor. No organic materials are to be used for seals, packing, etc. in the region 5 to 10 ft from the inlet end of the reactor, since the integrated radiation flux there will exceed their tolerance.

6.3 Description of Control System

The requirements stated in the sections above have been met in the system which has been designed. A descriptive account of this system is given in the present section; a more detailed analysis of system operation is given in Section 6.4. For a complete analysis from the viewpoint of servosystem theory, the reader is referred to a separate report.[20]

6.3.1 Nuclear Control Elements

Mechanical details of the control elements were presented in Section 4.1.1, and analysis of their neutronic behavior in Section 5.2.3. A brief review of some of their characteristics, with particular attention to their properties as control system elements, will be useful here.

It will be recalled that Tory II-A has two types of control elements, known as rods and cylinders (or vanes). All are contained in the radial graphite reflector. The eight cylinders are placed symmetrically around the reflector so that they occupy most of its volume. Each rotates on an axis parallel to the principal reactor axis, and thus shifts neutron-absorbing material toward or away from the reactor core. The four rods slide lengthwise through the reflector, into and out of channels placed very near the core, spaced evenly around the reflector. The rate at which motion of each element brings about change in reactivity depends on the position of that element as well as the position of all other elements, so that having accurate knowledge of the reactivity due to the control elements requires exact specification of the position of each of the 12 elements. Figure 6-1 shows the overall configuration of the reactor and elements of the control system.

Table 6-1 summarizes the mechanical and neutronic characteristics of the control elements. Section 5.2.3 may be consulted for a detailed discussion of the reactivity worth of the control elements, as a function of their positions.

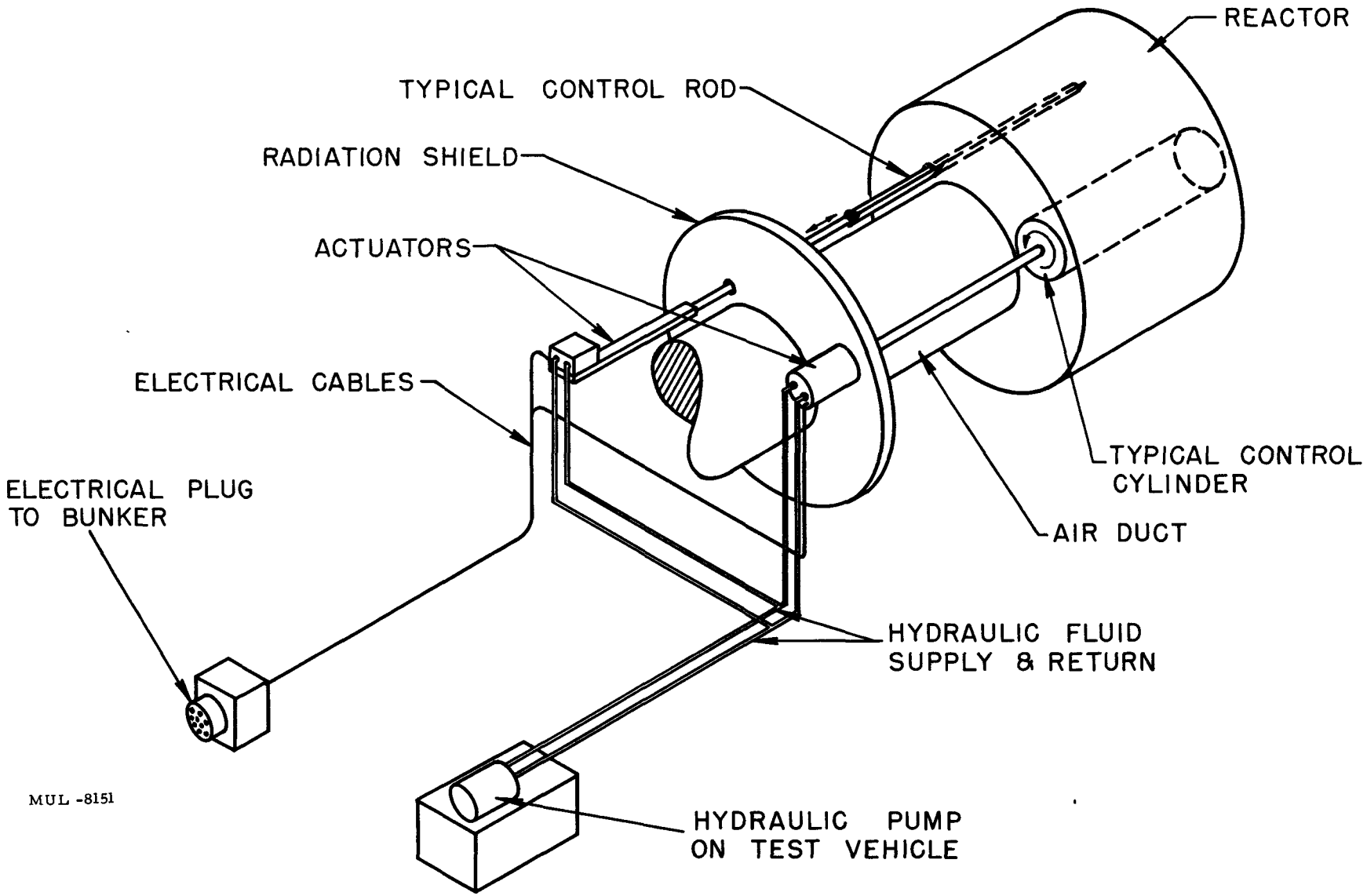

Fig. 6-1. Arrangement of control elements on reactor.

Table 6-1. Characteristics of control elements

Characteristic	Type: Rotating cylinder (Vane)	Sliding rod
Function	Large, slow reactivity adjustments	Power control, fast reset, calibration.
Number	8	4
Dimensions	22 in. diameter 49 in. length	1/4 in. thickness 4 in. width 40 in. length
Inertia	180 lb-in.-sec^2	45 lb
Travel	0° to 180°	40 in.
Material	2% boron steel	2% boron steel
Reactivity worth	0.12 absolute (all eight together)	0.0013 to 0.0060 abs (each rod).
Speed of response	Normal rate: 1-5 rad/min Fast reset rate: 0.55 rad/sec Scram rate: 3 rad/sec	180 in./sec

6.3.2 Control Actuation System

1. Actuation Subsystems

In Section 6.2, it was pointed out that there are four basic modes of power level control. In order to provide these four modes of control, there are two independent subsystems which can actuate each control element. These subsystems are defined and described as follows:

(a) Servo control actuation subsystem. This subsystem is a conventional electro-hydraulic position servo which is shown schematically in Fig. 6-2. It provides actuation of the control element in the automatic, manual, and fast reset modes. During automatic control it functions as a closed

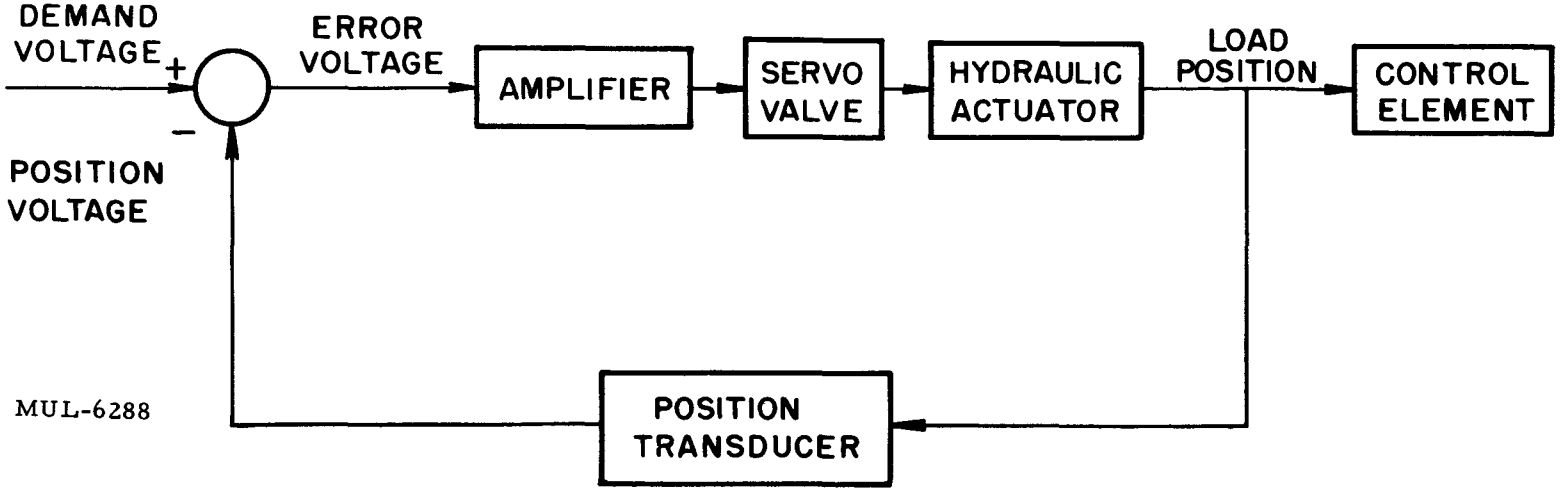

Fig. 6-2. Servo control actuation subsystem.

inner loop of the overall control system; in manual control and fast reset the position of the control element is directly controlled.

(b) Scram-override actuation subsystem. This subsystem which also employs electro-hydraulic actuation uses the same actuator, but operates independently of the servo actuation subsystem and is capable of overriding it, if both are attempting to actuate the control element at once. It provides actuation of the control element in the scram mode and is designed "fail-safe" such that, in the event of complete electrical or hydraulic power failure, each element is driven to the "full in" position by pneumatic-hydraulic accumulators located immediately adjacent to each actuator. In addition to the scram function, this actuation subsystem is capable of override positioning of a control element when the override method of actuation is selected for a particular control element. This can be done from the control point during reactor operation and all control elements can be controlled individually in this manner. When the override method of actuation has been selected there are three functions which can be performed: (1) In slow, (2) Out slow, (3) Hold. The "In slow" and "Out slow" rates are determined by the setting of a flow limiter which is set at assembly time and cannot be changed from the control point. These rates will be very low in order to maintain reactor safety. With these three functions, one can deactivate any control element in any desired intermediate position in case of malfunction of the servo actuation subsystem. In addition, if desired, one can "manually" move the deactivated member and, in the case of a control vane, it could be made to follow the other control vanes (such as during a transient). It is expected that override control of any control element will be a "flight engineer" type operation and will not be performed by the reactor operator.

2. Actuators

The power conversion elements of the control system are the fluid transfer valves and the hydraulic actuators. The actuators are mechanically connected to the control elements as indicated in Fig. 6-1.

The control rods are driven by hydraulic cylinders having a total stroke of 40 inches with approximately 2 inches at each end devoted to hydraulic buffing. These actuators have an effective area of 0.425 $in.^2$ which gives a maximum force output of 1275 lb in a 3000-psi system. This imparts a linear acceleration of approximately 913 ft/sec^2 to the 1.4-slug mass of the moving portion of the assembly. With the blade fully withdrawn, the overall length

of the control rod case and actuator is approximately 20 ft.

The vanes are driven by rotary-vane type hydraulic actuators with 180° of travel between mechanical stops. Internal hydraulic buffing is provided at the limit stops. These actuators develop a stall torque of approximately 10,000 lb-in. with a 3000-psi pressure differential across the moving vane. This stall torque will impart a rotational acceleration of approximately 55.5 rad/sec^2 to the 180 lb-in.-sec^2 inertia of the control vane. This results in a maximum peripheral acceleration of approximately 51 ft/sec^2 (1.58 g's).

Both the linear and rotary type actuators are fabricated entirely of radiation resistant materials. Conventional elastomeric seals have been replaced with seals using either all-metal, carbon, or graphited-asbestos materials. In other respects they are conventional components designed for simplicity and a maximum in reliability.

3. Fluid Control Valves

(a) Servo Valves

The servo control actuation subsystems employ two-stage, four-way, electro-hydraulic, linear, flow control servo valves. The servo valves driving the control rods are sized so that they have a flow capacity sufficient to provide saturated rod velocity of not less than 15 ft/sec. This allows a full stroke rod traverse in approximately 0.23 second. The servo valves driving the vane actuators are similar, but are sized to provide the very slow vane speeds required. All servo valves are fabricated of radiation-resistant materials and contain no organic seals.

(b) Solenoid Valves

Figure 6-3 shows schematically the electro-hydraulic circuitry of each control element actuation system with a solenoid chart showing energized and de-energized solenoids for the various control functions. This schematic applies to both the control rod and the control vane systems; the only differences in the two are the motion of the actuator and the maximum flows required.

The solenoid valves shown in Fig. 6-3 are specified for 3000-psi service with ac or dc solenoids; they are to be fabricated of materials which possess adequate radiation resistance. Valve A is a double solenoid 3-position valve to be mounted between the servo valve and the actuator. Valve B

SOLENOID CHART

OPERATION	A_1	A_2	B	C
SERVO CONTROL	x			
IN SLOW				x
OUT SLOW			x	x
HOLD		x		
SCRAM				

x - Indicates Energized

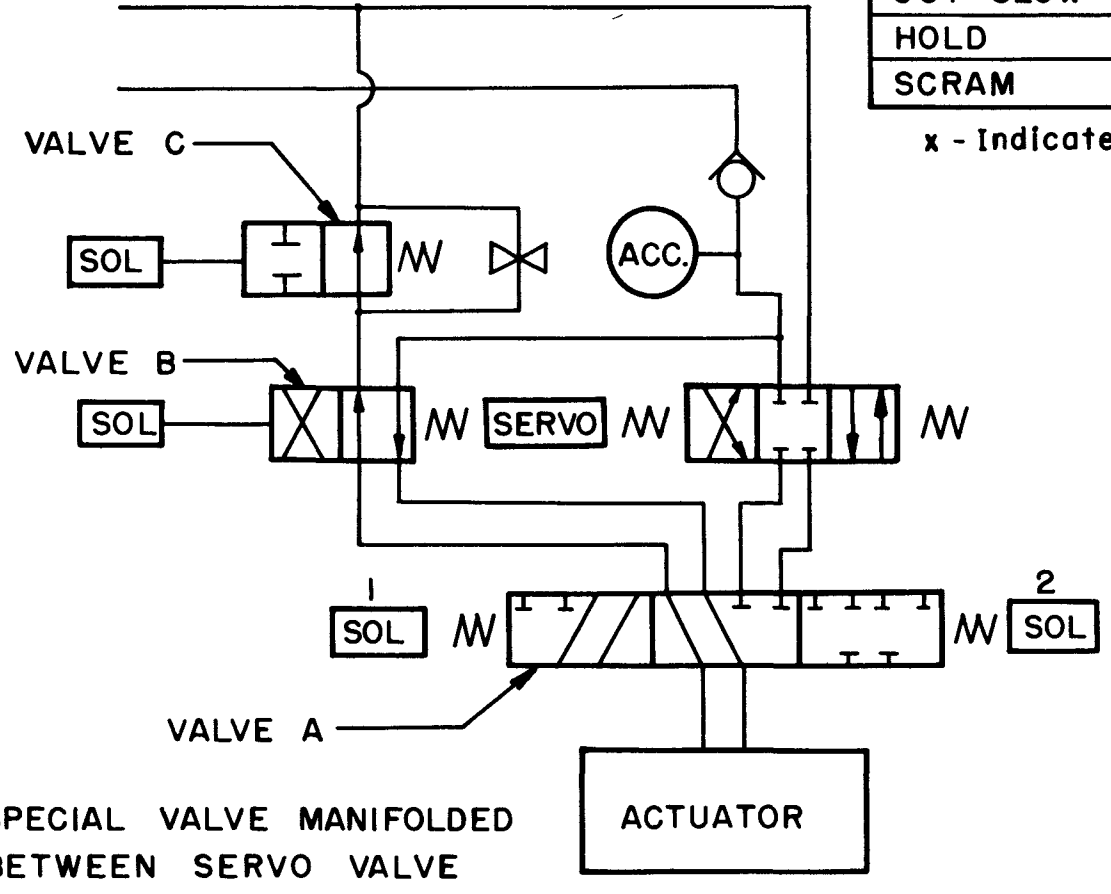

MUL-6188

Fig. 6-3. Electro-hydraulic circuitry used for actuation of control element.

is a 4-way, 2-position spring offset valve and valve C is a normally open shut-off type.

4. Power Supply

Hydraulic power will be supplied to the system by a positive displacement pump capable of delivering 10 gallons per minute at 3000 psi when driven by a 20 hp, 3-phase electric motor. The pump unit will also include a system pressure relief valve, 25-gallon tank, return check valve, hydraulic accumulator, heat exchanger, oil temperature control valve, strainer (air and oil), fluid-level indicator, fluid temperature transducer, and a 5-micron full-flow hydraulic oil filter with integral pressure relief.

Pressure and return lines will extend from the power supply unit to distribution headers and on to individual control assembly connection stations.

The entire pump unit will be located at a sufficient distance from the active core to allow the use of standard materials without danger of radiation damage.

5. Scram Energy Source

An individual pneumatic-hydraulic accumulator is located at each control actuator to serve as an emergency source of hydraulic power. The control rod accumulators will also supply transient, high power demands for rapid positioning of the vernier and safety rods. For a given gas precharge pressure, all accumulators will be continuously charged to full fluid capacity by the pump. Return flow in the pressure lines is prevented by check valves at each control assembly as well as the pump unit.

6. Position Transducers

Each control-rod actuator uses a linear differential transformer for position feedback and indication. This transducer is excited by a 5-kc sinusoidal input voltage and produces a secondary voltage proportional to the axial displacement of a moveable probe which is attached to the rod of the linear-type actuator. This voltage is demodulated by a phase-sensitive demodulator to provide the dc voltage for position feedback and indication. The total nonlinearity of the transducer-demodulator combination is less than $\pm 0.5\%$, and the resolution is $\leq 0.1\%$. The unit is both temperature and radiation insensitive.

High temperature dc potentiometers will be used for position feedback and indication on each control vane; they contain all radiation-resistant

materials. The nonlinearity of these transducers is below 0.3% and they possess a resolution capability of 0.17%.

7. Installation

The eight vane actuation assemblies are to be mounted on 45° annular segments of 1-inch-thick steel plate. These are to be fastened to the 3-inch-thick shield as shown in Fig. 6-4. The rotary actuator shaft coupling extends through the shield and connects with the 5-foot vane shaft extension. This shaft extension is essentially a pipe size to minimize mechanical compliance, with coupling arrangements at either end to allow for shaft misalignment.

In the event of component malfunction, the complete mounting plate can be removed to a location where remote manipulator facilities are available for further disassembly and checkout before the unit is put back into service.

The same "modular" approach is to be applied to the control rod actuation assemblies. Figure 6-5 shows the manner in which the actuator is coupled to the control blade.

6.3.3 Control Modes

This section describes the manner in which the reactor power level is controlled using the four basic control modes. It presents a functional description of how the reactor control system is switched from one mode to another.

The four basic modes of power level control of the Tory II-A reactor are (1) Manual, (2) Automatic, (3) Fast reset, and (4) Scram. During normal control the control system is in one of the first two modes (whichever one has been selected); the control system is placed in one of the latter two modes only when an accident or potential accident has been detected.

Control in each of these four modes is briefly described below.

1. Control in the Manual Mode

Here, control of the reactor power level and period is maintained by the reactor operator who programs rod and vane position demands. The rod position demand is normally programmed by means of a potentiometer on the manual control panel, but can also be programmed by means of a function generator input voltage. The latter might be used where it is desired to move the rod in some preset manner as a function of time. A combination of the two inputs can also be used. The vane position demand can be programmed only with the manual vane demand potentiometer. The rod and vanes are actuated by their closed-

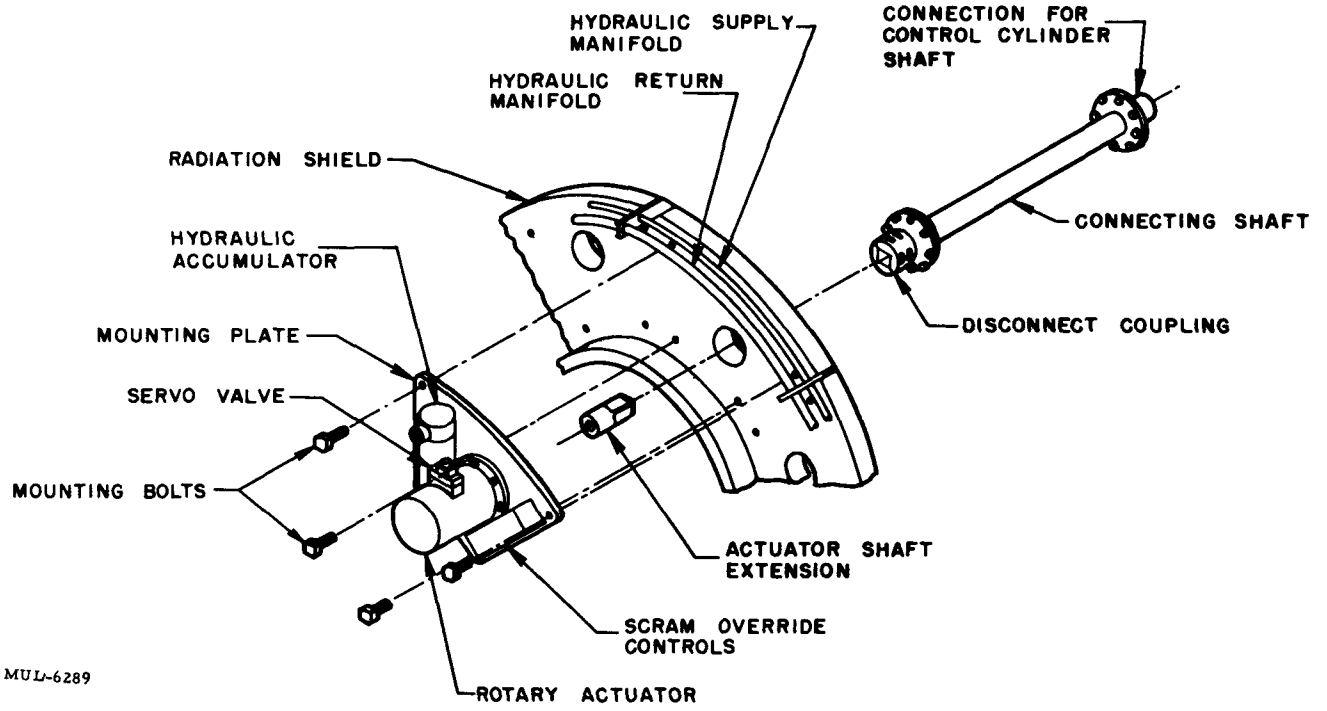

Fig. 6-4. Typical control vane actuation provision.

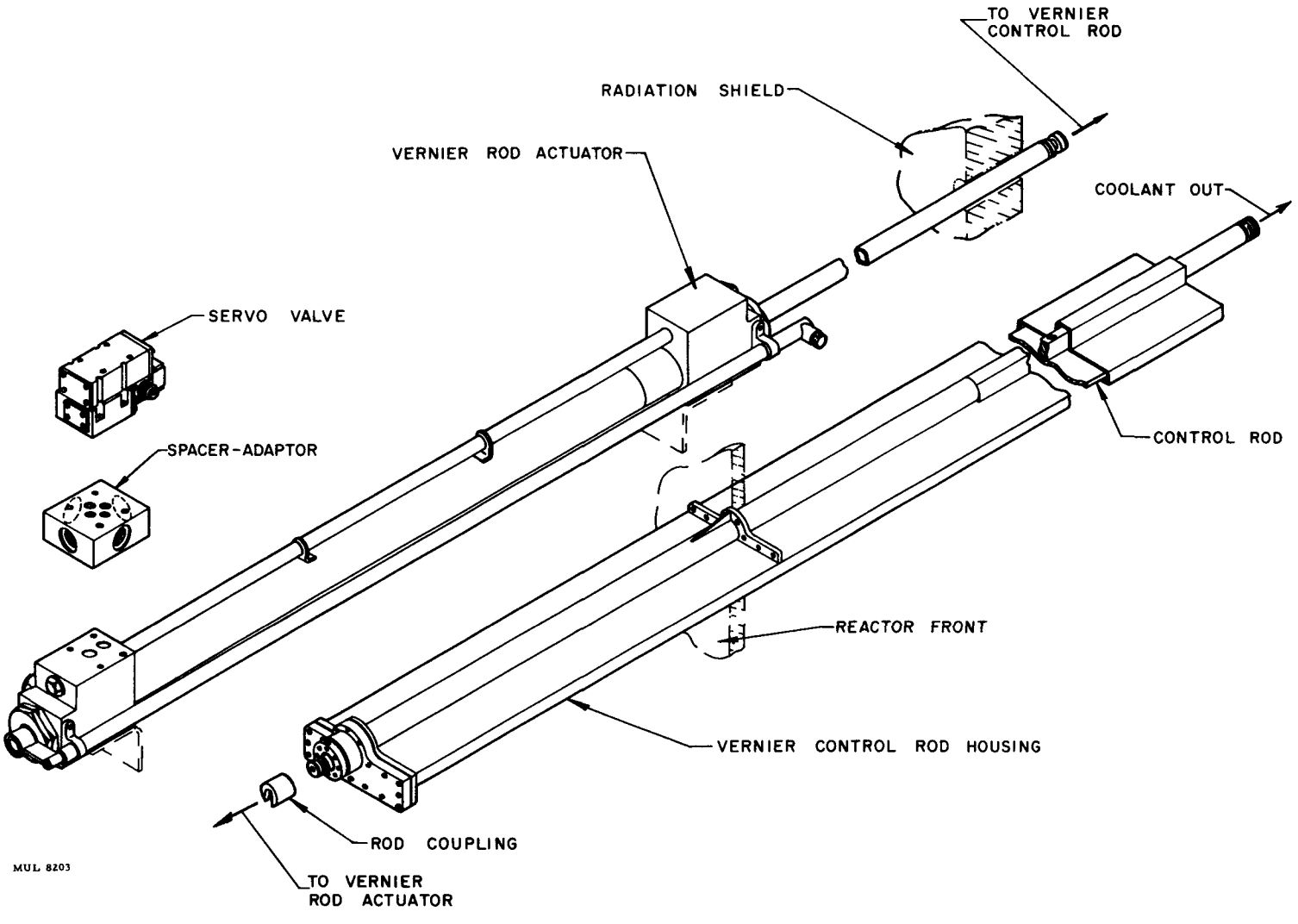

Fig. 6-5. Rod actuation assembly mounting.

loop servo subsystems which utilize position feedback. The vanes are electrically ganged by means of a common position demand voltage. The control system is stable in the manual mode because of the negative temperature coefficient of reactivity.

The reactivity rates which are possible while in the manual mode are those that correspond to the flow-limited saturation velocities. For the rod the saturation velocity of 15 ft/sec gives a reactivity rate of approximately 0.03 abs react./sec. For the vanes, the saturation velocity of 0.5 rad/sec gives a reactivity rate of approximately 0.016 abs react./sec. Rates of change of position demand voltage obtainable by the operator will be limited far below these maximum values. The rod, however, can be programmed to give the maximum rate when the function generator is used to provide the position demand voltage.

2. Control in the Automatic Mode

Control of the power level and period is maintained using the automatic control system which will be described in the next section. The operator can use either log power detection (for multi-decade automatic control) or linear power detection for fine control over 1 - 2 decades. In either case, the operator programs the demand power level by positioning a potentiometer on the automatic control panel, or by means of a function generator input voltage. The latter is used to program the power on a preset time schedule. Again, a combination of the two inputs can be used which allows manual "trimming" of the preset program during the course of a run.

The positive period demand is also programmed by the operator by means of a potentiometer on the automatic control panel. Normally, this will be set prior to the run and will remain fixed during any particular transient situation.

3. Control in the Fast Reset Mode

When the control system is placed in the fast reset mode, control of the reactor is again maintained through control of the position of the rods and vanes. Control in this mode is analogous to that in the manual mode, except that (1) the two safety rods are inserted in parallel with the vernier rod and all three control rod servo subsystems receive a position demand voltage which corresponds to the FULL IN position, (2) the control vanes are rotated toward the FULL IN position by insertion of a large negative voltage at the input to the integrator which produces the vane position demand voltage. Thus in the fast

reset mode, all control elements are inserted into the reactor very rapidly. All three rods are inserted at their maximum controlled rate, which is the flow-limited saturation velocity. For all three rods, the saturation velocity is 15 ft/sec, which gives a reactivity rate of approximately 0.06 abs react./sec (all three). During fast reset the vanes are inserted at an angular velocity of approximately 0.5 rad/sec which gives a reactivity rate of 0.016 abs react./sec. The total negative reactivity rate possible in the fast reset mode as a function of time is shown in Fig. 6-6, where it has been assumed that the reactor was operating at equilibrium at full power (rod at center, vanes at 1 radian) when the reactor was placed in the fast reset mode. Also shown is a plot of total reactivity inserted as a function of time.

The control system is placed in the fast reset mode:

(a) if the inverse-period exceeds its preset maximum limit (period set point); and

(b) if the power level exceeds its preset maximum limit (power set point).

The control system will remain in the fast reset mode only when one or both set points are exceeded. When both power and inverse-period are below their set points, the control system will be returned to the automatic or manual mode depending upon which has been selected. Thus, the reset action is nonlocking. When the control system has been returned to the normal control mode, the safety rods are withdrawn from the reactor at a very slow rate by means of a memory amplifier and integrator. The latter is an electronic device for memorizing the safety rod position voltage at the end of the fast reset action and integrating from this initial condition up to the +10-volt level. Since the output of this integrator is the position demand voltage into the safety rods during normal control, the rods are withdrawn by this action. (+10 volts corresponds to the FULL OUT rod position). The safety rods are withdrawn at a velocity of approximately 20 in./min which produces a positive reactivity rate of 0.01 abs react./min. This is less than a third of the rate at which the vanes can introduce negative reactivity when moving 1 rad/min, so it is easily compensated for.

4. Control in the Scram Mode

Here, the vernier rod, two safety rods, oscillator rod, and eight vanes are inserted completely into the reactor at their maximum rates. Hydraulic

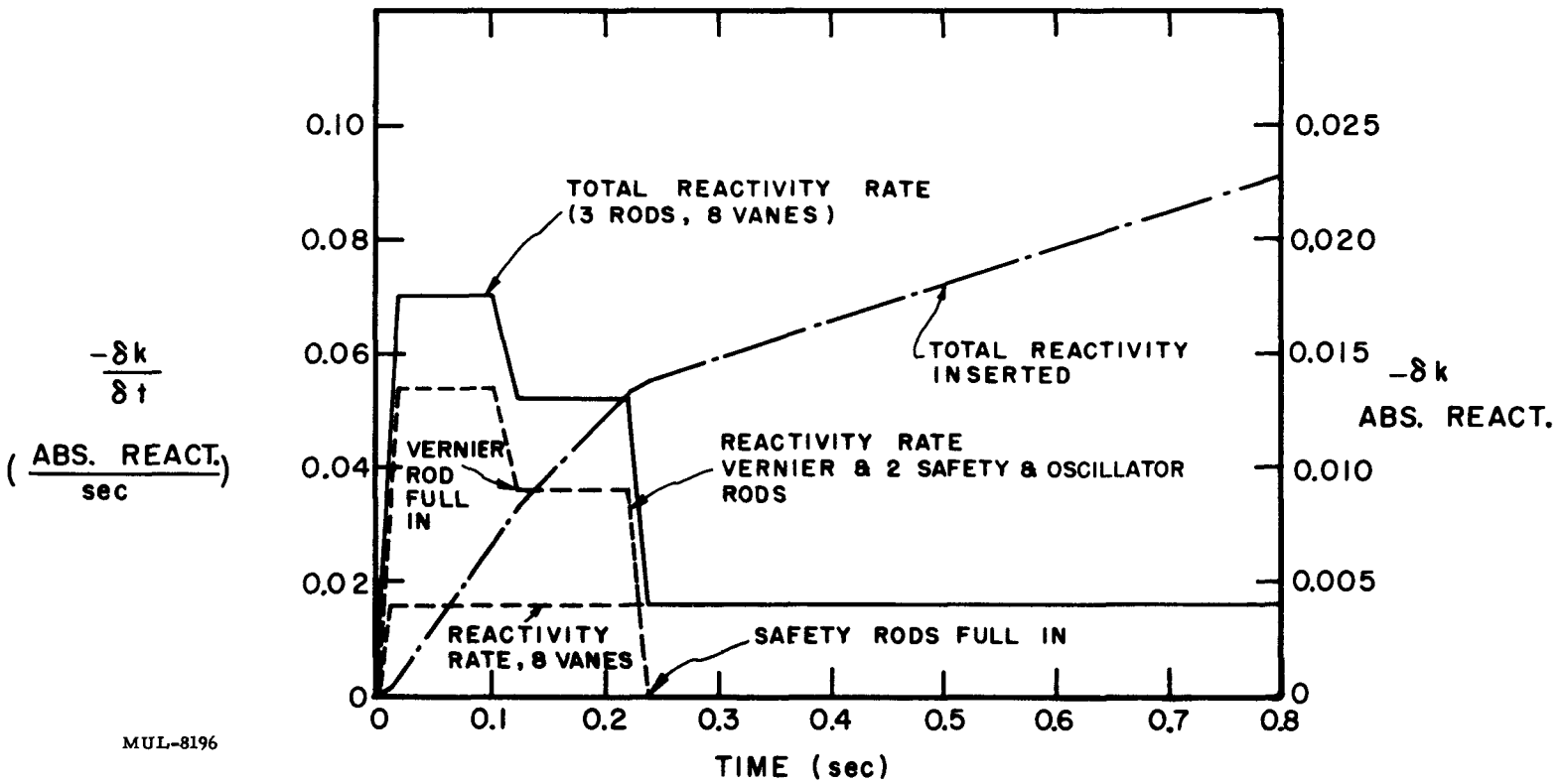

Fig. 6-6. Total negative reactivity rate and reactivity as a function of time in the fast reset mode.

power for this actuation comes from the scram accumulator through solenoid-type scram valves which have a response time of 0.05 second. In the scram mode all rods can be inserted at a velocity >15 ft/sec; the vanes are inserted at a rate of approximately 3 radians/sec. Figure 6-7 shows a plot of the reactivity rate and total reactivity as a function of time following the initiation of a scram action.

The scram mode is intended to be used only as a simple, foolproof, positive shutdown method; it will come into play only to prevent a reactor excursion if no other mode is operative.

5. Mode to Mode Transition

Automatic to Manual Operation:

The control system is taken from the automatic to the manual mode in two distinct steps. Interlocks insure that the transition is made in the prescribed manner. The steps are as follows:

(1) The vanes are first placed on manual control. Before this can be done, the vane position demand voltage, V_D, must be set equal to the voltage V proportional to actual vane position (see Fig. 6-2). When the vanes are switched from automatic to manual control, the rod is still maintaining power level in the automatic mode, so it is able to take any "bumps."

(2) The rod is placed on manual control. Before this can be done, the rod position demand voltage, V_D, must be set equal to the voltage V proportional to actual rod position.

Manual to Automatic Operation:

The control system can be taken from the manual to the automatic mode by simply depressing the designated button on the automatic control panel. It is important, however, to set the power level demand to the desired value before switching to automatic control. If no power jog is desired, the power level error meter should first be zeroed.

Linear to Log Power Operation:

Linear to log power operation can be effected by simply pressing the designated button on the automatic control panel. It is important that the log power error meter be zeroed before switching if a power jog is to be avoided. Log to linear power operation is carried out similarly; here, the linear power error meter should be zeroed. Figure 6-8 shows an operational diagram of the entire power, period control system in schematic form.

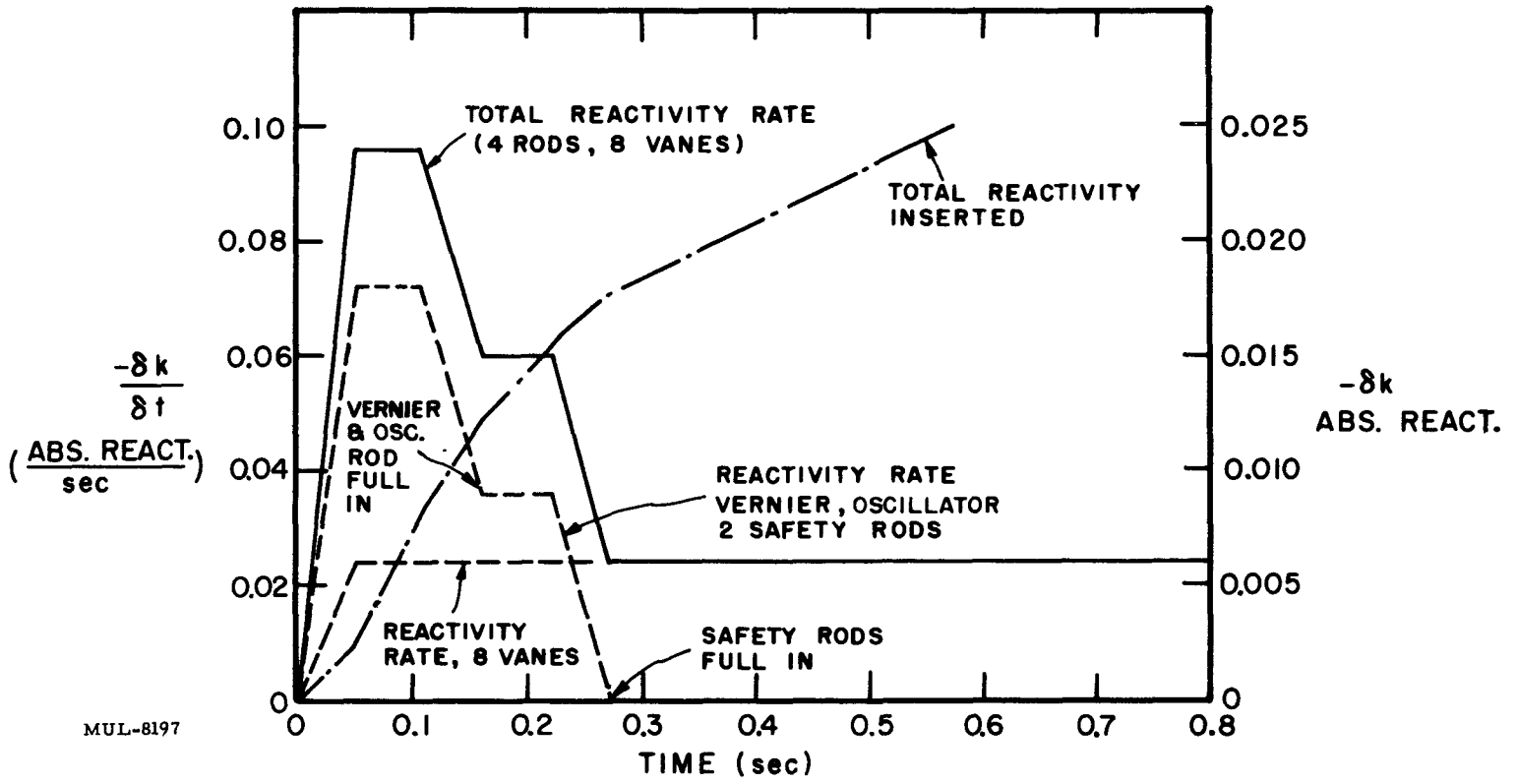

Fig. 6-7. Total negative reactivity rate and reactivity as a function of time in the scram mode.

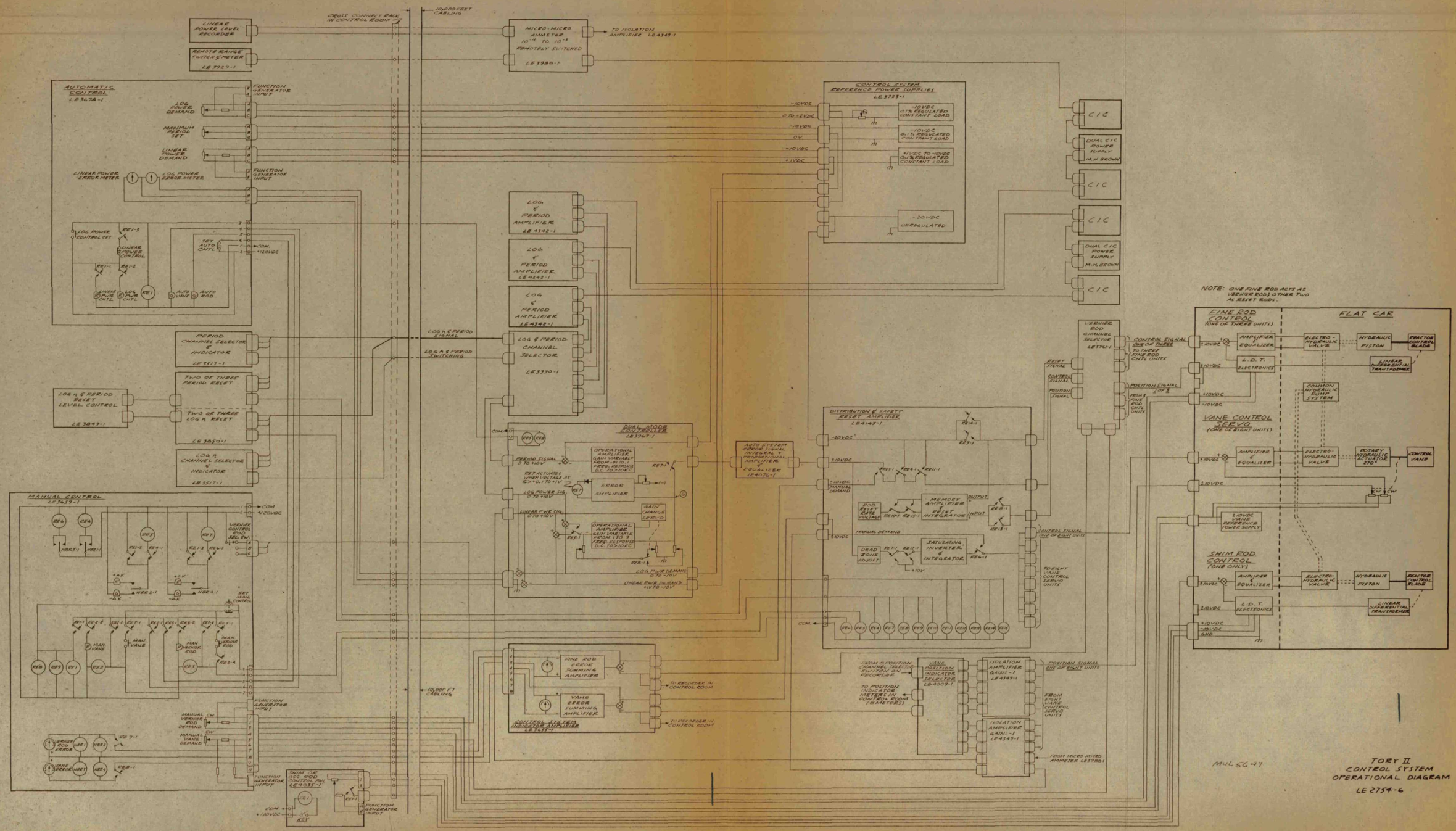

Fig. 6-8. Operational diagram of the reactor control system.

6.3.4 Design of the Automatic Control System

This section describes the system which provides automatic regulation of the power level and period. The method of control is characterized by the following:

(1) Closed-loop control of reactor power level at equilibrium or during negative power level excursions.

(2) Closed-loop control of reactor period during all positive power level excursions.

(3) Closed-loop control of power level and period over a number of decades using log n-period amplifier detection circuitry or alternate micro-micro-ammeter-detection circuitry for finer control of reactor power level; switching is required to use the latter type of detection over more than 1 or 2 decades.

(4) Use of fast vernier rod system and slow shim vane system in a parallel manner such that loss of one system (or part of it) does not cause loss of other. The rod and vane systems have been designed such that either one or both are capable of maintaining stable control of the reactor power level and period. Thus loss of rod does not produce instability, nor does loss of vanes.

Figure 6-9 shows in simplified block diagram form the system configuration which is employed to give this automatic control, where

T_c = core temperature
P = power level of reactor
$\dot{W}$ = flow rate through reactor
T_{gi} = air temperature at inlet to reactor
τ' = indicated period where $\frac{1}{\tau'} = \frac{1}{\tau}\left[\frac{1}{(1+0.01s)(1+0.1s)}\right]$
τ = actual reactor period
τ_D = demand period
δk_A = total excess reactivity inserted by control system
δk_R = excess reactivity inserted by vernier rod
δk_V = excess reactivity inserted by shim vanes
V_P = voltage proportional to power (or flux) level
V_{P_D} = voltage proportional to demand power level
ϵ_P = signal proportional to power level error
ϵ_τ = signal proportional to inverse period error
V_R = reference voltage at input to differential relay

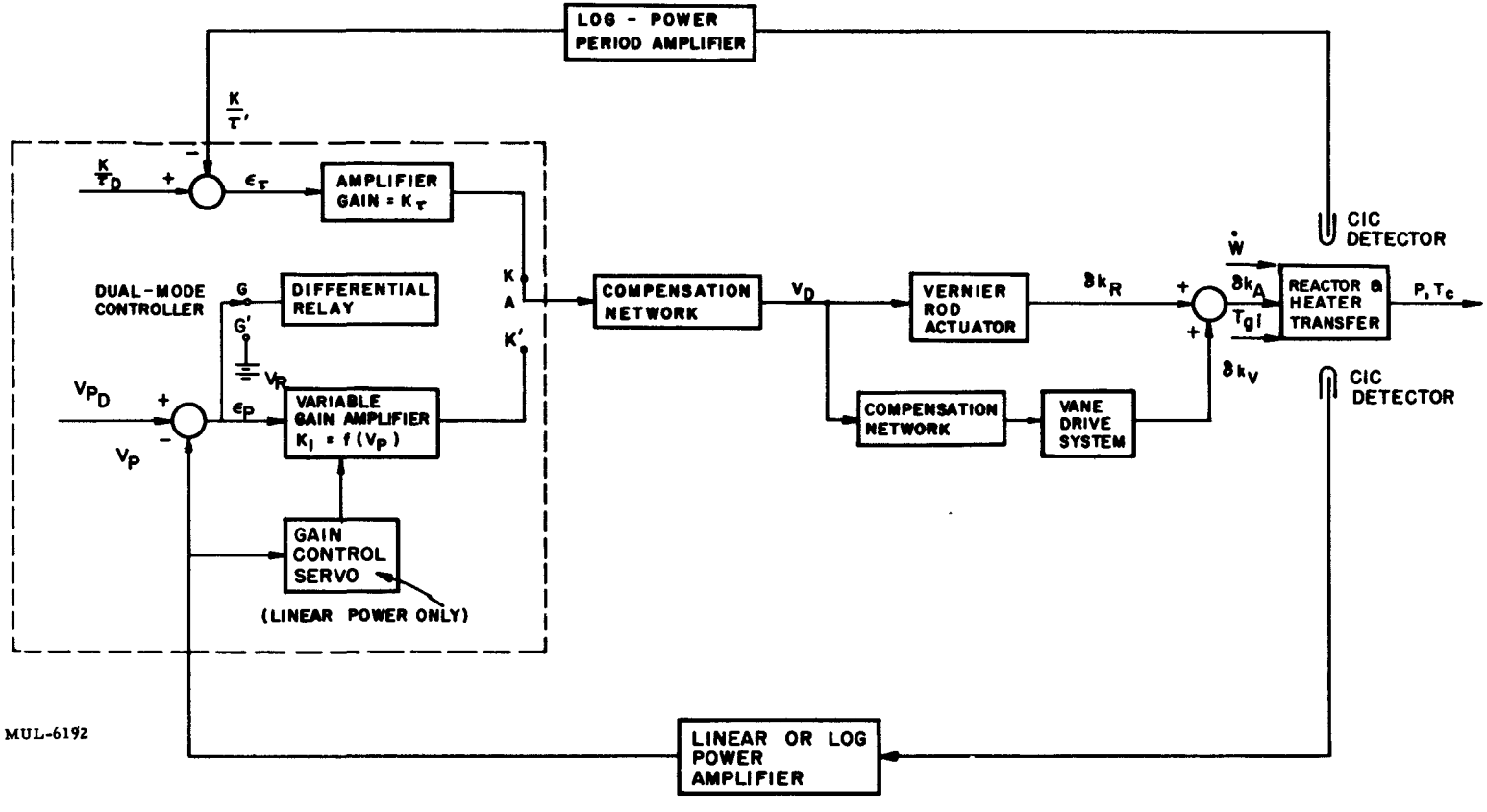

Fig. 6-9. Block diagram of the power, period automatic control system.

Shown within the dotted block is the "dual-mode controller," a simple logic circuit which serves the function of putting the control system in the power level or period control mode in the manner desired. The dual-mode controller operates as follows:

(1) If $\epsilon_P < V_R$, the differential relay is switched to the K' position, and the control system maintains control of the reactor power level. If V_R is some arbitrarily small voltage then this condition corresponds to equilibrium $\left[\epsilon_P = (V_{P_D} - V_P) = 0\right]$ or negative power excursions $\left[\epsilon_P = (V_{P_D} - V_P) < 0\right]$.

(2) If $\epsilon_P > V_R$, the differential relay is switched to the K position (as shown in Fig. 6-9) and the control system maintains control of the reactor period. The statement $\epsilon_P > V_R$ corresponds to the condition $(V_{P_D} - V_P) > V_R > 0$, hence period control is maintained during positive changes in power level.

It is seen that the power level and period systems share all control components except detection circuits and error signal amplifiers. Despite the number of common components, there are significant differences in these two systems, hence, the design of each will be considered separately. Response requirements are given below; system analysis is presented in Section 6.4.2.

1. Power Control System

The general requirements on the automatic power control system are included in the requirements given in Section 6.2. In addition to these, it is required that the automatic power control system

(1) possess an adequate margin of relative stability over the power range $10^{-5}\ P_0 \leq P \leq 10\ P_0$, where P_0 denotes full design power level. It is required that the system be stable with the rod loop alone and with the vane loop alone, as well as the normal situation where they are used together.

(2) show less than 5% overshoot to small step function inputs. (Note that this would apply only to negative power excursions, since the reactor is on period control during controlled positive power excursions.)

(3) possess a frequency response of approximately 10 cps for small signal inputs.

2. Period Control System

The requirements that are placed on the period automatic control system are as follows:

(1) It should be capable of providing stable control of period over the power range $10^{-5}\ P_0 \leq P \leq 10\ P_0$, with period variable from 1 to 20 seconds.

(2) It is desirable that the period control system show less than 10% overshoot to a step demand input and have a steady-state error which is less than 5% of the demand quantity $10/\tau_D$. Speed of response is relatively unimportant. The normal input to this system is a step function.

(3) It is required that this system share the control components used for the automatic power control system.

6.3.5 Air Control

At the time of writing, there is still insufficient quantitative knowledge concerning the air flow control system to include it in the system study. However, by design, the frequency response of the air flow automatic control system will be set about a decade below that of the power control system, so as to eliminate any interactions between the two systems. Because of this, the air flow can be regarded as constant over the time period of fast power transients as has been assumed in the synthesis of the power, period control system.

6.3.6 Reactor Operation

This section describes typical reactor operation as regards the power control system. It gives only a general outline of how the control system is used.

During a typical full power run, the reactor will be made critical and taken up to 10 kw under manual control. The latter operation will be done in approximately 10 minutes. At this point, the control system will be switched to the automatic mode using log power detection. After the core has reached 50% of the maximum design temperature, the power level will be programmed from 10 kw up to 10 Mw, this operation taking 1 minute or more. The operator can program this transient using either the power level demand potentiometer or a pre-programmed function generator input. The core temperature reaches its full design value in the 10-Mw power level range. After it reaches equilibrium, the power level is programmed from 10 Mw to full design power in approximately 15 seconds using log power detection. The flow rate is programmed concurrently so as to hold core temperature approximately constant. After a short period at full power and full temperature, the power level is returned to 10 Mw in approximately 15 seconds, the flow rate being reduced simultaneously. From this point the reactor can be shut down, if desired, in the inverse order.

There are many other operations preceding the full power run described above which place other requirements on the control system. For instance, the reactor will probably be taken as high as 10 Mw using the manual control system in order to check reactor parameters, behavior, and transfer functions before taking it through this level on automatic control. In the manual mode, the control system is stable so long as the reactor has a negative temperature coefficient of reactivity, regardless of the reactor transfer function. In the automatic mode, however, to have system stability it is required that the reactor behavior fall within certain predictable bounds. In either case, the fast reset action provides an additional safety factor.

Control in the automatic mode using linear power detection is also quite useful during certain operations. When it is desired that the reactor power level be held accurately at some level for long periods of time in order to calibrate or make measurements, linear detection is ideal, since then the system is much more sensitive to power variations than with log power detection. The power level can be programmed over a range of 1 to 2 decades without switching, when using linear detection, so the instrument range is sufficient for many experiments. One drawback of operation with linear power detection is that only 1 micro-micro-ammeter has been provided for control. In case of a detector malfunction, the operator is forced to switch to log power detection, which can introduce a power jog if the log power system does not have the same power demand as the linear power system.

No mention has been made, heretofore, of the manner in which the oscillator rod will be used. The oscillator rod will be used to give a measurement of the reactor transfer function when the control system is operating in the manual mode. Here the ratio $\frac{\delta P}{\delta k}(j\omega)$ is determined from measurements with small signal sinusoidal δk_A. When the control system is in the automatic mode, the oscillator rod can introduce δk disturbances to test the system response. It can also be used in the automatic mode to determine the worth of the vanes.

6.3.7 Accident Analysis

This section describes how the power control system would recover from several possible nuclear accidents using the fast reset mode of control. It is significant that the control system is capable of inserting more fast negative reactivity in the fast reset mode than in the scram mode, because of the much longer valve response time when in the scram mode (the scram solenoid valves

have a 50-msec response time vs a 3-msec response time for the servo valves). More important, however, is the fact that the fast reset action attempts to maintain the programmed power level while the scram action shuts down the reactor. During a full-power, full-temperature run, calculations indicate that a scram-type shutdown would produce thermal stress values high enough to entail danger of fuel element breakage. For this reason it is not considered desirable to put the control system in the scram mode as a result of excessive power or inverse period signals during high power runs ($P > 0.1\ P_0$). The fast reset mode actually provides more safety.

In order to illustrate the functional operation of the reactor control system, let us consider its action in two common accident situations: (1) The classical startup accident, from failure of power level detector; (2) The case where there are large reactivity perturbations due to loss of air or other unanticipated causes.

1. Failure of Power Level Detector. Before starting the run, the power level reverse set point would be set at a power level just above the highest anticipated operating level, e.g., 120% of full power. Similarly the period set point is set just above the maximum anticipated inverse-period level. With no feedback from the power level detector, assuming automatic control, the reactor power would go right by the demand power level at the demand period (since the system would be on period control). Upon reaching 120% P_0, the control system would be placed in the fast reset mode by the 2 out of 3 safety coincidence circuit and would remain there until the level was reset below 120% P_0, at which time it would again be placed in the automatic mode. This action would repeat itself and the reactor would oscillate about the set point until the operator switched another power detector into the control loop. Visual and audio warnings would be given to him until he did so.

2. Large Perturbations in Reactivity. The control system would act quite similarly when there are large perturbations in reactivity. Probably, inverse-period would exceed its set point first and the safety coincidence circuits would place the control system in the fast reset mode. It would remain there, until both power level and inverse period were below their set points. At this time, the control system would return to the selected mode. If this were the automatic mode, the control system would take the power level back to the demanded value. If the control system were operating in the manual mode, the operator would have to take the power back to the desired value.

Computed behavior of the control system during both of these accident situations is presented in Figs. 6-37 and 6-38.

The accidents that can be averted by use of the fast reset mode are obviously limited to those which introduce positive reactivity at a rate comparable to or less than the negative rate capabilities of the control system in this mode, and which have a total reactivity value less than that of the control elements. A "typical" air flow accident would introduce 0.002 to 0.004 (abs units) positive reactivity in a period of about 1 second. This can easily be counteracted by the control system in the fast reset mode, where the rods alone can introduce 0.03 abs react./sec.

The accident analysis outlined above considers only control of the primary control parameters: power level and period. It does not consider secondary parameters, such as core temperature and air flow. It is realized that a number of secondary parameters are most critical to safe reactor operation and wherever possible the primary parameter set points are placed so as to prevent secondary parameters from getting to dangerous levels. At present, analog computer studies are being made to determine suitable setback programs for the primary parameters which will give safe control of the secondary parameters in the event of some likely accident situations.

6.4 Servo-System Analysis

This section presents an analysis of the servo-systems involved in the Tory II-A control system, together with some calculated prediction of their behavior. An account of the servo control systems which regulate the position of individual control elements is given first; this is followed by a discussion of the operation of the overall power and period automatic control system.

6.4.1 Design of Servo-Control Actuation Subsystems

In the manual mode of control, the operator maintains the desired program on power and period by manually setting rod and vane position demands. Actuation is accomplished by means of the electro-hydraulic servo subsystems which position the vernier rod and the eight electrically ganged shim vanes. In the automatic mode of control, these same position servo subsystems become an inner loop in the overall control system; however, their performance dictates, more than any other factor, what performance can be realized with the reactor control system. In the fast reset mode of control,

the control elements are again positioned in an open loop manner using the position servo subsystems as in the manual mode (here, the maximum controlled shutdown rates are demanded, however). The scram mode of control uses an actuator common to all other modes, so one must consider the scram requirements as well as all others in selecting the actuator.

Hence, the position servo subsystems must be designed to provide certain requirements of each and all control modes, if a common actuation subsystem is to be used. This section outlines the requirements which the control rod and vane position servo subsystems must fulfill.

1. Control Rod Servo Subsystem

System Requirements

The requirements for the control rod servo subsystem, whether used as a simple position feedback system in the manual control and fast reset mode, or as an inner loop of the overall reactor control system in the automatic mode, are as follows:

(1) Position the control rod linearly within 3% over the 40 inches of travel with less than 0.05% dead zone.

(2) Possess a frequency response which is greater than 20 cps in the "small signal" linear region of operation.

(3) Show less than 12% overshoot to a step displacement input.

(4) Must be capable of completely inserting the rod in approximately 0.23 seconds in the fast reset mode. Hence, it must:

(a) Possess an orifice limited saturation velocity which is greater than 15 ft/sec.

(b) Possess an acceleration limit which is greater than 600 ft/sec^2 with 3000-psi pressure drop across the actuator.

The only scram requirement imposed on the actuator is the capability of complete rod insertion in less than 0.3 seconds. Since this requirement is less stringent than that imposed in (4) above, it will not be considered further.

Figure 6-10 shows the control rod servo subsystem in block diagram form, indicating the components which are to be located on the flat car with the reactor. The servo is a dc system, which uses voltages in the range 0 to ± 10 v.

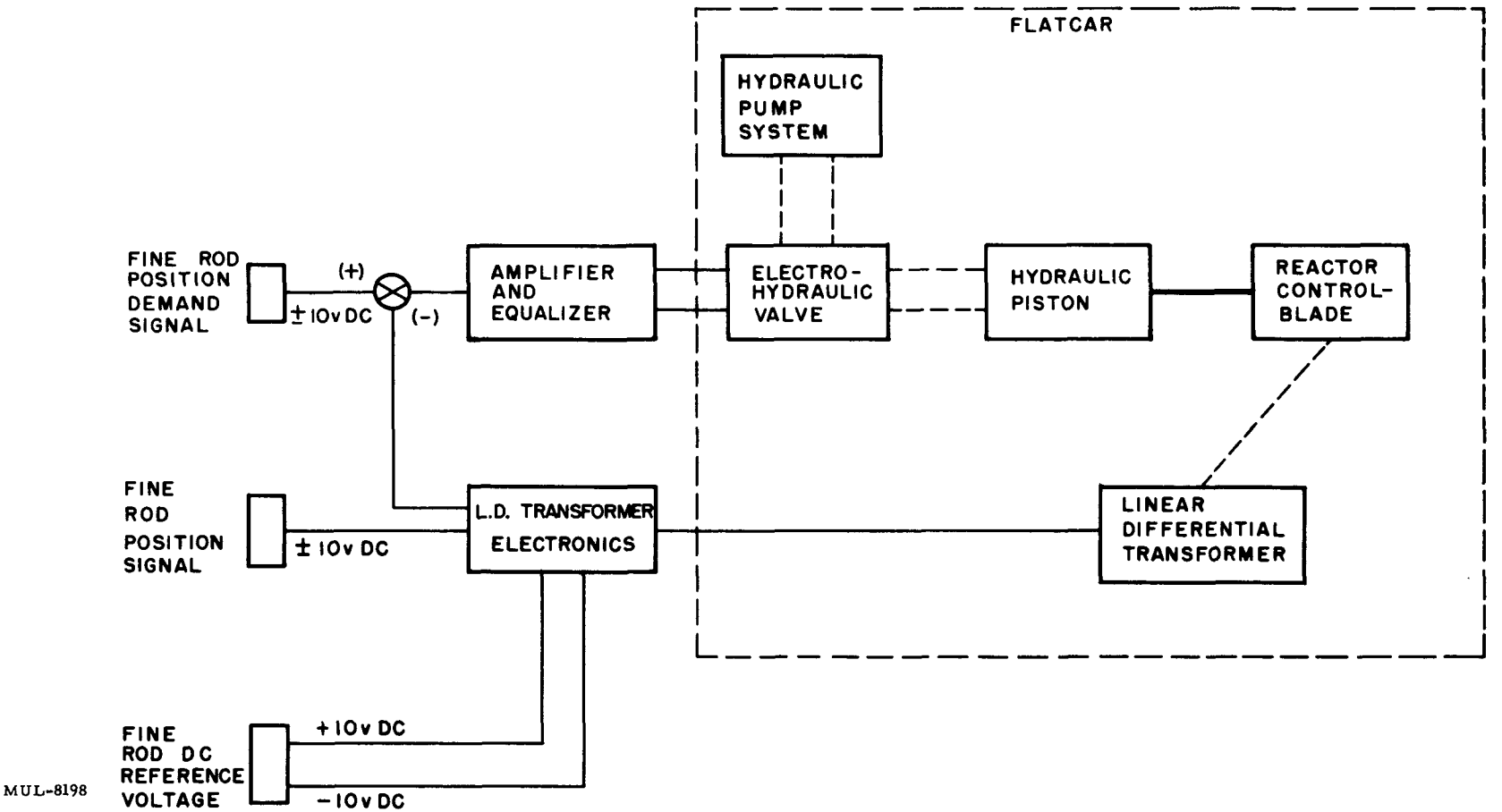

Fig. 6-10. Control rod subsystem block diagram.

Figure 6-11 shows a plot of the response of the system, in its linear (small-signal) region, to sinusoidal signals. The curve was calculated from the closed-loop transfer function.

The calculated performance of the servo system corresponds very closely to analog computer results obtained using the same basic system, but with all important nonlinearities included. The actual hardware is not available for comparison at the time of writing, but results obtained in the servo lab using similar hardware verify qualitatively the validity of the assumptions of linearity basic to this synthesis.

2. Control Vane Servo Subsystem

System Requirements

The system requirements for the control vane servo subsystem, whether used as a simple position feedback system in the manual and fast reset mode, or as an inner loop of the overall system in the automatic mode, are as follows:

(1) Position the control vane linearly within 0.3% over the 180° range with less than 0.1% dead zone.

(2) Possess a frequency response which is variable from 1-3 cps (variable by setting gain).

(3) Show less than 2% overshoot to a step displacement input.

(4) Possess an orifice limited saturation velocity greater than 3°/sec.

An additional requirement on the actuator is that it be capable of turning the vane to the full-in position in 1-4 seconds in the scram mode.

Figure 6-12 shows a block diagram of the control vane servo subsystem, indicating those components which are located on the flatcar near the reactor. As before, a dc system is used with voltages in the range 0 to ± 10 v.

Actuator position feedback is used rather than load position feedback, since the radiation level at the vane makes it impractical to place the transducer there. In the synthesis or analysis of this system, it can be assumed without appreciable inaccuracy that the load displacement signal is the quanity fed back.

Figure 6-13 shows a plot of the calculated small signal sinusoidal response of the system. Again, the calculated performance of the linearized servo system synthesized above compares very closely to the analog computer

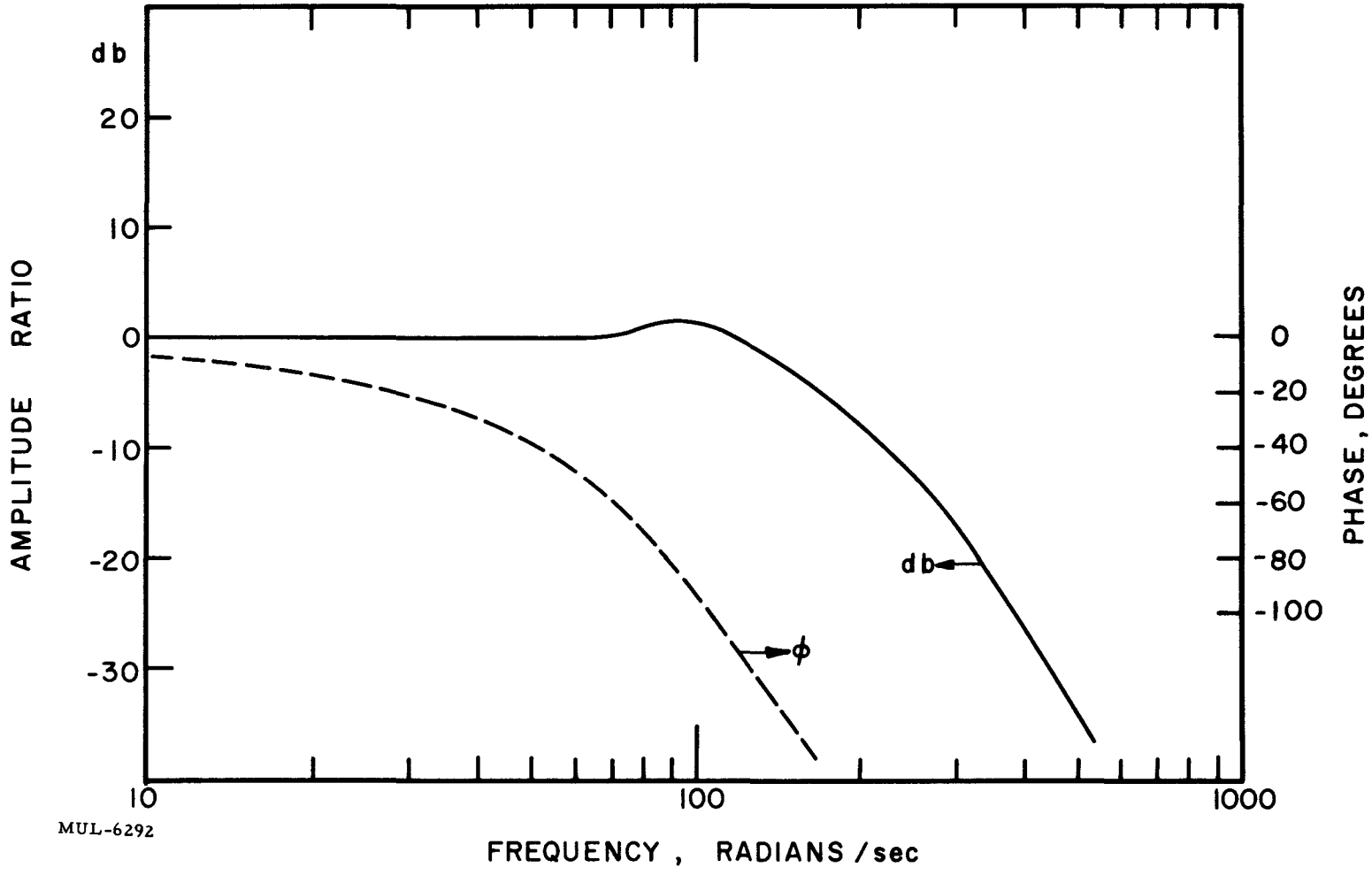

Fig. 6-11. Closed-loop response of the control rod servo subsystem.

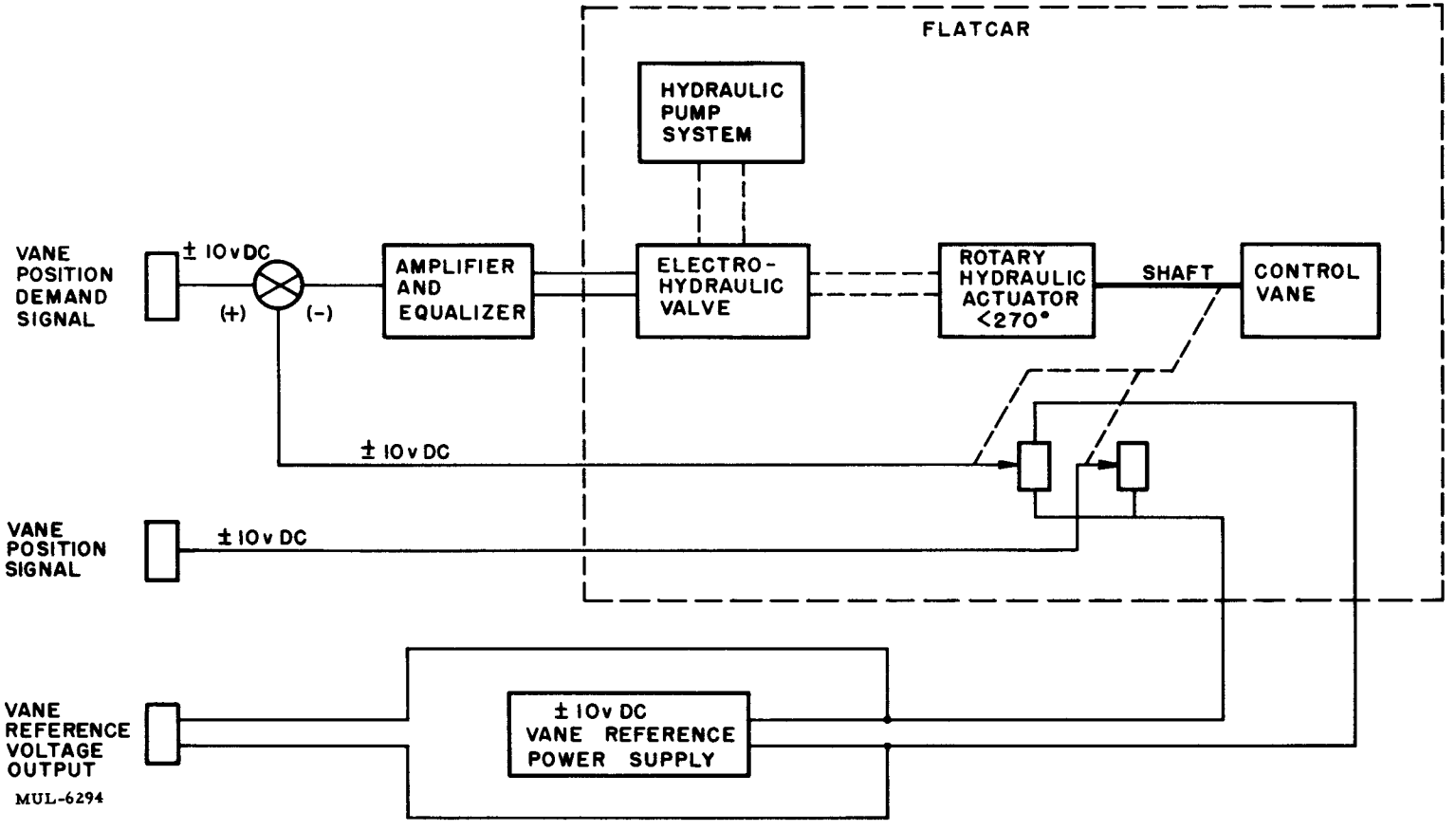

Fig. 6-12. Vane system block diagram.

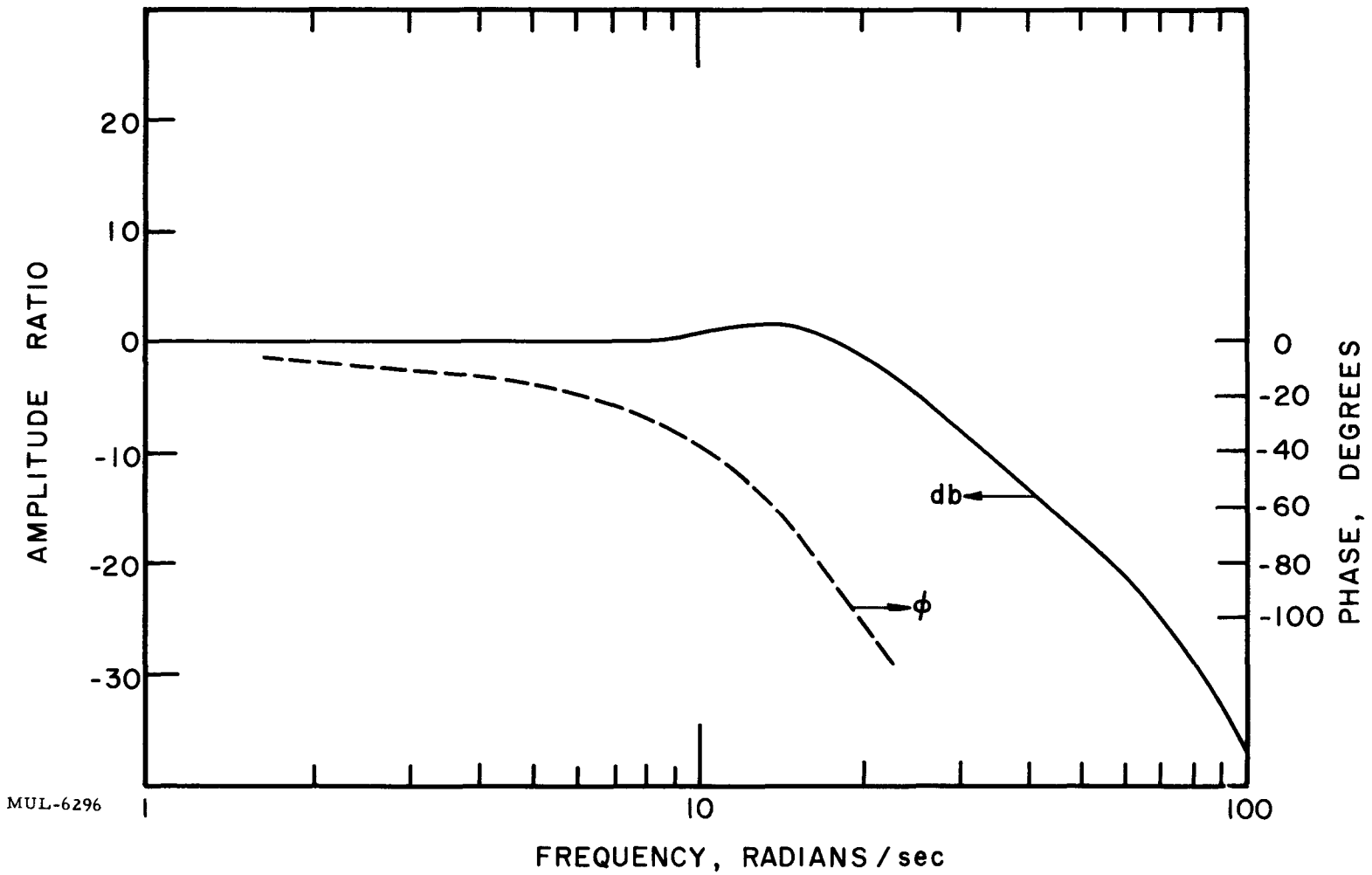

Fig. 6-13. Closed-loop response of the control vane servo subsystem.

results obtained using the same basic system, but with all important nonlinearities included. In addition, a graphical nonlinear analysis of this system has shown that linear methods of analysis are applicable.

6.4.2 Automatic Power and Period Control

As was pointed out in Section 6.3.4, the automatic power and period control systems consist of the same set of components, with one or two exceptions. In order to analyze each type of control, however, separate descriptions are given below.

1. Power Control

The basic control system configuration which has been selected for power control is shown in Fig. 6-14 in linearized transfer function form.

This system uses the vernier rod and the shim vanes in a parallel manner where the rod offset position (from center) and the vane rate are determined by the voltage V_D. Since the rod system has a frequency response approximately ten times that of the vane system, this means that the vane rate is approximately proportional to the rod offset, which is the desired condition. Use of proportional plus integral compensation makes the rod-only system (i.e., vanes assumed at a fixed position) at least a type 1 system (type 2 at low power) with a corresponding zero steady-state error to a constant power demand. The vane-only system is a type 2 system at full power (type 3 at low power) and so has a corresponding zero steady-state error to a constant power demand or a ramp-type power demand in its linear range.

As shown in Figs. 6-9 and 6-14, a variable gain amplifier has been included in the forward loop. The gain of this amplifier is set by a gain control servo such that at equilibrium

$$K_1 = K_A/V_P .$$

To prevent interactions with the power control system, the frequency response of the gain control servo has been set about a decade below that of the power control system so the gain setting is effectively a constant during the period of the transient response. In addition, interaction of the two loops is eliminated during positive power excursions because the reactor is on period control.

Figures 6-15 and 6-16 show plots of the amplitude and phase angle, respectively, of the overall reactor small signal transfer function $G'_{RT}(j\omega)$ at

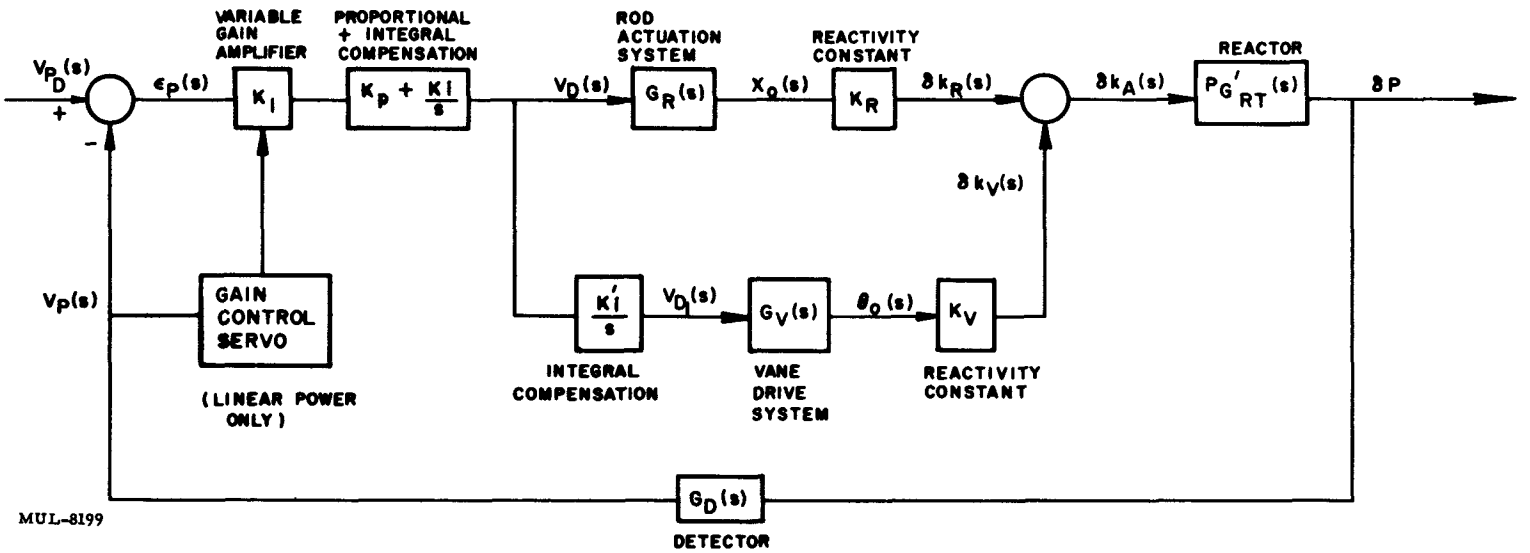

Fig. 6-14. Control system configuration for power control system.

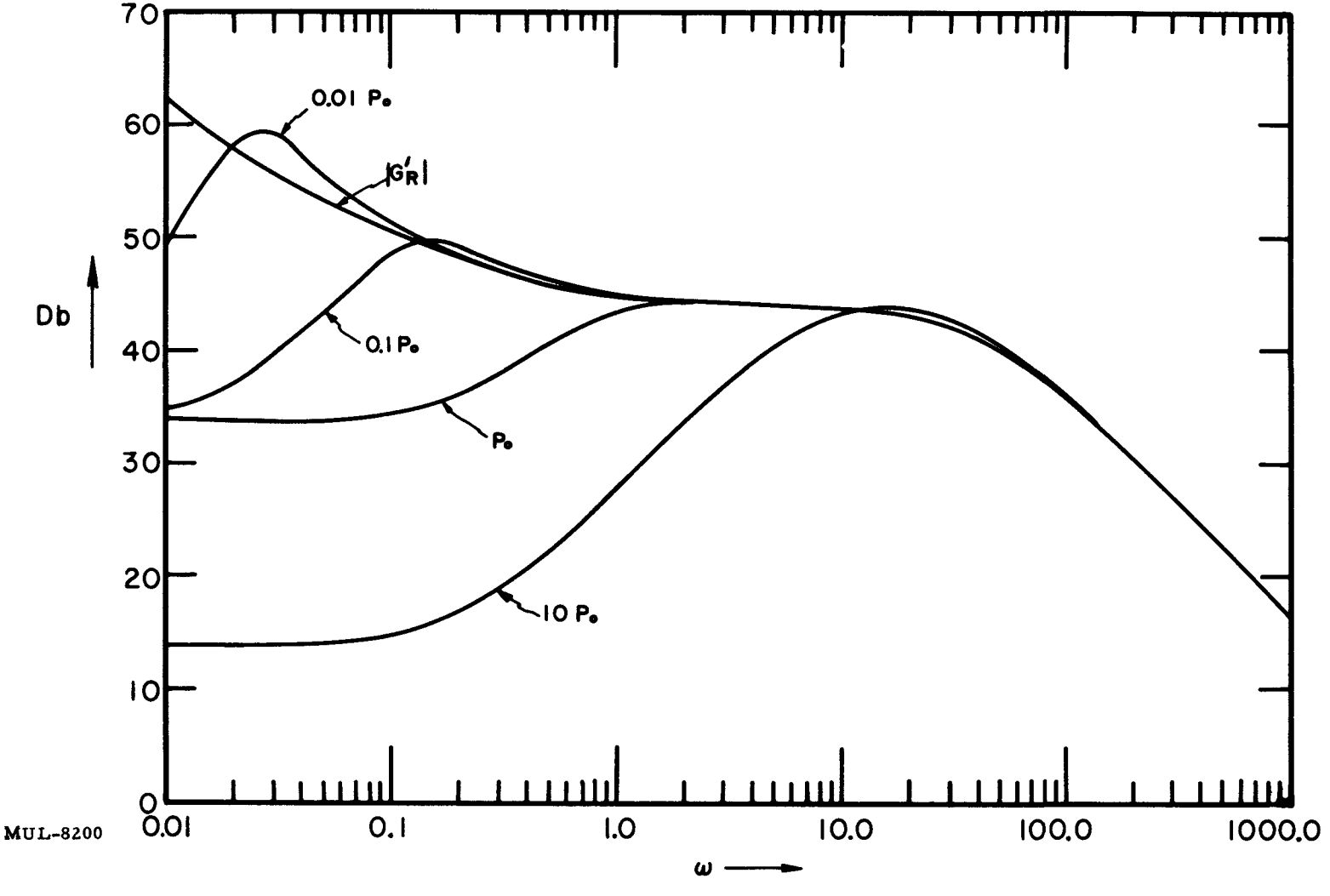

Fig. 6-15. Plot of $|G'_{RT}(j\omega)|$ in decibels at P = 0.01 P_0, 0.1 P_0, P_0, 10 P_0. Plot of $G'_R(j\omega)|$ in decibels.

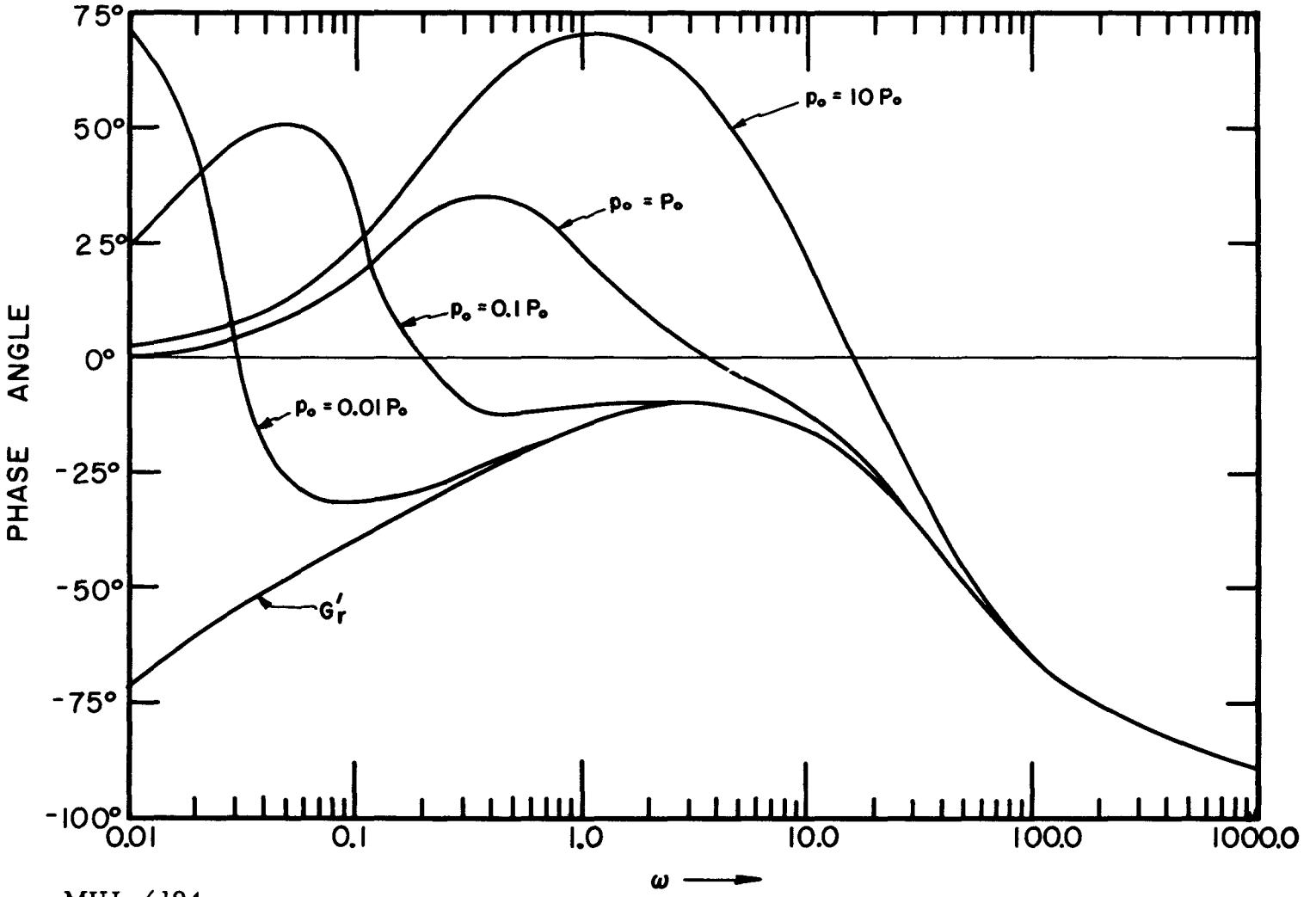

Fig. 6-16. Plot of ARG $G'_{RT}(j\omega)$ in degrees at $P = 0.01\,P_0$, $0.1\,P_0$, P_0. Plot of ARG $G'_R(j\omega)$.

full temperature and at several power levels, where

$$G'_{RT}(j\omega) = \frac{\delta P}{P \delta k_A}(j\omega) .$$

For values of power $P \leq 0.01\ P_0$, $G'_{RT}(j\omega)$ approaches $G'_R(j\omega)$, the transfer function of the reactor alone with no temperature effect. As P is increased, the function $G'_{RT}(j\omega)$ shows increasing phase lead and low frequency attenuation with a net effect of improving the relative stability of the overall system.

In Figs. 6-17 through 6-19 are shown the frequency response plots of the power control system when using linear power detection. These plots were obtained with an IBM 650 computer routine developed here. Figure 6-17 shows a "gain-phase" plot of the overall open-loop transfer function $G(j\omega) = \frac{\delta V_P}{\epsilon_P}(j\omega)$ at full power P_0, and at $0.01\ P_0$. Figure 6-18 shows a "gain-phase" plot of $G(j\omega)$ for the "vanes-only" and "rod-only" conditions at P_0 and $0.01\ P_0$. It can be seen that for values of $\omega > 2$ rad/sec, the transfer function of the combination system is approximately the same as that of the "rod-only" system. Figure 6-19 shows a Bode plot of the closed-loop transfer function $\frac{\delta V_P}{\delta V_{P_D}}(j\omega)$ at P_0 and $0.01\ P_0$. It is found that -90° phase shift occurs at $\omega = 2\pi\ (9.5)$ rad/sec, while the gain is down 3db at $\omega = 2\pi\ (15.3)$ rad/sec.

In all plots shown above, the air flow rate through the reactor is assumed constant at that value which produces full design core temperature and it is assumed that there is no interaction between the power and coolant loops. Since the frequency response of the coolant loop is more than a decade below that of the power or period loop, any interaction is negligible. Further, any variations in the coolant loop are felt only indirectly through the temperature coefficient of reactivity. In the frequency range of interest the power control system is fairly insensitive to the low frequency feedback through the temperature coefficient, as can be seen by comparing the overall system transfer function at low and high power levels ($0.01\ P_0$ and P_0) in Fig. 6-17.

An interesting situation, although one which is not expected to occur, is that in which the fuel elements suddenly become very porous, releasing all fission products to the air stream as soon as they are formed. In this case, the delayed neutron groups which provide normal control of the reactor are lost; and the reactor transfer function is represented by $G'_R(s) = \frac{1}{\ell^* s}$ with control of the reactor changed accordingly. Figure 6-20 shows a "gain-phase" plot of $G(j\omega) = \frac{\delta V_P}{\epsilon_P}(j\omega)$ at P_0 and $0.01\ P_0$ for the case of no delayed neutron

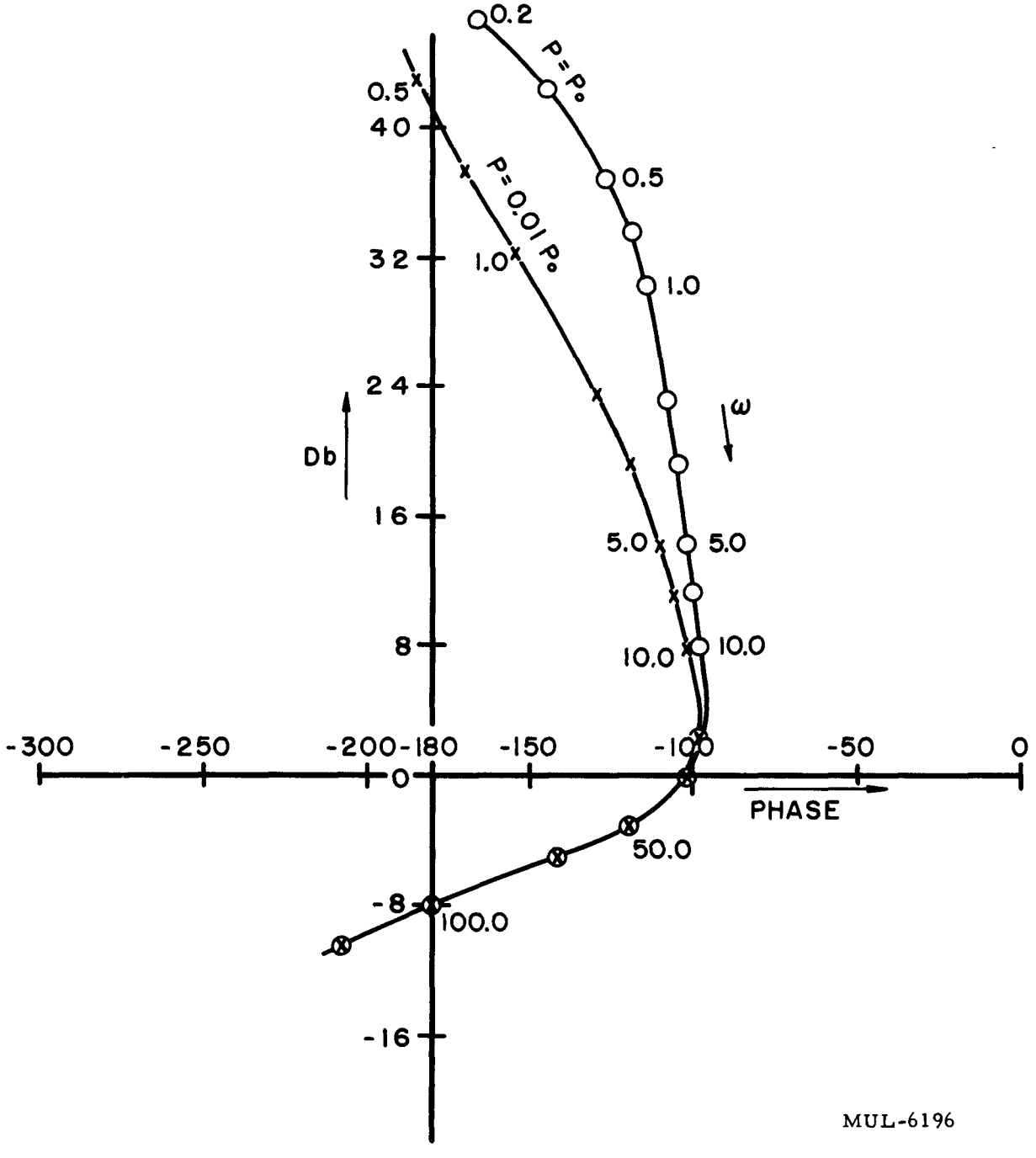

Fig. 6-17. Gain-phase plot of $G(j\omega)$ for $P = P_0$, $0.01\ P_0$.

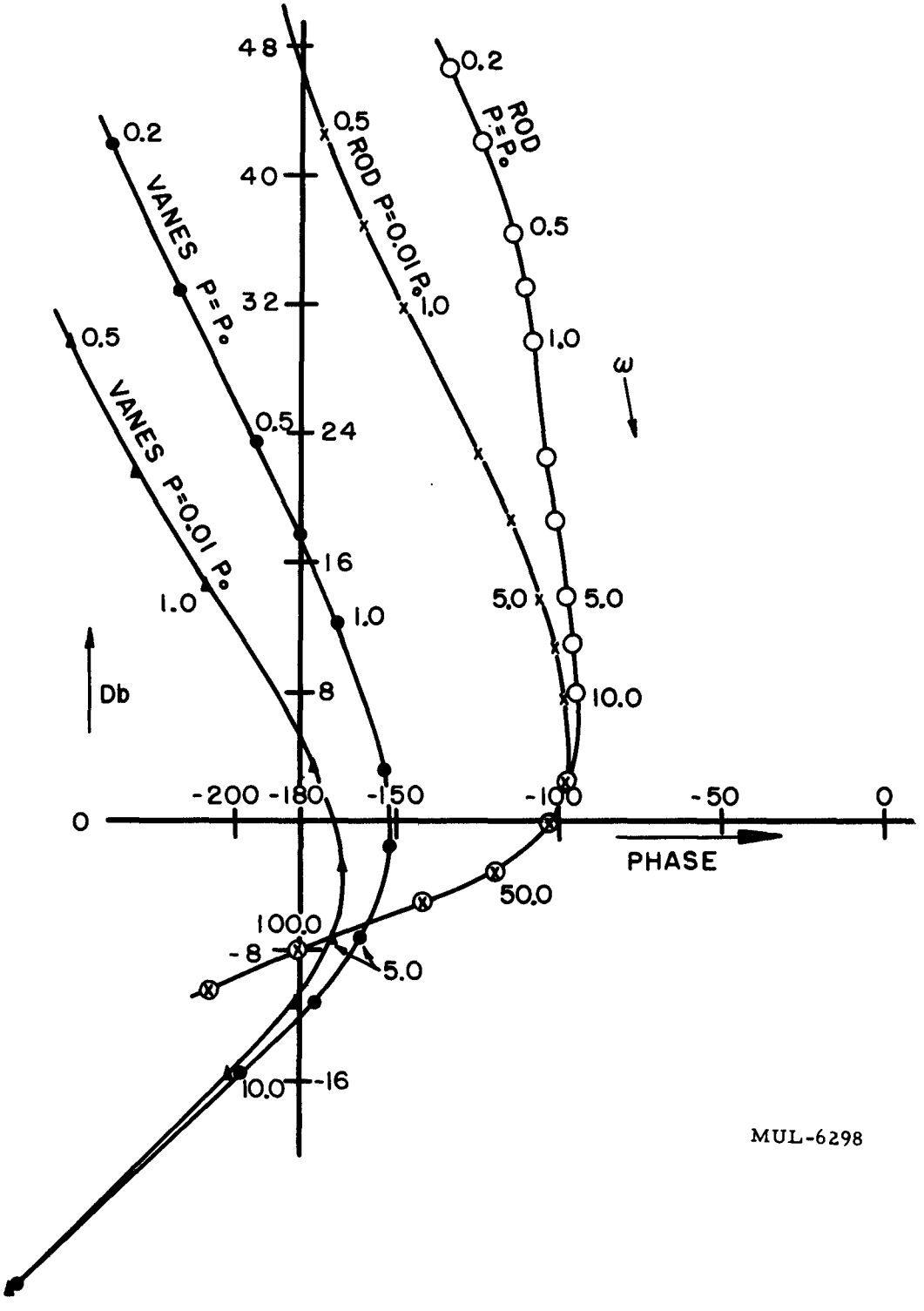

Fig. 6-18. Gain-phase plot of $G(j\omega)$ for "vanes-only" and "rod-only" for $P = P_0$, $0.01\ P_0$.

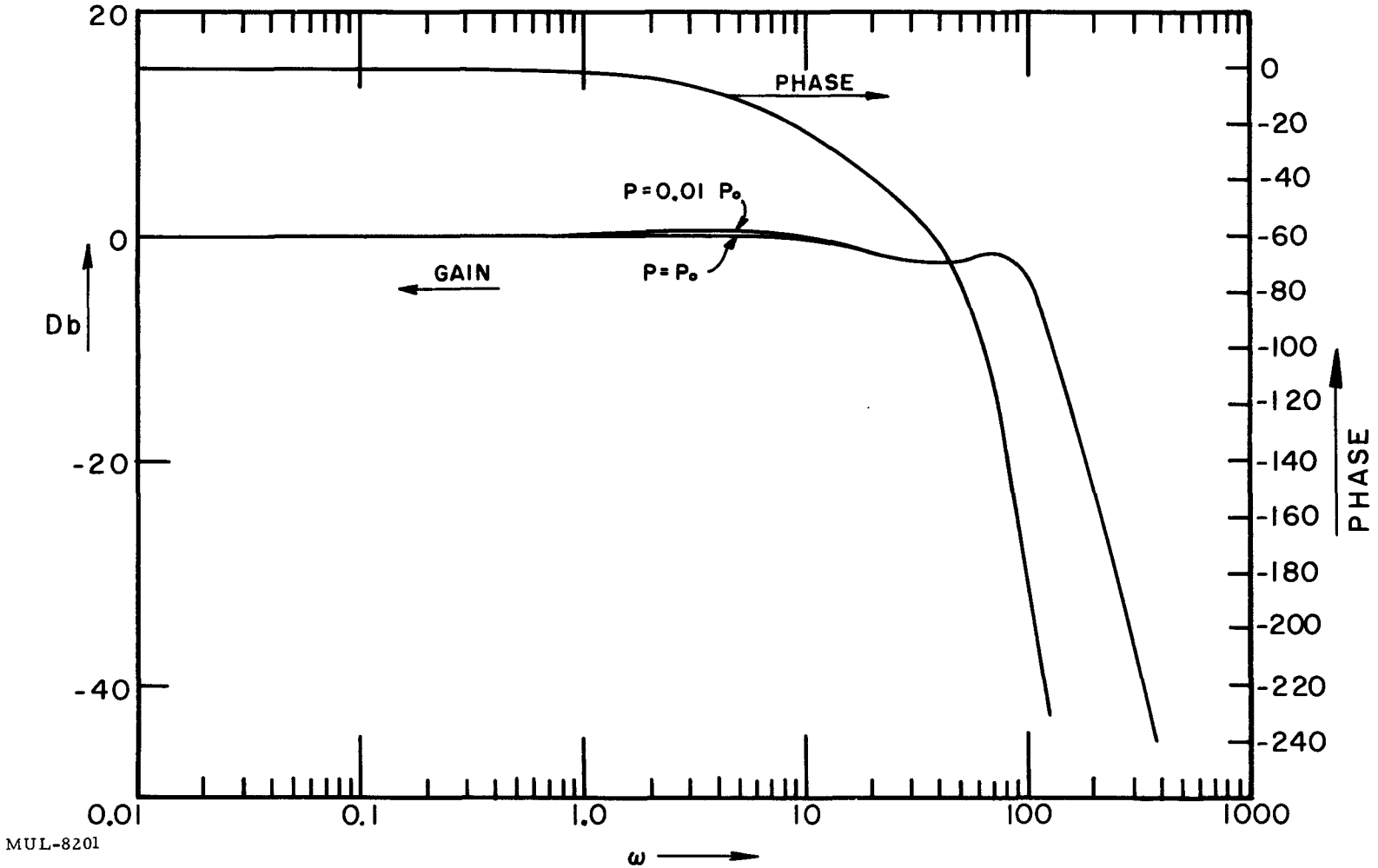

Fig. 6-19. Closed-loop response of power control system using linear power detection for $P = P_0$, $0.01\ P_0$.

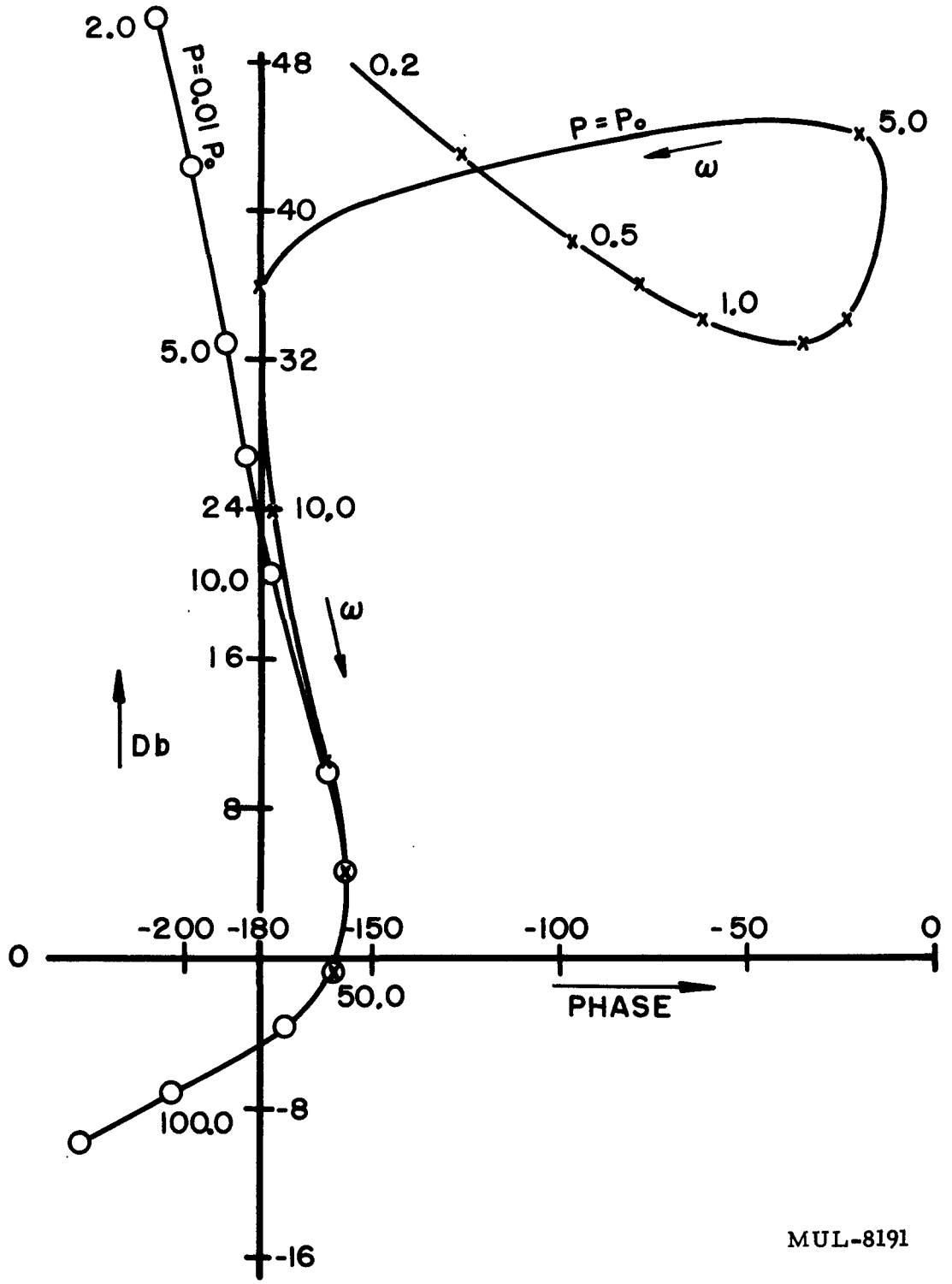

Fig. 6-20. Gain-phase plot of $G(j\omega)$ where $G'_R(j\omega) = \frac{1}{l^*(j\omega)}$ and $P = P_0$, $0.01\ P_0$.

groups. The system is still stable, but the margin of stability is significantly reduced from the normal control situation. The control system would be capable of recovery from this "accident" and would maintain demand power level following the accident.

In the above analysis, the neutron time-of-flight to the detector has been assumed negligible. For a detector approximately 50 ft from the reactor the neutron flight time is in the range 2 to 7 milliseconds, assuming that the propagation velocity for thermal neutrons is 2.2×10^5 cm/sec. This introduces a transport lag between the reactor and the detector which must be considered in the system stability analysis. The transfer function of this transport lag is simply $e^{-T_t s}$, so $|G(j\omega)| = 1$ and arg $G(j\omega) = -j\omega T_t$. Assuming $T_t = 5 \times 10^{-3}$ second, then the phase shift produced by the transport delay is that shown below

ω	arg $G(j\omega)$
1	0.3°
10	2.9°
50	14.3°
100	28.6°

Figure 6-21 shows a plot of the overall open-loop transfer function $G(j\omega)\, e^{-j\omega T_t}$ at P_0 when the transport lag is included, showing for comparison the transfer function $G(j\omega)$ without the transport lag. The effect of this lag is to reduce slightly the relative stability of the system. This affect can be offset by reducing the system gain by about 2 db; a slight decrease in the closed-loop frequency response results, but there is little other change in the system behavior.

The frequency and time domain characterictics of the power control system when using logarithmic power detection are shown in Figs. 6-22 through 6-25. Figure 6-22 shows a "gain-phase" plot of $G_1(j\omega)$ at P_0 and 0.01 P_0. Figure 6-23 shows a "gain-phase" plot of $G_1(j\omega)$ for the "vanes-only" and "rod-only" conditions. Figure 6-24 shows a Bode plot of the closed-loop transfer function $\frac{\delta V_P}{\delta V_{PD}}(j\omega)$ at P_0 and 0.01 P_0. The effect of the transport lag e^{-sT_t} on the system stability is shown in Fig. 6-25. It causes a slight decrease in the relative stability of the system, as in the linear power detection situation.

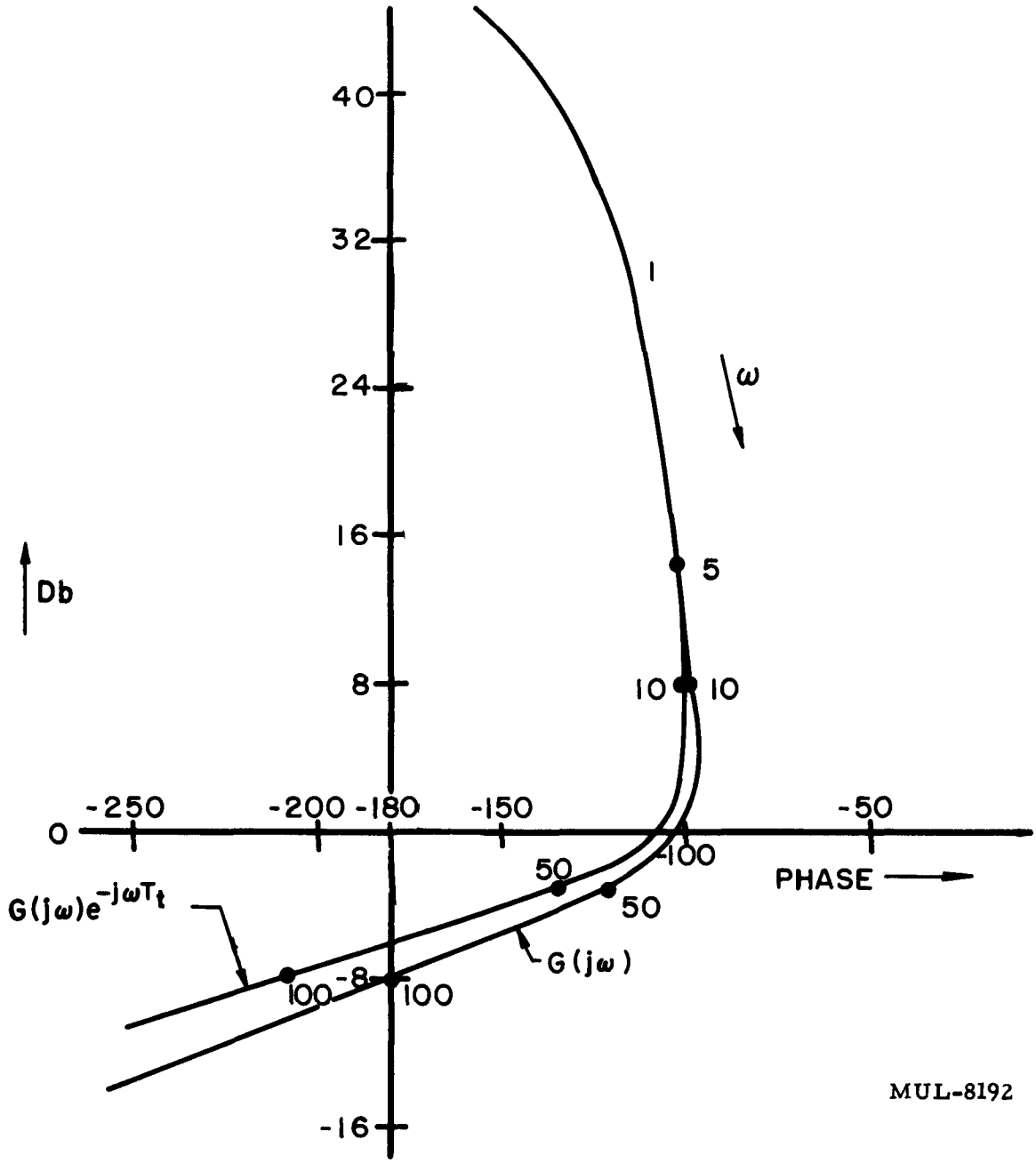

Fig. 6-21. Plot of $G(j\omega)$, $G(j\omega)e^{-j\omega T_t}$ for $T_t = 5 \times 10^{-3}$ second, $P = P_0$.

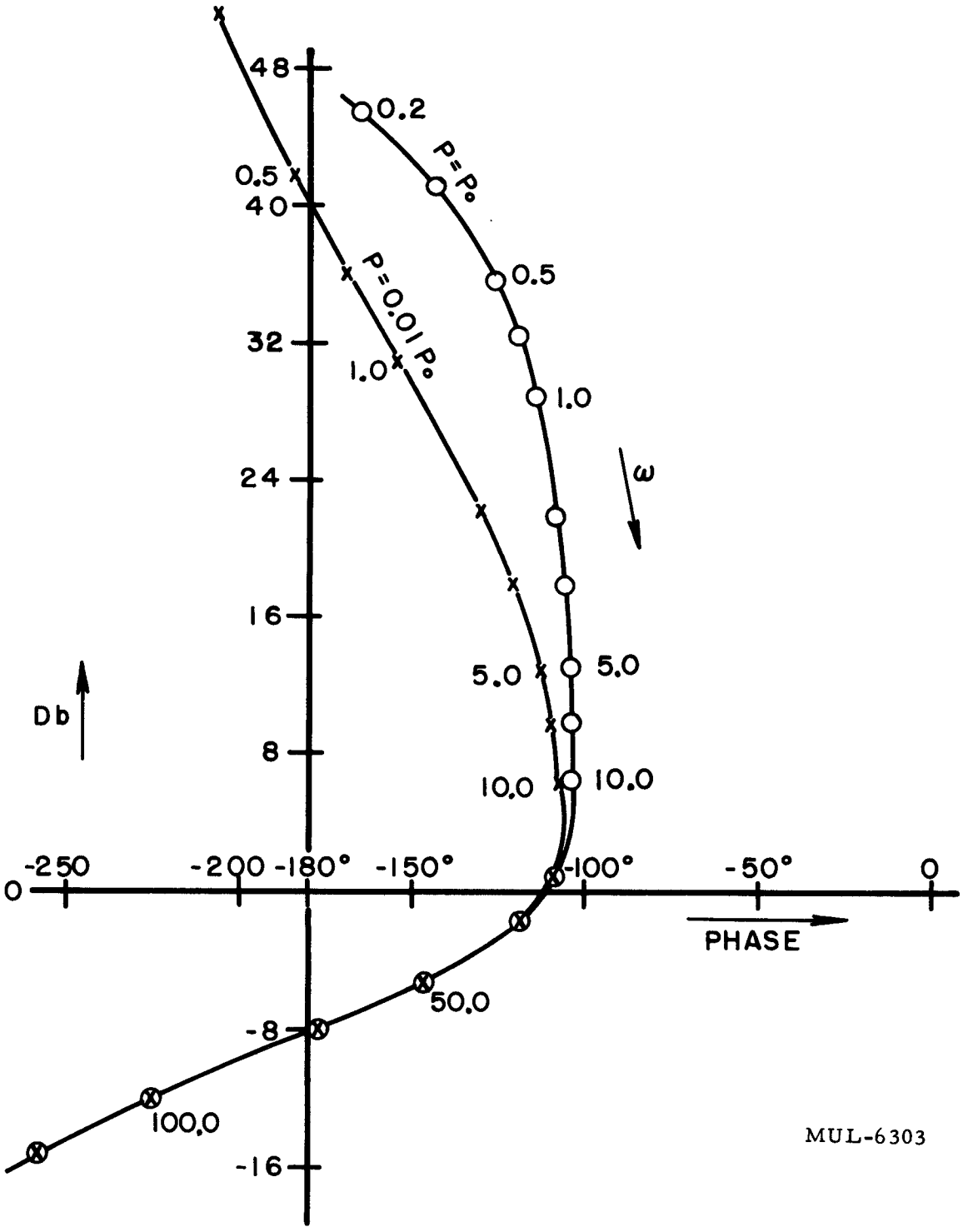

Fig. 6-22. Gain-phase plot of $G_1(j\omega)$ for $P = P_0$, $0.01\ P_0$.

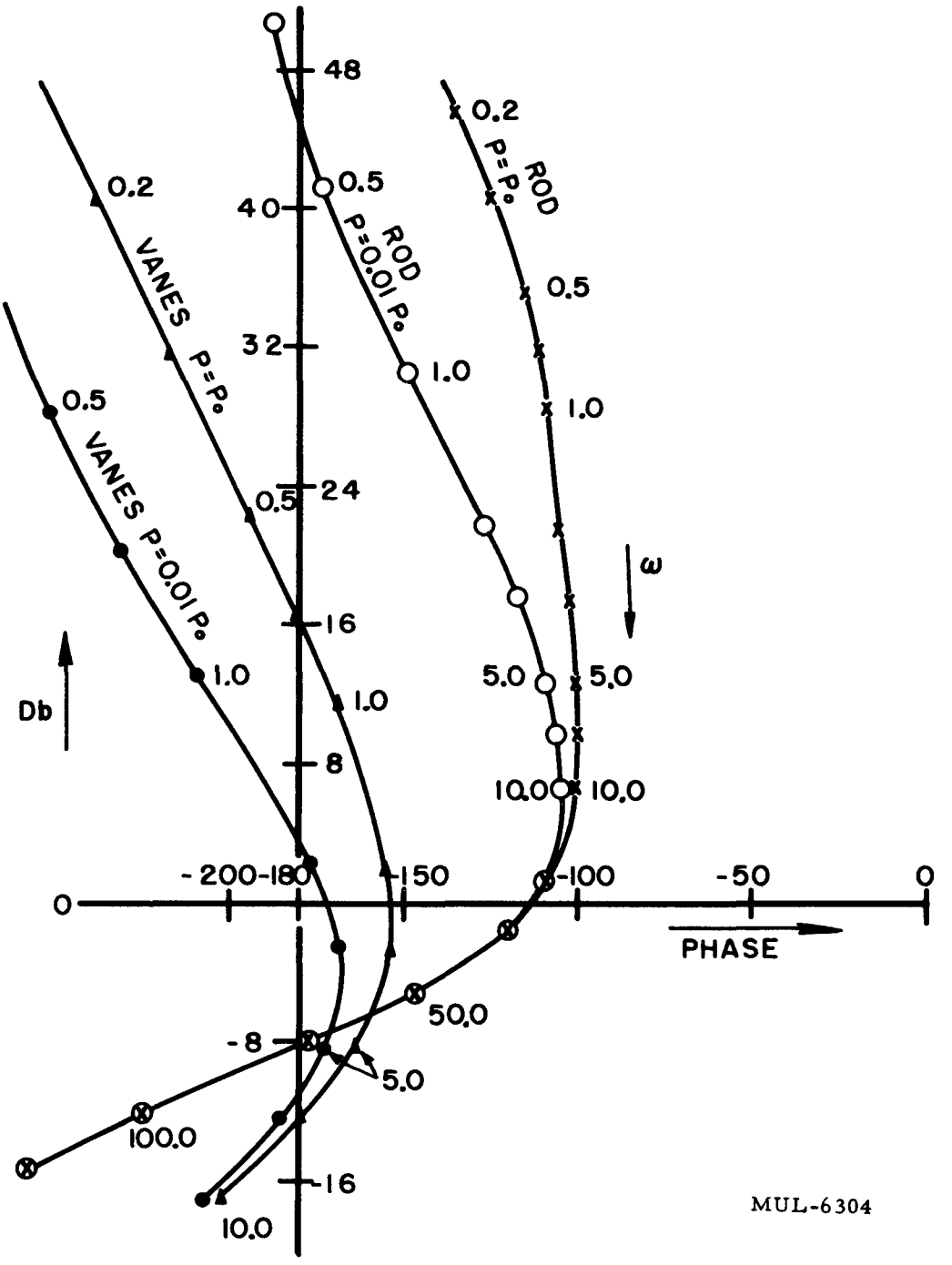

Fig. 6-23. Gain-phase plot of $G_1(j\omega)$ for "vanes-only" and "rod-only", with $P = P_0$, $0.01\ P_0$.

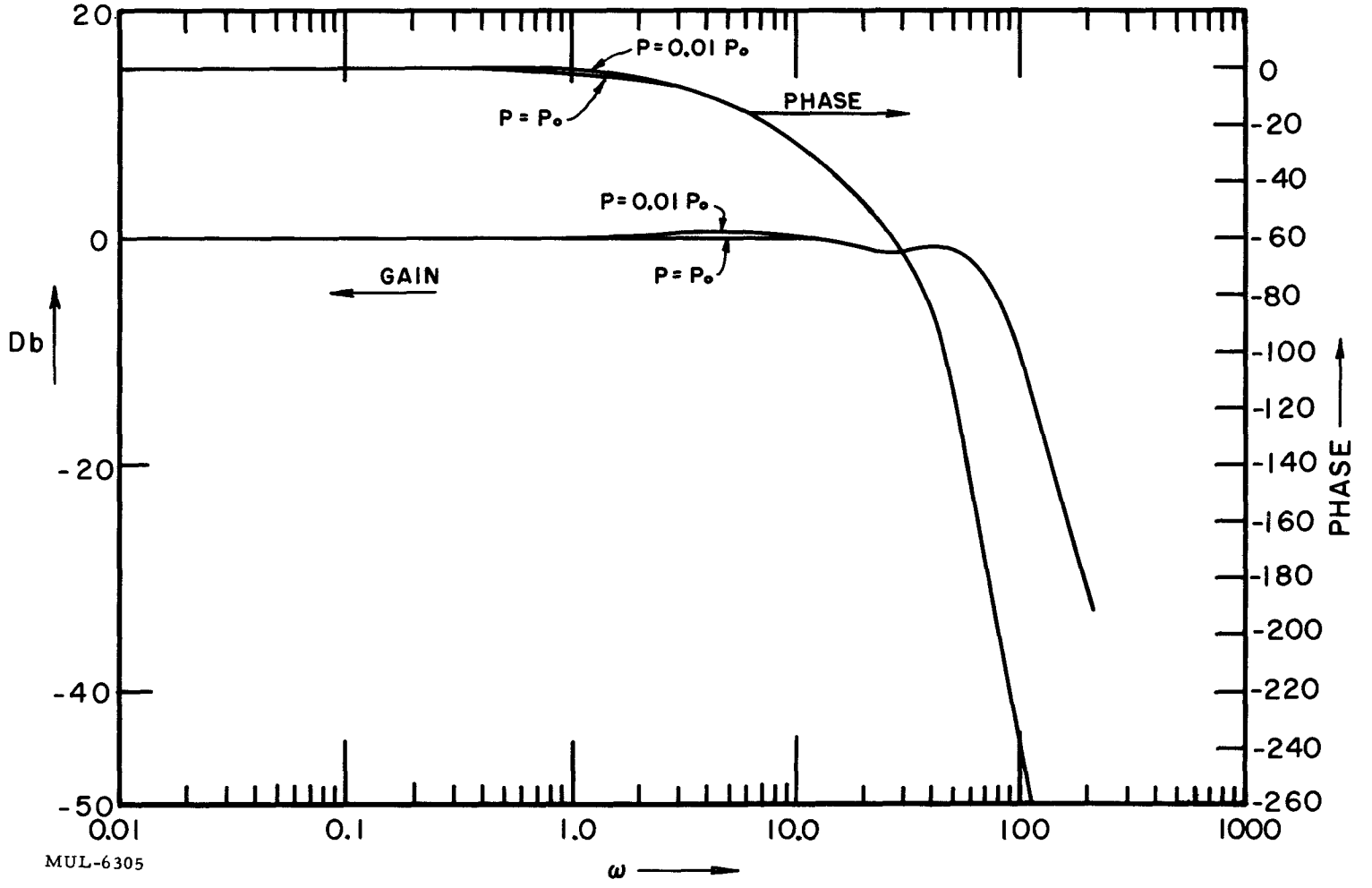

Fig. 6-24. Closed-loop response of power control system using log power detection for $P = P_0$, $0.01\ P_0$.

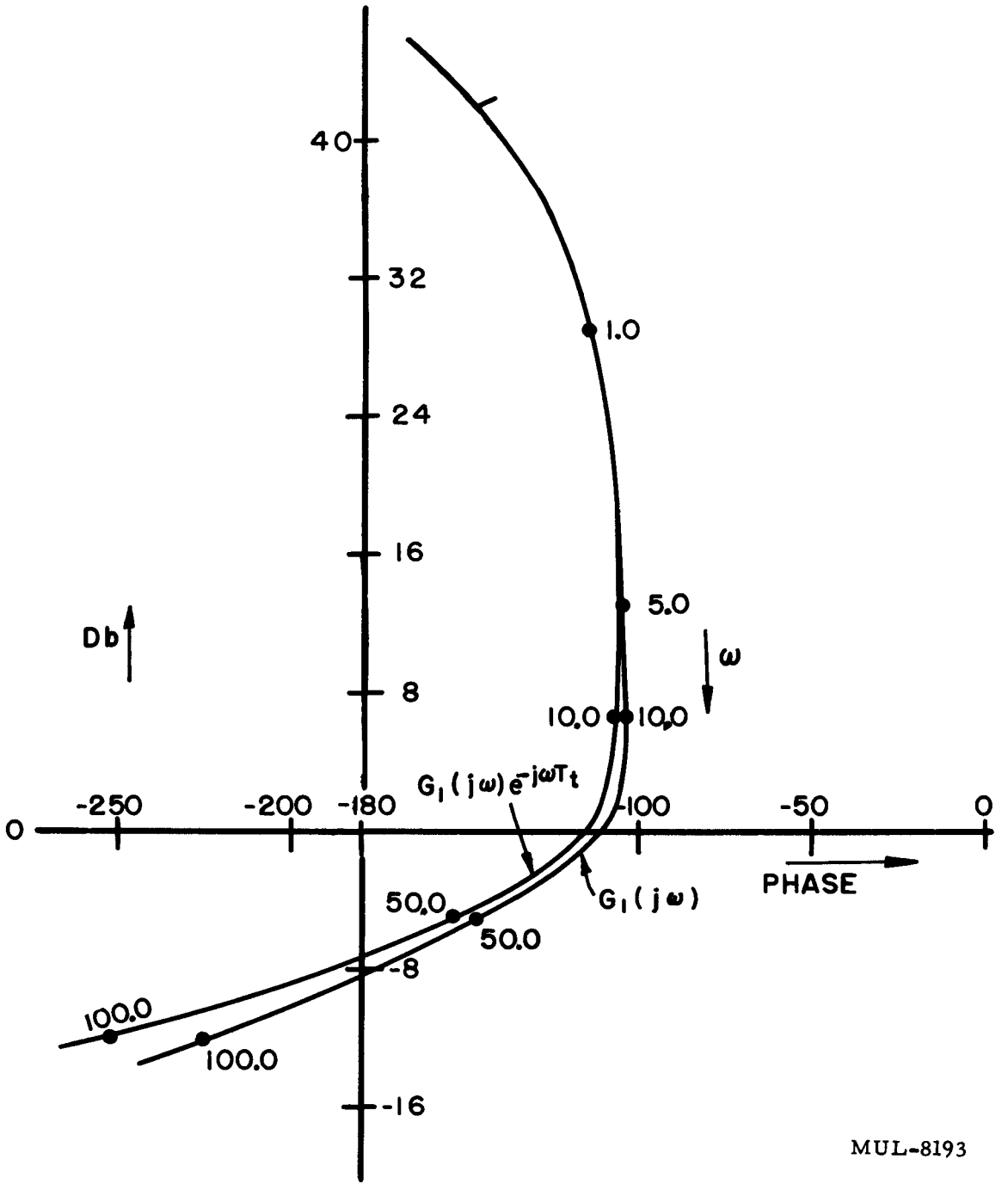

Fig. 6-25. Gain-phase plot of $G_1(j\omega)$, $G_1(j\omega)e^{-j\omega T_t}$ where $T_t = 5\times 10^{-3}$ second, $P = P_0$.

The synthesized power level control system has a zero steady-state error to a step change in power demand (V_{P_D}), but at full power has a finite steady-state error, ϵ_{Pss}, to a ramp-type power demand when considering the "rod-only" system (the effect of the vanes is negligible except over very long periods of time). With an input $v_p(t) = Rt$, it can be shown that

$$\epsilon_{Pss} = \frac{R}{K_0} ,$$

where $K_0 = \lim_{s \to 0} s\ G(s) = 622$

$$\therefore\ \epsilon_{Pss} = 0.0016\ R = 0.16\%\ R.$$

This steady-state error applies whether using linear or log power detection.

2. Period Control System

The design of this system follows in a manner similar to that of the power control system. Actually, the design of both systems was carried out jointly, and so most parameters were determined with both applications in mind. There are only two differences in this system from the power control system:

(1) The amplifier gain, K_τ, which adjusts the system gain.

(2) The detector transfer function, which changes in form when the controlled variable becomes inverse-period instead of power.

The overall open-loop transfer function $G'(j\omega) = \frac{10/\tau'}{\epsilon_\tau}(j\omega)$ is shown in Fig. 6-26 on a "gain-phase" plot for power levels P_0 and $0.01\ P_0$. Figure 6-27 shows a "gain-phase" plot of $G'(j\omega)$ for the "rod-only" and "vanes-only" conditions at P_0 and $0.01\ P_0$. It is seen that for $\omega > 5.0$ rad/sec, the transfer function of the combination system (both rod and vanes included) approaches that of the "rod-only" system. Figure 6-28 shows the closed-loop response function $\frac{10/\tau'}{10/\tau_D}(j\omega)$ at P_0 and $0.01\ P_0$. The gain of the period system is down 3 db at $\omega = 2\pi(12.8)$ rad/sec while -90° phase shift occurs at $\omega = 2\pi(7.8)$ rad/sec. Figure 6-29 shows the effect of the transport lag on system stability; a "gain-phase" plot of $G'(j\omega)\ e^{-j\omega T_t}$ is shown at $P = P_0$.

When on period control, the "rod-only" system (hence the combination system) exhibits zero steady-state error to a step-type input at low power levels, but at full power has a finite steady-state error. For a step input $\frac{10}{\tau_D}(t) = R$ for $t \geq 0$, the steady-state error is given by

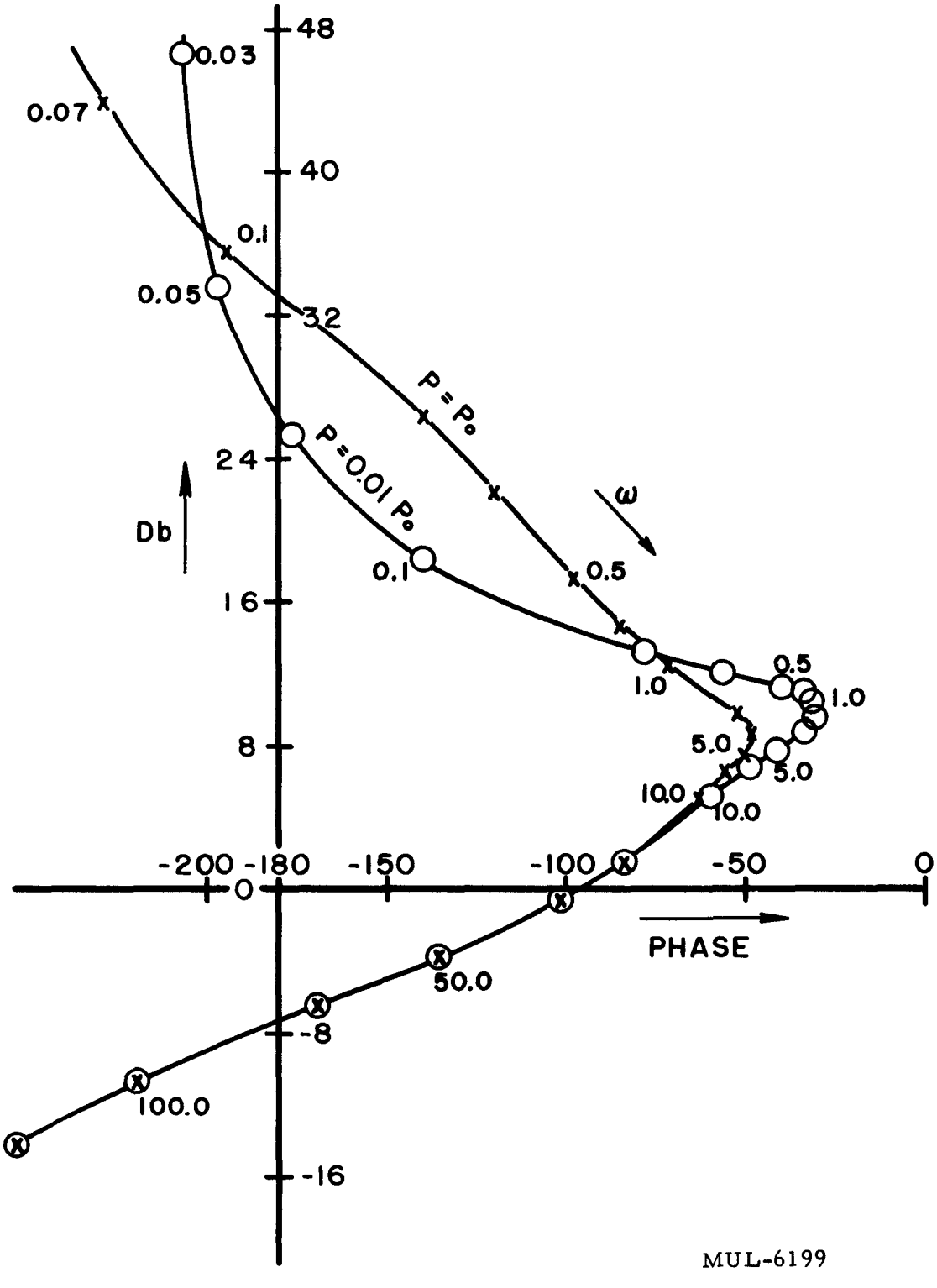

Fig. 6-26. Gain-phase plot of $G'(j\omega)$ for $P = P_0$, $0.01\ P_0$.

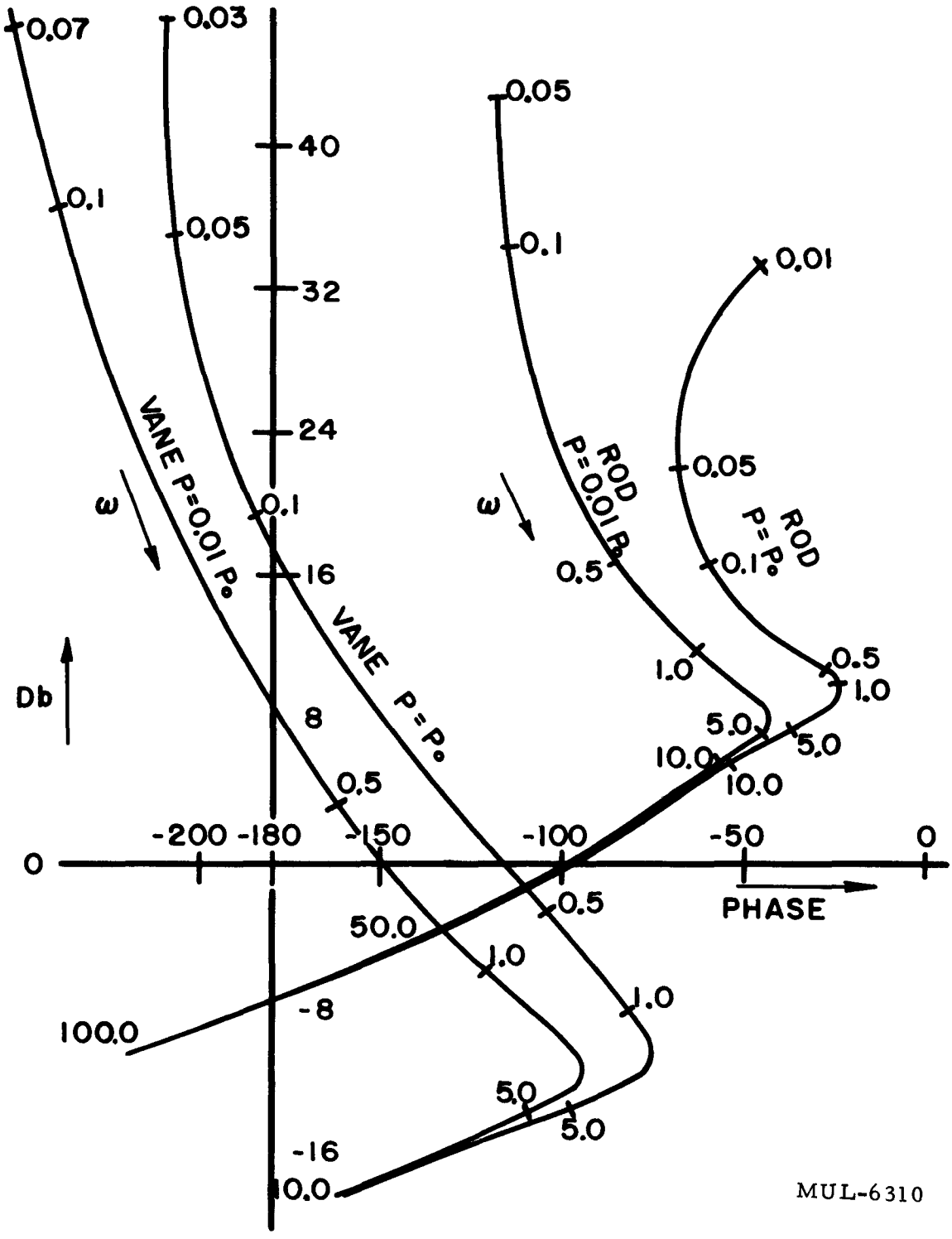

Fig. 6-27. Gain-phase plot of $G'(j\omega)$ for "vanes-only" and "rod-only" for $P = P_0$, $0.01\ P_0$.

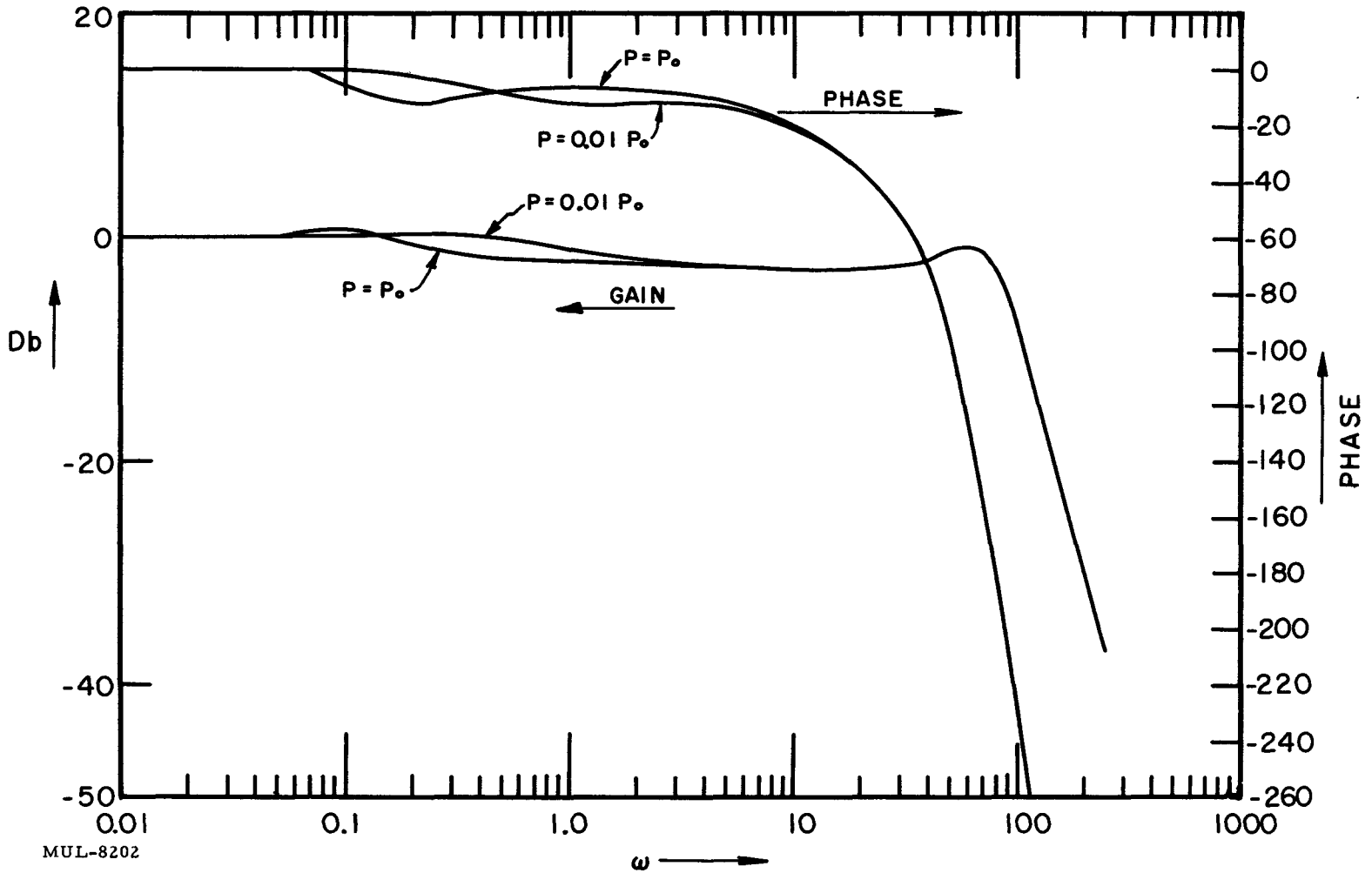

Fig. 6-28. Closed-loop response of inverse-period control system for $P = P_0$, $0.01\ P_0$.

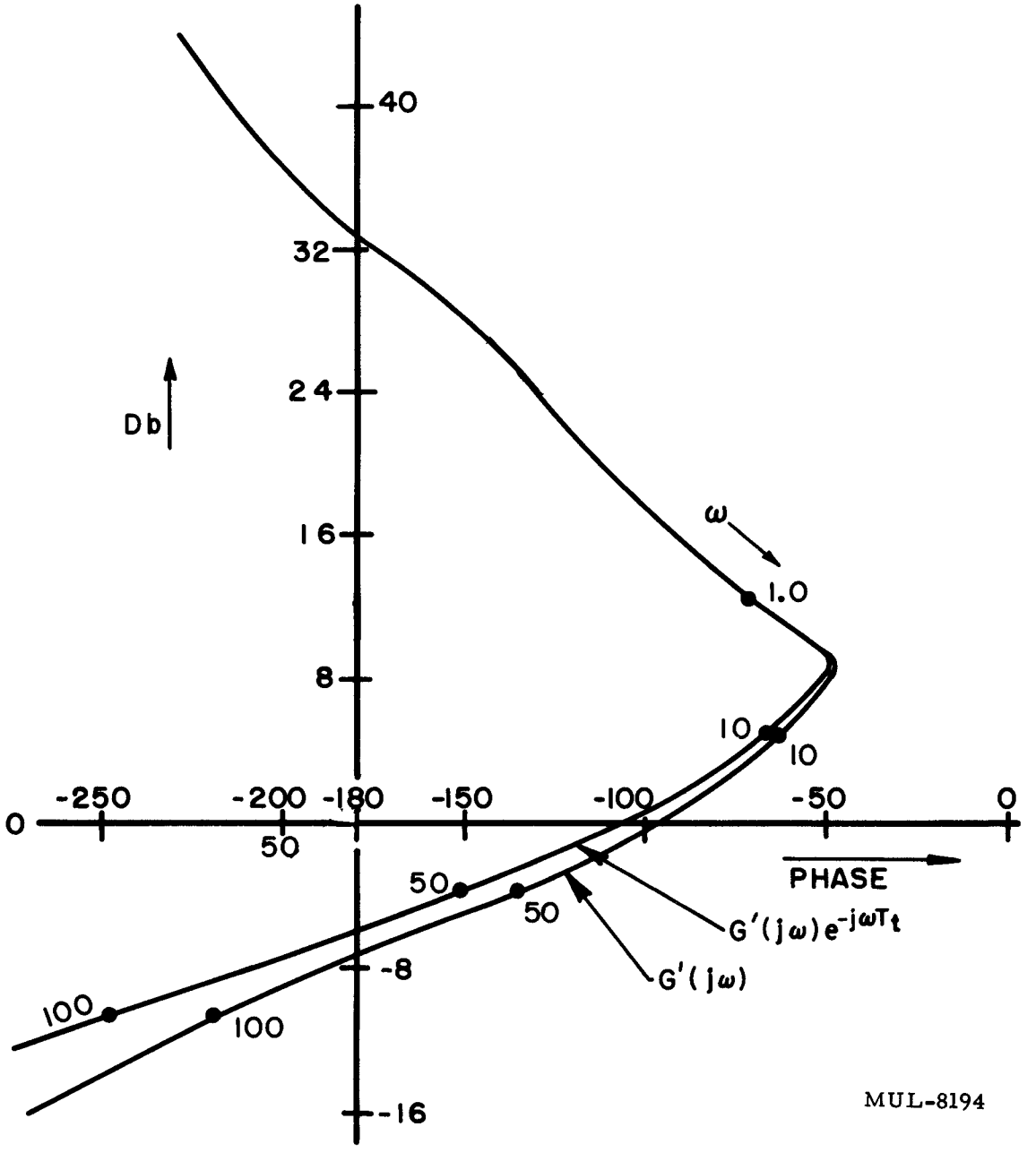

Fig. 6-29. Gain-phase plot of $G'(j\omega)$, $G'(j\omega)e^{-j\omega T_t}$ for $T_t = 5 \times 10^{-3}$ second, $P = P_0$.

$$\epsilon_{\tau_{ss}} = \frac{1}{1 + K'_0} R ,$$

where

$$K'_0 = \lim_{s \to 0} G'(s) = 65.7 .$$

Thus

$$\epsilon_{\tau_{ss}} = 0.015 \; R = 1.5\% \; R .$$

6.4.3 Analog Computer Results

The synthesis of the manual and automatic control system was performed using a combination of frequency domain, time domain and analog computer methods. In the synthesis stage, the analog computer was used primarily to simulate important nonlinearities and to show the transient behavior of the simulated system to typical inputs and disturbances.

The entire system has been simulated on electronic analog computers. This simulation includes the following features:

(1) Reactor simulation using the kinetic equations with 5 delayed neutron groups and one-zone approximation of the reactor thermodynamics. The simulation includes three second-order effects which alter the reactor behavior:

(a) Heat leakage out of the reactor.

(b) Reactivity changes introduced by the gas coolant.

(c) Variation of the gas friction coefficient.

(2) Simulation of the control actuation subsystems including such important nonlinearities as acceleration and velocity saturation and limited rod displacement.

(3) Simulation of the "dual-mode" controller using a differential relay circuit; simulation of the gain set servo-variable gain amplifier combination by means of a division circuit with a simple time delay network.

(4) Simulation of all other components using their linear representation.

The analog computer simulation included neither the neutron transport lag nor log power simulation. In the normal control situation, the effect of the transport lag on system stability was shown to be quite small. For that reason and because of a shortage of equipment, it has not been included in the present analog study. The principal change which this lag would introduce

into the system transient behavior would be the insertion of a 5-millisecond delay in the initiation of any corrective action by the control system following a disturbance or change in the system input. The study of the power control system using log power detection will be carried out as soon as the log power amplifier becomes available for insertion in the system analog. Use of a function generator in place of this component has proven unsatisfactory thus far.

The open and closed-loop transfer functions of the linear power and period control system were verified using the system analog with small signal sinusoidal inputs. The response of the automatic control system to typical inputs and disturbances is shown in the figures which follow. Figure 6-30 shows the system response to ±10% step changes in the power demand around full power with and without the dual-mode controller. It can be seen that the dual-mode controller provides period limiting only when positive power excursions are programmed. From Fig. 6-30, it is found that the settling time of the linear power control system is less than 0.1 second when the input is a small step change. The system exhibits less than 2% overshoot to a step type input and has a zero steady-state error. The period control system has a settling time of about 0.15 second and shows no overshoot to a step input. It has a small steady-state error and displays a small amplitude "tail" in its time response. Figure 6-31 shows the response of the system to step changes in demand power level at power levels other than full power. The steady-state reactor power level is varied from 50% P_0 to 110%. As seen the system response is independent of power level due to the action of the gain set servo. For the cases shown the time delay of the gain set servo was set at 1 second. Figure 6-32 shows the system response to a ±50% step-type input. Here, the system is driven into its nonlinear region as can be seen by examining rod position and vane velocity during the transient to the -50% change in demand power. The rod is driven full in and the vanes reach a peak velocity of 5 rad/min. Normally, the reactor will not be programmed in this manner, but rather in the manner shown in Fig. 6-33, which shows the system response to a ±50% ramp-type input. Here the slope of the ramp is set low enough that the system remains on power control throughout the transient.

Figure 6-34 shows a typical program which provides a +5% change in core temperature in 5 seconds. Flow rate through the reactor was maintained constant at full flow throughout the transient. As seen, the operator must overshoot the power a few percent if the temperature change is to be effected

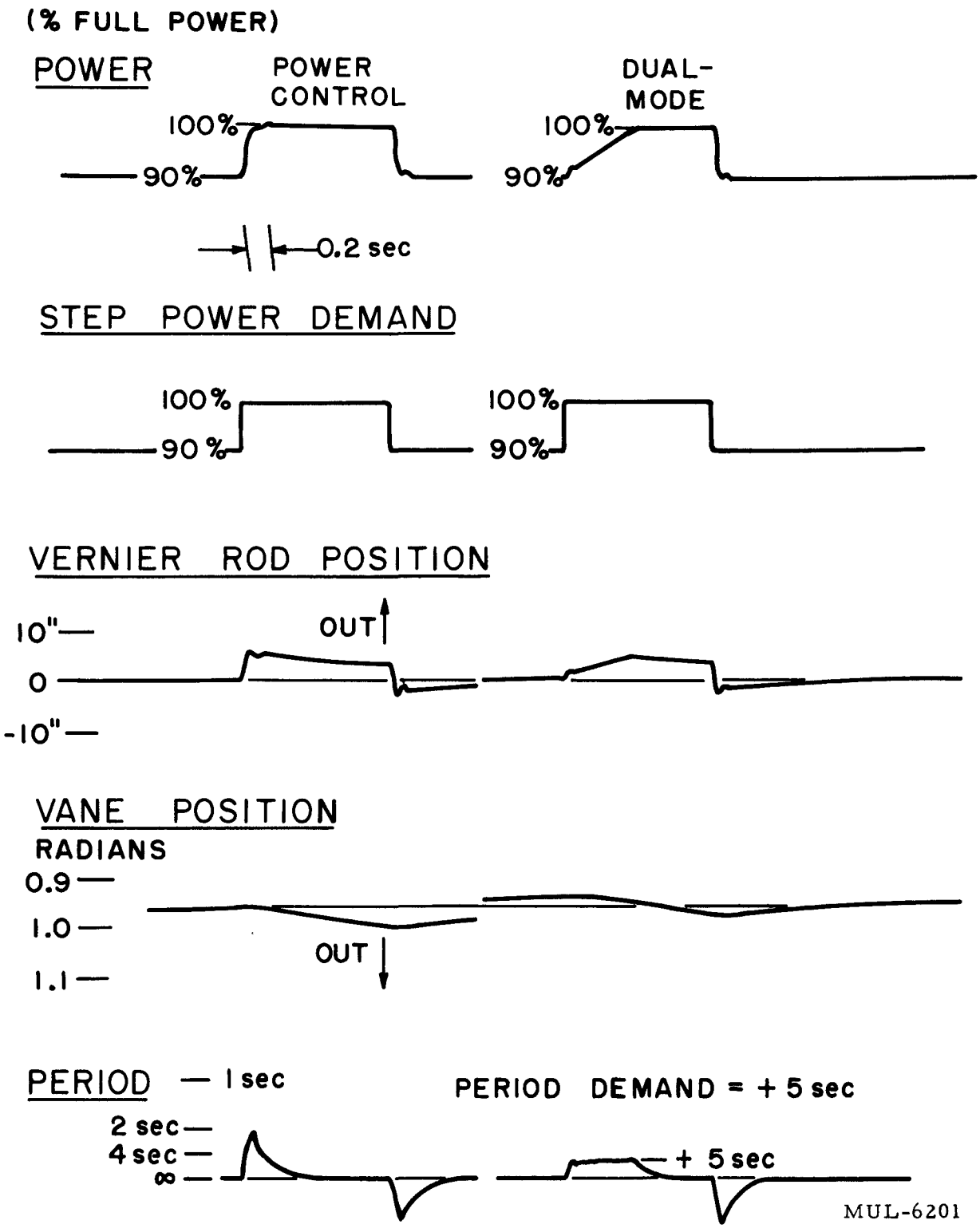

Fig. 6-30. System response to ±10% step changes in power demand at full power with and without dual-mode control.

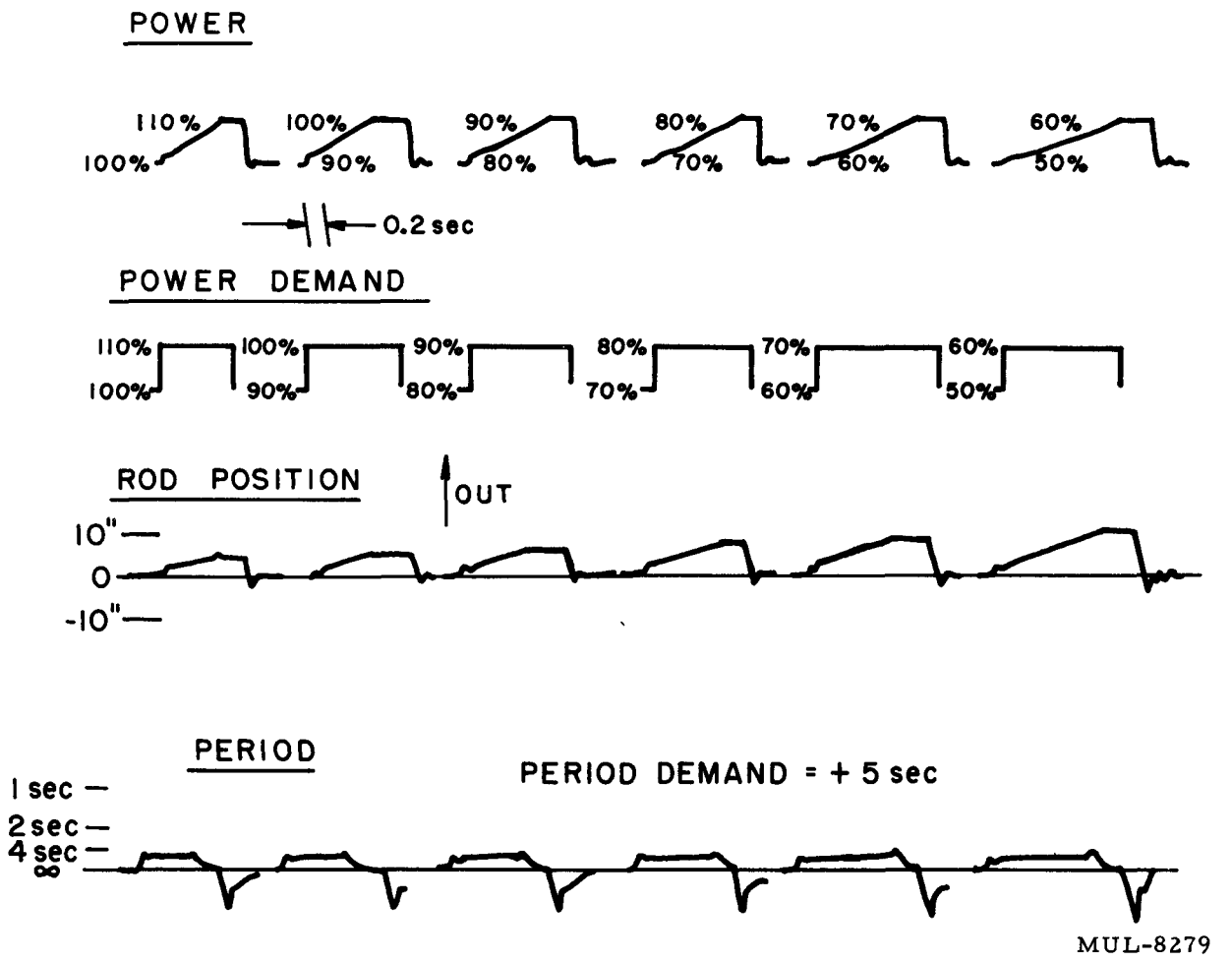

Fig. 6-31. System response to ± 10% step changes in power demand at intermediate power levels.

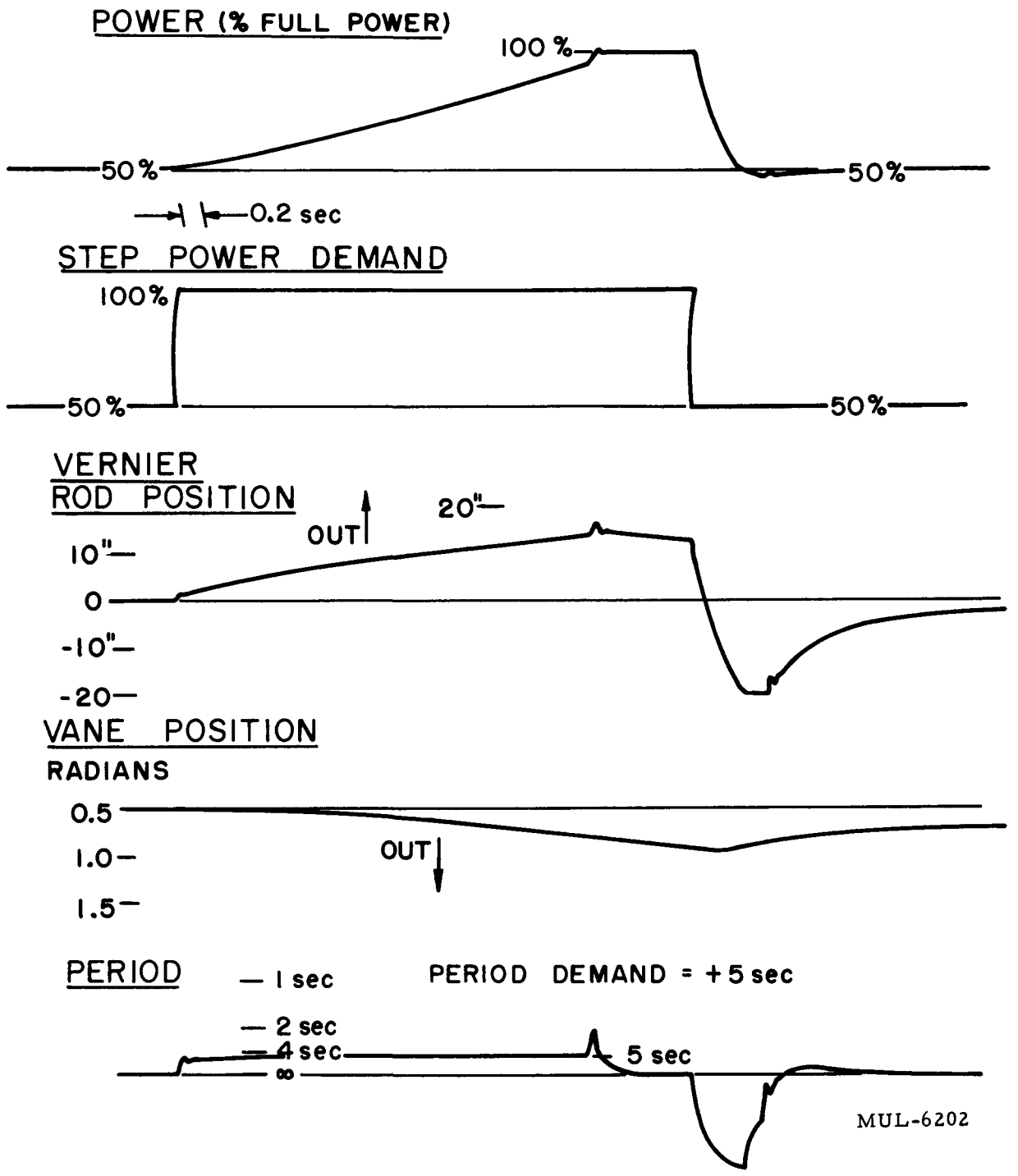

Fig. 6-32. System response to ±50% step changes in power demand.

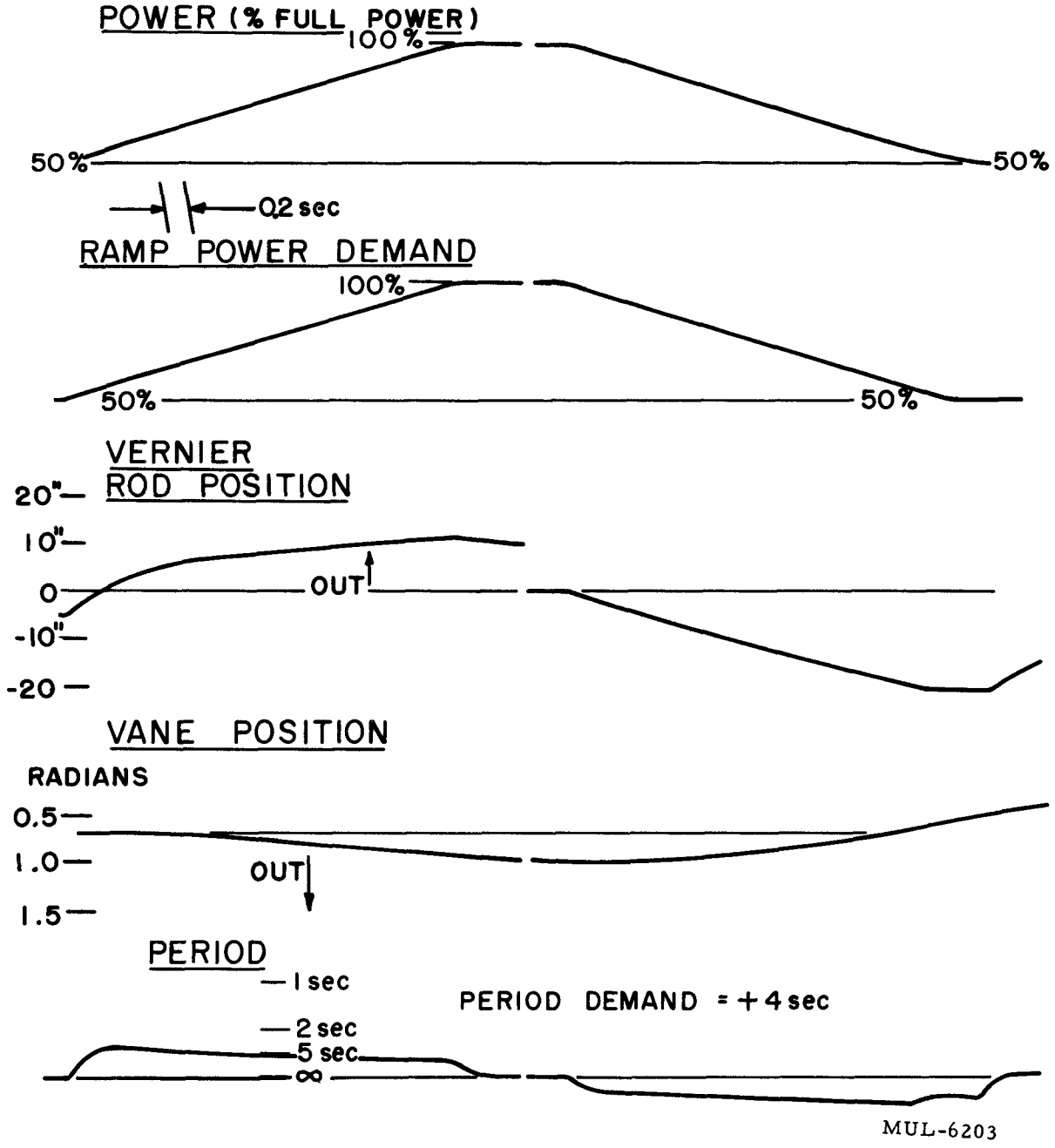

Fig. 6-33. System response to ±50% ramp changes in power demand.

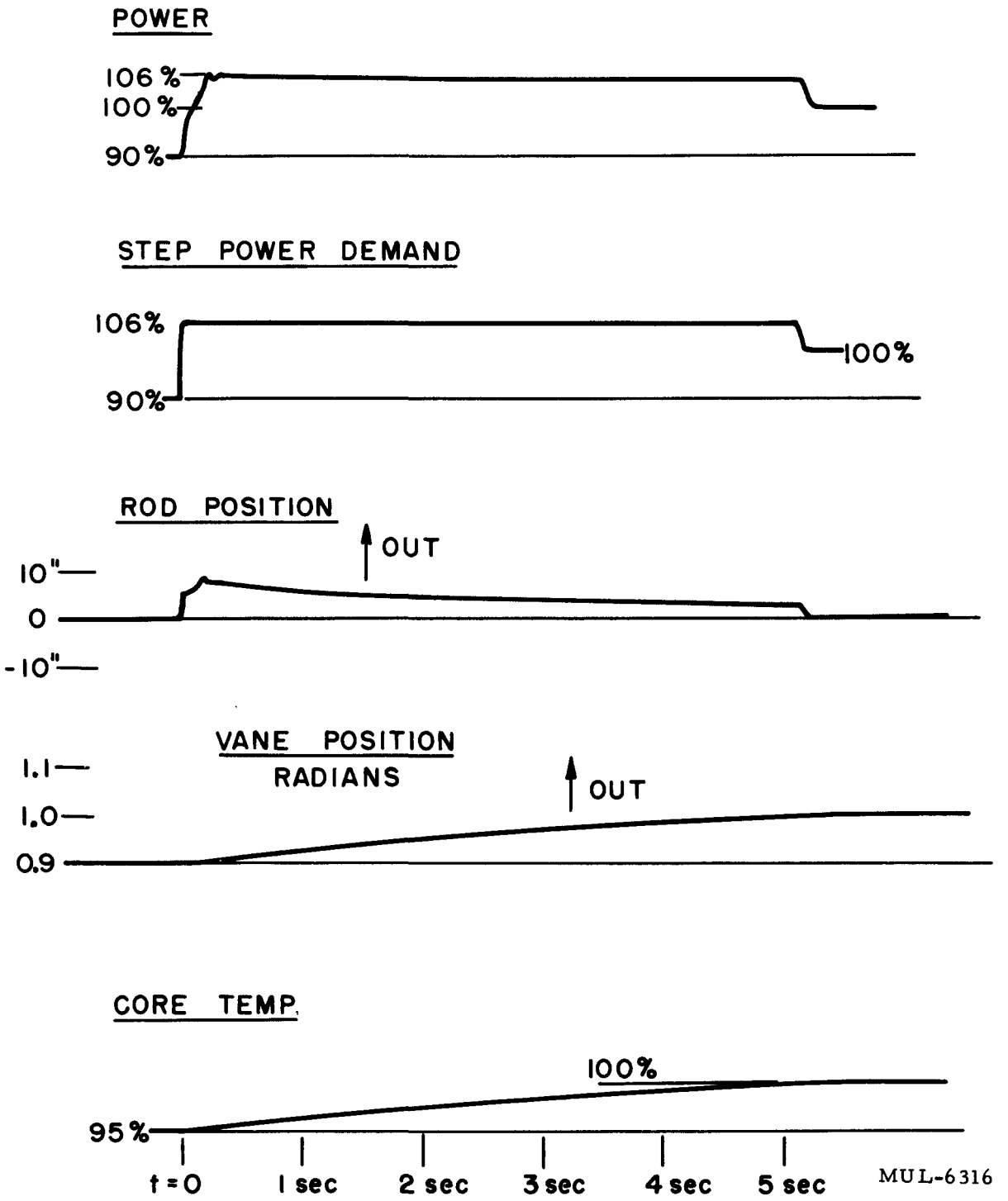

Fig. 6-34. Power program which produces 5% change in core temperature in 5 seconds. Flow rate was maintained constant at full flow.

in the required time. If both the flow rate and power level are varied, there are an infinite number of programs which will produce the required temperture change. The problem of optimum programming of these two variables will not be considered here.

Figure 6-35 shows the system response to step δk disturbances of ± 10¢ and ± 20¢ (where $1.00 = 0.0064 absolute reactivity). Figure 6-36 shows the system response to sinusoidal δk disturbances which have a peak amplitude of 10¢. The control system is capable of maintaining power level constant out to about 0.5 cps in the face of such a disturbance. This represents the "worst" type of disturbance insofar as desirable system response is concerned. The core temperature, however, is insensitive to these "high frequency" variations in power level.

The analog computer was applied to the accident analysis of Section 6.3.7, giving results which confirm that the control system will operate as intended in avoiding hazardous situations. Figure 6-37 shows the system response following failure of the power level detector during startup of the reactor. As intended, the power level is caught at the reverse set point (120% of full power in this case) and held close to that value until normal control is restored. Figure 6-38 shows the system response to step δk disturbances of ± $1.00. As seen, the temperature overshoot from a + $1.00 accident is less than 5°F; also, there is a fair amount of undershoot following the accident. This is due to the finite switching time of the fast reset circuitry.

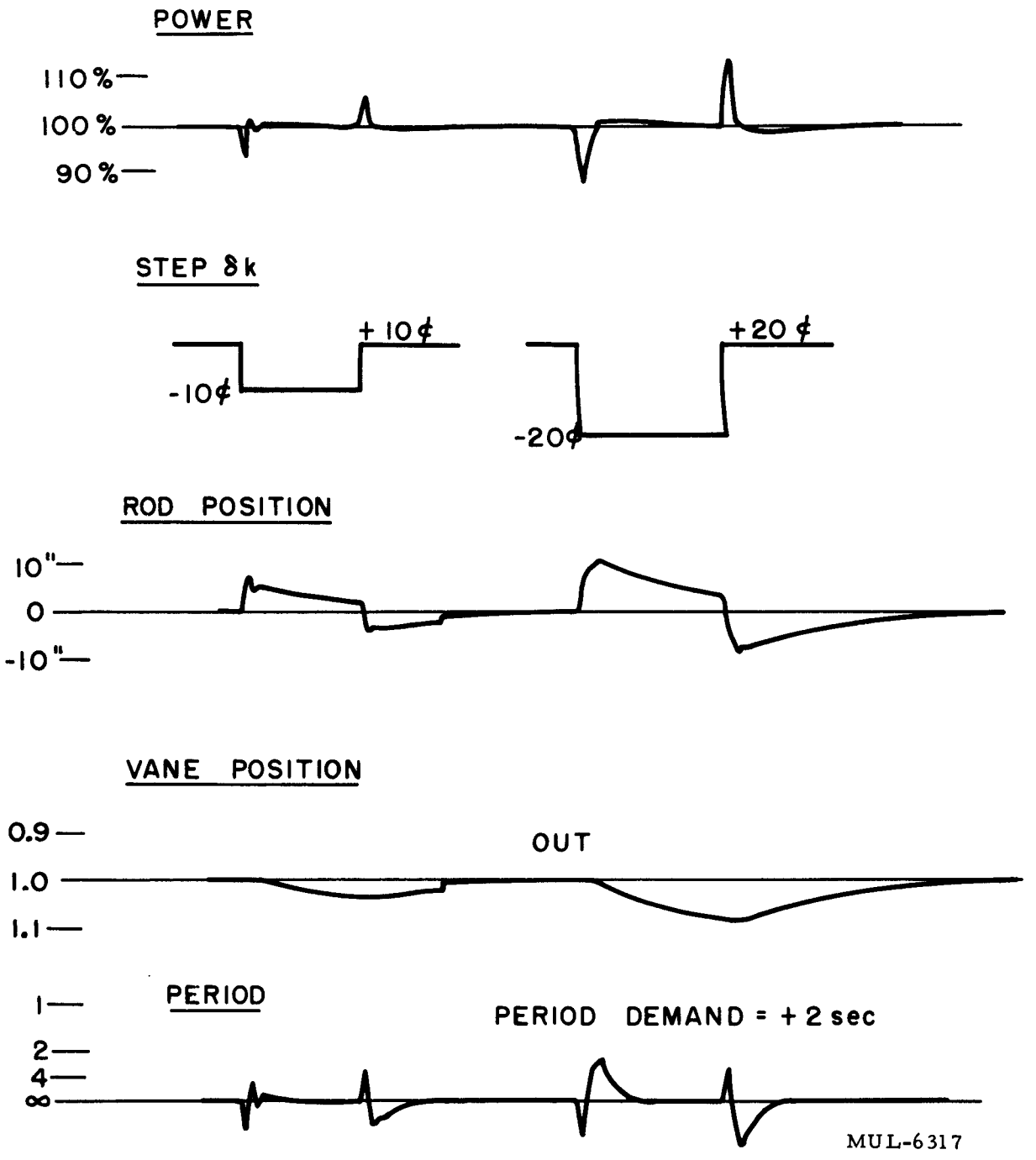

Fig. 6-35. System response to step δk disturbances of ±10¢ and ±20¢ (no fast reset action).

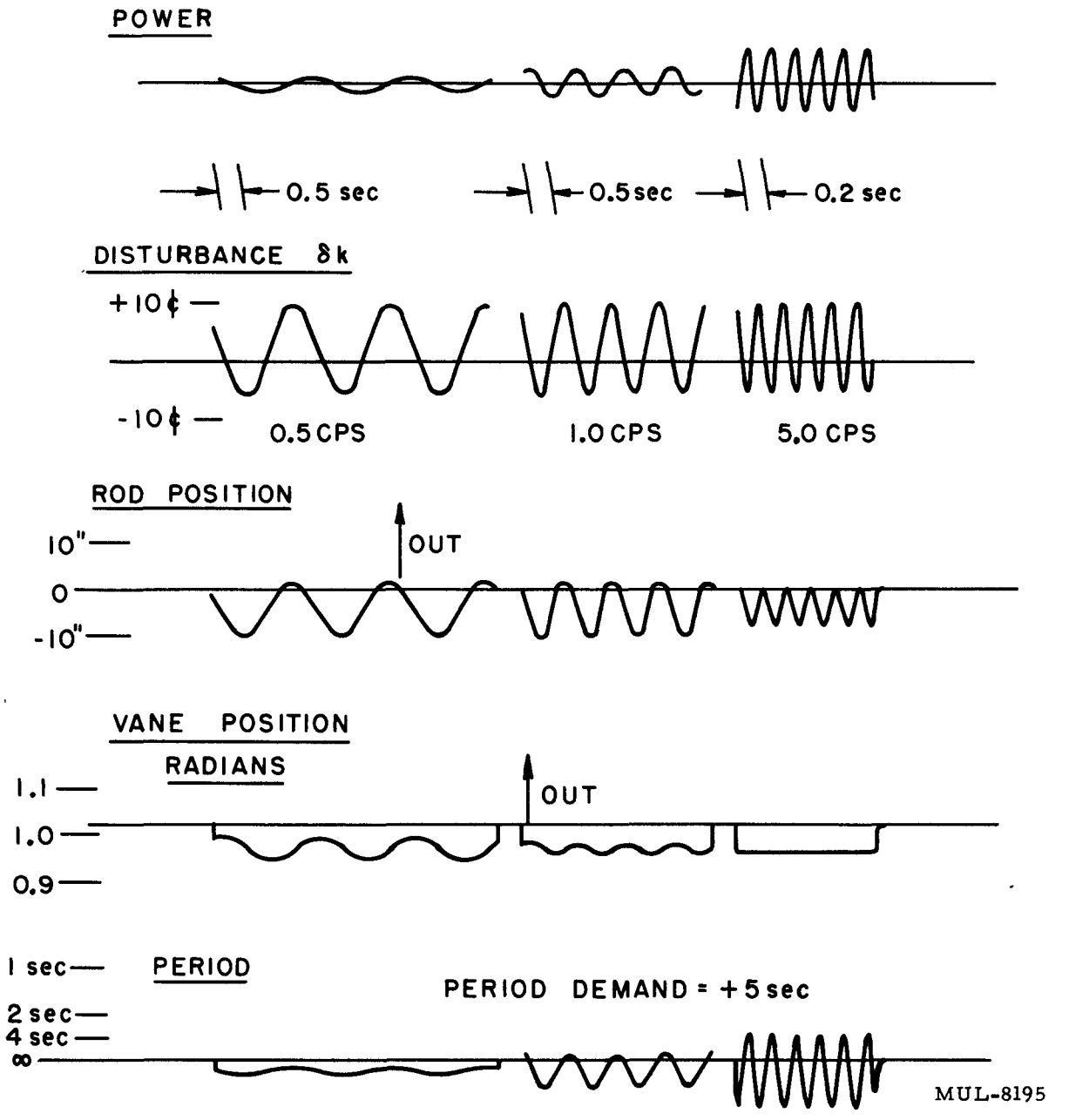

Fig. 6-36. System response to sinusoidal δk disturbances of amplitude 10¢ (no fast reset action).

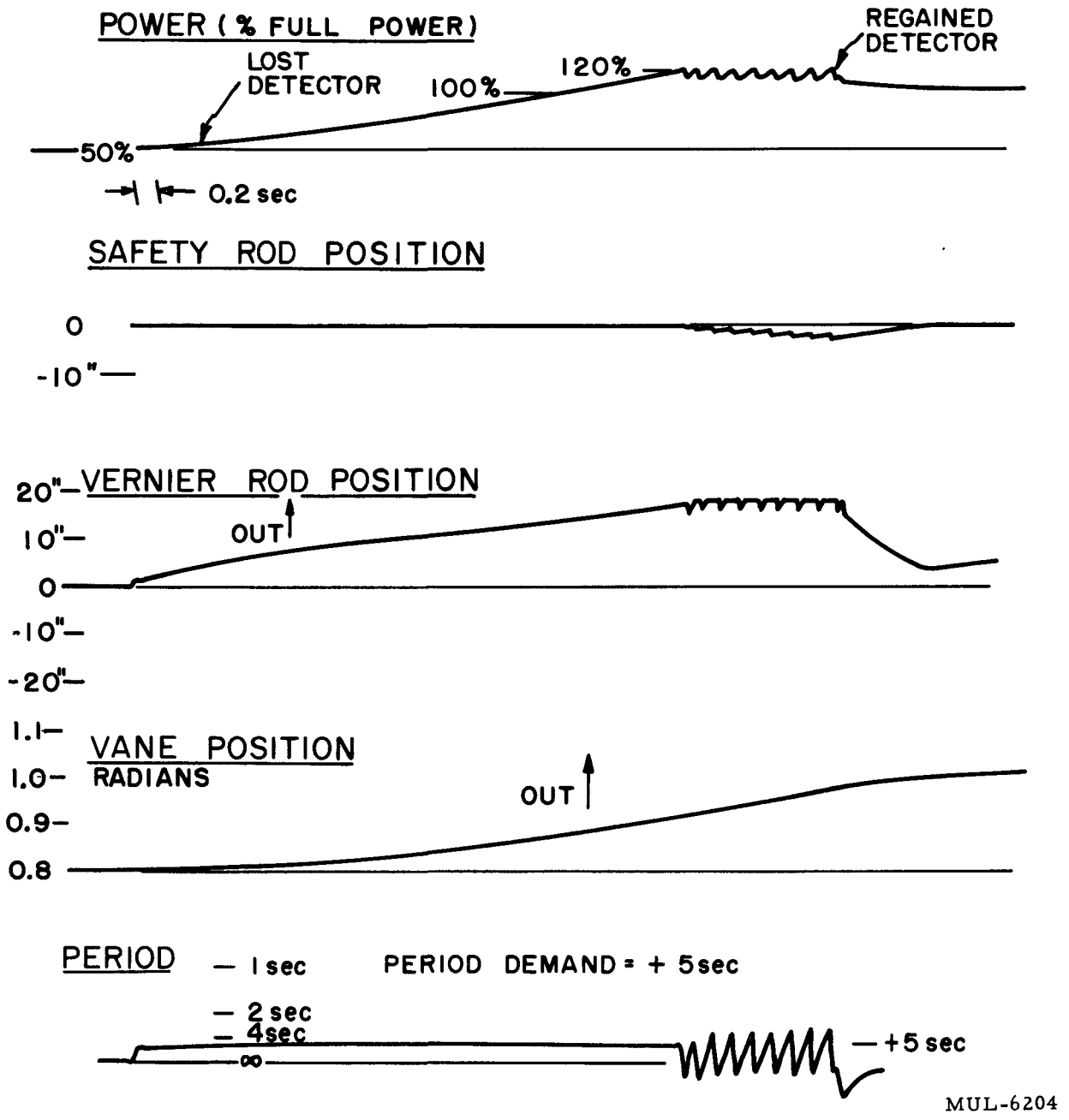

Fig. 6-37. System response and recovery in startup accident.

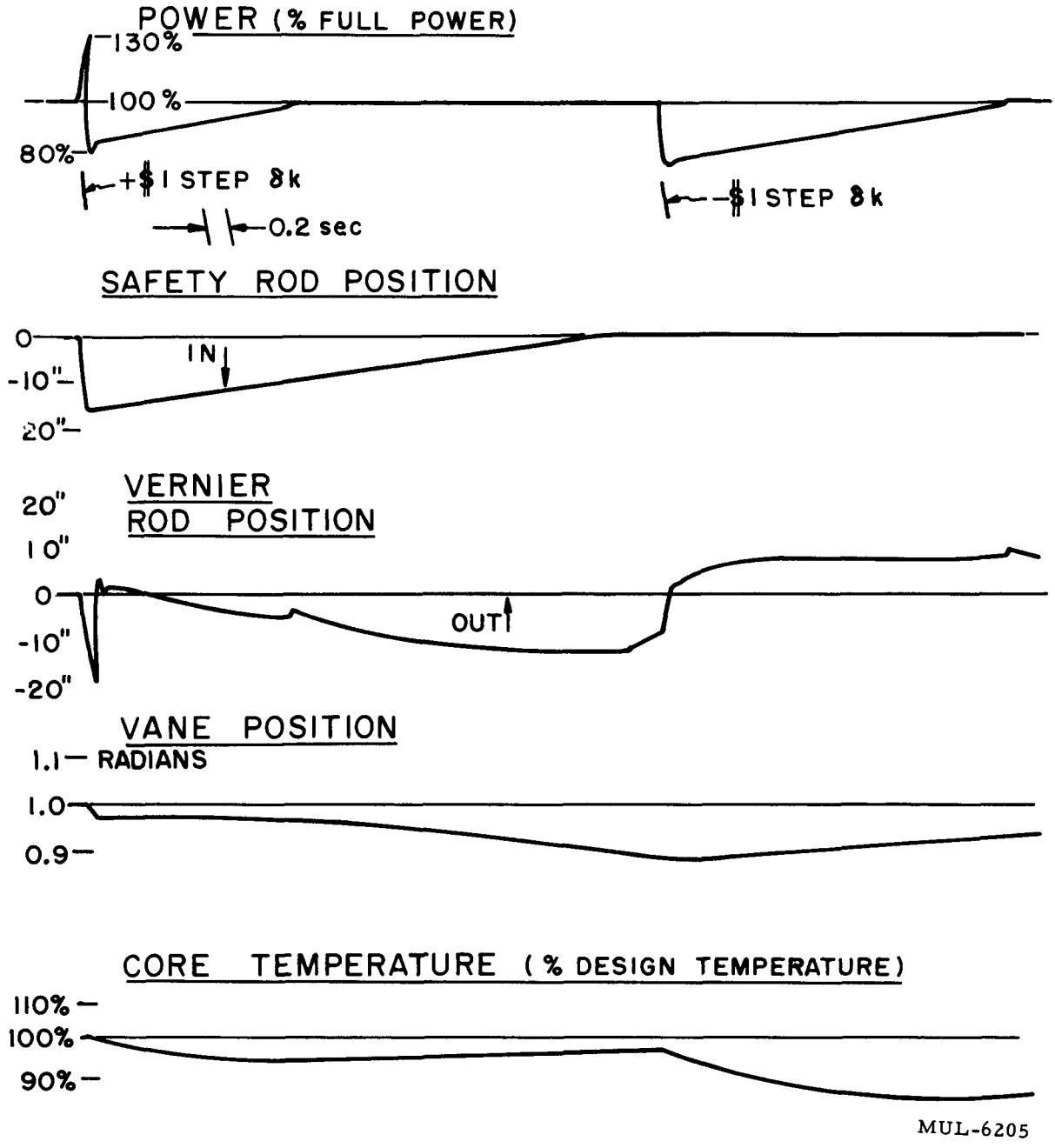

Fig. 6-38. System response and recovery to ± $1.00 perturbations in reactivity.

7. INSTRUMENTATION

7.1 Introduction

This chapter describes the system designed to gather data on the operating characteristics of Tory II-A. Included in the instrument system are sensing elements and transducers on the reactor, signal transmission equipment, and display or recording equipment.

The design of the instrument system was based, in a general way, upon a desire to answer questions such as the following:

1. What is the reactor neutron flux level, and at what rate is it changing? This information, which is needed for feedback to the automatic control system as well as for analysis of reactor behavior, will be supplied by the nuclear instrument system.

2. What is the temperature and pressure distribution of air entering and leaving the reactor core? Probes in the air stream near the core will supply this information, necessary for evaluation of the air flow and heat transfer characteristics of the core as well as for warning of conditions endangering the core during a run.

3. What is the temperature distribution in the core, and how does it change with power level and air flow rates? This question is of particular importance during startup and shutdown because of thermal stress problems. Core thermocouples serve to answer this question.

4. How is the core support structure stressed under static and dynamic loads during blowdown? Strain gauges are mounted on the tie rods and the shroud to answer this question. Only low temperature information can be obtained, however, since the strain gauges will become inoperative in the upper ranges of planned operating temperature.

5. What are the vibrational characteristics of the reactor? Are there any resonant tendencies or large-displacement, low-frequency vibrations? Velocity and acceleration pickups will be mounted on the core support structure and air duct to answer these questions.

6. Are the operating temperatures (due to gamma heating, for example) of auxiliary components excessive? Thermocouples have been placed in various places (reflector, rod and vane drive mechanisms, wiper seals, base plate springs, for example) to answer this question.

7.2 Nuclear Instruments

Figure 7-1 is a schematic diagram of the nuclear instrument system. This system consists of two source range, two intermediate range, and four power range channels. One intermediate range channel is spare. Seven of the eight channels display and record a signal proportional to the logarithm of the power level (log N); the eighth channel is equipped with linear level display and recording.

The detector signals pass through preamplifier and log and period computer stages (or a micromicroammeter for the linear channel) before transmission to the control building via coaxial cable. Provision is made for calibration "in service" of any one of the source range or intermediate range channels. The complete channel, except detector, can be checked by inserting a calibrated signal into the preamplifier.

In addition to displaying and recording information, the nuclear instrument system supplies one power and one period signal to the servo control system for automatic power level control use. Log N and period signals are also supplied to the fast reset circuits.

7.2.1 Detectors

1. Type – The source range and intermediate range detectors are BF_3 counters. Some operating characteristics are: (a) neutron flux range – zero to 2.5×10^4 nv; (b) sensitivity – 4.5 counts/n/cm^2; (c) output pulse – minimum of 10^{-3} volt with inherent rise time of less than 5×10^{-8} second.

Power range detectors are compensated ion chambers. Some operating characteristics are: (a) thermal neutron flux range – 2.5×10^2 to 2.5×10^{10} n/cm^2/sec; (b) neutron sensitivity – 4×10^{-14} amp/n/cm^2-sec; (c) approximate signal electrode output impedance – 160 μμf, 10^{14} ohms.

2. Location – Present plans call for mounting the source range detectors on a tramway located about 10 feet from the reactor center line and running parallel to the reactor axis. This makes it possible to vary detector-reactor separation, hence detector sensitivity. This should ensure that overlap of the source and intermediate ranges is adequate.

The intermediate range and power range detectors are located in the bunker on the air duct centerline just behind the duct turning section.

3. Power Level Coverage – The expected power level range coverage of the detectors is as follows:

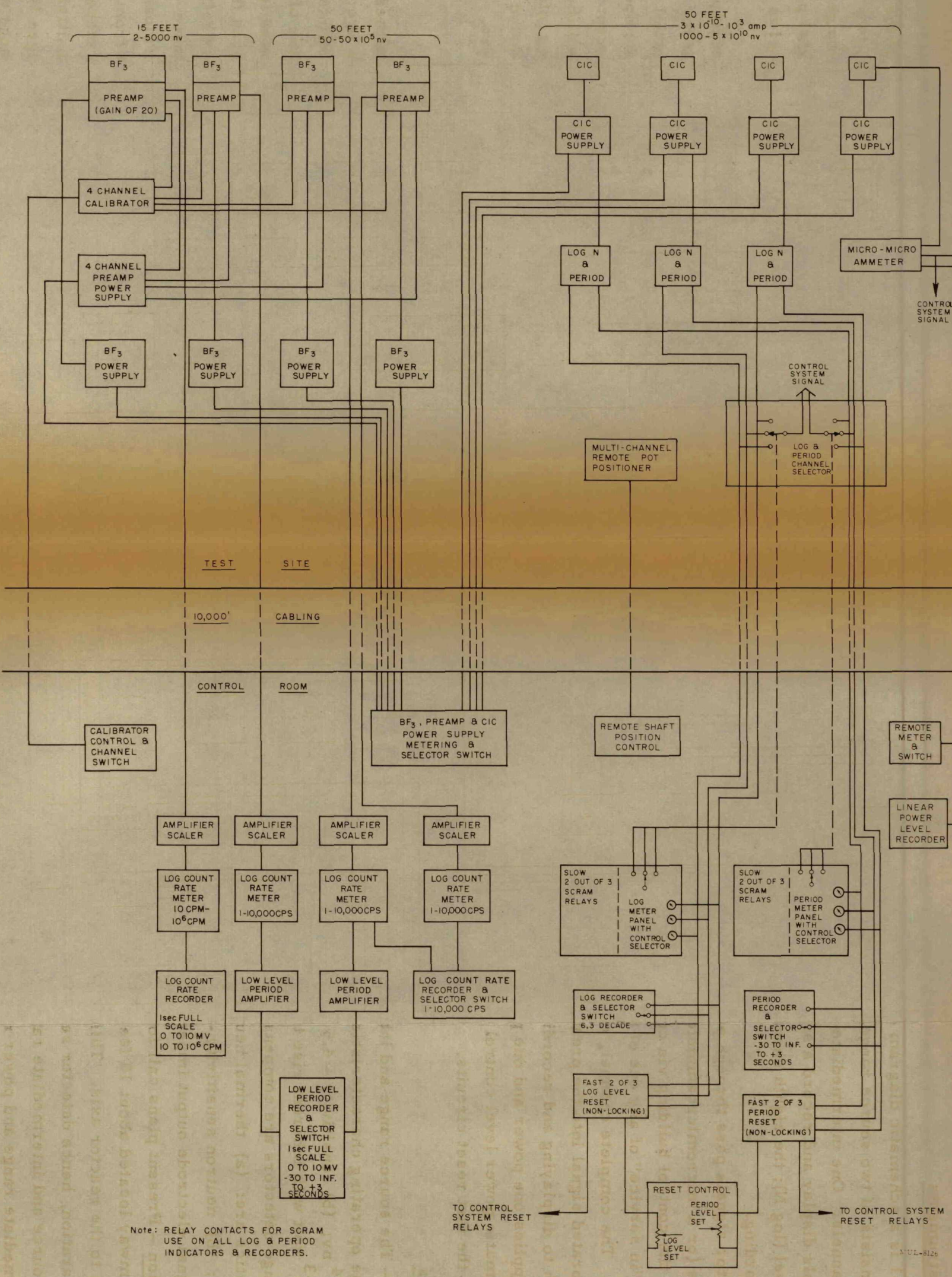

Fig. 7-1. Nuclear instrument system schematic diagram.

Source range — minimum to 2 watts
Intermediate range — 0.1 to 10^4 watts
Power range — 10^2 to 10^9 watts.

Figure 7-2 shows expected signal strengths and thermal neutron flux levels at detector stations vs reactor power level.

7.2.2 Transmission, Display, and Recording

As mentioned above, signals from all eight neutron detectors are modified before being transmitted to the control point via direct cable. The BF_3 counters feed into preamplifiers. Three of the compensated ion chamber signals are operated on by log N and period computers; the fourth (linear channel) feeds a micromicroammeter.

Each source range channel is equipped with a scaler and log count rate meter. One has a log count rate recorder; the other shares a low-level period recorder with the intermediate range instruments.

The intermediate-range instrument channels each include a scaler and a log count rate meter. A log count rate recorder is shared by these two channels; a low level period recorder is shared by one of them with a source range channel.

As indicated in Figure 7-1, there are three log N channels and one linear channel in the power range. The period and log N signals are displayed on meters at the control point; one log N and one period signal can be recorded on strip chart recorders.

The fourth power range channel feeds a linear meter and recorder. This linear channel operates over the full range of compensated ion chamber output. A range switch with about twelve steps is provided for changing the linear channel sensitivity.

The relation of the nuclear instrument system to the control system is discussed in the next section.

The recorders will be comparable to the well-known Brown or Leeds and Northrup strip chart recorders. Chart speeds are variable up to several inches per minute, and full scale pen travel time is about 0.4 second. Pen travel time for a step change smaller than full scale takes a correspondingly smaller time. In addition, the channels which are being used by the control system are recorded on 120-cycle equipment.

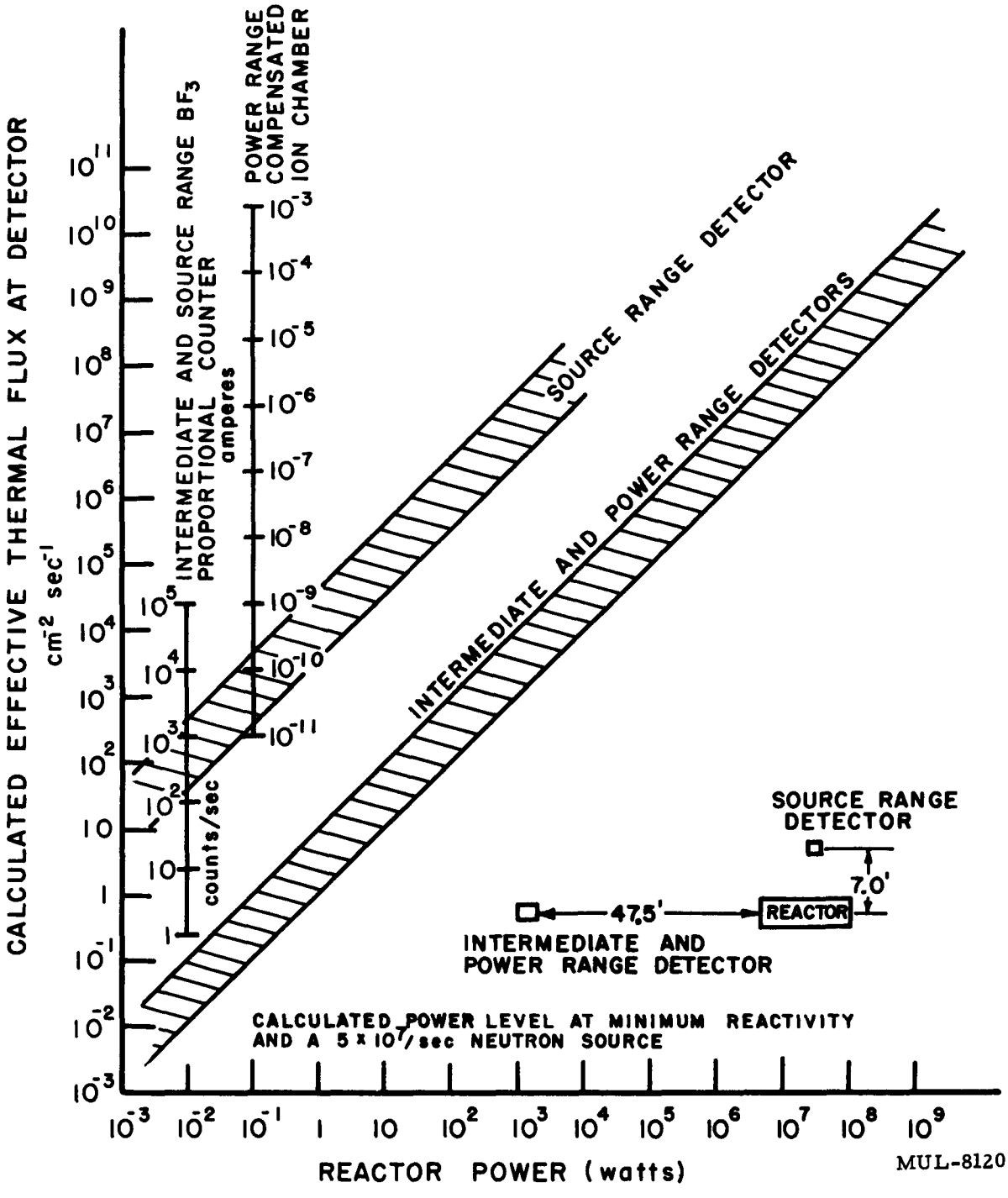

Fig. 7-2. Detector station neutron flux vs reactor power level.

7.2.3 Signals Supplied to Control System

One of the more important functions of the nuclear instrument system is to supply signals to the control system which are utilized to maintain desired power level and to deliver setback signals in the event of an undesirable excursion.

Three compensated ion chambers are available for supplying log power level and period information to the control system. Any one of these three channels can be chosen for control use by a remote switch located at the control point. The control system requires both a power and period signal, and the selector switching arrangement is such that the ion chamber chosen to supply the log N signal may or may not be the same as that chosen to supply the period signal. This choice is left to the operator. The control system may also regulate power according to the linear signal from the fourth compensated ion chamber. A period signal would still be taken from one of the log N channels.

The three log N channels have the additional function of supplying information to the fast reset system. If any two of the three indicated power levels exceed a specified limit, or if two of the three indicated period signals fall below a fixed limit, fast reset action will be initiated to prevent an uncontrolled power excursion. Section 6 describes the fast reset system in detail.

7.3 Temperature Instruments

Since high temperature is one of the more distinguishing characteristics of Tory II-A, measurement of temperatures is a very important part of the instrumentation program. Core temperature distribution is important from the standpoint of temperature dependence of material behavior and from thermal stress considerations during thermal transients. In addition, core temperature distribution will serve to check the extensive heat transfer calculations. The temperatures of auxiliary equipment on the test car, such as rod-drive mechanisms, reflector, and pressure vessel, must also be known, for safety as well as analysis of reactor operation.

A total of 184 temperatures are measured on the test vehicle. Of these 92 are located in the core and core support structure.

7.3.1 Transducer Selection

Selection of high-temperature thermocouples will be determined by the results of a test program to be carried out at Livermore. Some of the questions which this test program should answer are:

1. How is the resistance of commercially available (MgO or Al_2O_3) thermocouple insulation affected by temperatures in the 2000°F range?

2. Both shielded twin lead and co-axial thermocouple wire is available. What is the relative mechanical performance at high temperature? It is planned to temperature-cycle samples with bends of various radii to determine the tendency to short circuit.

3. Finally, it is important to determine reproducibility of thermocouple calibration.

Test program results were not yet available when making the tentative choice of thermocouples described in the following section.

7.3.2 Core Measurements

Accurate core temperature measurements will be the most difficult to make. "High temperatures" here refer to temperatures in the 1500-2300°F range. This exceeds "high temperature" as normally encountered in instrumentation by several hundred degrees.

The primary temperature elements will probably be platinum-rhodium thermocouples, specifically 94 Pt-6 Rh against 70 Pt-30 Rh. The melting points of these alloys are such that they will withstand the expected temperatures with a margin of safety. Unfortunately, platinum is a very good gamma-ray absorber, so wire must be kept small to reduce reading error (maximized surface-to-volume ratio). Difficulty has been encountered in fabricating suitably small wire.

Calculations using 0.040 in. o.d. × 0.007 in. wall sheath with 0.010 in. diameter center lead co-axial wire indicate errors of the order of 15-20°F. Co-axial wire is not presently considered compatible with the remainder of the system because of ground loop problems. Use of a double-lead, shield-sheath couple greatly reduces the noise problems but must, of course, be larger. In either case, fabrication difficulties must be overcome.

Installation

1. Fuel Elements

The core is approximately 3 ft diam × 4 ft long with several thousand longitudinal air passages through it. These air passages are less than 1/4 inch in diameter, and the core is assembled from many thousands of small pieces of fueled ceramic. Thus, core thermocouples must be carefully

installed in the core during the initial core assembly.

Dummy tubes (same as others except unfueled) will be incorporated in the core as thermocouple lead-wire passages. To carry the leads from the dummy tubes to the desired couple locations, some type of drilling and porting of fuel elements must be made. Several techniques have been tried, with two general methods of drilling investigated. The first, ultrasonics, appears at this time to have an effectiveness decreasing rapidly with increasing depth of cut. From work done on alumina, it appears that this method could be used to "clean up," straighten, and size the bores of core elements but would be impractical to use for drilling holes as small as 0.040 inch diameter. The second method, diamond drilling, has been very effective for every operation tried. Holes as small as 0.030 in. and as large as 1/2 in. diam have been drilled in beryllia at relatively high rates of speed.

Of the various methods tried for physical placement of the thermocouples within the core, the least troublesome, from the standpoint of fabrication of core elements and assembly of the core, is that shown in Fig. 7-3. This method requires, as do all others tried, that drilling and porting be done prior to assembly. As indicated in the figure, the junction is located in a blind hole in the end of a core element, adjacent to the dummy tube. The element immediately above is ported to allow an accurate fit. Leads installed in this manner will be sufficiently well clamped by the core elements in which they are installed that they will not require bonding to resist displacement by the air stream. It may prove necessary to provide some sort of clamp at intervals along the dummy tubes to avoid the possibility of lead failure due to whipping in the air stream.

It has been suggested that a sort of "semi-bonding" might be accomplished in such a fashion that the danger of failure from thermal stress is minimized and yet the contact surface between the thermocouples and the ceramic is maximized. This would tend to reduce the error from gamma heating.

Two methods appear feasible for this. The first is a light shrink fit — i.e., drill the blind hole in the core element slightly undersize, heat the element, insert the junction and allow the ceramic to shrink onto the lead by cooling to room temperature.

The second approach is to use "liquid platinum" (a suspension of finely divided metal in a vehicle normally used for ceramic decoration) in the blind hole, insert the junction end of the thermocouple lead, and bake. Either method

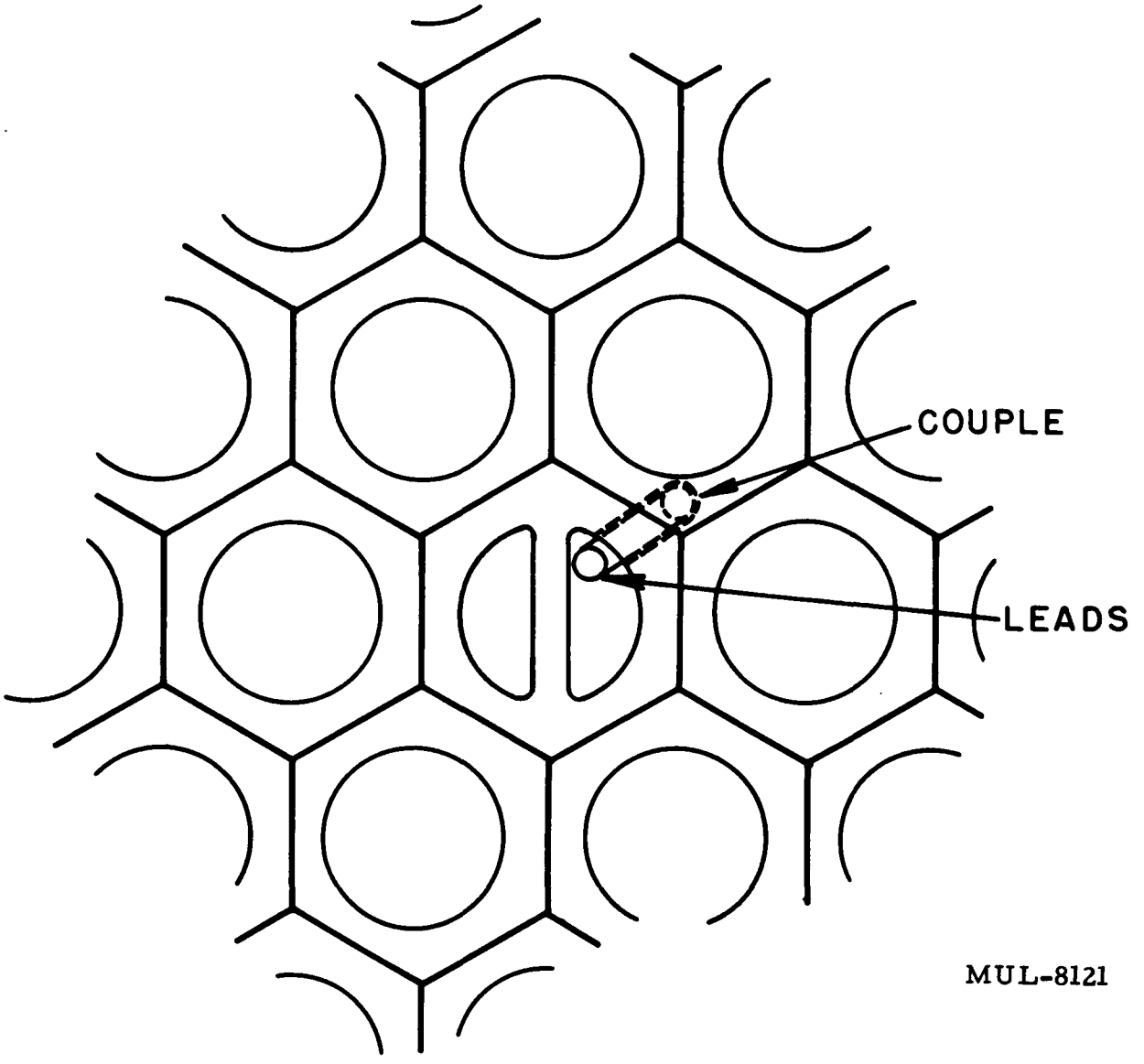

Fig. 7-3. Dummy tube and thermocouple installation in core.

should result in good contact and, since both would be performed prior to the time of final core assembly, each would affect final assembly in the same way.

The best information currently available on coefficients of expansion indicates that the thermocouple wire coefficient is very nearly equal to that of the ceramic. Therefore, a tight fit installation appears feasible.

2. Dogbones, Outer Links

Although the foregoing deals with the fuel elements, the discussion applies equally well to the dogbone ribs, inner dogbone eyes, and outer links. These are all basically the same material, so although wire routing, wire passages, etc., may have to be modified to suit the particular item involved, none of these installations really differ one from another.

3. Base Plates

Attachment of thermocouples to the coated molybdenum base plates presents a difficult problem which has not yet been solved. Bonding must be good, but the protective coating may not be removed unless it is replaced after the couples are attached.

4. Support Structure, Tie Rods

The front support structure, shroud, tie rods and wiper seals are all nickel-chrome alloy. With these materials welding becomes a feasible method of attachment. It is conceivable that one of the ceramic "cements" might also be useful for the front support structure installation. Here the temperature is low enough (about 1200°F) that such a cement could reasonably be expected to function. It is felt, however, that welding or brazing techniques would be more suitable.

Location

In general the location of thermocouples in the core is based on a need to know the temperature distribution of core elements throughout the core volume. Obviously this need must be compromised with cost and mechanical interference problems.

As far as temperature measurements are concerned the core is asymmetrical in several respects. First, the heat transfer calculations predict maximum temperatures in the $x/L = 0.7$ plane, so core components in this plane are heavily instrumented (see Table 7-1 and Figs. 7-4 and 7-5). Second,

Table 7-1

Longitudinal location of Pt-Rh/Pt-Rh core thermocouples

x/L is fractional core length, measured from front face of inlet end reflector.

Core component on which mounted	Transverse plane in which located	Quantity
Fuel elements	x/L = 0.175	5 Active 5 Spare
	0.320	1 Active 1 Spare
	0.540	1 Active 1 Spare
	0.700	23 Active 23 Spare
	0.910	6 Active 6 Spare
Dogbone ribs	0.175	2 Active 2 Spare
	0.700	8 Active 8 Spare
	0.910	2 Active 2 Spare
Inner dogbone eyes	0.700	3 Active 3 Spare
Shroud	0.700	2 Active 2 Spare
	0.910	2 Active 2 Spare
Tie rods	0.700	6 Active
	0.910	6 Active
Outer links	0.175	2 Active
	0.700	5 Active 5 Spare
	0.910	2 Active

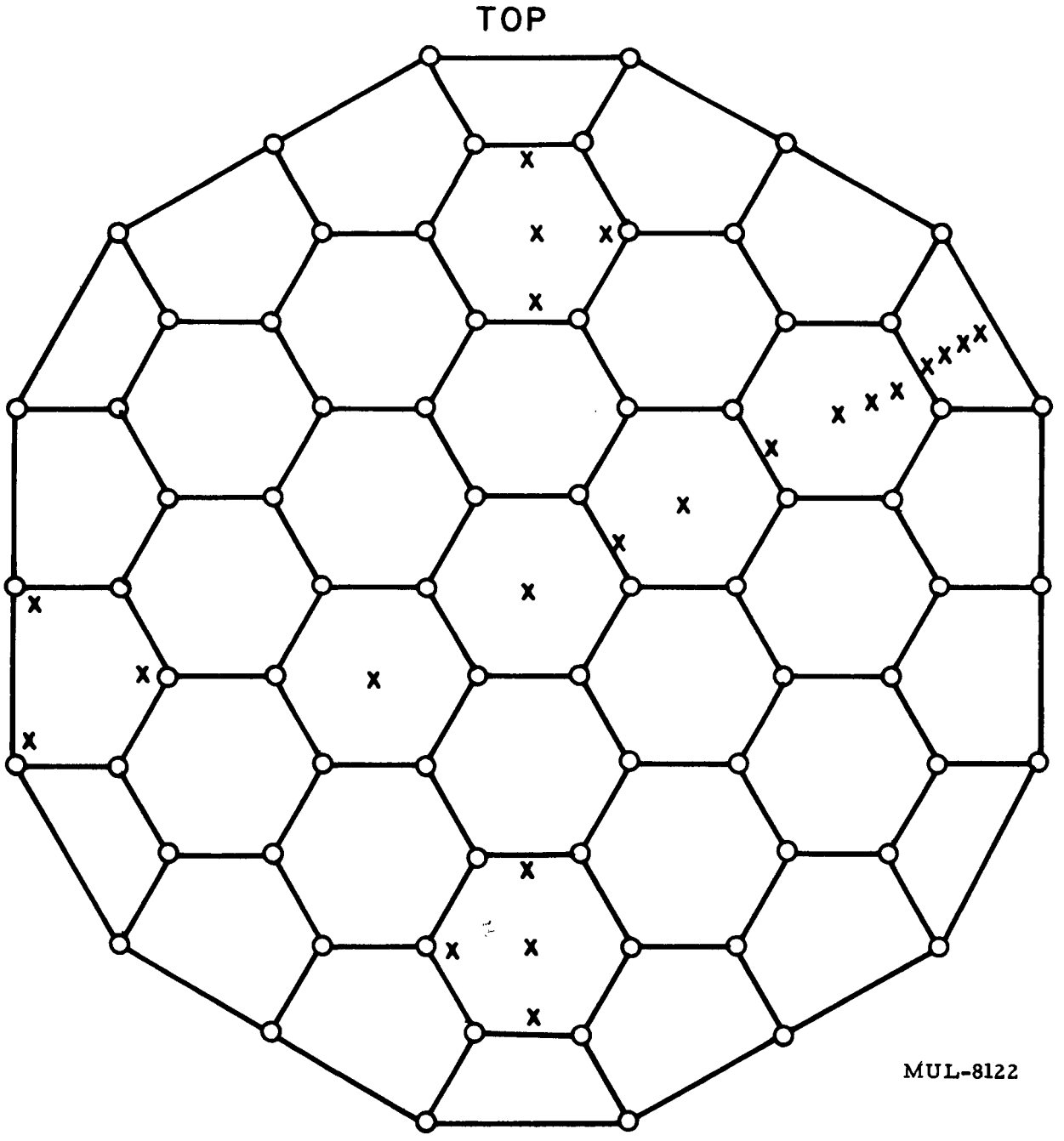

Fig. 7-4. Fuel element thermocouple location in the X/L = 0.7 plane.

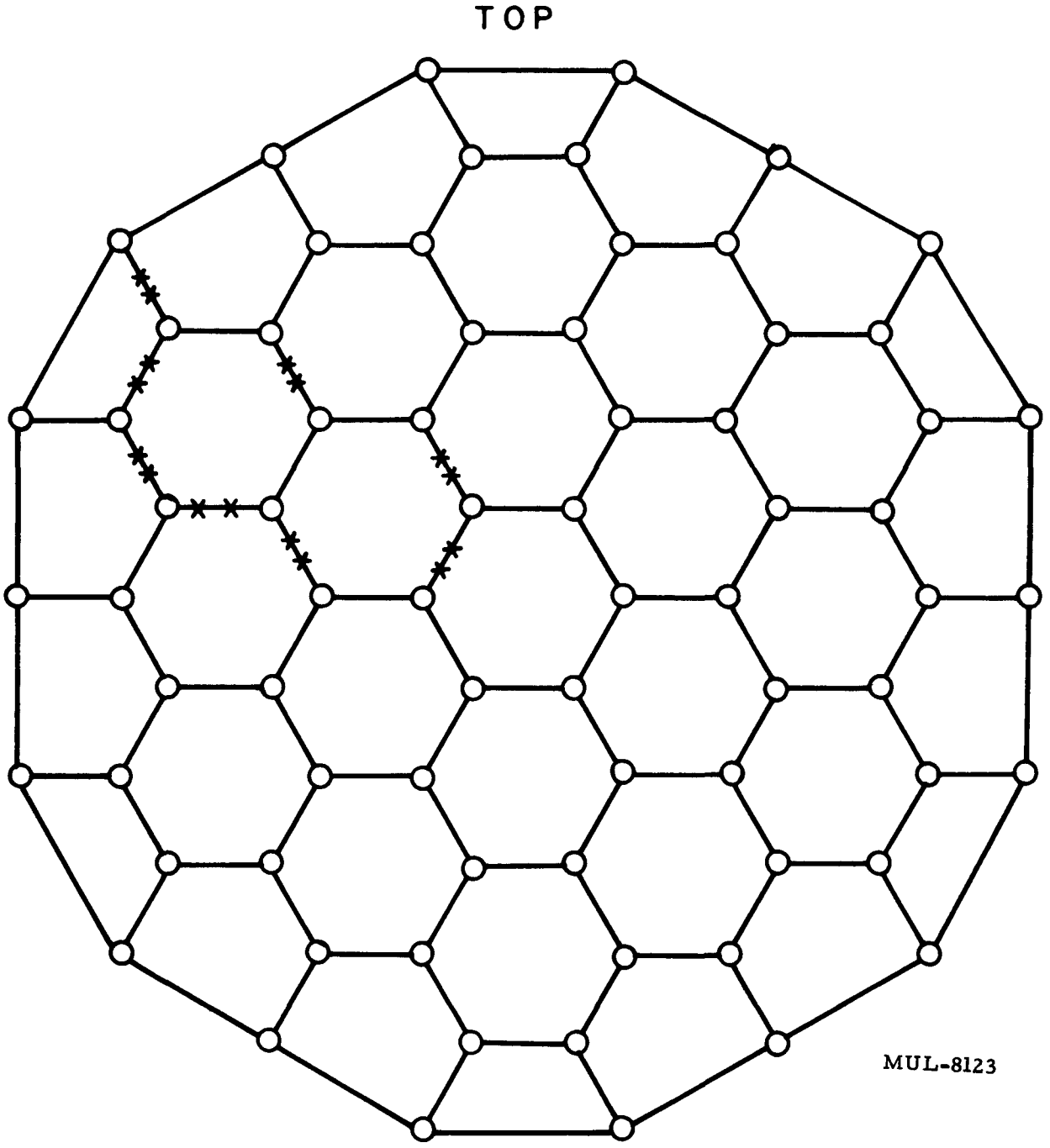

Fig. 7-5. Dogbone web thermocouple locations in the X/L = 0.7 plane.

the vernier rod is partially inserted during normal control operation, so there is a flux depression in its vicinity. Therefore, core elements in the vernier rod area have been given special attention. Third, the bottom outer links are more heavily stressed than those at other locations, so more thermocouples are located on bottom links. Fourth, the difference between fueled and non-fueled core component temperatures is greater in the forward portion than in the rear portion of the core. This tends to make the thermocouple population greater in the forward part of the core.

7.3.3 Measurements Exclusive of the Core

There are several areas of temperature interest other than the core. The temperatures of hydraulic actuator equipment, core support structure, gamma shield, and air stream, for example, are important. These temperature measurements are not as unique and difficult as core measurements and need not be discussed in detail.

As shown in Fig. 7-6, the exit air total temperature distribution is measured by 19 Pt-Rh/Pt-Rh thermocouples mounted on a horizontal and vertical temperature rake at the reactor rear face. In addition, diffuser inlet air total temperature is measured.

Table 7-2 shows the general disposition of all test-vehicle temperature transducers.

7.3.4 Transmission and Display

Figure 7-7 shows the types, number, and use of the data transmission, recording, and display channels. All test-vehicle thermocouple measurements will be carried on channels B, C, and G.

Slow Response Channel – Channels B and C are 86-signal ASCOP data transmission systems. In this system each measured variable is sampled ten times per sec, amplified, used to modulate a pulsed carrier, then transmitted to the control point via direct cable. Frequency response is 1.5 cycles per second.

Each of the two channels of ASCOP equipment is supplied with a 17-inch oscilloscope for display of the entire 86 variables per channel. The display appears as a series of vertical lines on the oscilloscope face, the length of each line being proportional to the magnitude of the measured variable. Each channel is supplied with a magnetic tape recorder which records all 86 variables being supplied to it. In addition, five selected variables can be displayed

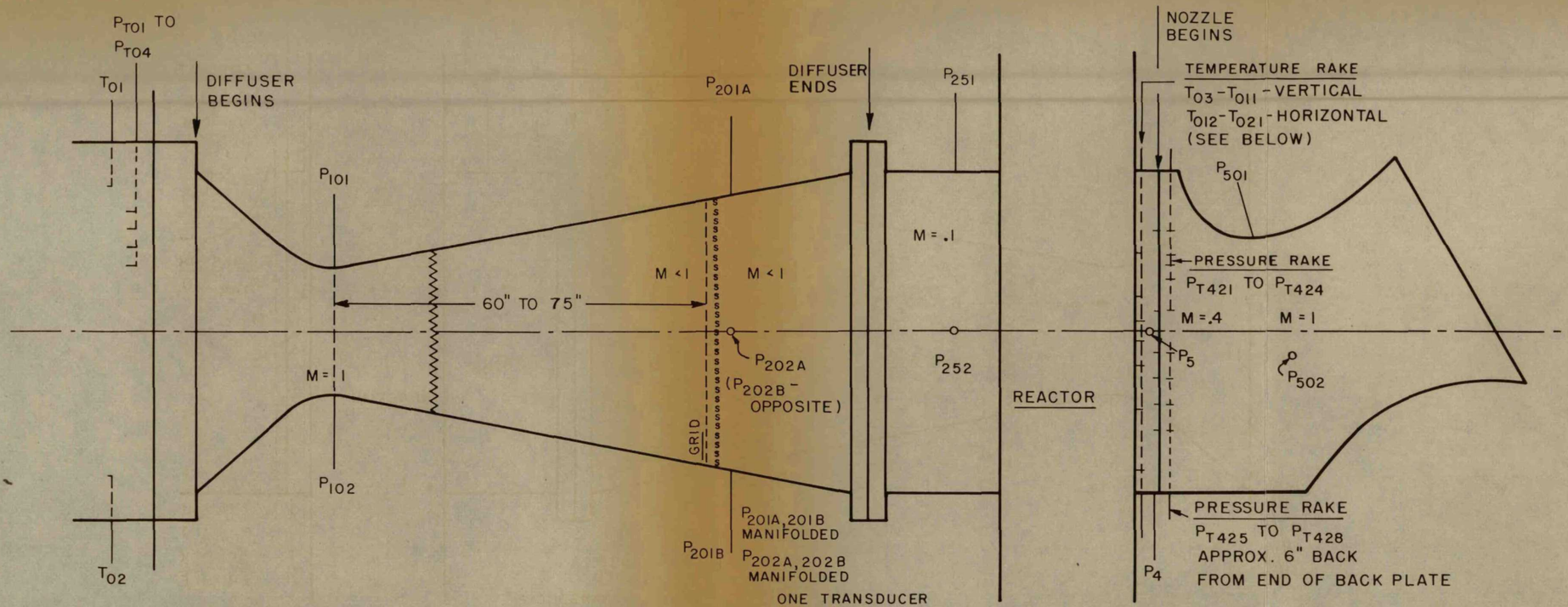

PRESSURES AND TEMPERATURES

PRESSURE ITEM	TEMPERATURE ITEM	No. REQ'D PRESS.	No. REQ'D TEMP.	No. TELEMETERED PRESS.	No. TELEMETERED TEMP.	RANGE	ACCURACY DESIRED
$P_{T01,2,3,4}$		4		4		0-500 PSI	1%
$P_{101,102}$		2		2		0-300 PSI	10%
$P_{201A,201B}$							
$P_{202A,202B}$		2		2		0-500 PSI	5%
$P_{251,252}$		2		2		0-500 PSI	1%
$P_{4,5}$		2		2		0-300 PSI	5%
$P_{T421-T428}$		8		8		0-300 PSI	1%
$P_{501,502}$		2		2		0-200 PSI	10%
	$T_{01,02}$		2		2	100-1500°F	2%
MUL-8124	T_{03-021}		19		19	MAX. 2300°F	1%
		22	21	22	21		

TEMPERATURE RAKE

VERTICAL SECTION :	PROBE LOCATIONS
1 AT ~ 0" RADIUS	LOOKING UP FUEL ELEMENTS AND 0.66" BACK FROM END OF BASE PLATE
2 AT ~ 8" RADIUS	
2 AT ~ 11.5" RADIUS	
2 AT ~ 14" RADIUS	
2 AT ~ 16" RADIUS	

HORIZONTAL SECTION :	PROBE LOCATIONS
2 OUTER LINKS	(ALL THE SAME)
2 HEAT SHIELD	(INNER HOLE)
2 TRIANGLES AT DOGBONES	(CENTER REGION)
4 TIE RODS	(CENTER MODULE)

ALL 0.66" FROM END OF BASE PLATE OR OUTERMOST HOST PROTRUSION APPROX. LENGTH, EACH SECTION : 34"

Fig. 7-6. Schematic diagram of air temperature and pressure measurements.

Table 7-2. Test-vehicle temperature measurement locations

Type of transducer	Quantity	Transducer location
High-temperature Pt-Rh/Pt-Rh thermocouples	60 Active 56 Spare	Ceramic core components
	30 Active 14 Spare	Core support structure, shroud, tie rods, base plates, wiper seals, base plate springs
	2 Active 2 Spare	Core gamma shield
Pt/Pt-Rh thermocouples	2 Active	Diffuser inlet air
High-temperature Pt-Rh/Pt-Rh thermocouples	19 Active	Temperature rake at reactor rear face
Chromel-constantan thermocouples	24 Active	Control system hydraulic reservoir, control vanes and rods
	14 Active 6 Spare	Core vessel and water system
Chromel-Alumel thermocouples	2 Active	
Contact-making thermometers	12 Active	
Chromel-constantan thermocouples	6 Active 4 Spare -	Nozzle (internal and external), nozzle turning section, test car miscellaneous
Chromel-Alumel thermocouples	5 Active 1 Spare	

on strip chart recorders. Arrangement is such that after a run the magnetic tape recording can be played back and displayed on the oscilloscope at will.

Fast Response Channel — System G (Fig. 7-7) consists of 56 channels of 120-cycle response analogue recording equipment comparable to Sanborn or Offner type strip chart recorders.

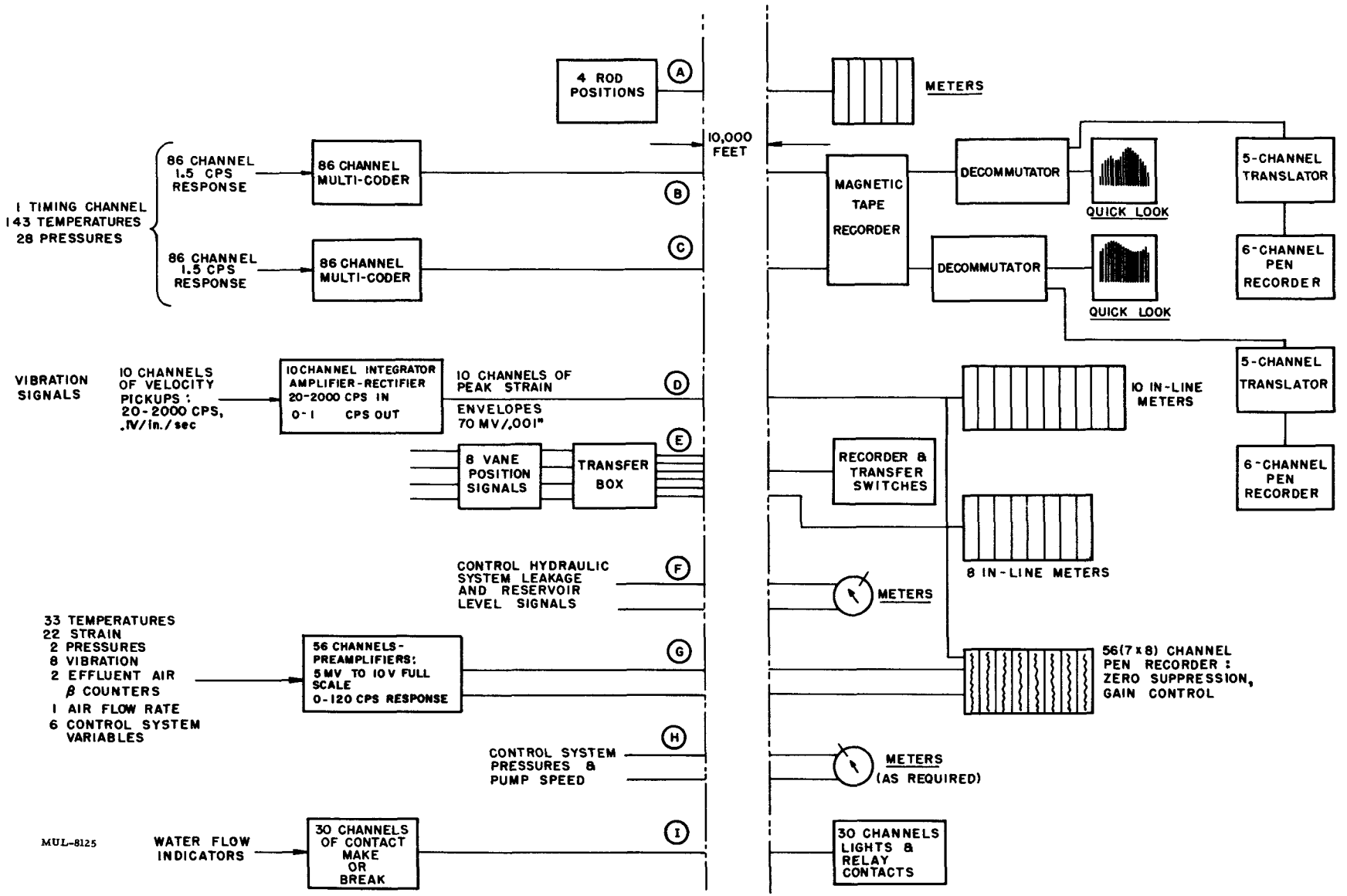

Fig. 7-7. Data collection system.

Present plans call for all thermocouple measurements within the core and closely associated with the core to be displayed on the ASCOP system, and the remainder on system G. However, the arrangement is such that any measurement can be displayed on either system by simple wiring changes.

Common Timing of Recorders – All recording channels in Fig. 7-7 are to be tied to a common timing signal generator which sends out identifiable pulses at intervals of 1 sec, 10 sec, 1 min, 10 min, and 1 hour.

7.4 Strain and Vibration Measurements

At high air flow rates the core components, core support structure and air ducting will be subjected to significant static and dynamic loads. Consequently, strain and vibration transducers are being located at points of particular interest. Measurement techniques are highly developed for normal environments, but difficulties are encountered in high-temperature applications and high-level radiation fields.

7.4.1 Strain Measurements

Location

Pre-nuclear-power strain measurements will be made on two tie rods in the upper core region and on six in the lower region. In addition, the following shroud measurements are planned: inside and outside on shroud front at (1) two top locations (2) two bottom locations, plus (3) one measurement on each of the sides.

Transducers

Present state of the art is such that precise (±5%) strain measurements can be made up to about 300°F; ±20% measurements are possible up to about 700°F. Above 700°F results are of questionable value.

Present plans call for using foil-type gauges cemented to the test piece. Published reports on the use of such techniques are available.[21] At each measurement location a temperature-compensating gauge at right angles to the line of strain will be used.

Display and Recording

Electrical strain gauge outputs will be taken to the bunker and amplified. Wire transmission will take the signals to the control point for recording on a 120-cycle, strip-chart recorder (System G, Fig. 7-7).

7.4.2 Vibration

Measurements of vibration on both the core structure and the air duct will be made during air flow tests, with moderate temperature and little or no nuclear power (non-nuclear phases). During runs involving high temperature and power (nuclear phases), vibration data from the core and its support structures will no longer be available, since the transducers cannot operate under these conditions.

Nuclear phase vibration will be measured along the three orthogonal axes at one location on the inlet duct, on the core vessel, and on the outlet duct.

Non-nuclear phase vibration will be measured on the core front support structure and baseplate, with transverse vibration measured at the top of the center module, vertical vibration at the 2 o'clock position, and longitudinal vibration at the 4 o'clock position of the center module. Vibration will also be measured on the rear of the core shroud in the transverse and vertical directions.

Transducers

Nuclear phase vibration velocity will be measured externally at about 300°F, with radiation-resistant pickups which generate a voltage proportional to velocity. This output will be electronically integrated to give a voltage proportional to displacement and will be wire-transmitted to the control point.

Prenuclear internal vibrational acceleration will be measured up to 700°F by an unbonded strain gauge accelerometer developed for use at this temperature without cooling. Output voltage, proportional to acceleration, will require amplification in the bunker for wire transmission to the control point.

Display and Recording

Nuclear-phase vibration will be displayed on in-line meters; all vibration will be recorded on 120-cycle response strip chart recorders (System D, Fig. 7-7).

7.5 Pressure Measurements

Measurements of static and total air pressure in the vicinity of the core are required for diagnosis and analysis of reactor-air stream behavior. In addition, the coolant water and control hydraulic systems require pressure

measurements for safety and assurance of proper operation.

Location

Figure 7-6 shows the location and range of cooling air total and static pressure probes which comprise the bulk of the pressure measurements. In addition, the cooling water inlet and outlet total pressure, the hydraulic pump discharge pressure, and the hydraulic system filter pressure drop are measured.

Transducers

The hydraulic system pressures will be sensed by potentiometer-type pickups. The remaining transducers will probably be unbonded strain gauge pickups. These were especially developed for the Aircraft Nuclear Power Program and have been found to operate satisfactorily in reactor environments.

Display and Recording

The two potentiometer outputs will not require amplification and will be transmitted by direct wire to display meters; no recording is planned. The balance of the pressure pickup outputs will be transmitted via the ASCOP system, tape recorded, and displayed on a quick-look oscilloscope.

7.6 Air Flow Rate

The measurement of total air flow rate is necessary not only for analysis of reactor behavior but also to provide a feedback signal for the automatic air flow control system.

Flow rate will be measured through pressure and temperature data taken at venturis just down stream from the two main air control valves (see Section 4.4). Values of individual pressures and temperatures will be recorded to 1% accuracy on strip charts. In addition, an analogue computer will use this data to provide the total flow rate. Accuracy of the flow rate measurement will not be constant over the range of operation conditions; six specific combinations of pressure and flow rate have been chosen as representing desirable operating points. The flowmetering system will be designed to give 5% accuracy at those points, shown in Table 7-3.

In addition, pressure and temperature data measured in the air duct on the test vehicle can be used to determine total air flow rate, at high flow rates.

Table 7-3. Standard operating points

Flowmetering venturi	Air flow rate	Static pressure at venturi
1	870 lb/sec	360 to 500 psia
1	300	165
1	90	65
1	25	18.5
2	15	40
2	3	20

7.7 Control Rod and Vane Positions

Provision is made for indicating and recording rod and vane positions (Fig. 7-7). All eight vane positions are indicated on in-line meters and any one can be chosen for recording on a Brown strip chart recorder. Rod position is also displayed on in-line meters, and any one may be recorded on system G (120-cycle response). Also by simple wiring changes any vane position may be recorded on system G.

7.8 Exhaust Air Monitor

A continuous air sample will be pumped from the exit nozzle to shielded beta counters in the test bunker, providing information on emission of radioactive fission products from the core. Some fission products may be deposited on the walls of the tube leading from the nozzle to the bunker, causing a loss in counting rate which depends on air temperature and flow rate. To provide an indication of this effect, two counting heads will be used, separated by a length of tubing equal to that reaching from the nozzle to the bunker. Only overall counting rate will be measured, with no attempt to sort out individual isotopic activities.

This system will provide a means of studying the relative importance of recoil and diffusion fission product loss from the core fuel elements, and will also be of value for personnel safety in giving an early warning of high rates of emission of radioactive material in the exhaust stream.

Outputs of the two counters will be displayed and recorded on system G of Fig. 7-7.

8. TEST FACILITY

8.1 Site Description

8.1.1 Location and Size of Area

The Tory II-A test facility, Site 401, is located within the Nevada Test Site at Mercury, Nevada. This experimental area is situated in the Cane Spring Valley east of Jackass Flats and west of Frenchman Flat.

The Tory II-A activities are confined to an area of approximately 8 square miles, within which is also situated the Hot Box hot critical experiment facilities.* Figure 8-1 shows a topographic map of this area.

8.1.2 Relief and Elevations

The Cane Spring Valley floor is at an elevation of 4000 ft above sea level at the lowest point. The bordering mountains rise to 5200 ft on the north and 6000 ft on the south.

The valley floor is composed of alluvium eroded from the surrounding volcanic mountains. The mountains are composed of tertiary volcanics which, when faulted, expose layers of tuff and dark-colored rhyolites.

8.1.3 Drainage

During heavy rains the water runs off, sometimes as flash floods, into impervious playas, from which it disappears by evaporation.

8.1.4 Vegetation

Mountain areas are free of soil, hence of vegetational growth. The valley, however, supports sage brush, saltgrass, cactus and mesquite.

8.1.5 Access

Access to the Pluto area, Site 401, is by a 60-mph highway, known as road A, originating at Mercury. The distance from Mercury to Pluto is 28 miles.

8.1.6 Weather

A study of typical weather conditions was necessary in order to choose a site where operations would not be inconvenienced by frequent likelihood of

---

*Hot Box is described by H. L. Reynolds and C. E. Walter in UCRL-5483 (see ref. 22).

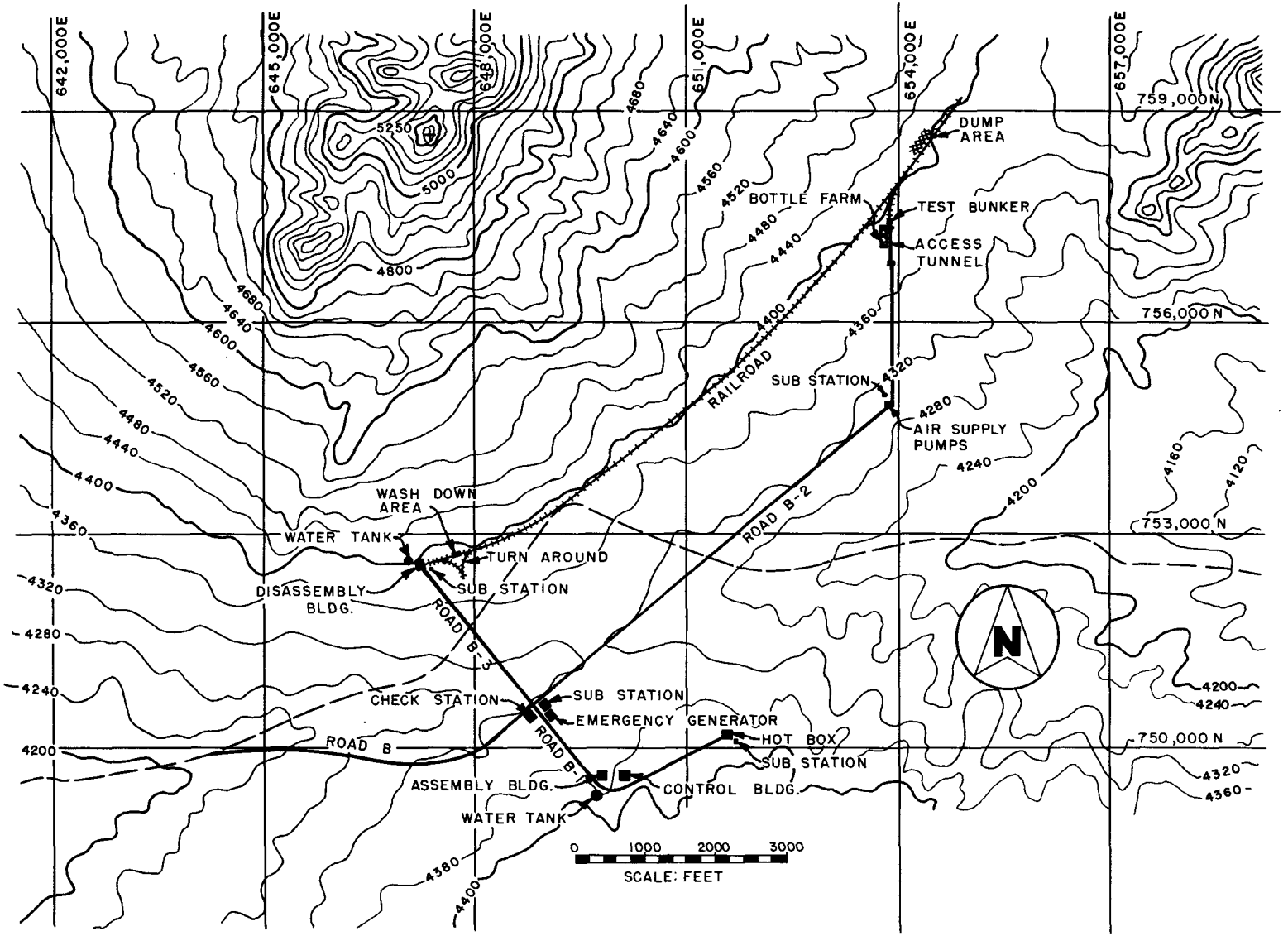

Fig. 8-1. Test Site 401.

transport of radioactive exhaust products to the site control area or other nearby inhabited areas. Effluent activity is not expected to be large enough to present any off-site hazards (see Section 11.2.1), but on-site personnel are not protected by the diffusion and decay attenuation of activity which take place over large distances, and therefore cannot tolerate air motion from the reactor test point towards themselves. Such air motion might necessitate suspension of test operations, with possible great loss of time. Data such as that described in the following paragraphs indicate that the test site chosen will be as free of this difficulty as any available in the vicinity.

The U.S. Weather Bureau Research Station at the Nevada Test Site maintains two recording wind and temperature locations in the 401 area. The location designated as T-2 is near the Tory II-A control building and has been in operation since March 1, 1956. The location designated as T-1A is near the test bunker and has been in operation since November 13, 1957. The wind-measuring equipment is mounted atop 96-ft towers and the information is telemetered and recorded in a Weather Bureau trailer. The temperature 5 ft above the ground is recorded at T-2 and temperature and relative humidity are recorded at T-1A.

Winds

The general feature of the winds in the 401 area is that southerly winds predominate in summer and northerly winds in winter. East and west winds are of minimum frequency during all seasons. Figures 8-2 through 8-6 show the seasonal wind roses for T-2 and T-1A.

The total number of observations are shown in the bottom half of the wind rose circle, each observation being an average over the 15-minute interval before each hour. The percentage of calm is recorded in the top half of the circle, while the length and shading of each direction arm (wind from south points down) represent the frequency of occurrence of speeds and direction over 16 points of the compass: Lengths of the arms indicate percentage of total time in which the wind blew in the given direction; the scale is shown in Fig. 8-2. Division of the arm indicates proportion of the time during which the wind speed was between 1 and 10 mph (line segment), between 10 and 20 mph (white segment), and greater than 20 mph (black segment). The change of wind direction and speed from hour to hour in a season is depicted by the mean diurnal resultant hodographs shown in Figs. 8-7 and 8-8. Each point

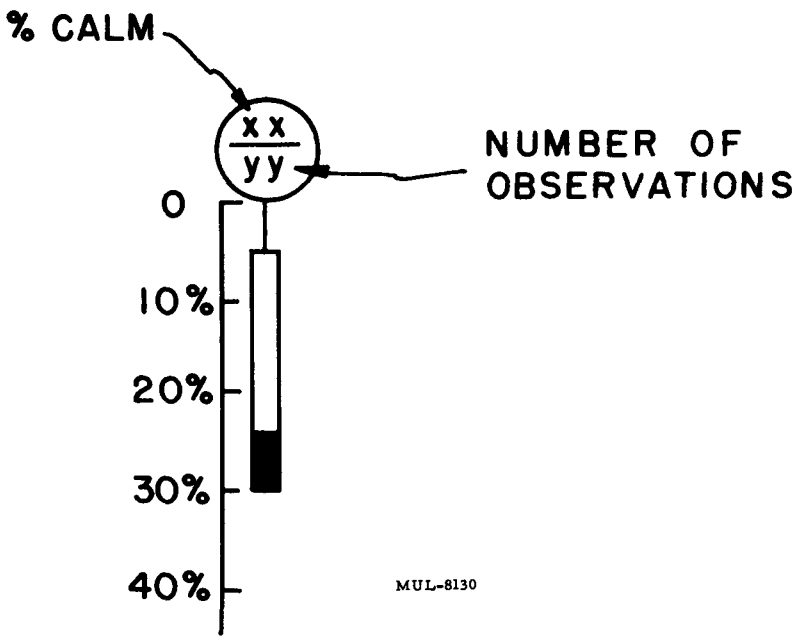

Fig. 8-2. Key to wind rose figures.

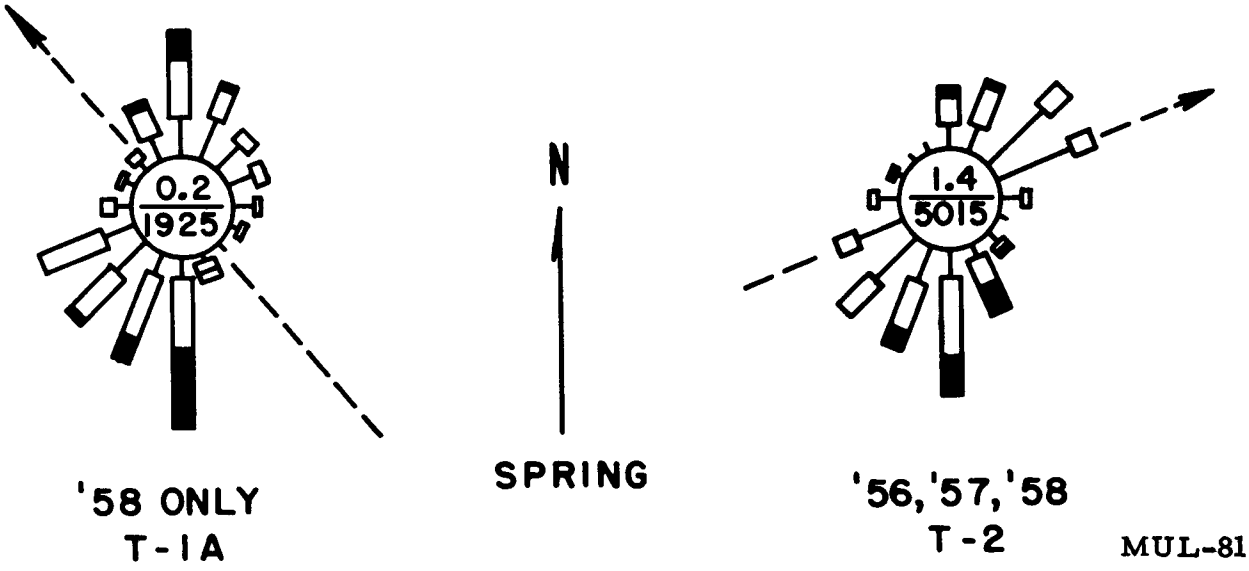

Fig. 8-3. Wind roses.

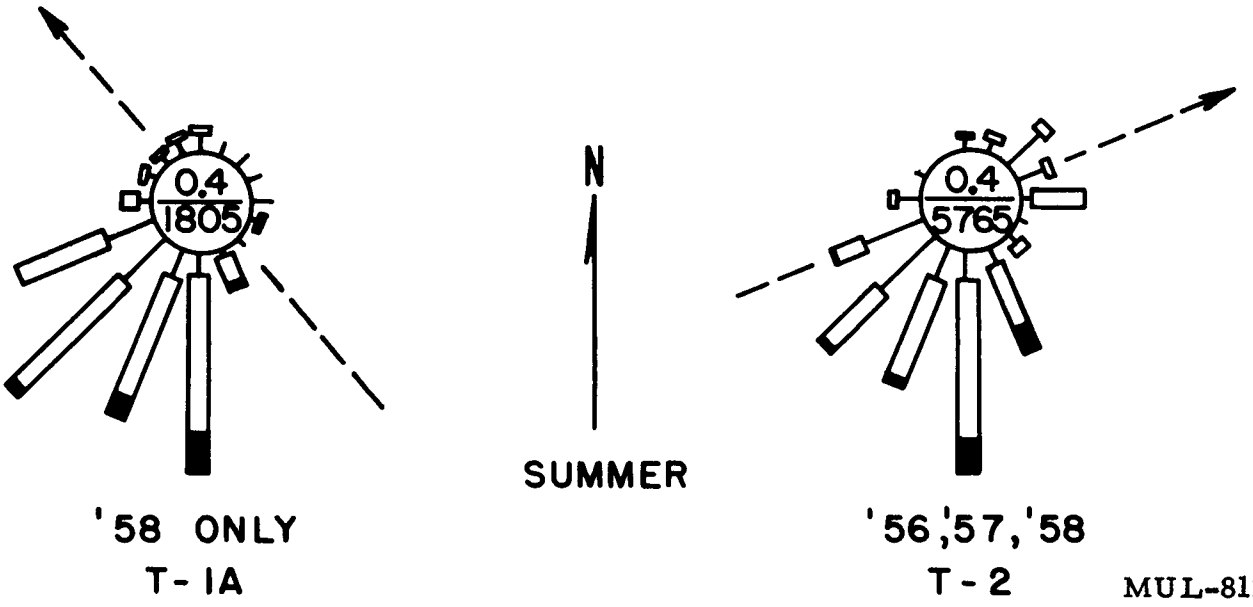

Fig. 8-4. Wind roses.

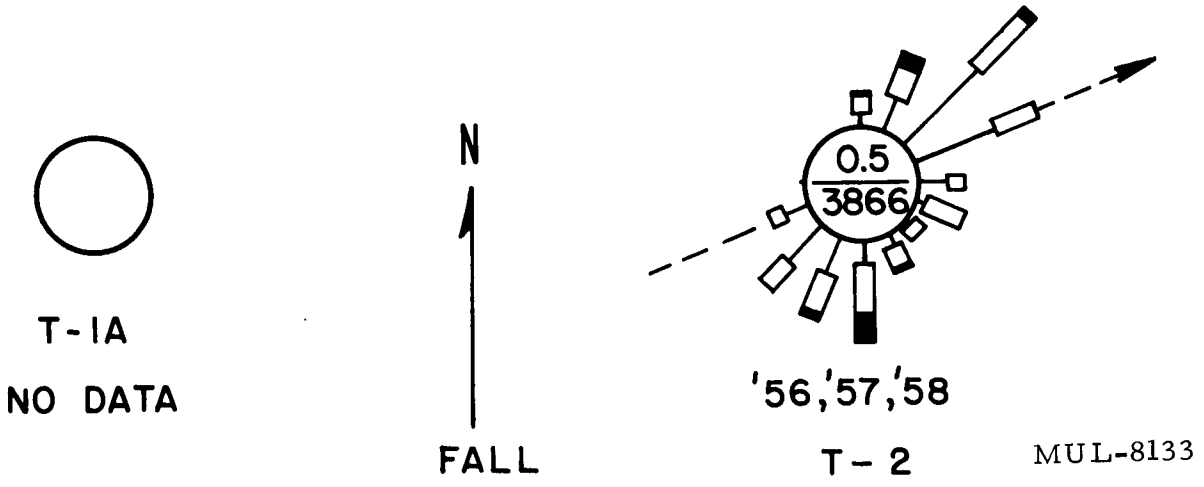

Fig. 8-5. Wind roses.

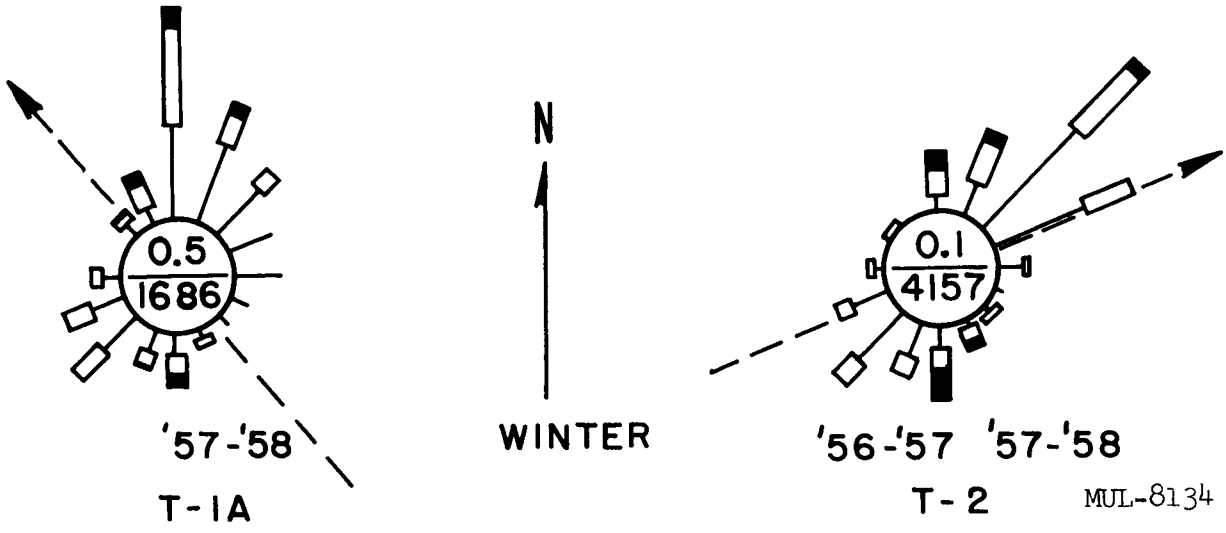

Fig. 8-6. Wind roses.

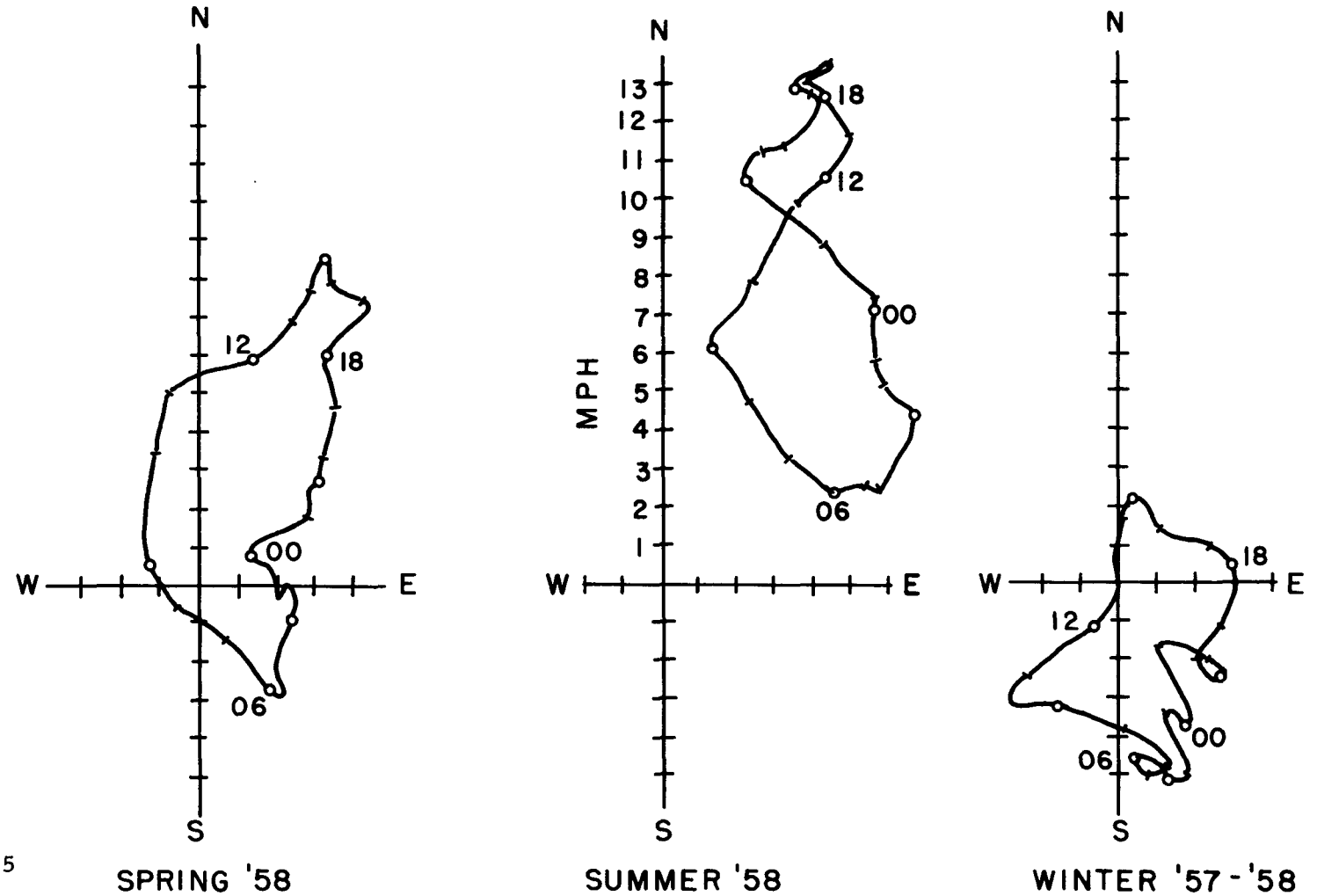

MUL-8135

Fig. 8-7. Hourly variation of wind velocity vector at Tower 1-A.

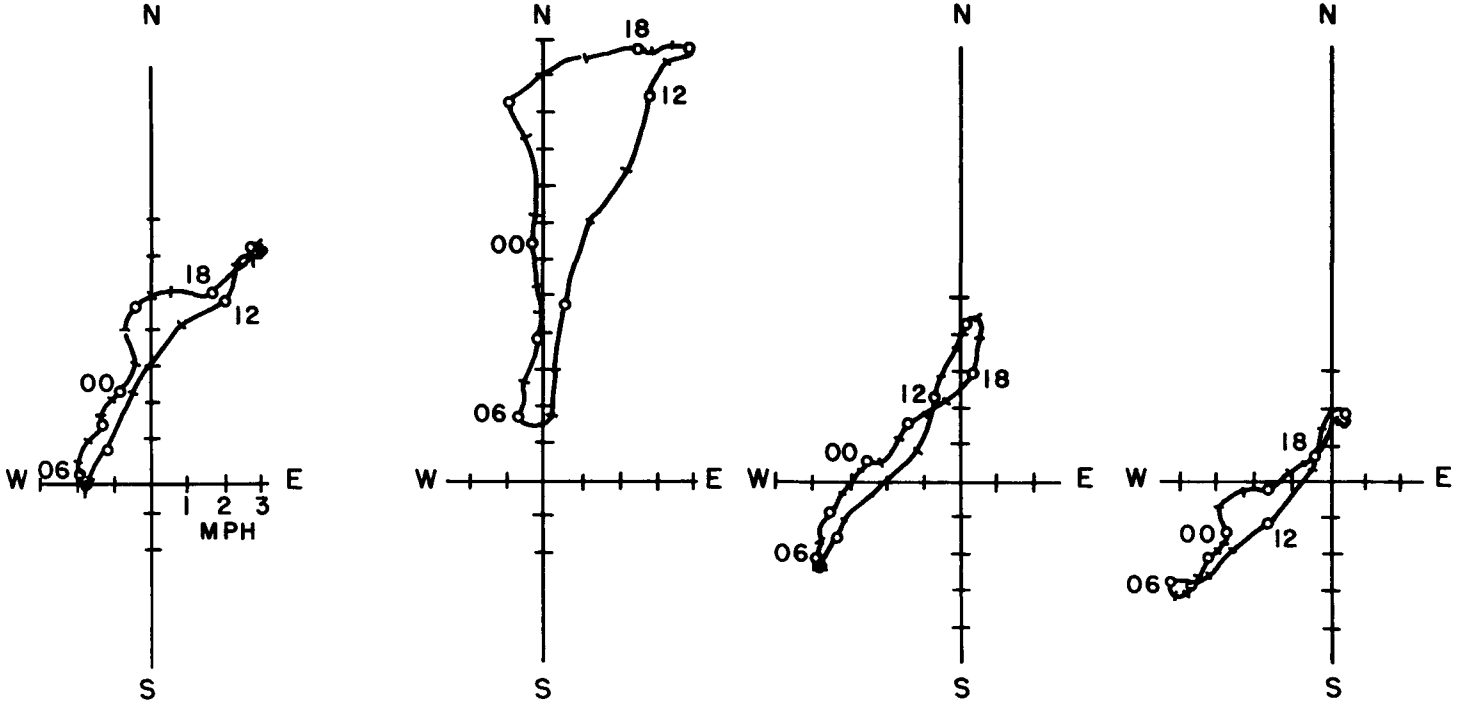

Fig. 8-8. Hourly variation of wind velocity vector at Tower 2.

represents the end of a vector starting at the origin (see Fig. 8-9). The top right-hand quadrant would consequently represent a wind blowing from a south through west direction. Only three seasons are available for T-1A. However, the general feature still holds for T-1A, i.e., southerly winds predominate during all hours in summer with minimum speeds at about 0600 h and maximum speeds at about 1600 h. This is in contrast to the summer winds occurring in the lower central portion of the flat where light northerly winds show up on the hodograph during the early morning hours.

Winter winds at T-1A show northerly winds during almost all hours with only light southerly winds appearing during the late afternoon (1400 to 1800 h). The terrain at T-1A slopes up towards the northwest and the nighttime downslope wind is from the northwest.

The mean diurnal resultant hodograph for T-2 (Fig. 8-8) shows the same features as T-1A during summer. The winter hodograph for T-2 shows a downslope wind direction from the north east during the early morning hours, agreeing with the slope of the valley.

A computation was made of the wind speed profile between heights of 10 and 100 feet at T-1A. Using 15-minute average wind speeds taken once an hour at these two levels, the average "n" value (Sutton's Stability Index) was computed. For the period January to April 1958 the average daytime (0800-1600) n value was 0.14 and for nighttime (1900-0500), 0.24. These values are slightly lower than similar computations in the central portion of the flat and indicate slightly better atmospheric diffusion qualities near the surface in the higher, relatively flat portions of Jackass Flats.

Temperature and Relative Humidity

Table 8-1 lists by months the average temperature, the average maximum and minimum temperature, the average daily range of temperature, and the absolute highest and lowest temperatures recorded and the year recorded. The T-1A location has less than one year of record while T-2 has over two years of record. The highest and lowest temperature recorded at T-2 during the last two years was 104 and 11°F, respectively.

Table 8-2 lists the average relative humidities in percent for a year's record at T-1A. The data is presented in a fashion similar to the temperatures in Table 8-1.

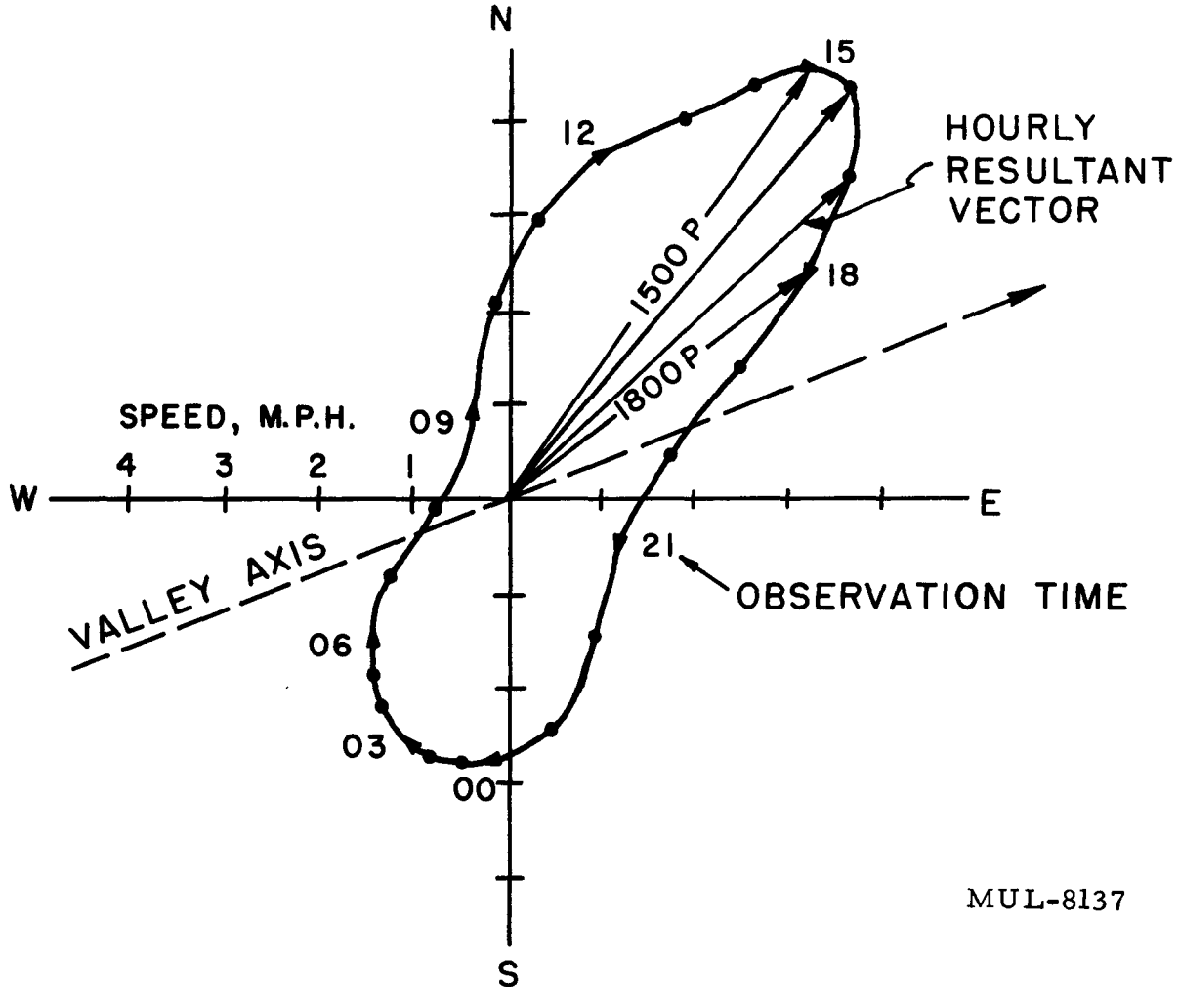

Fig. 8-9. Key to wind velocity diagrams.

Table 8-1. Jackass Flats area temperatures (°F)

	Jan.	Feb.	Mar.	Apr.	May	June	July	Aug.	Sept.	Oct.	Nov.	Dec.
Tower 1A (12/57-8/58)												
Av temperature	44	47	44	54	70	74	81	83	--	--	--	46
Av maximum	54	55	52	65	81	85	92	94	--	--	--	54
Av minimum	35	38	36	44	59	64	70	73	--	--	--	40
Av range	19	17	16	21	22	21	22	21	--	--	--	14
Highest/year	63/58	68/58	64/58	82/58	90/58	97/58	102/58	101/58	--	--	--	66/57
Lowest/year	25/58	26/58	26/58	30/58	46/58	53/58	64/58	64/58	--	--	--	29/57
Tower 2 (8/56-8/58)												
Av temperature	41	46	45	53	70	78	80	80	75	55	44	42
Av maximum	48	56	55	65	82	89	93	92	86	66	55	53
Av minimum	33	37	35	42	57	64	68	68	61	45	35	32
Av range	15	19	19	24	25	25	25	24	25	21	21	21
Highest/year	63/58	70/57	68/57	84/58	90/59	104/57	104/58	102/57	99/57	80/56	72/56	67/57
Lowest/year	11/57	20/57	24/57, 58	28/58	43/58	49/58	59/56	52/57	49/57	26/56	15/56	16/56

Table 8-2. Jackass Flats area relative humidities (%)

	Jan.	Feb.	Mar.	Apr.	May	June	July	Aug.	Sept.	Oct.	Nov.	Dec.
Tower 1A (11/57-11/58)												
Av rel. hum.	31	44	43	27	20	14	14	22	24	21	30	30
Av max rel. hum.	44	62	63	41	30	22	20	32	37	30	41	42
Av min rel. hum.	18	25	23	13	9	7	8	12	11	12	19	17
Av range	26	37	40	28	21	15	12	20	26	18	22	25
Highest/year	85/58	91/58	88/58	76/58	74/58	44/58	48/58	74/58	86/58	84/58	88/58	74/57
Lowest/year	9/58	12/58	12/58	3/58	3/58	3/58	3/58	4/58	4/58	4/58	10/58	3/57

Trajectories

Surface air trajectories under conditions when the air essentially flows downslope in the 401 area show a flow both eastward to Frenchman Flat and westward to the central portion of Jackass Flats. This is due to the fact that the downslope flow essentially follows the "water-course" and the 401 area is at the crest of a large pass between the two flats. T-1A is east of the crest while T-2 is west. As indicated previously, the nighttime air flow in winter shows the eastward and westward drainage.

The daytime southerly air flow at the surface generally follows a straight-line trajectory, tending to flow over topographical obstacles such as the hills to the north and east of the 401 area.

8.2 Installations

8.2.1 Description

The site has three functional areas, namely, control, disassembly, and testing. The nature of the activity in these areas requires the geographical separation shown in Fig. 8-1, to avoid danger of overexposure of personnel to radiation.

Control Area

This area includes the Control Building, Assembly Building, Emergency Shelter, Rad-Safe Check Station and the Hot Critical Test Building.

The Control Building will be used jointly to operate the Hot Box and Tory II-A reactors. Figure 8-10 shows the internal arrangement of this building. The air supply system, locomotive, truck switching and reactor controls will be operated from the Tory II-A control room. During a full-scale test the only personnel within the Site 401 area will be in the Control Building. It is not planned to conduct a Hot Box test and a Tory II-A test concurrently.

The Assembly Building will be used to assemble and fabricate subassemblies and will serve as a materials receiving station and for vault storage of classified and accountable materials.

The Emergency Shelter will be used only when, by virtue of an accident, personnel in the Control Building must seek shelter because of intolerable radioactivity. Water and food supplies will be stored for approximately 20 persons for 24 hours.

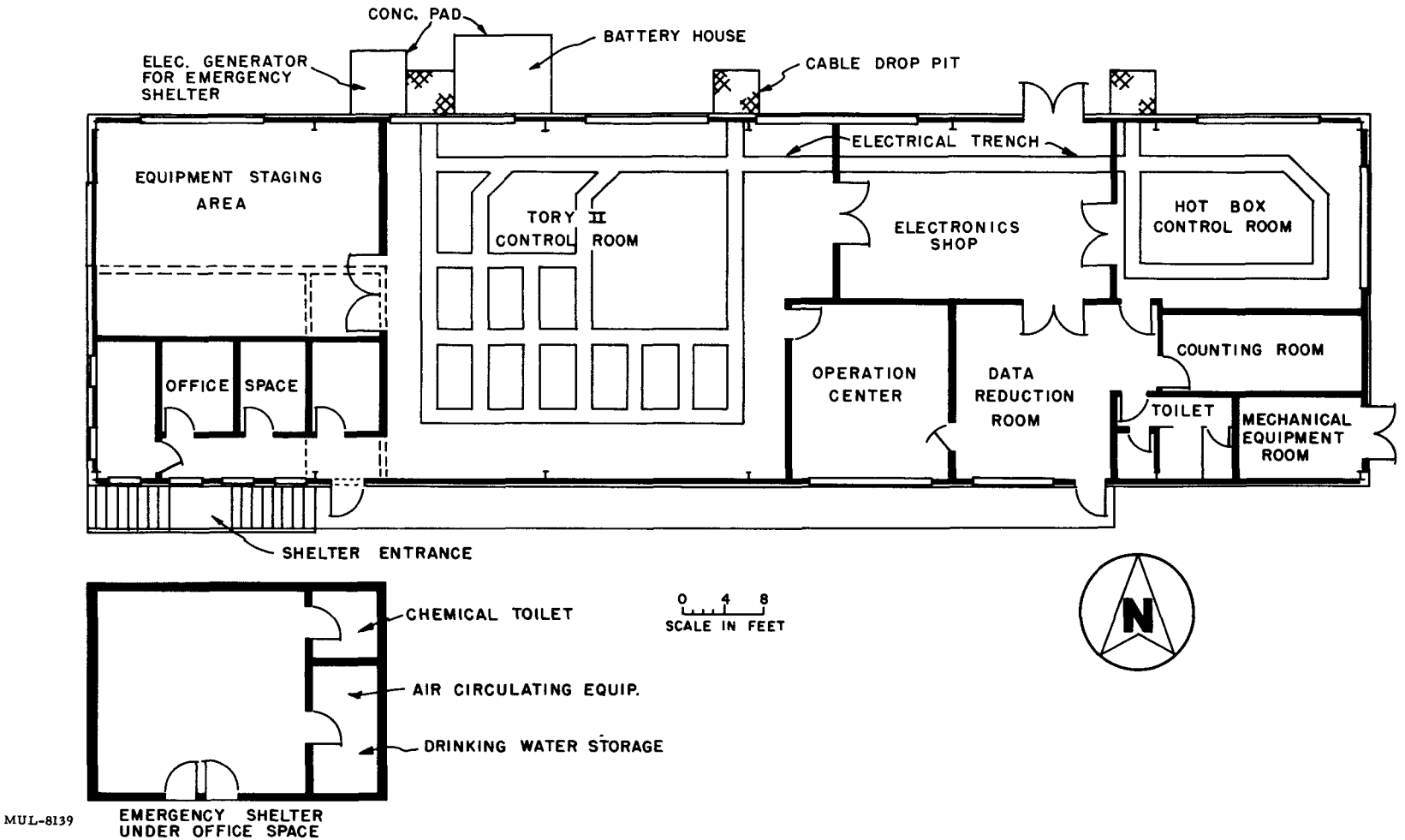

Fig. 8-10. Control building plan view.

Check Station

This building, placed at the road junction, will provide for controlled access and personnel safety activities in the test and disassembly areas. This facility includes change rooms, showers, rad-safe clothing, safety equipment, hot-car wash, and hot and cold parking lots.

Test Area

This area includes the Bunker, Access Tunnel, Head House, air storage and heater systems and a cooling water system. Figure 8-11 shows the general bunker area.

The bunker complex consists of three connected structures, namely, the Head House, Tunnel, and Test Bunker. The main function of the Head House is to provide a sheltered entrance to the bunker. It includes an off-loading area and ventilation fans which provide air in the bunker for personnel comfort, heater furnace combustion, and reactor low-power coolant air.

The concrete bunker, shown in Fig. 8-12, contains electronic recorders and amplifiers, remotely controlled valves, and disconnects, reactor cooling blowers, heater combustion equipment, and reactor car alignment apparatus. Adjacent to the bunker is the air storage bottle farm, stored energy air heater, and cooling water tanks.

The bottle farm consists of a series of high pressure pipes with a capacity of 120,000 pounds of air, charged by two compressors. While air charging is in progress, heat energy is being stored in the air heater. During an actual test run the stored air is split, part going to the heater and part going directly to the air-mixing chamber. Here the air streams are regulated and mixed to provide the proper test air temperature and mass flow. Section 4.4 gives a more detailed account of the air supply system.

The cooling water system is a closed circuit with de-ionizers, pumps, and hot and cold storage tanks. Its sole purpose is to provide cooling water for the reactor during test runs.

Figure 8-13 shows the test vehicle in place at the Test Bunker.

Disassembly Area

This area includes the Disassembly Building, railroad car wash down, track turn-around, and locomotive service facilities.

The building, Fig. 8-14, has two basic functions, namely, test vehicle assembly and car and core disassembly. The Cold Assembly Bay provides

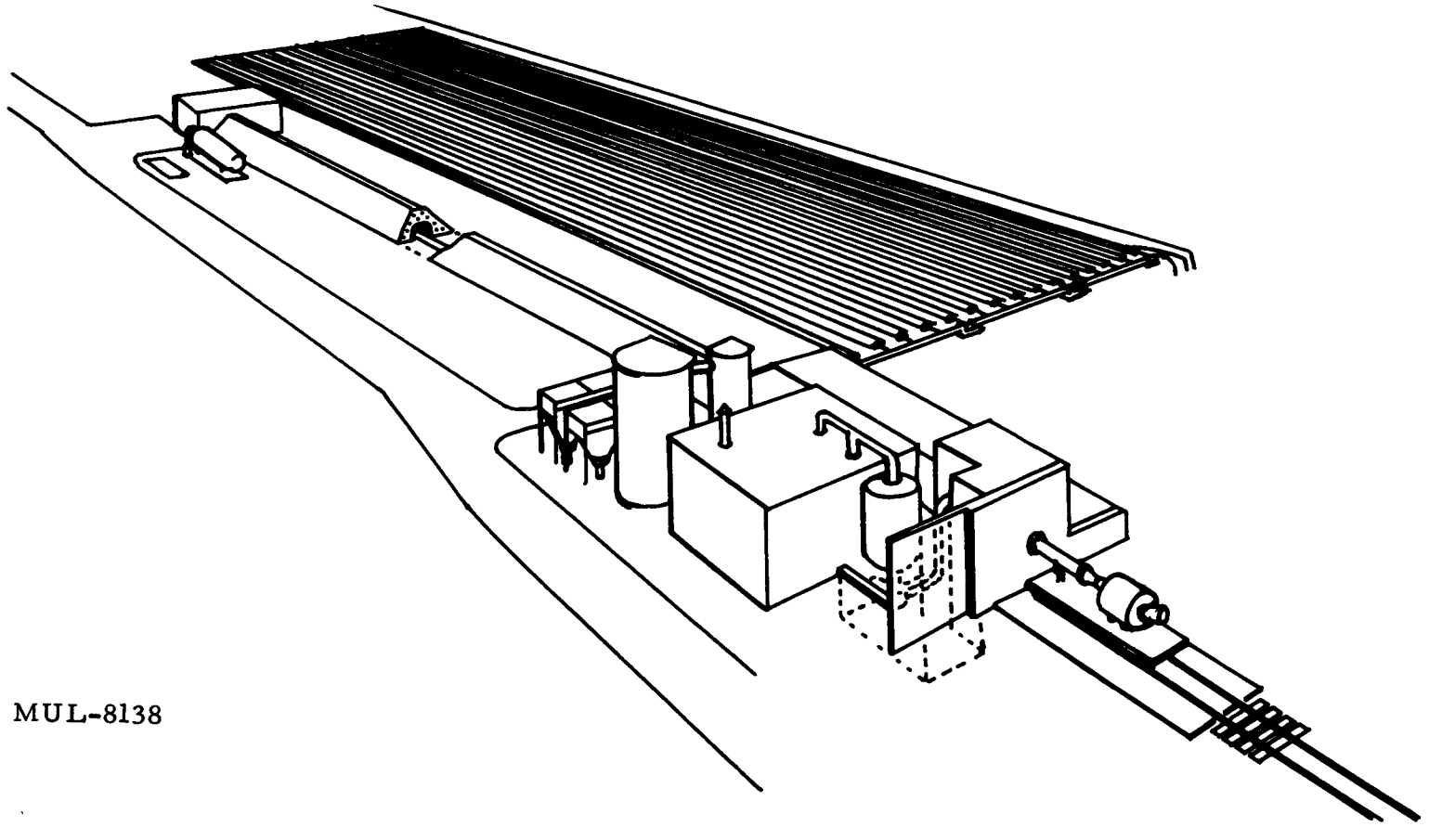

MUL-8138

Fig. 8-11. Test point—general area.

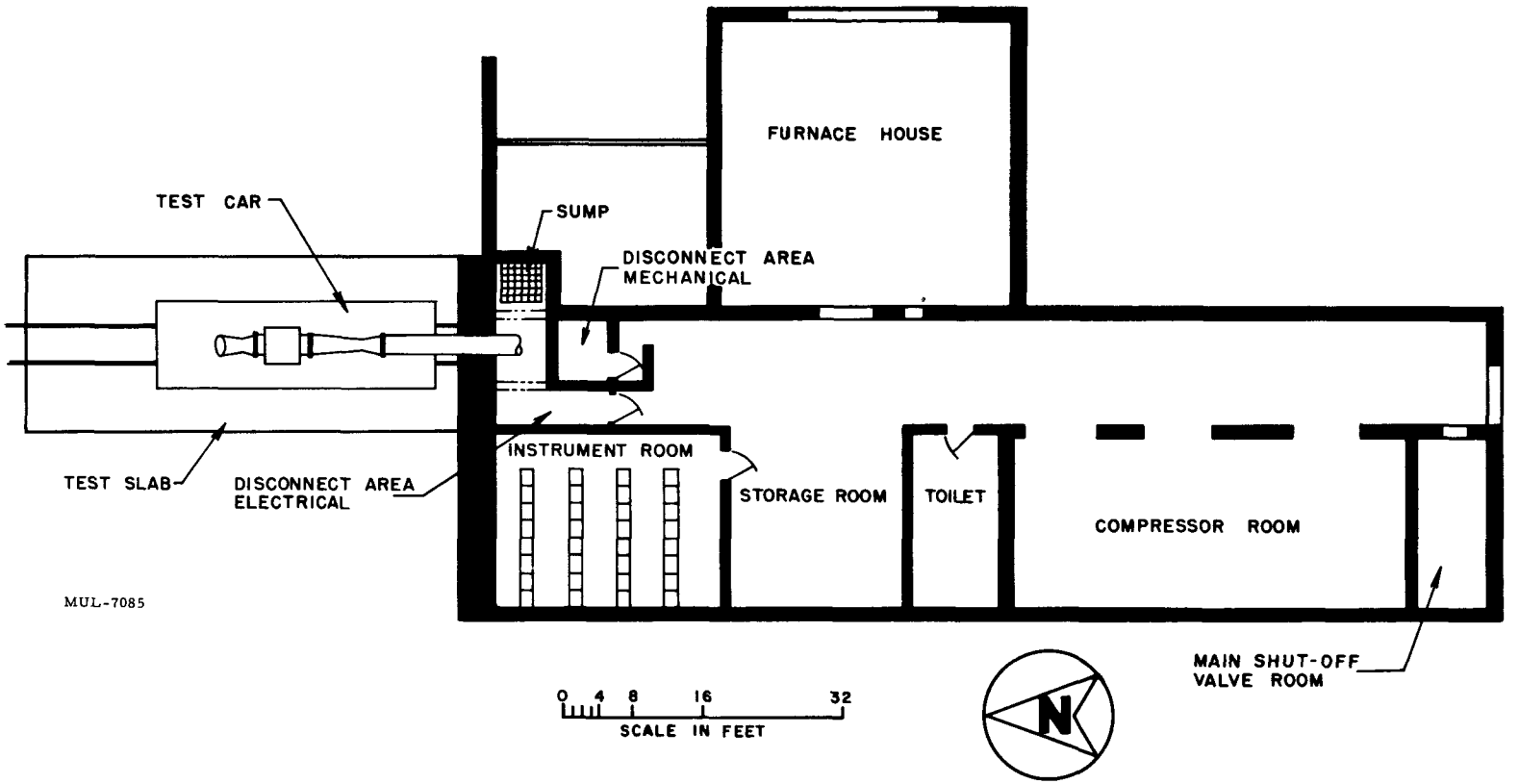

Fig. 8-12. Test bunker plan view.

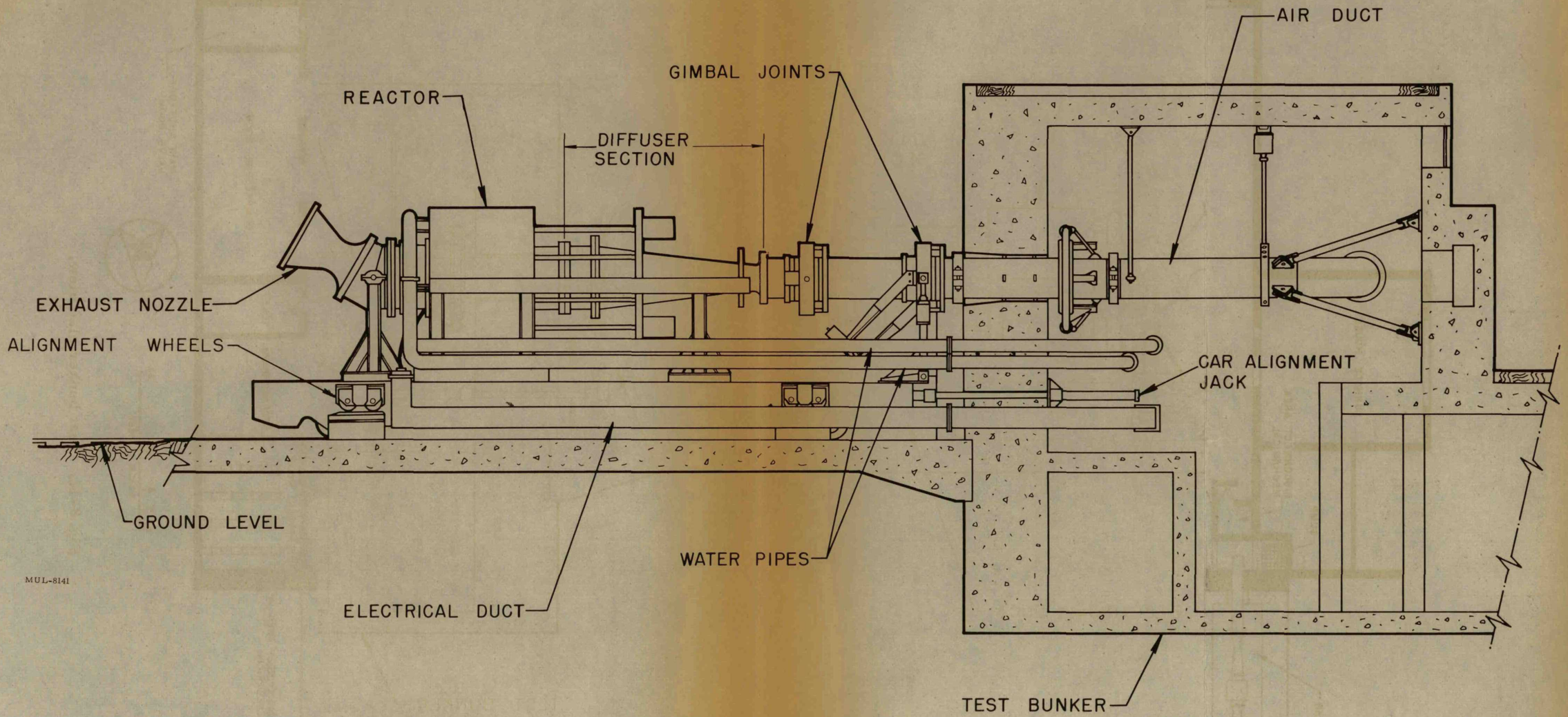

Fig. 8-13. Test vehicle at bunker wall.

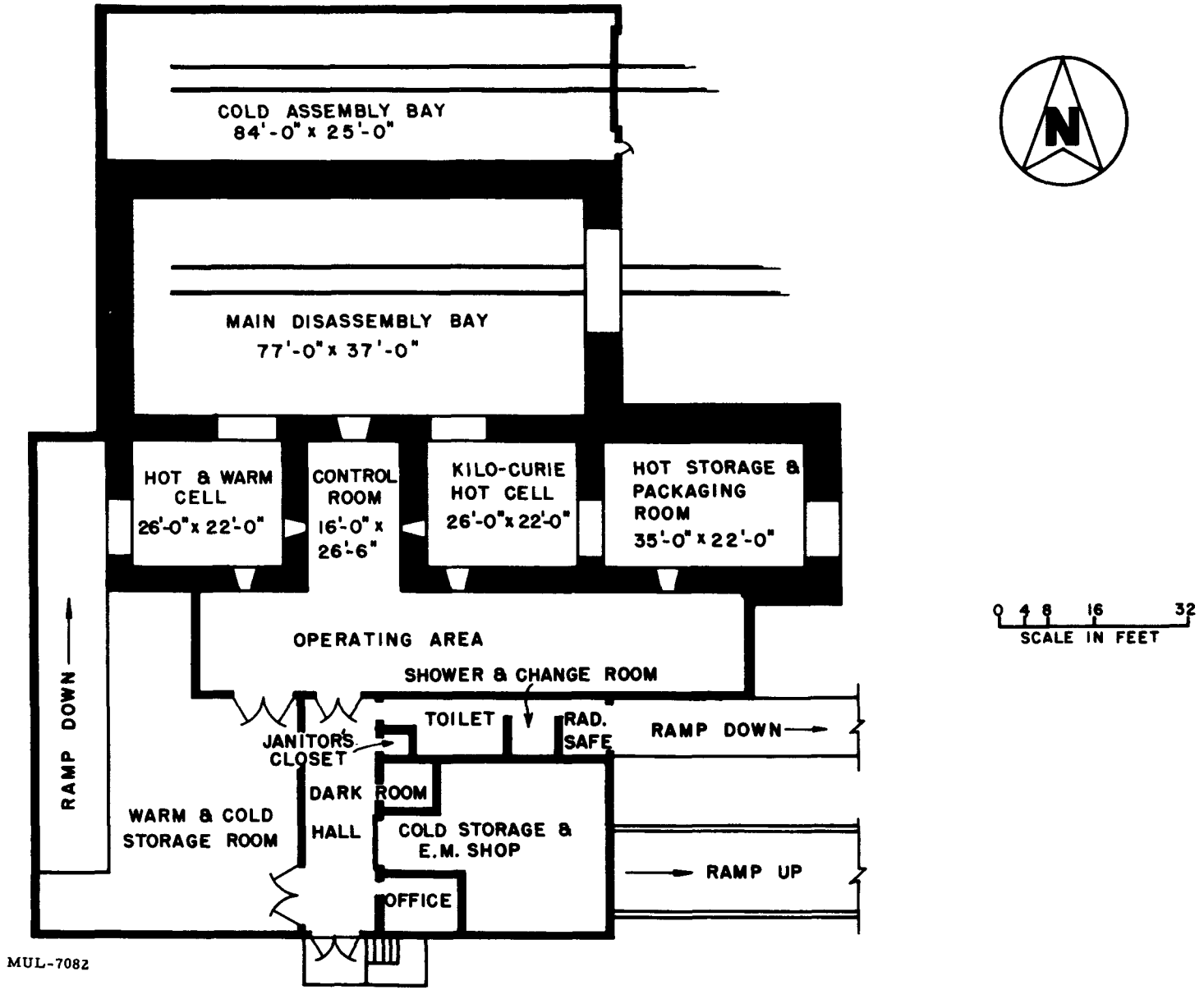

Fig. 8-14. Disassembly building — plan view.

space for test vehicle assembly, locomotive storage, and locomotive battery charging. In the Hot Bay the major assemblies of the test vehicle are removed. Subsequent components are then moved to the various hot cells for further autopsy or repair. The remaining area is used for disassembly, control operations, equipment repair, and building services.

8.2.2 Test Facility Data List

Control Area

1. Substation power for Site 401: 2.5 Mw; 69/12.5 kv
2. Water storage tank capacity: 30,000 gal
3. Assembly Building area: 2880 ft^2
4. Control Building area: 2880 ft^2
5. Hot Box Building area: 3700 ft^2
6. Distance, Control to Hot Box: 1200 ft
7. Hot Box load center power: 1000 kva
8. Distance, Control to Disassembly: 3600 ft
9. Distance, Control to Test Bunker: 8200 ft

Disassembly Area

1. Disassembly Building area: 15,700 ft^2
2. Water tank capacity: 5000 gal
3. Disassembly Building major equipment includes one 15-ton crane, three 7-1/2-ton cranes, four 3000-lb-capacity manipulators, six lead-glass windows 4 ft thick, three positioning turntables, and two master-slave manipulators.
4. Load center power: 500 kva
5. Locomotive: 15-ton, standard gauge, battery-powered, 10-channel radio-controlled

Air Storage System

1. Compressor Building area: 3750 ft^2
2. Compressor capacity: 2 each, 750 cfm at 4000 psi
3. Air storage capacity: 120,000 lb
4. Air heater capacity: 900 lb/sec for 90 sec, 0° to 1050°F
5. Load center power: 1500 kva

Test Bunker

1. Bunker area: 4800 ft^2
2. Reactor cooling water capacity: 60,000 gal
3. Bunker equipment includes ventilation fans, reactor cooling blowers, heater combustion system, electronic racks, hydraulic power unit, air supply piping and controls, television cameras.

9. CERAMIC COMPONENTS

9.1 Introduction

With the exception of the ceramic components, the reactor is to be constructed of metals whose properties are fairly well known and for which extensive data are available in the literature. Because of their unusual nature as structural elements, a special discussion of the ceramic fuel elements and structural links ("dogbones") will be given here. Both fuel elements and links will be made of high-density beryllium oxide.

An extensive discussion of the ceramic parts and the problems associated with their fabrication will be found in Pluto Programmatic Report I.[2] A discussion of stress in the fuel elements has also been given in a separate report.[14]

Potential problems associated with the ceramic parts are concerned with:

1. Ability to withstand mechanical loads.
2. Ability to withstand repeated thermal stresses.
3. Ability to withstand chemical and mechanical attack by the air stream.
4. Distortion due to creep under stress.
5. Distortion or cracking upon thermal cycling (increased in severity for fuel-loaded parts).
6. Retention of uranium in fuel elements.

The mechanical and physical properties of beryllia are strongly dependent upon the starting material (powder), the method used to densify it, the presence of impurities and additives, and, in the case of the fuel elements, the manner of incorporating the uranium, and the amount of it in the BeO. A specific combination of variables has evolved which results in a fuel-element material having satisfactory properties, and therefore, the latitude within which these parameters are allowed to vary is quite narrow. On the other hand, several methods for producing the structural links are under consideration and therefore the latitude of the variables is great.

9.2 Parts Fabrication

9.2.1 Fuel Tube Fabrication

The method chosen to produce fuel tubes is extrusion and firing, possibly followed by grinding to final dimensions.

The following "standard recipe" has resulted in a satisfactory fuel-element material: Enriched uranium in the form of a uranyl chloride (UO_2Cl_2) solution is mixed with BeO powder. U_3O_8 is precipitated in the slurry by the addition of excess ammonia. After drying and adding plasticizer the material is extruded, dried and fired, the U_3O_8 being converted to UO_2 in the process. The starting material is Brush UOX grade of beryllia powder, or a substantially equivalent grade. Other grades of beryllia and other methods of incorporating the urania into the beryllia have been investigated but to date none has appeared to be markedly superior to those adopted, although the matter is under continuous investigation. It is possible that other materials and/or methods may be adopted.

Fuel element-like specimens tentatively considered satisfactory have been produced at this laboratory and by several commercial contractors.

One company has proposed to produce fuel elements of a different shape from the extruded tubes by a novel combination of cold- and hot-pressing methods. The resulting fuel element is essentially a hexagonal biscuit several inches across, 1/2 to 1 inch thick, and pierced by holes according to the same pattern as with the tubular fuel elements. These fuel elements are geometrically compatible with the reactor mechanical components and are interchangeable with the tubular fuel elements. Therefore, both biscuits and tubes can be used in the same core. A problem to be overcome is achievement of the specified radial variation in urania loading, especially in the outer regions of the core where the loading must vary considerably across one module. However, in the central region of the core the loading can be uniform. It is possible, although unlikely, that this kind of fuel element will be developed soon enough to be used in an early Tory II-A core. With this kind of fuel element it is quite likely that the structural links and the baseplates can ultimately be eliminated, resulting in a tremendous simplification of fabrication and assembly.

9.2.2 Structural Link Fabrication

Structural links have been produced by a variety of methods: Among those under consideration are: grinding from a hot-pressed blank; direct hot-pressing to finished dimensions; and slip-casting of a rough blank, followed by high firing and grinding. Investigations of producing the structural links by isostatic pressing, by extrusion, by cementing several pieces together, and by cold pressing are also being pursued. A study of the practicability of machining in a low-fired state followed by high-firing with little or no subsequent

grinding is being made. Finally, tests are being made of ultrasonic cutting of links from hot-pressed blanks.

9.3 Operating Requirements

9.3.1 Structural Links

Working stresses to be withstood by the structural links are approximately the following:

tension: 12 psi; bending: 500 psi; thermal: 1600 psi.

As mentioned earlier, the material and fabrication technique have not been specified, and, in fact, several different methods might be used to produce the links used in a given core. At the present time complete data on representative specimens produced by the various methods are not at hand. However, we do have the following data on specimens of hot-pressed material:

Temperature	Modulus of rupture
1200°C	4,900 to 16,600 psi
1400°C	3,600 to 11,200 psi

It is apparent that the strength of hot-pressed material is well in excess of expected mechanical stresses at the reactor operating temperature of 1300°C. Only a factor of 2 exists between strength and calculated thermal stress, however. Since the accuracy of calculation of thermal stress remains somewhat in doubt, this may be a serious problem.

Mechanical and chemical attack by the working fluid, and dimensional instability, are less severe problems for the structural links than for the fuel elements.

9.3.2 Fuel Elements

1. Mechanical Stresses. The mechanical loads acting on the fuel elements are expected to be small. An axial compressive stress of 220 psi will result from the fluid pressure drop. A small mismatch between the fluid pressure inside and outside the fuel elements may occur, resulting in tensile or compressive hoop stresses. These stresses are not expected to exceed 200 psi. A lateral force acts on the fuel elements due to the weight of the fuel elements above. In the worse case this weight might be applied at the center of a fuel element while the ends are supported, resulting in bending stresses of 110 psi.

Compared with the modulus of rupture data for the hot-pressed material, these stresses are quite low, and the mechanical forces should present no difficulty even if the extruded material should be substantially weaker than the hot-pressed material.

2. Thermal Stresses. The thermal stresses present a potentially serious problem. Thermal stress is a function of the shape, the power density, and of the familiar material properties E, α, k, ν. The difficulties associated with independent evaluation of these quantities are obvious, especially with a material whose properties are a function of so many variables. A test was devised by which the thermal stress resistance of tubes of approximately the correct size could be determined directly. A tube is heated on the outside by thermal radiation from an electrically heated graphite tube and is cooled on the inside by forced convection heat transfer to a gaseous coolant, usually helium. This is not a true simulated service test in that the heat is not generated uniformly throughout the volume of the material but rather is deposited on the surface. The test results are correlated with the Tory II-A requirements by means of the elastic theory (if, however, the state of the material is plastic, the correlation by the elastic theory is not directly applicable). The results obtained to date include gradually applied thermal loads, suddenly applied loads, and repeated loading through about 10 cycles on pure BeO specimens, and one test on a urania-loaded specimen. The tests indicate that the mechanical integrity of the tubes is likely to be maintained but that some cracking will probably occur.

3. Urania Retention. The ability of a variety of BeO-UO_2 materials to retain UO_2 in air at elevated temperatures has been determined; specimens were discs 2 mm thick by 1 to 2 cm in diameter. UO_2 loss was determined by subjecting the specimens to flowing air, both dry and moist, for 4 hours at 1510°C. Specimens were produced by isostatic pressing at 30,000 psi followed by sintering for 3 hours in hydrogen at 1735° or 1790°C. It is felt that the results are representative of those that one would obtain with extruded specimens. The following variables were investigated:

1. Grade of BeO powder (3 grades).
2. Effect of calcining the "as received" powder in helium at 1230°C.
3. Method of adding uranium (3 methods).
4. Effect of pre-oxidizing in air at 1010°C followed by hydrogen reduction.

5. Sintering temperature (1735°C and 1790°C).
6. Addition of 0.5 and 1.0 wt % of nine different metallic oxides, including Y_2O_3.

The pertinent results, insofar as Tory II-A is concerned, are that BeO produced by the adopted recipe has satisfactory urania retention, without requiring the addition of special metallic oxides. Loss was less than 5 wt % in 4 hours.

4. Thermal Cycling: Earlier it was felt that oxidation of UO_2 to U_3O_8 in the fuel elements, at lower temperatures, might result in dimensional instability and cracking. Tests performed on specimens having up to 12 wt % uranium show no evidence of such effects.

10. OPERATION AND TEST PROGRAM

10.1 Experimental Objectives

As mentioned earlier, the operation of Tory II-A is intended as a test of the behavior of a reactor core that embodies most of the features essential to the core of a nuclear ramjet engine. Only two compromises have been made in order to simplify the design of the Tory II-A core: no control elements will be placed in the core, and the structure will not be designed for the large maneuvering loads which a flying engine would encounter. In addition, a very large graphite side reflector is being used in Tory II-A. This reflector does not resemble any part of a realistic engine, but does provide more than ample nuclear control for reactor safety, and permits the somewhat secondary areas of engine reflector and control design to be sidestepped until experience has been gained with design and construction of the first core.

Several general values to be provided by the Tory II-A program are quite apparent: First, it forms a basis for the establishment of an experimental facility of continuing usefulness to the Pluto program. The experience and personnel training gained during operation of Tory II-A will be essential to the design and testing of succeeding reactors. Further, the Tory II-A program is now providing experience in developing means of parts manufacture, in working out acceptance criteria and inspection procedures, and in accomplishing assembly and checkout of components in the field; these areas all present problems quite comparable in difficulty to those that must be overcome in theoretical design and analysis of the reactor.

There is, moreover, a set of definite experimental objectives to be realized in the operation of Tory II-A. The testing of a device as complex as this reactor has not at all the aspect of a proof test, in which the test objectives may almost be covered in the question, "Does it work?" Operation of Tory II-A and its auxiliaries will involve the simultaneous activity of a variety of different processes, each important in its own right as well as in its relationship to the rest of the system. Important data for evaluation of reactor operation will be obtained at all levels of power, temperature and air flow rate, starting from the very lowest. The test program will thus consist of a long sequence of stages leading from room-temperature operation of a barely critical reactor up to the achievement of maximum design conditions. A variety of information, necessary to the study of Tory II-A behavior and to initiation

of the design of successive reactors, will be gained at each point along the way.

The kinds of information sought are grouped below under several classes. A great deal of experimental data on these processes have already been or will be obtained by laboratory tests of individual parts or materials; the full information desired, however, can only be obtained by testing of actual components in the reactor environment, with all mutual interactions given full play.

1. Materials Tests

Thermal stress-strain; creep relief or breakage.

Corrosion-erosion of beryllia and metal parts.

Radiation damage: loss of strength, change of heat conductivity, dimensional changes.

Impregnation stability: retention of urania in fuel elements.

Fission product release into air stream.

2. Air Flow and Heat Transfer

Enthalpy gain of air stream through reactor.

Air flow distribution among reactor tubes; stability against unbalanced flow.

Total pressure loss in irregular passages.

Hot spot formation; possible overheated areas in core.

Heat load in non-fueled elements; effectiveness of heat removal provisions.

Temperature distribution throughout core in startup or shutdown; differential expansion problems caused by unbalanced heat deposition and removal.

Net axial thrust on core.

3. Nuclear Processes

Criticality.

Reactivity value of control elements, singly and together.

Temperature coefficient of reactivity.

Power distribution; comparison with desired profile at design temperature, and variation with core temperature.

Reactivity interaction of core air.

Effect of fission-product loss on reactivity.

Effect on power distribution, and temperature distribution, of individual control-element motion.

Radiation heat deposition in structural materials.

External neutron and gamma radiation level and distribution.

4. Design Feasibility

Test of a specific engineering design with respect to load distributions, dimensional tolerances, stability under partial loss of strength or breakage of some elements, ease of handling.

5. Control and Dynamics

Feasibility of control system design; effectiveness of automatic level and period controls, safety provisions.

Study of reactor-control system dynamics, with full interaction among all elements and processes.

10.2 Test Program

Each run in the Tory II-A test program will be directed toward specific objectives, with appropriately limited power, temperature and air flow levels. In general, since risk of damage to the reactor increases as the level of these variables is raised, their levels will be kept very low at first and gradually raised during progress of the tests.

Following such a program will provide an opportunity to gain operating experience under relatively nonhazardous conditions, so that behavior of the reactor will be fairly well understood by the time it is taken into the risky area of maximum power and temperature runs. It is hoped that possible sources of failure may be found and corrected or avoided during early runs, when they are least likely to cause a serious breakdown. Furthermore, a great deal of physics and engineering experimental information can be gathered during the early runs; this bird in the hand may prove to be worth several in the bush if damage at high temperature causes extensive shutdowns later.

Another strong reason for obtaining as much information as possible at very low power levels involves activation of the core: Operation at levels above 10 watts or so will raise the residual core radioactivity to an extent involving difficulty in closely inspecting or working on the core for more than a few minutes at a time. Eventually remote handling equipment becomes necessary, and any approach to the core is very awkward and time-consuming.

A tentative scheduling of operating conditions during the test program has been started, based on the principle of keeping the ratio of information gained to risk incurred as high as possible at every stage. Sources of risk

of reactor shutdown may be listed under several classes, the main area being the following:

1. High Temperature and Power

Some components may overheat, owing to unforeseen high heat deposition rates or failure of cooling provisions. Failure could occur through loss of strength, or through high stresses imposed by temperature differences through the core. In particular, fuel-element breakage may occur due to stresses imposed by thermal gradients in the tube walls.

2. High Air Flow Rate

Stress on the core tension rods, baseplates, and front support structure, as well as on the air duct, increases with high flow rate. In addition, vibration stresses may be felt at high flows.

3. Transients

High rates of increase of neutron level occur at high reactivity values, when slight disturbances in the reactor or control system may be enough to take the reactivity beyond prompt critical, leading to large power and temperature excursions before setback action can be taken. Even aside from this hazard, rapid transient conditions imply that very little time is available for the operators to notice and correct dangerous conditions.

The core is primarily designed for steady-state operation, although every effort will be made to provide for satisfactory operation in anticipated transient conditions. The greater the departure from steady-state conditions, the greater the degree of cooling and dimensional mismatches will be and the greater the consequent likelihood of failure of some component.

To assist in estimating the risk involved in each test phase, and to provide a basis for specifying limits of power, period, temperature and flow rate for each scheduled run, extensive use is being made of analogue computer simulation of the reactor, control system, and air supply, in part or as a whole. Eventually, many parts of the actual reactor control system will be incorporated in the analogue studies.

An operation schedule based on the preceding considerations is given below, with division into phases according to experimental objectives:

PHASE 1: Connection and Mechanical Checkout

1st month, days 1 through 12

Conditions: Reactor subcritical.

Poison rods inserted in core to permit any control position without criticality.

Direct access of personnel to car will be possible.

Objectives: Checkout of control operation; check cooling water, electrical, hydraulic systems, low-flow air instrumentation.

Disconnect and reconnect car at least once.

PHASE 2: Approach to Criticality

1st month, days 13 through 15

Conditions: Poison rods removed from core.

Reactor subcritical or just critical at zero power.

Objectives: Gradual removal of safety poison rods from core, with continual tests of neutron multiplication.

First criticality at NTS.

PHASE 3: Very Low Power Measurements

1st month, days 16 through 22

Conditions: Power 0.01 to 10 watts

Ambient temperature

Period > 30 sec

No cooling air.

Manual control

Running Time: Five 1-hour runs, totalling about 10 watt-hours

Objectives: Foil activation in reactor.

Measurement of gamma and neutron flux outside of reactor.

Check rod and vane reactivity; period vs control position.

PHASE 4: Very Low Power, Intermediate Temperature

1st month, days 23 through 30

Conditions: Like phase 3, but temperatures up to 1000°F; heated by air stream.

Running Time: Five 1-hour runs, totalling about 10 watt-hours.

Objectives: As in phase 3, with effects of elevated temperature.

PHASE 5: Non-critical Blowdown Tests

2nd month, days 1 through 10

Conditions: Power zero

Temperature 700-800°F

Air flow – 900 lb/sec

Objectives: Check mechanical behavior of core and duct at high air flow rates; check air instrumentation.

PHASE 6: Low-Power Measurements

2nd month, days 11 through 20

Conditions: Power < 100 kw

Ambient temperature

Period > 30 sec

No cooling air.

Manual or automatic control.

Running Time: Ten 1-hour runs, totalling about 200 kw-hr

Objectives: Continuation of previous measurements.

Determination of reactor transfer function for ambient temperature, large periods: oscillator, step changes in k_{eff}.

Measure heat deposition in core, reflector, and other parts.

Probable first detection of recoil fission-product escape.

PHASE 7: Intermediate Temperature, Low Power

2nd month, 21st day through 3rd month, 5th day

Conditions: Power < 100 kw

Temperature $\leq$ 1100°F, supplied by heated air.

Period > 30 sec

Sufficient air to hold core temperature.

Running Time: Ten 30-minute runs, totalling about 100 kw-hr

Objectives: Measure effects of elevated temperature on reactor neutronics.

PHASE 8: Fast Transient Tests

3rd month, days 6 through 9

Conditions: Power < 100 kw

Ambient temperature

Period $\geq$ 1 sec

No cooling air

Automatic control

Running Time: Ten 5-minute runs, totalling about 100 kw-hr

Objectives: First checkout on short periods; test of response to fast transients under fairly safe conditions.

Further neutronic information; better measurement of prompt neutron lifetime.

PHASE 9: Reactor Self-Heated

3rd month, days 10 through 25

Conditions: Power < 1 Mw

Air supplied by blower.

Running Time: Ten 1-hour runs, totalling about 5 Mw-hr

Objectives: Further neutronic measurements — transient response, reactivity, power distribution.

Investigation of fission-product escape at elevated temperature.

Determine integrity of core at high temperature.

PHASE 10: Medium Power, High Temperature

3rd month, 26th day through 4th month, 25th day

Conditions: Power $\leq$ 15 Mw

Temperature $\leq$ 2000°F

Blower cooling

Running Time: Ten 30-minute runs, totalling about 25 Mw-hr

Objectives: High-temperature neutronics studies.

Study behavior of reactor and air stream as a heat exchanger system.

Measure escape of BeO and fission products.

Determine core integrity at high temperature.

PHASE 11: Approach to Peak Power at Peak Temperature

4th month, 26th day through 5th month, 30th day

Conditions: Power $\leq$ 160 Mw

Temperature $\leq$ 2250°F

Blowdown cooling air to 800 lb/sec

Running Time: Twenty 90-second runs at high power, with forty 30-minute runs at about 15 Mw; totalling about 200 Mw-hr

Objectives: As in phase 9, with additional test of core integrity at high power.

Figure 10-1 shows approximate upper limits on power and temperature during the test program, as well as an estimate of integrated operating power at any point in the program, all taken from the schedule above.

10.3 Operation of Reactor

Before a high-temperature, high-power run can be started, a great deal of preparation of the facility will be necessary. When this preliminary work, such as air storage and heater charging, checking of electrical circuits, mechanical connections, and so forth, has been completed, all personnel except the operating crew and others in the control building will be cleared from the test site. All operations will then be conducted from the control consoles in that building.

Every run will have specifically outlined objectives and limiting values of power, period, temperature, and other variables. Runs involving any rapid changes in power or temperature levels, and probably any runs at high values of power or temperature, will proceed according to a definite schedule, often with partially or wholly automatic programming of important variables.

10.3.1 Control Building

During reactor operation, personnel will be cleared from all parts of the facility except for the control building. The final pre-operation checkout, the test run itself, and the initial shutdown procedures will all be conducted from that building. Figure 10-2 shows a diagram of those sections of the control building (Bldg. 2101) which will be involved in Tory II-A operation. Operation of the reactor will be carried on in the large room, labeled Reactor Control Room. All controls and data displays necessary for reactor operation during a test will be located in this main room. All doors will be closed during a test, with no entry permitted except through an anteroom. This anteroom, labeled Operation Center, will contain communication facilities and display of data of secondary importance to a test run, such as wind and weather data, site radiation levels, general facility condition, and so forth.

Figure 10-2 shows a tentative control room layout. The nuclear controls and the air supply controls are located separately at central consoles. Other racks provide control and monitoring of secondary systems: cooling water, hydraulic fluid pressure, voltage levels, etc. Detailed data, other than that necessary for the attention of the nuclear and air operators, are

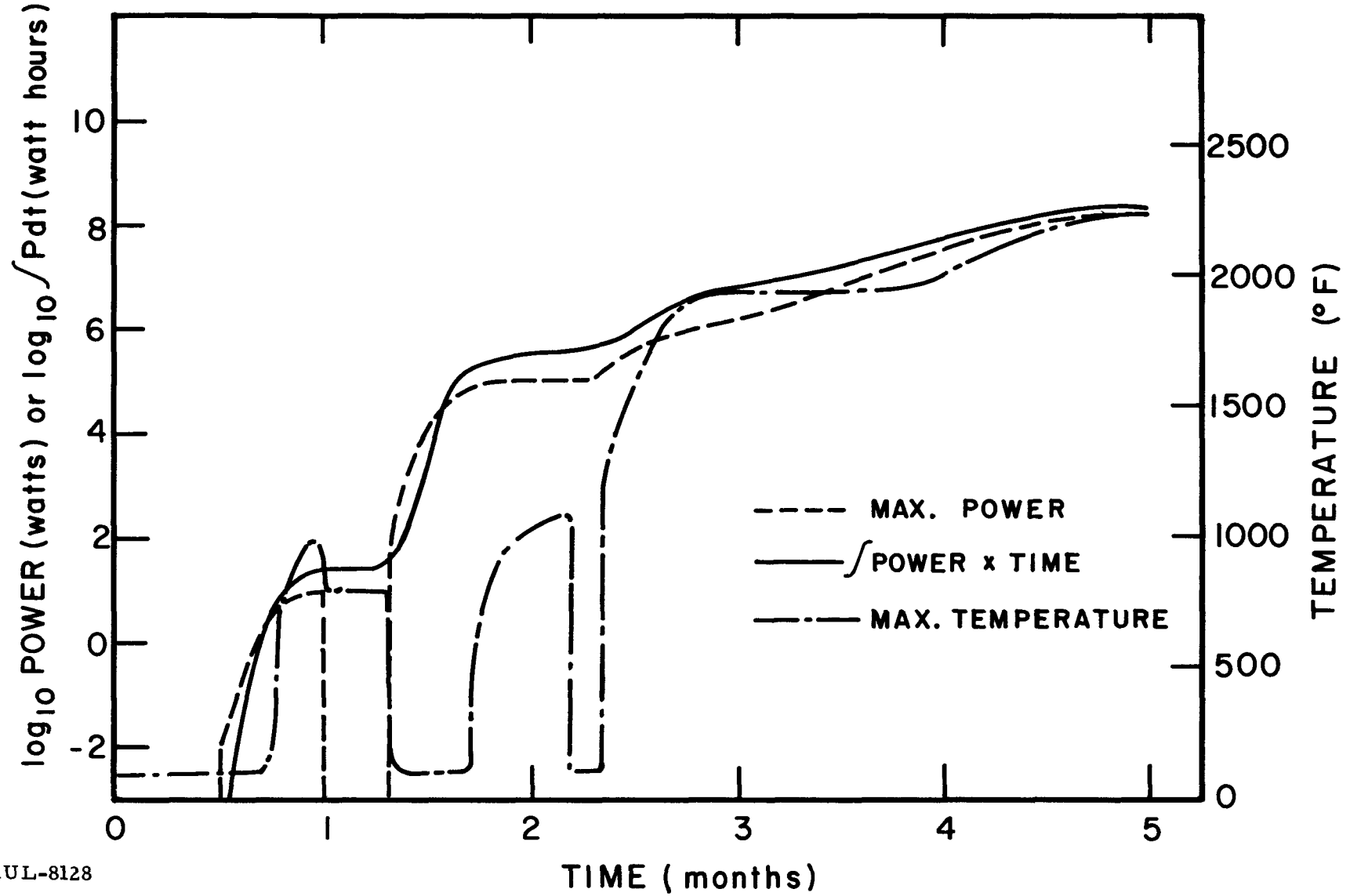

MUL-8128

Fig. 10-1. Tory II-A operating conditions.

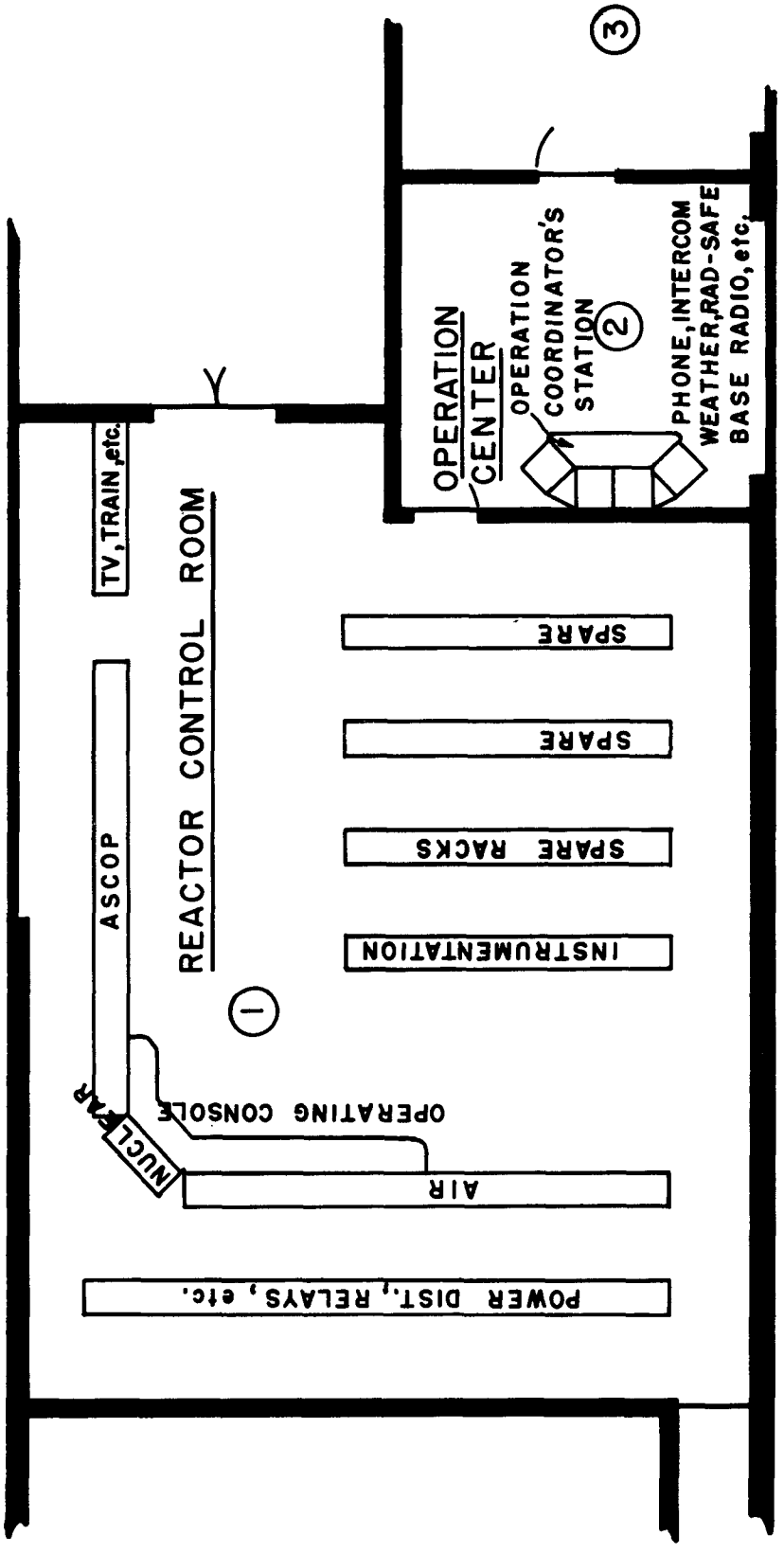

MUL-8129

Fig. 10-2. Tory II-A control area.

displayed at one location. Finally, television monitors and electric locomotive controls are located in another set of racks.

The operating consoles will be assembled in Livermore as soon as they are available. Analogue computers connected to the consoles will provide simulated reactor and air supply response to operation of the controls, permitting early training of personnel. Studies of typical operation sequences can be made with this equipment in time to correct faults before actual installation at Nevada.

10.3.2 Operation Staff

Chief Experimenter

During a test run, operation of the reactor and facility will be in charge of a Chief Experimenter, specifically designated for that run. He will not operate any controls directly, but will give generalized commands to individual operators at the air supply and nuclear control consoles. Thus he will be free to give his attention to the overall reactor condition, to the progress of the experiment, and to general requirements for action, rather than to the specific details of how desired power and air flow conditions are attained.

The Chief Experimenter will have complete authority during a test run, overriding possible conflicting opinions by other members of the operating staff. His attention will be given completely to operation of the reactor, with routine control of incidental activities being supervised by an Operation Coordinator (see below).

The Chief Experimenter's post will be in the area of Station (1) in the Reactor Control Room, Fig. 10-2. Here he will be able to observe all data of primary importance, and to communicate with the individual reactor operators.

Operation Coordinator

Data which is of importance during a run, but which will not require immediate action at the reactor control console, will be gathered in the Operation Center at Station (2) of Fig. 10-2. This station will be in charge of an Operation Coordinator, whose function will be to relieve the Chief Experimenter of all concern with outside activities, or with any situation not immediately affecting the course of the test run. He will control the only means of communication with the Chief Experimenter, and will use it only to

receive information on the progress of the test, or to supply information which may require a change in the course of the test. The decision of what action to take in such a case will be made by the Chief Experimenter.

The Operation Coordinator will receive information from site radiation detectors and from wind and weather monitors. He will monitor the conditions that might influence the test. All outside communications will come to him, and he will be in charge of all incidental site activities during the course of a test run.

Reactor Operators

Direct control of reactor conditions during a test will be carried on by four operators seated at the control console. In addition, two to three data observers will be required, to maintain a continuous awareness and evaluation of data displayed at the console or its adjoining racks. Operator functions will be the following:

a. Nuclear Operator

Control of nuclear power level through selection of operation modes, control element positions, demand levels, or automatic programs.

Receives commands from the Chief Experimenter, calling for achievement of stated power levels or rates of change; has responsibility of carrying out these instructions while insuring safe nuclear operation.

Initiates preplanned remedial action in case of emergency.

If reactor is to be controlled to give a specified temperature program, this shall be the responsibility of the Nuclear Operator.

b. Nuclear Control Engineer

Assistance in nuclear control operation by monitoring of system condition indicators, operation of manual vane overrides in case of single vane failures, etc. No direct control of reactor power.

c. Air Flow Operator

Control of mass air flow rate or inlet pressure to reactor.

d. Air Temperature Operator

Regulation of reactor inlet air temperature by trimming balance of flow through and around heater.

This division of controls provides for essentially complete control of individual variables by single operators, so that a minimum of interference exists between the operators. Thus the Nuclear Operator has complete control, within limits, of reactor power; his control system has very fast response and can immediately override any reactivity perturbations introduced by changes in air flow. The Nuclear Control Engineer does not regulate a primary reactor variable; changes in reactivity which he may cause are readily corrected by the Nuclear Operator. The Air Flow Operator will have sole control of mass flow rate, with the ability to overcome incidental flow variations caused by the Air Temperature Operator. The latter, finally, has the only means of regulating air temperature. Reactor core temperature regulation is an exception to this principle, because of the strong dependence of core temperature on all of the control variables. Even here, however, in regulating this quantity there should be little difficulty with interference among the three operators, since the nuclear system responds much faster than the air controls, and so will predominate.

The Chief Experimenter will always be in charge of reactor operation; the operators will follow his commands, generally calling for specified levels of power, reactor temperature, air flow rate or inlet temperature. In the event of sudden failures or other emergency conditions, however, the individual operators will be responsible for initiating remedial action according to prearranged plans. These planned emergency responses will be kept as simple as possible, and in the event that a conflict between air and nuclear control actions could occur, the principal activity will be assigned to the Nuclear Operator.

Typical emergency responses initiated by the operators will be quite simple; for instance, the Nuclear Operator may find it necessary to switch control to a different neutron detector when one behaves erratically.

After taking necessary prompt action to avert immediate danger, the operator will report status to the Chief Experimenter, who will evaluate the reactor position and assign new objectives, such as: "Go into shutdown program," or "Adjust power to hold temperature steady at present level."

The condition to which this description applies is that of a high-power test run, with the complete control and instrumentation systems in use. Not all test runs will require full use of these systems, or attendance of a complete

operating crew, but the same general procedures will apply to all reactor operations.

As mentioned above, the control console with simulated reactor responses will be set up in Livermore. The operating procedures described here, as well as some possible alternates, will be tested on that console and evaluated for suitability before the start of actual operation in Nevada.

11. HAZARDS OF OPERATION

11.1 Overall Hazard Aspects

The Tory II-A design is advanced well beyond the scope of present reactor experience in the areas of high temperatures and rapid automatic control. Thus its operation will necessarily involve greater risk of accidental power excursions or other accidents than is the case for conventional reactors. In addition, the coolant air stream is to be released directly to the atmosphere, bearing with it radioactive fission products and some amount of the chemical poison, beryllium oxide.

In order to avoid a hazard to the general population, Tory II-A operation is to be carried out at the Nevada Test Site. Careful reactor operation and control of personnel location will also reduce hazard to on-site personnel to a negligible level.

As shown in Section 10, reactor operation will start with very low power levels, ambient temperatures, and low rates of change of power level. At this stage radiation levels are low, no air flow will pass through the reactor, and no rapid control maneuvers will be attempted. A very careful program of increases of power, temperature and control speeds will then lead up, over a period of several months, to operation at maximum design capabilities. This approach is vital, not only to the assurance of maximum yield of information from the reactor, but also to the achievement of a minimum hazard condition. The key point is this: thorough study of reactor behavior and measurement of radiation levels and exhaust contamination, will be carried out in each phase of operation, before going on to the next. Thus no sudden entry into unfamiliar modes of operation will take place; instead, such modes will be reached through a gradual approach, with careful study and analysis assuring at all times a good understanding of reactor behavior and site radiation levels.

The following sections will discuss some specific aspects of possible hazards associated with operation.

11.2 Radioactive Materials in Exhaust

Release of radionuclides in the Tory II-A exhaust should be expected during high-power operation. Inasmuch as the fuel elements are not coated, and are exposed directly to the air stream, fission products can enter the stream by recoil, erosion of the BeO, or diffusion. Activation of the cooling

air is found to be an insignificant issue.

The radioactive hazard due to escaping fission products has been reviewed carefully with emphasis placed on off-site radiation levels. The source strength was determined on the basis of running for 375 Mw-hr per core, and about two cores per year.

A radionuclide distribution appropriate to thermal neutron fission was assumed;[23] this is compatible with a loss mechanism of particle recoil from the heat transfer surfaces into the cooling air, which is thought to be the main contributor. The recoil loss was estimated to be 0.1-0.2% of the formation rate. It depends on the power, for at lower power levels the cooling air will be less dense and so will have a reduced stopping power. This will enable some fission fragments to completely traverse the air stream and become imbedded in the opposite wall of the fuel tube.

Loss by erosion at high power is expected to account for a fragment loss less than 0.01% of the formation rate. Erosion is expected to occur from reaction of water vapor in the air with BeO. The above value is based on undried air which may be used for power levels below 20 Mw; however, at high power runs, dried air will reduce the above value by a few orders of magnitude.

Diffusion losses are sensitive to the fuel-element temperature as well as the duration of a high-power run. Also, the method of fabricating the fuel elements markedly influences the loss rate. Some early experimental work[24] on urania-loaded BeO (i.e., 10% by weight) of poor uniformity led to diffusion constants that would imply diffusion losses from the Tory II-A not in excess of the recoil losses. Inasmuch as the quality of the loaded BeO that will be used in Tory II-A is expected to be far superior to that of the samples which were tested, it is reasonable to anticipate that the major loss mechanism will be particle recoil, and this will amount to about 0.2% of the fission-fragment formation rate.

Conventional procedures were employed to determine the degree of atmospheric dilution at various distances from the reactor.[25] Sutton's formula was used, with constants recommended by the Las Vegas Research Station of the U. S. Weather Bureau. The hazard to people several miles from the reactor was determined by first observing the isotopic composition of the radioactive cloud at the point in question; decay and buildup of the radioisotopes were taken into account.[23] Exposure time at distant points was equated to reactor operating time. It was then relatively straightforward to compute

the total dose received per year by various body organs.[26] Figure 11-1 summarizes the results; it was assumed, to be very conservative, that 1% of the fission fragments escape from the core. This is a factor of 5 greater than what should be expected. Since the meteorological assumptions are quite approximate, and since several assumptions have been made in the calculation, it is reasonable to be conservative.

Figure 11-1 shows that the thyroid received a higher exposure than any other organ. However, for a valid comparison in terms of equivalent body damage, one would reduce the exposure (i.e., in roentgens per year) by about 2.5.[26] In this case, one finds that for distances closer than 11 miles from the reactor, the total body exposure is critical, and at greater distances, the thyroid is the critical organ. At 20 miles, the total body received 0.04 roentgens per year which is much less than the maximum dose to the population-at-large recommended by the National Academy of Sciences. The recommendation gave an upper limit of 0.3 roentgens per year.

Damage to the gastro-intestinal tract, bone, kidney, and muscles are found to be lower than that to the total body and gonads, and the thyroid gland.

It is felt, therefore, that high-power operation of Tory II-A at NTS Site 401 does not constitute a radiation hazard to people beyond the site boundary.

11.3 Site Radiation Levels

Radiation levels in areas to which personnel access is desired will, of course, be measured directly to establish tolerable exposure times. However, it is well to predict these values beforehand in the most critical locations. Two such areas are taken up here.

11.3.1 Radiation Levels in Zero Site Bunker

The bunker is designed to provide enough radiation shielding so that its principal rooms and corridors may be occupied within a day or so after a full power run, with a reactor which has accumulated several hundred megawatt-hours of integrated power, without removing the reactor from the test point. Table 11-1 below shows estimated radiation levels in several specific locations, 24 hours after such a run. During the earlier parts of an operating program, with runs at lower power, radiation levels will, of course, be lower, permitting access at earlier times after shutdown of the reactor.

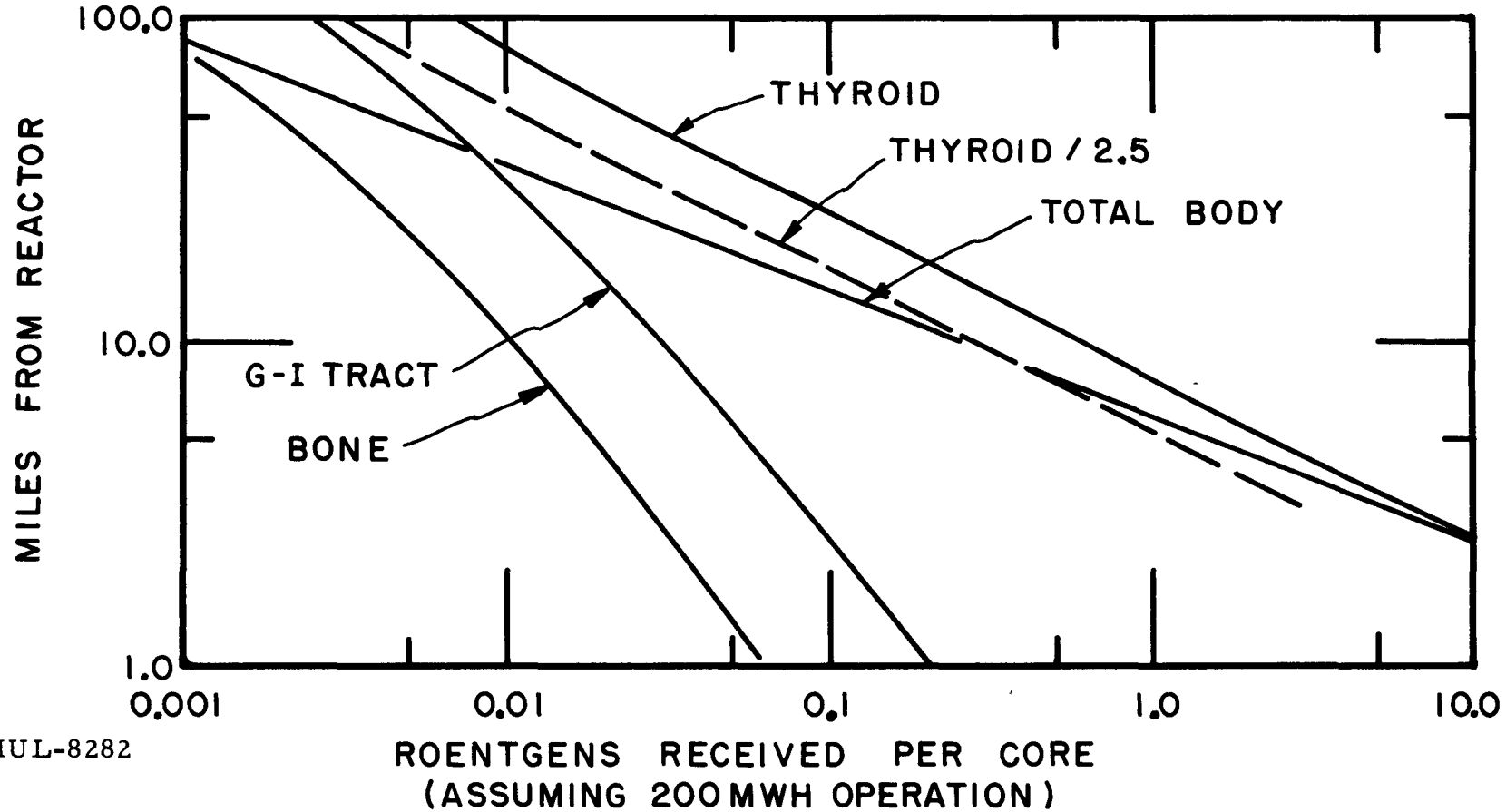

Fig. 11-1. Radiation dose vs distance from reactor.

Table 11-1. Estimated radiation levels, 24 hours after a full-power run, in roentgens per hour

1.	Inside plenum chamber (direct beam exposure)	3×10^{2}
2.	Disconnect room (6 ft below air pipe)	5×10^{-1}
3.	Passageway between disconnect room and electronics room	4×10^{-3}
4.	End of access tunnel (in front of maze)	4×10^{-2}
5.	Electronics room	5×10^{-3}

Because of the presence of sensitive components in the electronics room, radiation level in this area has been evaluated during high-power operation. For a power level of 160 Mw the radiation level was found to be 10^{3} r/hr; for a run of 3 minutes the integrated dose is ~50 r. These values are well below the damage threshold of electronic equipment.

11.3.2 Radiation Dose at Control Point

During the high-power operation of Tory II-A, it may be expected that personnel at the control building, which is 9000 ft from the zero site, will recieve a radiation dose. Both gammas and fast neutrons are capable of travelling over large distances. Thermal neutrons tend to be absorbed by the ground,[27, 28] and so may be neglected in the present calculation.

For estimating the neutron attenuation over large distances, it was found that age theory was not appropriate; rather, a first-collision modification in which slowing-down occurs after the first collision[29] was seen to be in general agreement with nuclear weapons test information and so was applied. The integral describing the slowing-down density, $q(r, \tau)$ was derived explicitly and gave:

$$q(r, \tau) = \frac{\Sigma_0 \, e^{-\Sigma_0 (r - \tau \Sigma_0)}}{4\pi r(r - 2\tau\Sigma_0)} ,$$

where Σ_0 = macroscopic cross section for the first collision (cm^{-1})

τ = "age" of neutron at energy E; initial energy, E_0.

An attenuation length, Σ_0^{-1}, of 221 meters ($\rho_{air} = 1.08 \times 10^{-3}$ g/cc) was found from comparison of the above expression with data from nuclear weapons tests.[30, 28] The neutron dose rate was then determined by employing the source strength listed in Section 5.4. The anisotropy of emission of the source was ignored; in the worst case, the radiation level may be three times higher than the following estimates.

A conversion factor, P(u), which relates neutrons/cm^2 sec to milli-rem/hr enters into the calculation for dose (D):

$$D = \int_{N_E} dN_E \int_{u(E)}^{u(0)} \frac{\phi(u)\, du}{P(u)} \quad \text{m-rem/hr} ,$$

where $\phi(u) = q/\xi\Sigma_t$,

ξ = logarithmic energy decrement per collision

Σ_t = macroscopic collision cross section (cm^{-1})

u = lethargy

N_E = number of neutrons with source energy E.

The integration, therefore, is carried out over the entire spectrum at a distance r. The second integration (i.e., over N_E) is required because the neutron source is not monoenergetic.

If $\Sigma_t = \Sigma_0$, which is a quite reasonable assumption, one finds that for r = 9000 ft, the dose rate from neutrons above 0.03 Mev is 0.5 milli-rem which is quite tolerable.

Gammas are found experimentally to have an attenuation length in air of 325 meters.* The total gamma energy release is about 1.0×10^{18} Mev/second. If, once again, one ignores non-isotropic emission, and considers a distance from the zero point of 9000 ft, a flux of 2.3×10^2 Mev/cm^2 second is realized. Since this spectrum is likely to be hardened, a conversion factor of 1.2×10^{-6} rad/hr per Mev/cm^2 sec (i.e., for 5 Mev gammas) seems appropriate. Therefore, the dose rate is about 3×10^{-4} rad/hr, or 0.3 milli-rad/hr. This is seen to be insignificant compared to the fast-neutron effect.

One may, therefore, expect a dose rate of 20 milli-rem/hr, and a total dose of 0.5 milli-rem, during full power operation. This is due primarily to fast neutrons.

11.4 Failure of Control System

The control system is designed to respond to any likely situation in a way such that power and temperature excursions will be prevented. In general, as explained in Section 6, power and temperature control will be maintained in spite of the failure of any individual control components or the introduction of

* Reference 28, p. 61.

unexpected excess reactivity. A "scram," or sudden reduction of power, such as conventional reactors use to deal with hazardous situations, will not in general be tolerated for Tory II-A, because of the resulting thermal stresses in the core. Instead, steps will be taken to maintain or restore a condition of zero reactivity.

In spite of the unlikelihood of such an occurrence, it is desirable to know what to expect if all precautions fail and control of the reactor is lost. Several such hypothetical situations are therefore considered here.

11.4.1 Cutoff of Coolant

Sudden loss of air pressure during a high-power run, as for instance by inlet duct rupture, would result in a positive temperature excursion in the reactor core if the power were not immediately reduced. The principal effect would be from the sudden cessation of heat removal, although the positive reactivity increment ($\Delta k \cong 0.0009$) caused by the reduction in nitrogen density in the core would also contribute.

Let us assume, then, that the control system fails completely at the same time that such a loss of air takes place. No further motion of the control elements takes place, but negative reactivity is introduced by the increasing core temperature until the power is reduced to a negligible value. The overall increase in core temperature may be obtained by integrating well-known time-dependent neutronic equations* coupled with the proportional relationship of power to rate of temperature change.

The result may be written as

$$\Delta T = \frac{\Delta\rho_g}{\partial\rho/\partial T} + \left\{\left[\frac{\Delta\rho_g}{\partial\rho/\partial T}\right]^2 + \frac{2P_0}{\sigma_c C_{pc}\,\partial\rho/\partial T}\left[\ell^*(1-\Delta\rho_g) + \Sigma_i\beta_i/\lambda_i\right]\right\}^{1/2}$$

where ΔT = core temperature increase

$\Delta\rho_g$ = reactivity increment on removal of air

$\partial\rho/\partial T$ = temperature coefficient of reactivity

P_0 = steady power, just before accident

* See for instance, Glasstone and Edlund, The Elements of Nuclear Reactor Theory, 1954 edition, Chapter 10.

σ_c = average core density
C_{pc} = specific heat of core
ℓ^* = prompt neutron lifetime
β_i = fractional yield of ith group of delayed neutrons
λ_i = decay constant of ith delayed group.

This and similar analytic expressions are used here as well as an IBM 704 computer code (Dane) for reactor excursion analysis.

Substitution of the following numerical values:

$\Delta\rho_g = 0.002$
$\partial\rho/\partial T = 2 \times 10^{-5}$ per deg K
$P_0 = 7.5$ Mw/ft^3 (core average)
$\sigma_c = 1.5$ g/cm^3
$C_{pc} = 0.5$ cal/g deg K
$\ell^* = 2 \times 10^{-4}$ sec
$\Sigma \beta_i/\lambda_i = 0.084$

leads to the result

$$\Delta T = 995°K.$$

The peak temperature increase, near the center of the core, will be 30% higher than this average value, hence 1300°K. Added to an initial peak temperature of 1550°K, this gives a final maximum of 2850°K or 2580°C. The melting point of BeO is listed variously from 2440 to 2550°C, so that some melting in the center of the core might take place in this accident. Certainly none of the core would be vaporized, and no explosion would occur, so that no hazard to on-site or off-site persons would be present.

Another interesting result may be noticed in the equation given above. If the initial power is very low, $P_0 = 0$, then the final temperature reached is twice that necessary to compensate for the added reactivity $\Delta\rho_g$. That is,

$$\Delta T = 2 \frac{\Delta\rho_g}{\partial\rho/\partial T} .$$

This result, of course, applies not only to the air loss accident, but to any noncooled excursion starting from low power.

11.4.2 Slow Addition of Reactivity

Now another type of control failure will be supposed, in which the vanes

all move out together, introducing reactivity at a maximum rate of 0.0025 sec^{-1}. Results of a number of calculations, starting under various conditions, have shown that the temperature very nearly follows a value giving zero reactivity for the instantaneous vane position. Thus the temperature rises at a rate given by

$$\frac{dT}{dt} = \frac{d\rho/dt}{\partial\rho/\partial T} = \frac{25 \times 10^{-4}}{2 \times 10^{-5}} = 125°C\ sec^{-1}.$$

If this temperature rise is not stopped very quickly, it would lead to fracture and melting in the core, but it is far too slow to produce any explosive disassembly.

11.4.3 Sudden Addition of Reactivity

The sliding control rods are worth up to about $0.60 each in reactivity, the specific amount depending on the position of the rotating control vanes. If the control system were to fail in such a way that the vernier rod and both of the reset rods were withdrawn at their maximum rates, reactivity could be introduced at a rate of as much as 0.06 sec^{-1}. One might also imagine some other means of introducing large amounts of reactivity very suddenly, perhaps even by deliberate sabotage. Studies have therefore been made of this situation.

Two problems were considered. In one, $\Delta\rho$ = $1.00 was added abruptly (i.e., $\Delta t = 0$), while in the other, $\Delta\rho$ = $3.00 was added abruptly. The core power density was initially 7.5 Mw/ft^3, and the gas flow corresponded to steady-state operation. The temperature coefficient of reactivity was taken as $-2.0 \times 10^{-5}/°K$, and the prompt lifetime as 1.5×10^{-4} second; initial core temperature was 1505°K. The Dane 704 code was used, so that all six delayed neutron groups were included. A simple equation relating the rate of core temperature change to core power and coolant flow allowed the core temperature history to be determined. The results are shown in Fig. 11-2.

It is observed that for the problem where $\Delta\rho$ = $1.00 (i.e., $\Delta\rho = 0.0064$) the temperature rises in a few seconds to the value $\Delta\rho/(\partial\rho/\partial T) + T_0$. That is, there is no overshoot in the temperature history. Such is not the case for $\Delta\rho$ = $3.00; here we have a 40% overshoot. The maximum temperature in the former problem was 1820°K while in the latter problem, T_{max} = 2800°K, about equal to the BeO melting point. Since the calculations dealt with core average temperatures, melting should definitely be expected in the center of

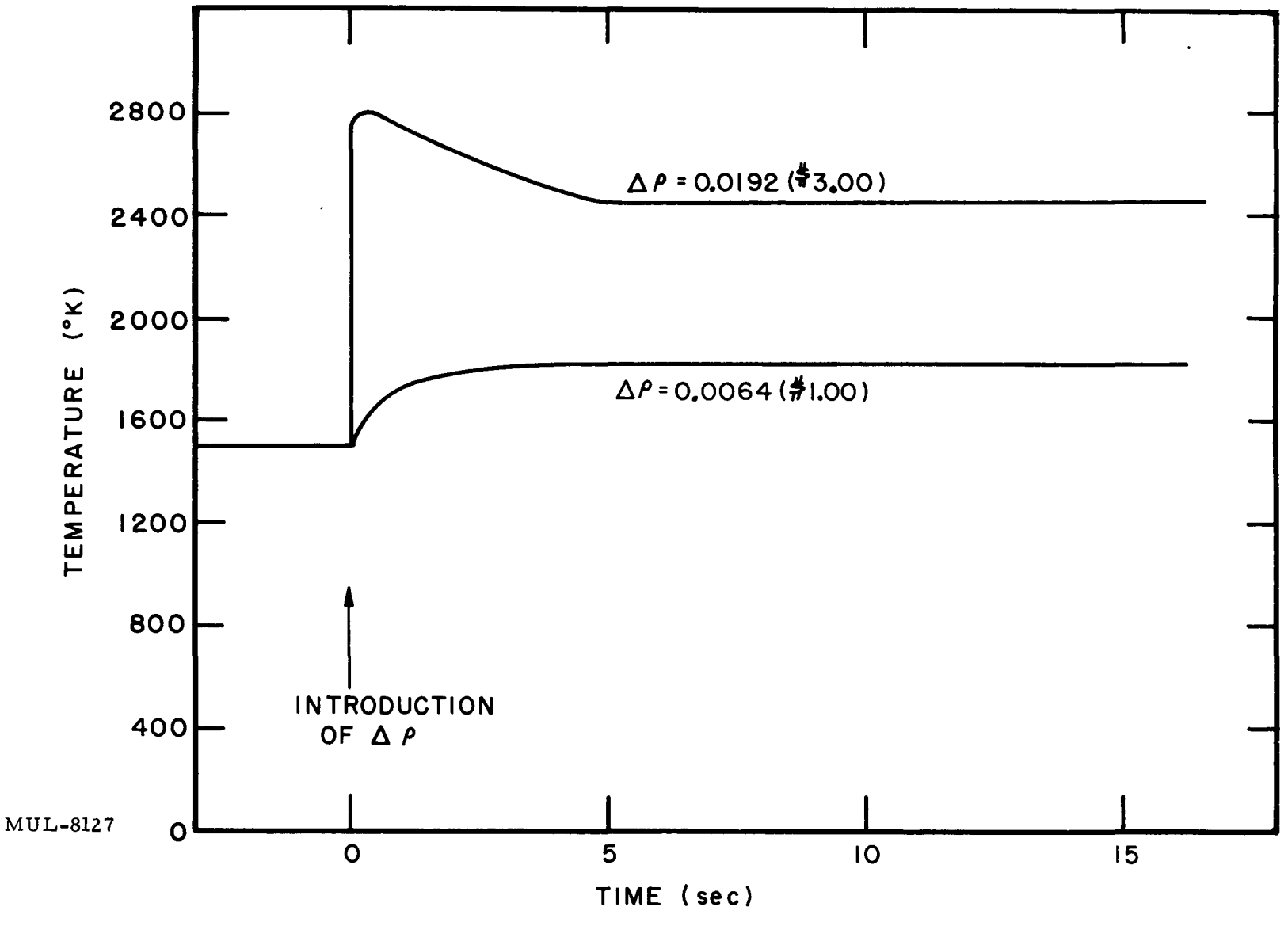

Fig. 11-2. Reactor temperature excursions resulting from sudden introduction of reactivity.

the core, where the temperature rise will be 30% above the average. The boiling point will still not be attained (~4000°K) but this accident almost approaches a situation where some vaporization, and the possibility of violent disassembly, would occur. The sudden introduction of more than $3.00 of reactivity is practically inconceivable, however.

A thorough analysis of reactor excursion hazards would involve consideration of a variety of possible conditions and occurrences, and cannot be complete until the reactor is actually constructed. The cases discussed above are felt to give a clear indication that a negligible chance of reactor explosion will be present, even if the control system were to fail in a very unlikely manner.

REFERENCES

[1] Finke, Meuser, Reynolds, and Tyson, "Sea-Level Nuclear Ramjet Parameter Study," UCRL-5397, March 1959.

[2] Pluto Programmatic Report I, UCRL-5515, January 1959.

[3] Stuart, Canfield, Dougherty, and Stone, Zoom, a One-Dimensional, Multigroup, Neutron Diffusion Theory Reactor Code for the IBM 704, UCRL-5293, November 1958.

[4] R. Stuart and S. Stone, Angie, A Two-Dimensional, Multigroup, Neutron Diffusion Reactor Code for IBM 704, UCRL-5019, September 1957.

[5] D. J. Hughes and R. S. Carter, Neutron Cross Sections, Angular Distribution, BNL-400, June 1956.

[6] L. Rosen and L. Stewart, Neutron Emission Probabilities from the Interaction of 14-Mev neutrons with Be, Ta, and Bi, Phys. Rev. 107, 824 (1957).

[7] H. Reynolds et al., Critical Measurements and Calculations for Enriched-uranium Graphite-moderated Systems, Second United Nations International Conference on the Peaceful Uses of Atomic Energy, Geneva, 1958, Paper No. P/2408; this paper is also report No. UCRL-5175, March 1958.

[8] Argonne National Laboratory, Reactor Physics Constants, ANL-5800, (1958).

[9] Humble, Lowdermilk, and Desmon, Measurements of Average Heat-Transfer and Friction Coefficients for Subsonic Flow of Air in Smooth Tubes at High Surface and Fluid Temperatures, NACA-1020, (1951).

[10] Durham, Neal, and Newman, LASL Technical Memorandum N-3 (1956).

[11] A. H. Shapiro, The Dynamics and Thermodynamics of Compressible Fluid Flow, vol. I, Fluid Mechanics (Ronald Press Co., New York, 1953) p. 231.

[12] Appendix I of UCRL-5515 Sup 1 (Appendices I-VI for Pluto Programmatic Report I), January 1959.

[13] Private communication.

[14] R. Meuser and R. Finke, Thermal Fracture Resistance of Simulated Beryllia Fuel Elements for Pluto, UCRL-5381, November 1958.

[15] C. D. Bopp, Gamma Radiation Induced in Engineering Materials, ORNL-1371, May 1953.

REFERENCES (Contd.)

[16] D. J. Hughes and J. A. Harvey, Neutron Cross Sections, BNL-325, July 1955.

[17] R. J. Howerton, Tabulated Neutron Cross Sections, UCRL-5226 (Pt I (Vols. I-III)), May 1958.

[18] Broadway, Youtz, Zaring, and Palinchak, The Effect of Nuclear Radiation on Elastomeric and Plastic Materials, Battelle Memorial Institute Report No. REIC-3, May 1958.

[19] S. L. Cosgrove, The Effect of Nuclear Radiation on Lubricants and Hydraulic Fluids, REIC-4, April 1958.

[20] R. E. Finnigan, Control Concepts for Nuclear Ramjet Reactors, UCRL-5465 (Summary), February 1959.

[21] American Society for Testing Materials, Symposium on Elevated-Temperature Strain Gauges, ASTM Publication No. 30.

[22] H. L. Reynolds and C. E. Walter, Hot Box, A High-Temperature Critical Facility, UCRL-5483, March 1959.

[23] R. C. Bolles and N. E. Ballou, Calculated Activities and Abundances of U^{235} Fission Products, USNRDL-456, August 1956.

[24] J. E. Wilson, Diffusion of Fission Products from Beryllia Fuel Rod Material, CT-3765, February 1956.

[25] Weather Bureau, Washington, D. C., Meteorology and Atomic Energy, AECU-3066, July 1956.

[26] British Journal of Radiology, Supplement No. 6, 1955, Recommendations of the International Commission on Radiological Protection (Revised Dec. 1, 1954); also NBS Handbook No. 52, March 1953.

[27] Hurst, Harter, Hensley, and Mills, Neutron Flux and Tissue Dose Studies with Fission Threshold Detectors, ORNL-1671, March 1954.

[28] R. I. Schnittke and C. W. Horn, Full Scale Test of Atomic Shell. Phase III. Shell Effects and Performance. Operation Upshot-Knothole. September 1954.

[29] A. M. Weinberg and L. C. Noderer, Theory of Neutron Chain Reactions: Extracts from Volume I, Diffusion and Slowing Down of Neutrons: Chapter III. Slowing Down of Neutrons, May 1951, p. III-40.

REFERENCES (Contd.)

30 W. A. Biggers and F. Waddell, External Neutron Measurements 1946 Through 1956. General Report on Weapons Tests. WT-9004, March 1957.

/bc